Universitat de València - CSIC

Departament de Física Atòmica, Molecular i Nuclear

Institut de Física Corpuscular

Isospin mixing and in-beam study of non-yrast states in ^{56}Co

VNIVERSITAT DE VALÈNCIA

Author:
Ana Montaner Pizá

Supervisor:
Dra. Berta Rubio Barroso

València, Març de 2018
Programa de Doctorat en Física
Tesi presentada per obtenir el títol de Doctor per la Universitat de València

Dra. Berta Rubio Barroso, Profesor de Investigación del Consejo Superior de Investigaciones Científicas (CSIC)

CERTIFICA:

Que la presente memoria "Isospin-mixing and in-beam study of non-yrast states in ^{56}Co" ha sido realizada bajo su dirección en el Instituto de Física Corpuscular (Centro Mixto Universidad de Valencia - CSIC) por **Ana Montaner Pizá** y constituye su Tesis doctoral dentro del Programa de Doctorado en Física del Departamento de Física Atómica, Molecular y Nuclear de la Universidad de Valencia.

Y para que así conste, en cumplimiento con la legislación vigente, presenta ante el Departamento de Física Atómica, Molecular y Nuclear la referida memoria, firmando el presente certificado en Paterna (Valencia) a 27 de Marzo de 2018.

Berta Rubio Barroso.

Abstract

In the present work we have studied the fusion-evaporation ^{56}Fe(p,nγ)^{56}Co reaction with an incident 10 MeV proton-beam at the Maier-Leibnitz-Laboratory (MLL) of the Technische Universität München (TUM, Germany). The γ-rays emitted in the de-excitation of the odd-odd ^{56}Co nucleus were measured in-beam with four high-resolution MINIBALL-triple germanium (Ge) detectors.

The experiment provided excellent data in γ-γ coincidences. A total of 223 γ-transitions have been observed and placed in the level scheme, 169 of which were previously unobserved.

A total of 77 excited states have been observed: 37 of them were previously known states for which no γ-de-excitation had been observed and 14 of them have been observed in this work for the first time. In 42 cases the precision of the excitation energy has been improved.

The spin and parity assignments to the excited states were made based on their γ-decay pattern and the angular distributions of the γ-ray de-excitations measured. The angular distributions of 53 γ-transitions were measured, obtaining the corresponding angular coefficients A_2. A total of 36 new J^π assignments have been made, 10 improvements of previous J^π assignments have been suggested and in 4 cases J^π-assignments ambiguities have been resolved. For the remainder of states, previously assigned J^π values have been confirmed.

Contents

List of Figures

List of Tables

Chapter 1

Motivation and basic physics

1.1 Introduction

The investigation of the ^{56}Co nucleus is interesting for a variety of reasons. From the shell-model point of view, in the simplest analysis ^{56}Co ($Z = 27$, $N = 29$) is just one proton hole and one neutron added to the doubly magic nucleus ^{56}Ni ($Z = N = 28$) (see Fig. 1.1). Ideally, spectroscopy of ^{56}Co ought to yield direct information on the particle-hole residual interaction in the fp-shell.

On the other hand, the ^{56}Ni nucleus is the most abundantly produced isotope in the silicon burning stage of a $\geqslant 10$ solar-mass star, and together with its daughter ^{56}Co plays an important role in the radioactive power of most supernovae. A wider knowledge of the properties of ^{56}Co is also important for nuclear astrophysics, more generally (See Appendix A).

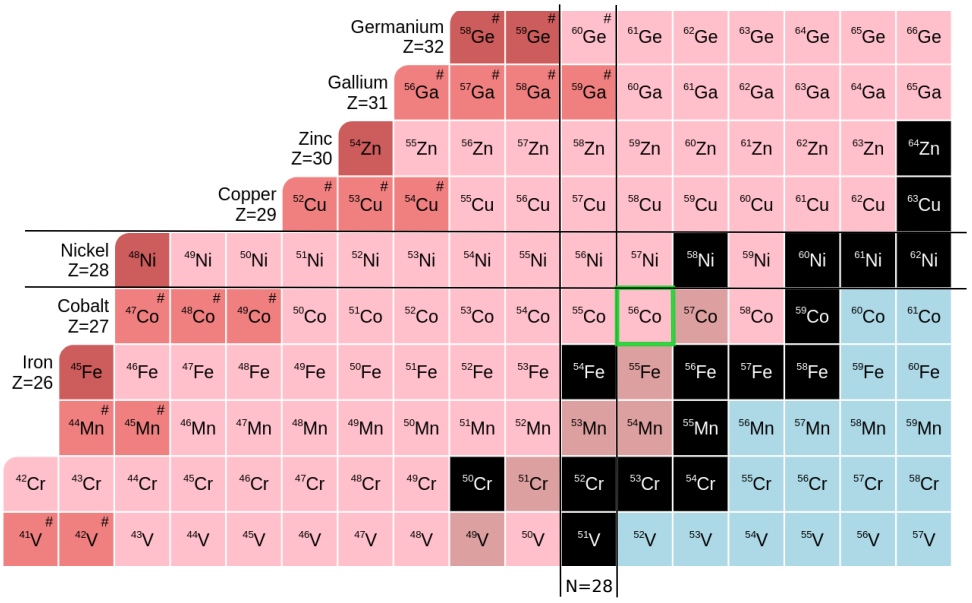

Figure 1.1: ^{56}Co region in the chart of nuclides.

In the present work we have studied the (mainly) fusion-evaporation ^{56}Fe(p,nγ)^{56}Co reaction with an incident 10 MeV proton beam to study in detail the γ-de-excitation of excited states in ^{56}Co. In the first chapter, we will explain the main motivations to perform the present work. The previous knowledge of ^{56}Co is summarised and the main physics involving the fusion-evaporation ^{56}Fe(p,nγ)^{56}Co reaction is explained.

In Chapter 2 the experimental setup and analysis techniques used will be presented. The construction of the γ-γ coincidence matrices and angular distributions of γ-rays depopulating excited states will be explained in detail. Chapter 3 brings together all the experimental results obtained in this thesis. In Chapter 4 we will make the theoretical interpretation of the results and dedicate an individual section for the two isospin-mixed 0^+ states in ^{56}Co which both have a component of the IAS of the ^{56}Fe ground state and whose study was one of the main motivations of the present work (see later).

1.2 Main motivations of the present work

The mechanism of beta (β) decay is well understood and dominated by allowed Fermi (F) and Gamow-Teller (GT) transitions. The Fermi transition (τ operator) connects the initial state in the parent nucleus and the *isobaric analogue state* (IAS) in the daughter nucleus having the same structure and quantum numbers spin-parity J^π and isospin T, although the third component of isospin $T_z = (N-Z)/2$ is changed in one unit. Thus the Fermi transition is characterized by $\Delta L = 0$, $\Delta S = 0$ (therefore $\Delta J = 0$) and $\Delta T = 0$. On the other hand, Gamow-Teller transition ($\sigma\tau$ operator) can be identified by $\Delta L = 0$, $\Delta S = 1$ (therefore $\Delta J = 1$) and $\Delta T = 1$.

The study of ^{56}Co in this work was initially motivated by the observation of two 0^+ states in its mirror nucleus ^{56}Cu in a ^{56}Zn β^+-decay experiment carried out at GANIL (Caen, France) [1]. These two states are populated through Fermi-type decay and correspond to the splitting of the IAS. Two very similar states exist in ^{56}Co and were recently investigated in the ^{56}Fe(^{3}He, t)^{56}Co charge exchange (CE) reaction performed at the Research Centre for Nuclear Physics RCNP in Osaka (Japan) with high-resolution [2]. No γ detection was possible in this work.

Beta decay and CE reactions can be compared under certain experimental conditions namely when the CE is carried out [3, 4]:

- at low angles close to 0°,
- at intermediate incident energies, generally ($E \geq 100$ MeV/u).

The motivation for the present work is defined in this context. Figure 1.2 shows the mirror symmetry of the $T = 2$ isobaric multiplet for $A = 56$. The multiplet is composed of $2T + 1$ members. The third component of isospin $T_z = (N - Z)/2$ is

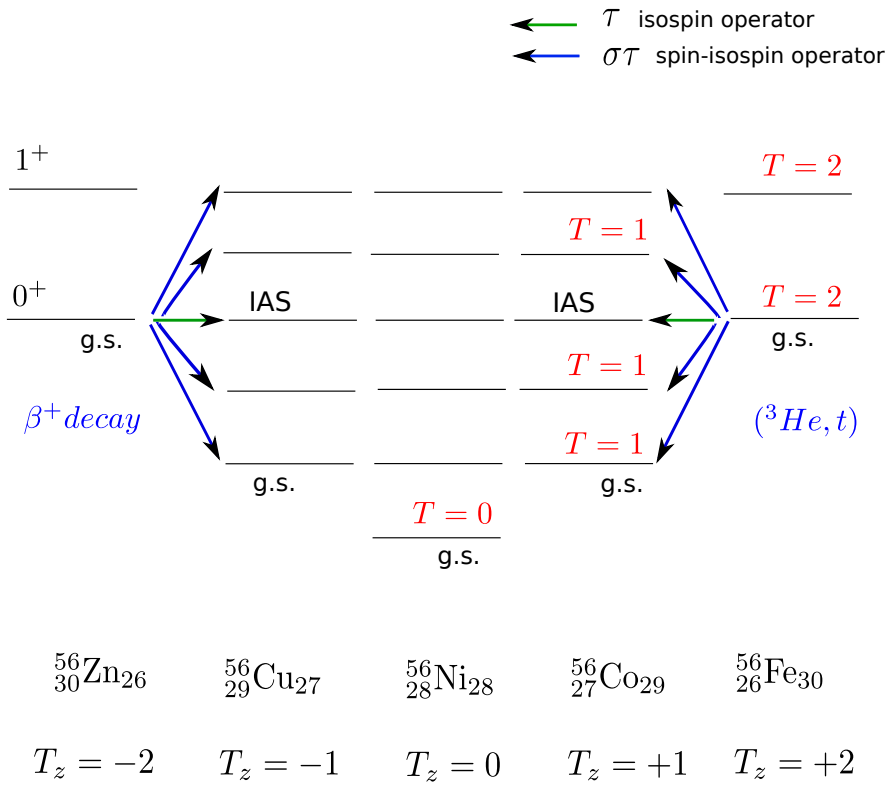

Figure 1.2: Graphical scheme of the $T = 2$ isobaric multiplet for $A = 56$. Beta decay and CE reactions can be compared under certain conditions (see main text). The Fermi transition (τ operator) connects the $T = 2$ initial state in the parent nucleus and the IAS in the daughter nucleus having the same structure, spin-parity $J^\pi = 0^+$ and isospin T. The third component of isospin $T_z = (N - Z)/2$ is different by one unit between neighbouring members of the multiplet. The transitions to the $T = 1$, 1^+ states are of Gamow-Teller type ($\sigma\tau$ operator).

different by one unit between neighbouring members. The $T_z = -2 \rightarrow -1$, β^+ decay connects the ^{56}Zn and ^{56}Cu nuclei. On the other hand, the excited states in ^{56}Co are populated via the $T_z = +2 \rightarrow +1$, (p,n)-type CE reaction on ^{56}Fe. The ground states (g.s.) of the $\mid T_z \mid = 2$ parent nuclei, the even-even ^{56}Zn and ^{56}Fe nuclei, have quantum numbers $J^\pi = 0^+$ and $T = 2$. Thus two kinds of state are expected to be populated in these processes: the $T = 2$, 0^+ IAS (through the Fermi transition), and a number of $T = 1$, 1^+ states (mainly through Gamow-Teller type transitions). The doubly magic ^{56}Ni nucleus ($N = Z = 28$) corresponds to the $T_z = 0$ member of the multiplet.

One of the main purposes of the experiment we present in this work was to study in detail the γ-de-excitation of the two isospin-mixed 0^+ states in ^{56}Co which both

have a component of the IAS of ^{56}Fe and compare the results with what is observed in its mirror nucleus.

1.2.1 The ^{56}Zn β-decay experiment

The β^+ decay of ^{56}Zn to ^{56}Cu was carried out at GANIL in 2010 [1]. The experiment was performed in inverse kinematics at the LISE facility using a ^{58}Ni^{26+} primary beam accelerated to 74.5 MeV/u. The primary beam was fragmented using natural Ni targets of approximately 200 mg/cm^2. Fragments were selected by the LISE3 separator and Wien filter and implanted into a Double-Sided Silicon Strip Detector (DSSSD) surrounded by four EXOGAM germanium (Ge) clover detectors for the γ detection.

This experiment was motivated in turn by the comparison with the mirror CE reaction on ^{56}Fe (which will be discussed in the next section), which populates the excited states in ^{56}Co, the mirror nucleus of ^{56}Cu.

In the β decay of medium to heavy nuclei, close to stability, the de-excitation of the parent nucleus proceeds via β-delayed γ decay. As the nuclei become more exotic, the particle separation energy decreases and the strong interaction causes decay to occur via β-delayed particle emission. In proton-rich nuclei proton decay is expected to dominate for states well above, namely > 1 MeV, the proton separation energy S_p. Nevertheless, the proton decay from the IAS is usually isospin forbidden. In this case competition between β-delayed proton- and β-delayed γ-decay modes becomes possible.

Thus, proton decay from the $T = 2$ state at 3508 keV in ^{56}Cu (which had been identified as the IAS in previous works) to the ^{55}Ni$_{gs}$ ($T = 1/2$) is expected to be isospin forbidden, which makes the competing γ-de-excitation possible. Actually competition between β-delayed proton- and β-delayed γ-emission in states well above S_p was observed in this nucleus for the first time (see Fig. 1.3). Moreover, β-delayed γ-rays that populate proton-unbound levels that subsequently decay by proton emission were also observed. This rare and exotic decay mode, β-delayed γ-proton decay, was observed in this work for the first time in the *fp* shell.

On the other hand, the total Fermi transition strength has to be $|N - Z| = 4$. The state at 3508 keV in ^{56}Cu (previously known as the IAS) had a Fermi strength $B(F) = 2.7(5)$. The comparison with the mirror case showed that the missing strength had to be hidden in the broad peak that was observed at 3423 keV. This was a confirmation that the IAS in ^{56}Cu is fragmented due to isospin mixing and thus part of the feeding to the 3423-keV level corresponded to the Fermi transition.

The off-diagonal matrix element of the charge-dependent part of the Hamiltonian $\langle \mathcal{H}_c \rangle$ and consequently the isospin impurity α^2 can be deduced if isospin mixing

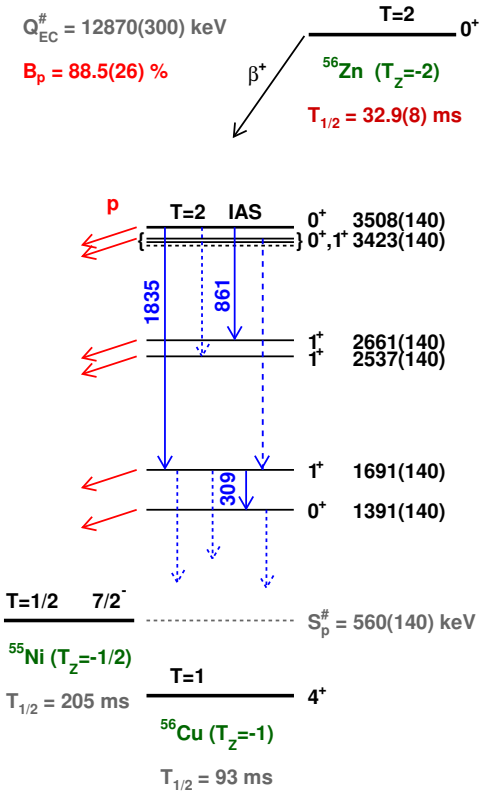

Figure 1.3: ^{56}Zn decay scheme deduced from the ^{56}Zn β-decay experiment at GANIL. Observed proton or γ decays are indicated by solid lines. Transitions corresponding to those seen in the mirror ^{56}Co nucleus but not seen in ^{56}Cu are shown by dashed lines. The 140 keV-error comes from the uncertainty in S_p.

exists and experimental data allows (see Appendix B). Thus an isospin impurity of $\alpha^2 = 33(10)\%$ was deduced from the ^{56}Zn β-decay experiment.

Figure 1.3 shows the ^{56}Zn decay scheme deduced from the β-decay experiment. Observed proton or γ-decays are indicated by solid lines. Transitions corresponding to those seen in the corresponding counterpart levels in the ^{56}Co nucleus but not observed in ^{56}Cu are shown by dashed lines. It could be that these unobserved transitions exist but were below the gamma-sensitivity threshold of the experiment; it should be noted that this nucleus is exotic and the statistics obtained in the experiment was poor.

The 1834.5(10) and 861.2(10) γ-rays were observed and attributed to transitions de-exciting the state at 3508 keV (the one having the largest component of the IAS). However no γ-transitions were observed de-exciting the state at 3423 keV. At the time of this β-decay experiment was done, the homologous state of the 3423-keV

level in the ^{56}Co nucleus, which is the state at lower excitation energy of the two isospin-mixed 0^+ states, was known to de-excite by one γ-ray. Then, considering that the isospin mixing is quite large in ^{56}Cu, interesting open questions are the following: should the two close-lying 0^+ states in ^{56}Cu de-excite in a similar way? And in turn, should they de-excite in a similar way to their counterpart levels in ^{56}Co?

1.2.2 The ^{56}Fe(^{3}He, t)^{56}Co charge exchange reaction

The isobaric analogue state in ^{56}Co was identified for the first time in the early 1960s in a direct-exchange ^{56}Fe(p,n) reaction [5]. Later this state was found to be a doublet by several authors through the (p, n)-type CE reactions on ^{56}Fe such as the ^{56}Fe(p,n) [6, 7] and ^{56}Fe(^{3}He, t) [8, 9] reactions.

In order to ensure the possibility for the splitting of the IAS it is necessary that both states of the doublet have the same spin and parity, and are not too far apart in energy. Previous work had demonstrated that the members of the doublet observed in ^{56}Co and described in terms of the IAS (with $T = 2$) and a nearby 0^+, $T = 1$ state, lied at excitation energies of 3522 $\pm$ 9 keV and 3592 $\pm$ 9 keV [8].

A high-energy-resolution ^{56}Fe(^{3}He, t)^{56}Co CE reaction was performed at the Research Centre for Nuclear Physics (RCNP) in Osaka [2] using 140 and 100 MeV/u beams of ^{3}He. The good energy resolutions achieved made it possible to study the fine structure of the doublet in ^{56}Co and the nearby excited states (see Fig. 1.4).

The measurements were made at forward angles including 0°, i.e., an orbital momentum transfer of $\Delta L = 0$ was favoured. Therefore mainly 0^+ and 1^+ states were populated in ^{56}Co.

In order to distinguish between the possible 0^+ and 1^+ nature of the states, the fact that the τ- and $\sigma\tau$-type effective interactions strengths have different dependencies on the incoming energy of the projectile can be used. In CE reactions at intermediate energies and near 0°, there is a good proportionality between the GT and Fermi reaction cross sections, σ_{GT} and σ_F, and the square of the transition matrix elements. Because the reduced transition strength, B, is proportional to the squared transition matrix element (see equation 1.9 from section 1.6.3), we can write:

$$\sigma_{GT}(0^\circ) = \hat{\sigma}_{GT} B(GT) \tag{1.1a}$$

$$\sigma_F(0^\circ) = \hat{\sigma}_F B(F) \tag{1.1b}$$

where $\hat{\sigma}_{GT}$ and $\hat{\sigma}_F$ denote GT and Fermi unit cross sections, respectively. A systematic study in (p, n) reactions below $E_p = 200$ MeV showed that the ratio of

the unit cross section, $\hat{\sigma}_{GT}/\hat{\sigma}_F$, is almost proportional to the squared value of the incoming energy of the proton beam [3]. This is caused by the fact that the strength of the τ term of the free nucleon-nucleon interaction becomes larger at lower incident energies, while the strength of the $\sigma\tau$ term remains nearly the same [10]. Therefore it is expected that $\hat{\sigma}_F$ will become larger relative to $\hat{\sigma}_{GT}$ at lower incident energies. Thus the states excited through the Fermi transition will be enhanced relative to the states excited through the GT transition in the spectra obtained.

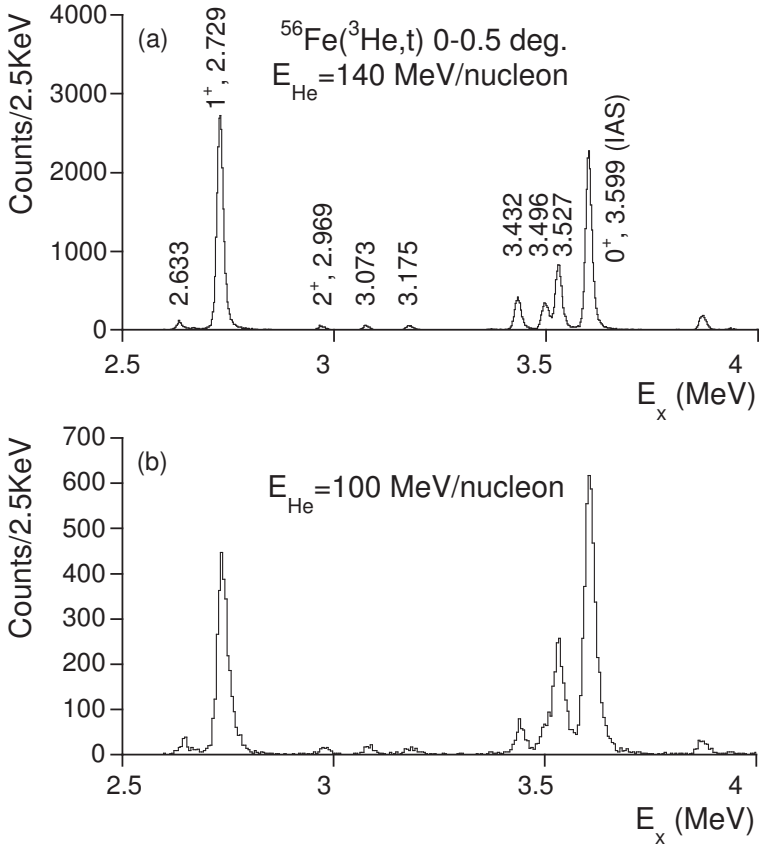

Figure 1.4: Excitation energy spectra of ^{56}Fe(^{3}He, t)^{56}Co reactions at 140 and 100 MeV/u are shown. The isolated strong GT state at 2.729 MeV was used as the normalization standard.

The excitation energy spectra for the ^{56}Fe(^{3}He, t) reaction at 140 and 100 MeV/u are compared in Fig. 1.4. They correspond to the triton (t) energy spectra measured and the peaks are labelled according to the corresponding excitation energies in ^{56}Co. The isolated strong GT state at 2.729 MeV was used as the normalization standard.

The ratio of the cross sections at 100 and 140 MeV/u show how much the relative cross sections increase in the measurement of the former compared to the latter. As

can be clearly seen, the 3.599 MeV state is enhanced in the spectrum at 100 MeV/u. It can be observed that the 3.527 MeV state is also enhanced. While ratios of $\simeq 1$ were obtained for the several 1^+ states, which suggest that they are excited by $\sigma\tau$-type interactions, values of 1.85(12) and 1.91(15) were obtained for the state at 3.599 MeV and the nearby state at 3.527 MeV. From this result, it was concluded that the τ-type operator excites both states and therefore there is a splitting of the Fermi transition strength and, consequently, a splitting of the IAS exists. Therefore both states have $J^\pi = 0^+$ (the same as the ground state of the even-even ^{56}Fe nucleus). The previous results suggest that the state at 3.527 MeV is excited through the isospin impurity part (T=2) of the wave function and carries part of the Fermi transition strength.

An isospin impurity of $\alpha^2 = 28(1)\%$ was deduced in this experiment (see Appendix B). This value is compatible with that obtained in the ^{56}Zn β-decay experiment (see previous section), showing a good isospin symmetry.

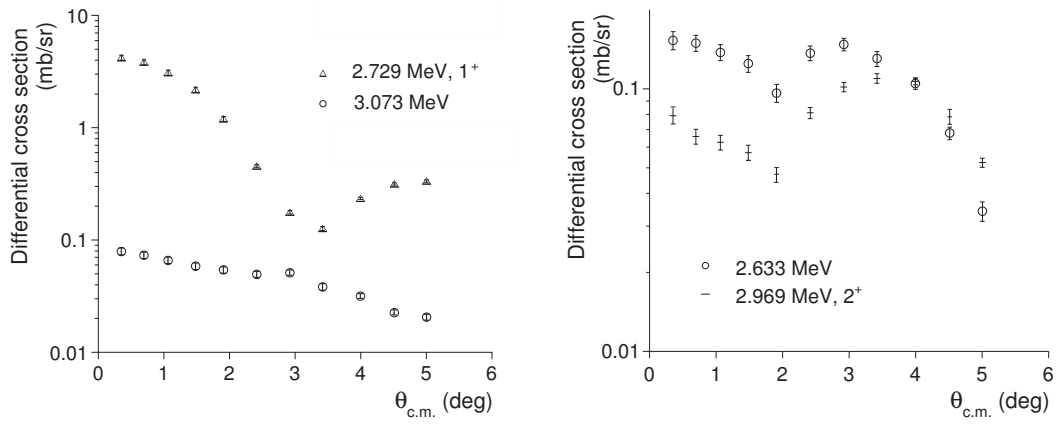

(a) (b)

Figure 1.5: Angular distributions of reaction cross sections for the states at 3.075 MeV (a) and 2.633 MeV (b) studied in the $(^3\mathrm{He}, t)$ reaction on ^{56}Fe at an incoming energy of 140 MeV/u. The well-known angular distributions for the 1^+ state at 2.729 MeV and the 2^+ state at 2.969 MeV are shown for comparison.

It is worth remembering that both Gamow-Teller and Fermi transitions have a $\Delta L = 0$ nature. These transitions can be identified by the characteristic shape, peaked at 0°, of the angular distribution of the reaction cross sections. Thus their study is useful to perform a J^π identification of the levels. The typical 0° peak of the angular distributions for the 0^+ states corresponding to the splitting of the IAS (the states at 3.527 MeV and 3.599 MeV) and various 1^+ states was confirmed. However the angular distributions for the 2.633- and 3.073-MeV states, assigned to 1^+ from previous work, differed from the expected shape (see Fig. 1.5). As an example of

this typical $\Delta L = 0$ transition, the angular distribution for the well-known $J^\pi = 1^+$ state at 2.729 MeV is shown in Fig. 1.5(a). In Fig. 1.5(b) the angular distribution for the well-known 2^+ state at 2.969 MeV is presented in order to show the similarity to the shape of the 2.633-MeV angular distribution. Thus, the possible improvement on the J^π assignment of those levels was an extra motivation to study in detail the ^{56}Co nucleus.

Summary of open questions

After the analysis of the results of both experiments, three questions remained open. If the two close-lying 0^+ states in ^{56}Co are mixed, should they de-excite in the same way? And, based on mirror symmetry, should the states in ^{56}Co and ^{56}Cu have a similar γ-decay pattern? On the other hand, are the two states at 2.633- and 3.073-keV excitation energy 1^+ states and can a detailed study of the γ-decay of these two states confirm or dismiss this assignment?

These open questions summarise our motivation for a detailed study of the γ-de-excitation of low-spin states in ^{56}Co.

1.3 Previous knowledge of ^{56}Co

The ^{56}Co nucleus cannot be formed by the familiar methods of inelastic scattering or single-particle transfer reactions. Consequently, the only available means to investigate it are decay experiments, two-particle transfer, direct charge exchange or fusion-evaporation reactions.

Two-particle transfer plays an important role in the study of ^{56}Co. The two-particle stripping reactions ^{54}Fe(^{3}He,p) [11, 12] and ^{54}Fe(α,d) [13–16]; and the two-particle pick-up reactions ^{58}Ni(d,α) [11, 17–22] and ^{58}Ni(p,^{3}He) [23] have been extensively studied. Usually (^{3}He,p) reactions have been used to search for 0^+ and 1^+ states formed by $L = 0$ orbital momentum transfer. On the other hand, it has been shown that under suitable kinematic conditions, high-spin states with stretched configuration are preferentially excited in (α,d) [14–16] and (d,α) [19–22] reactions.

The (p, n)-type CE reactions ^{56}Fe(p,n) [5–7] and ^{56}Fe(^{3}He, t) [2, 8, 9] have also been explored. However, the former is impeded by the well-known difficulties of neutron spectroscopy.

The level scheme of ^{56}Co can be determined through the β-decay of ^{56}Ni [24–26] and by means of the transfer reactions ^{56}Fe(p,nγ) [24, 27, 28], ^{54}Fe(^{3}He,pγ) [29], ^{54}Fe(α,pnγ) [30] and ^{58}Ni(d,$\alpha\gamma$) [31]. Information about electromagnetic transitions and lifetimes of low-lying states can also be obtained from such studies. The β-

decay studies are obviously limited by the Q_β-value ($Q_\beta = 2.136 \pm 0.011$ MeV in ^{56}Ni$\rightarrow^{56}$Co).

Given the extensive work previously done studying ^{56}Co, one would initially expect that its structure is very well known. However, a large amount of new information has been obtained in the present work and will be presented in Chapter 3.

1.4 Population of the 0^+ states in ^{56}Co

Aiming at answering the open questions presented in section 1.1 we performed an experiment to study in detail the γ-de-excitation of excited states in ^{56}Co and, especially, the splitting of the IAS among two close-lying 0^+ states.

The reaction and beam energy for the experiment were carefully chosen in order to guarantee that the 0^+ states in ^{56}Co were populated up to 3.6-MeV excitation energy (the location of the two 0^+ states of interest was already reported). Due to the fruitful results obtained in the study of these 0^+ states in previous works using the reactions ^{54}Fe(^{3}He,pγ) [29] and ^{56}Fe(p,nγ) [24, 27, 28], these two types of reactions were considered at first. However, due to practical reasons the latter option was finally chosen. Calculations using the TALYS software [32] were made to investigate the p + ^{56}Fe reaction and in particular the population of the excited energy states in ^{56}Co (see Appendix C for details). These calculations showed that two primary reaction channels were open: the (p,p') channel populating excited states in ^{56}Fe and the (p,n) channel populating excited states in ^{56}Co, with a higher total cross section in the former. The ratio between the total cross sections of both reaction channels, $\sigma_{(p,p')}/\sigma_{(p,n)}$, remained almost constant in the energy range $E_p = 8 - 12$ MeV, with a ~ 1.5 value. At lower and higher energies the (p,p') channel became clearly dominant. Therefore we chose to perform the ^{56}Fe(p,nγ)^{56}Co reaction at an incident-proton energy of ~ 10 MeV. The definitive energy value was chosen during the experiment aimed at maximising the population of the two 0^+ states in ^{56}Co of interest. According to the TALYS calculations, the 0^+ states of interest were populated with sufficient cross section to be investigated at these incident energies. On the other hand, calculations also showed that the excited states in ^{56}Co were mainly populated through a fusion-evaporation reaction instead of a direct reaction in this energy regime (see Appendix C).

1.5 The ^{56}Fe(p,nγ)^{56}Co fusion-evaporation reaction

As mentioned above, the reaction under study in this work is the ^{56}Fe(p,nγ)^{56}Co reaction. At high projectile energies (> 100 MeV/u) the direct charge-exchange reaction would be favoured. However at the energy regime of our experiment ($\sim$

10 MeV/u), it becomes very likely that an intermediate step takes place and a compound nucleus is formed (^{57}Co in our experiment).

The angular momentum transferred in the collision process must be dissipated by the emission of neutrons (unless the compound nucleus lies close to the proton drip line, where proton emission would occur, which is not the case for ^{57}Co) and the succeeding gamma cascade. Thus, after equilibration, the ^{57}Co nucleus evaporates neutrons until the excitation energy becomes smaller than the separation energy of the neutron S_n (S_n = 11.4 MeV in this nucleus). This type of reaction is known as fusion-evaporation. Depending on the number of emitted particles various final nuclei are produced. We are interested in the case where only one neutron is emitted after the formation of the compound ^{57}Co nucleus leading to excited states in ^{56}Co:

$$^{56}Fe + p \rightarrow {}^{57}Co \rightarrow {}^{56}Co + n \tag{1.2}$$

Figure 1.6 shows a simple energy diagram for the p +^{56}Fe reaction at an incident 10 MeV proton beam. The proton separation energy in ^{57}Co is $S_p \approx 6$ MeV. Therefore, the energy window available for the population of excited states in ^{56}Co is $\Delta E = 10 + 6 - 11.4 = 4.6$ MeV. We will see in Chapter 3 that this value is in perfect agreement with the highest excited state in ^{56}Co reached in our experiment.

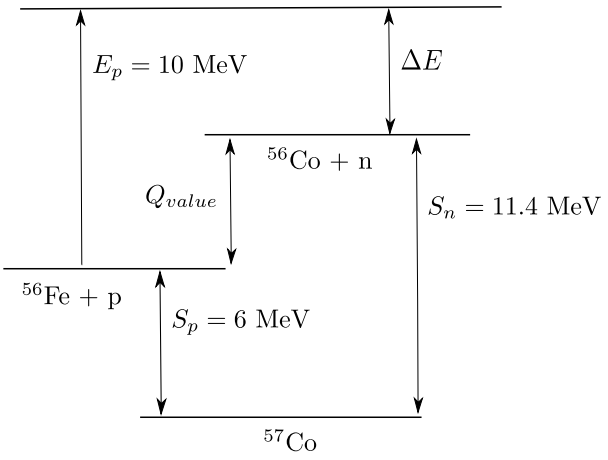

Figure 1.6: Energy diagram for the p +^{56}Fe reaction at E_p = 10 MeV. After the reaction, the compound nucleus ^{57}Co is formed. The proton and neutron separation energies in ^{57}Co are S_p = 6.0 MeV and S_n = 11.4 MeV, respectively. After equilibration, the ^{57}Co nucleus evaporates neutrons leading to states in ^{56}Co, until its excitation energy becomes smaller than S_n. Thus the energy window available for the population of excited states in ^{56}Co is ΔE = 4.6 MeV.

The neutron evaporation lowers considerably the excitation energy of the nu-

cleus. However, the mean angular momentum taken away by each neutron is only $\approx 1\hbar$. After the emission of the last neutron ($\approx 10^{-15}$ s after the collision) the angular momentum as well as the excitation energy must be dissipated by γ-rays (and internal conversion). Since the γ-rays are even more inefficient in taking away the angular momentum, the gamma cascade should have a strong tendency to lead first to the lowest energy state for a given spin and then to cascade down further along the lowest energy-highest spin level sequence, which is known as the "Yrast" line, till finally coming to the ground state of the residual nucleus (see Fig. 1.7). Thus the highly-excited states would de-excite at first by the emission of a few high-energy γ-ray transitions of predominantly electric dipole character (E1) which on average take away a lot of excitation energy but little angular momentum. If states which lie a few MeV above the Yrast line are reached, the emission of stretched ($\Delta J = 2$) electric quadrupole E2 transitions or M1 transitions can favourably compete with the emission of E1 transitions. In our case, we see predominantly M1 transitions, partially due to the dominance of positive-parity states up to 3.3-MeV excitation energy.

Since the nucleus of interest in this work is the odd-odd ^{56}Co nucleus, a schematic idea of the flow of population after a fusion-evaporation reaction ending in an odd-odd residual nucleus is shown in Fig.1.7:(a) reaction populating relatively high-spin states, (b) reaction aiming at non-yrast relatively low-spin states. As can be seen in the picture, in a reaction such as (a) we could have never populated the low lying 0^+ states in ^{56}Co.

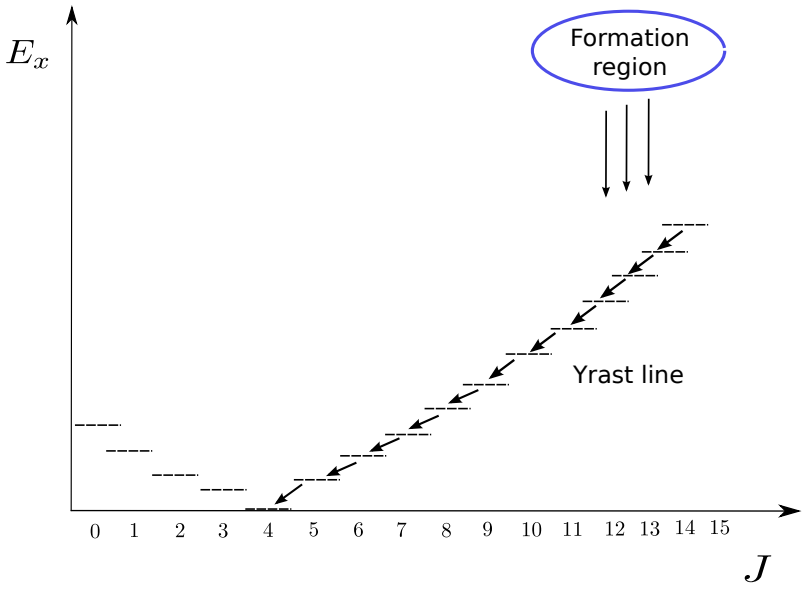

(a)

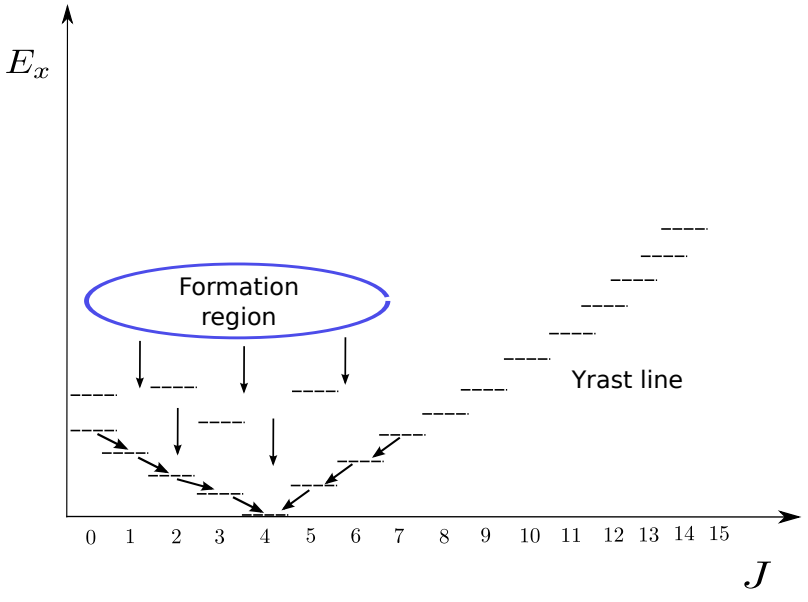

(b)

Figure 1.7: Flow of population in a relatively high-spin fusion-evaporation reaction ending in an odd-odd nucleus (a), and in the present experiment (b).

1.6 Principles of in-beam γ-spectroscopy

The study of in-beam γ-ray spectroscopy was initiated in 1963 by Morinaga and Gugelot [33] by the observation that discrete γ-rays can be detected in the de-excitation of excited states of nuclei produced in nuclear reactions. They carried out the first "in-beam" γ-spectroscopic experiments utilizing NaI(Tl) detectors to measure the γ-radiation emitted promptly from the target. The development of in-beam γ-spectroscopy since then is related to the continuous improvement of the features of γ-ray detectors, viz. the energy resolution, peak-to-total ratio and total photopeak efficiency. The main break through occurred when Ge detectors, with almost two orders-of-magnitude better resolution, were implemented.

In this chapter we shall discuss the spectroscopic uses of γ-rays de-exciting excited states in nuclei formed in nuclear reactions.

1.6.1 In-beam γ-spectroscopy techniques

A detailed study of the properties of excited nuclear states requires high-resolution γ-ray spectroscopy. The nuclear states are characterized by their basic eigenvalues and quantum numbers, such as excitation energy E_{level}, spin J and parity π. In order to determine these quantities the features of the γ-ray transitions depopulating these excited states have to be measured. They are the transition energy E_γ, the multipole order $L \geq 1$ and the character of the radiation (magnetic M or electric E). If the features of the final state, populated by the γ-ray, are known, then those of the initial state can be determined considering energy conservation $E_i - E_f = E_\gamma$ and the selection rules $|J_i - J_f| \leq L \leq J_i + J_f$, $\pi_i \pi_f = (-1)^L$ for electric radiation and $\pi_i \pi_f = (-1)^{L+1}$ for magnetic radiation. In most cases the lowest one or two multipole orders, being in agreement with the selection rules, are allowed for a γ-ray transition, e.g., a mixture of M1 and E2 radiation. The peak area in the γ-ray energy spectrum provides information on the intensity of the transition, I_γ.

In order to establish the complex level scheme of a nucleus it is necessary to place the observed γ-ray transitions in the level scheme and to determine their intensity. This information can be deduced from γ-γ coincidence measurements, since the determination of coincidence relationships between γ-ray transitions forms the basis for their placement in the level scheme. In order to place weak transitions or members of unresolved multiple γ-ray peaks, high-fold coincidence measurements are required. Thus arrays with many γ-ray detectors, placed at different angles with respect to the beam direction, are needed.

1.6.2 Angular distribution of γ-rays

As previously mentioned, γ-γ coincidence measurements give us information about the energies E_{level} and the intensities I_γ of the transitions connecting them. However, to make spin and parity assignments one needs to investigate the character and the multipolarity of the transitions.

The excited states in a nucleus formed in nuclear reactions are in general oriented with respect to the beam direction. The degree of orientation depends on the process of formation and therefore is subject to the reaction mechanisms. Thus one can use the fact that the intensity of a γ-transition emitted from an oriented excited state has an anisotropic spatial distribution, which provides information about the multipole orders and multipole mixing of the γ-radiation.

One way of preparing an oriented ensembled of nuclei is through nuclear reactions. They provide orientation to the nuclei by the angular momentum transfer from the projectile of well defined direction and occasionally defined polarization too. In in-beam γ-spectroscopy experiments, the spins $\vec{J}$ of nuclei in excited states formed in the nuclear reactions are generally aligned in a plane perpendicular to the beam. As a consequence, γ-rays depopulating these states exhibit characteristic angular distributions relative to the beam direction depending upon the multipolarities of the radiation and the spins of the nuclear states involved. When alignment is incomplete, partial alignment may be represented by a Gaussian distribution of the substates with quantum number m (m=-J,...,J), resulting from the projection of the angular momentum on the beam axis as quantization axis. The substate population distribution then fulfils the condition $P(m)$=$P(-m)$, centred around m=0, and is characterized by a parameter σ which is the half-width of the assumed Gaussian distribution.

The directional angular distribution (or anisotropy) of γ-radiation from oriented nuclei may be written as:

$$W(\theta_\gamma) = \sum_k A_k(\gamma) P_k(cos(\theta_\gamma)) \tag{1.3}$$

where $k = 2l$, and l is the multipolarity of the transition. The A_k are the angular distribution coefficients which depend on the substate population distribution of the initial state, the spins of the initial and final states (J_i and J_f), the multipole orders and the multipole mixture of the γ-radiation. $P_k(cos(\theta_\gamma))$ are the Legendre polynomials and θ_γ is the emission angle of the γ-ray with respect to the beam direction.

For real cases, where the alignment is partial, and expanded up to second order, the previous expression can be rewritten as:

$$W(\theta_\gamma) = 1 + A_2 P_2(cos(\theta_\gamma)) + A_4 P_4(cos(\theta_\gamma)) \tag{1.4}$$

The angular distribution coefficients can be written as,

$$A_n = \alpha_n * A_n^{max} \tag{1.5}$$

where α_n are the attenuation coefficients, which depend on the spin J and the distribution of the nuclear state over its m substates, and the A_n^{max} are the angular coefficients for complete alignment.

As mentioned earlier, in most cases the lowest one or two multipole orders, being in agreement with the selection rules, are allowed for a γ-ray transition, e.g., a mixture of M1 and E2 radiation. In these cases the parameter δ can be defined,

$$\delta = \frac{\langle J_f \| L_2 \| J_i \rangle}{\langle J_f \| L_1 \| J_i \rangle} \tag{1.6}$$

which is the ratio of the amplitudes of the mixed multipolarity.

1.6.3 Transition probabilities

In this section we will briefly describe some basic features of electromagnetic transition probabilities, which will be useful for the analysis of empirical data.

Transition probability

The transition probability for gamma-ray emission of energy E_γ and multipolarity λ (with its component μ) is expressed by [33]:

$$T_{fi}(\sigma\lambda, \mu) = \frac{8\pi(\lambda+1)}{\hbar\lambda(2\lambda+1)!!}\left(\frac{E_\gamma}{\hbar c}\right)^{2\lambda+1} |\langle f|\mathcal{M}(\sigma\lambda, \mu)|i\rangle|^2 \tag{1.7}$$

where σ denotes electric (E) or magnetic (M) transitions, and $|\langle f|\mathcal{M}(\sigma\lambda, \mu)|i\rangle|$ is the transition matrix element.

Reduced transition probability

Equation 1.7 gives the transition probability for one sub-process μ. The total transition probability from a state J_i to a state J_f (summed over all possible m_f substates

and all μ substates which satisfy $\mu = m_i - m_f$) is given by the following equation [33]:

$$T(\sigma\lambda, J_i \to J_f) = \frac{8\pi(\lambda+1)}{\hbar\lambda(2\lambda+1)!!}\Big(\frac{E_\gamma}{\hbar c}\Big)^{2\lambda+1} B(\sigma\lambda : J_i \to J_f) \tag{1.8}$$

where,

$$B(\sigma\lambda : J_i \to J_f) \equiv \sum_{\mu,m_f} |\langle f|\mathcal{M}(\sigma\lambda,\mu)|i\rangle|^2 = \sum_{\mu,m_f} \langle J_i m_i \lambda\mu | J_f m_f\rangle^2 |\langle f\|\mathcal{M}(\sigma\lambda)\|i\rangle|^2 \tag{1.9}$$

is called the *reduced transition probability* [34]. The term $\langle f\|\mathcal{M}(\sigma\lambda)\|i\rangle$ is the *reduced transition matrix element*. The reduced transition probability does not depend on energy. Therefore it is usually very convenient to convert $T(\sigma\lambda)$ into $B(\sigma\lambda)$.

Using the symmetry and completeness of the Clebsch-Gordan coefficient equation 1.9 can be rewritten as:

$$B(\sigma\lambda : J_i \to J_f) = \frac{2J_f+1}{2J_i+1}|\langle f\|\mathcal{M}(\sigma\lambda)\|i\rangle|^2 \tag{1.10}$$

Thus reduced matrix element B depends upon the direction of the transition. The definition used in equation 1.9 makes it transform in the same way as a Clebsch-Gordan coefficient under exchange of J_i and J_f. Then using this transformation property one can obtain the following relation between the excitation $B(\sigma\lambda)\uparrow$ and the decay $B(\sigma\lambda)\downarrow$ of a given transition:

$$B(\sigma\lambda : J_i \to J_f) = \frac{2J_f+1}{2J_i+1} B(\sigma\lambda : J_f \to J_i) \tag{1.11}$$

Chapter 2

The experiment

2.1 The experimental setup

All measurements analysed and presented in this work were carried out at the Maier-Leibnitz-Laboratory (MLL) of the Technische Universität München (TUM, Munich, Germany). The excited states of the odd-odd nucleus ^{56}Co were populated in the (mainly) fusion-evaporation reaction ^{56}Fe(p,nγ)^{56}Co. The γ-rays emitted in the de-excitation of these states were measured in-beam with four high-resolution MINIBALL-triple germanium (Ge) detectors.

2.1.1 The Maier-Leibnitz-Laboratory

The experiment analysed in the present work was performed at the Maier-Leibnitz-Laboratory (MLL) of the Technische Universität München (TUM, Munich, Germany). A schematic map of the laboratory is shown in Fig. 2.1(a).

The MLL operates a Tandem-van-de-Graaff accelerator (see Fig. 2.1(b)) which accelerates ions to high velocity with a voltage of up to 14 million volts. For our experiment, protons were accelerated to 9, 10 and 12 MeV. These energies were chosen aiming to optimise the population of the two 0^+ states of interest in ^{56}Co (see Chapter 1). The reaction using 10-MeV incident protons turned out to be the optimal scenario for the purpose mentioned before and therefore the experiment was performed at this energy during almost all of the beam-time. The accelerated protons were transported from the Tandem Hall to the spot #14 in Fig. 2.1(a), where the detector array was placed. A specially shielded beam dump was mounted for our experiment about 3 meters behind the target chamber, which had an inner shield of lead followed by 1 m^3 of plastic to slow down (and finally stop) the neutrons.

2.1.2 The MINIBALL detector array

The MINIBALL array is a γ-ray spectrometer optimized to achieve a high photo-peak efficiency in combination with position-sensitive γ-ray detection. The detectors

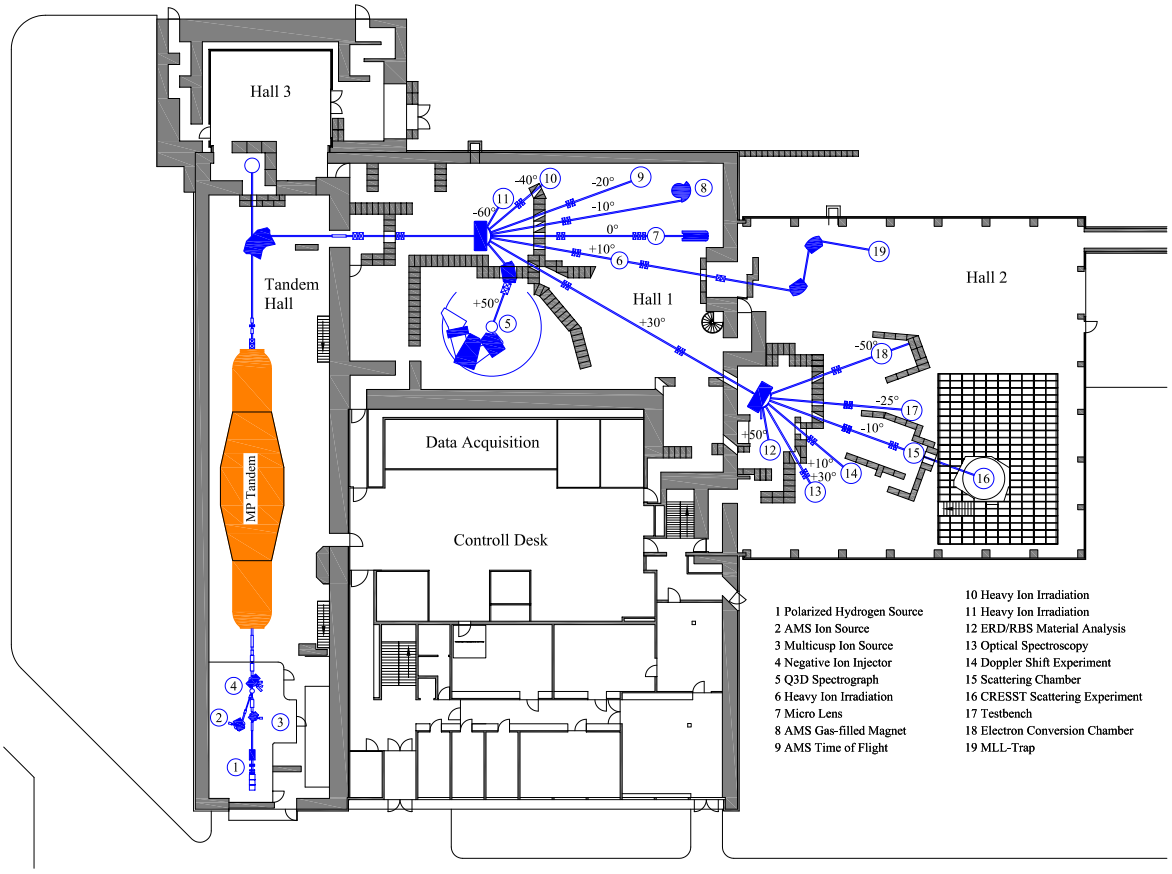

(a)

(b)

Figure 2.1: An schematic map of the Maier-Leibnitz-Laboratory in the Technische Universität München is shown in (a). View of the Tandem-van-de-Graaff accelerator (b).

are six-fold segmented, tapered, encapsulated high-purity Ge-crystals disposed in clusters of three (*triple* detectors). The layout of one single crystal is shown in Fig. 2.2. The cryostat configuration combined each triple detector with a common vacuum chamber, cryostat and dewar.

The whole array consists of eight clusters and was specially designed for low multiplicity experiments with low-intensity radioactive ion beams (RIBs). High granularity and high efficiency were achieved by the segmentation of the charge-collection electrodes of the Ge detectors and the use of pulse-shape analysis to determine the position of the first interaction of the γ-ray within the Ge crystal. The MINIBALL array has been used in numerous Coulomb-excitation and transfer-reaction experiments with exotic RIBs with energies up to 3 MeV/u, produced at the REX-ISOLDE facility at CERN. The detectors have also moved around for a limited period of time. The experiment performed in June 2013 was part of the MINIBALL campaign at Munich. Before that the whole detector array had been operational at ISOLDE for over 10 years. For the experiment at the TUM, four MINIBALL clusters were available. Figure 2.3 shows the experimental setup used. Two detectors were located forward and two backward with respect to the beam, as can be seen. A schematic drawing is presented in Fig. 2.4 where the clusters have been labelled. MINIBALL detectors were positioned at slightly different distances from the chamber, trying to maximise the solid angle covered. The distance $d_{tar \to det}$ between the target position and the frontal face of the detectors was approximately of 9.5 cm.

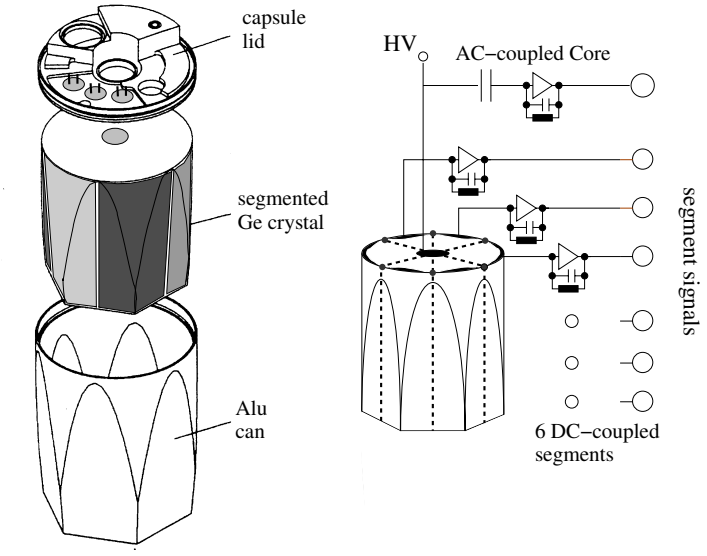

Figure 2.2: Layout of one six-fold segmented germanium crystal: the drawing shows an exploded view of the capsule assembly.

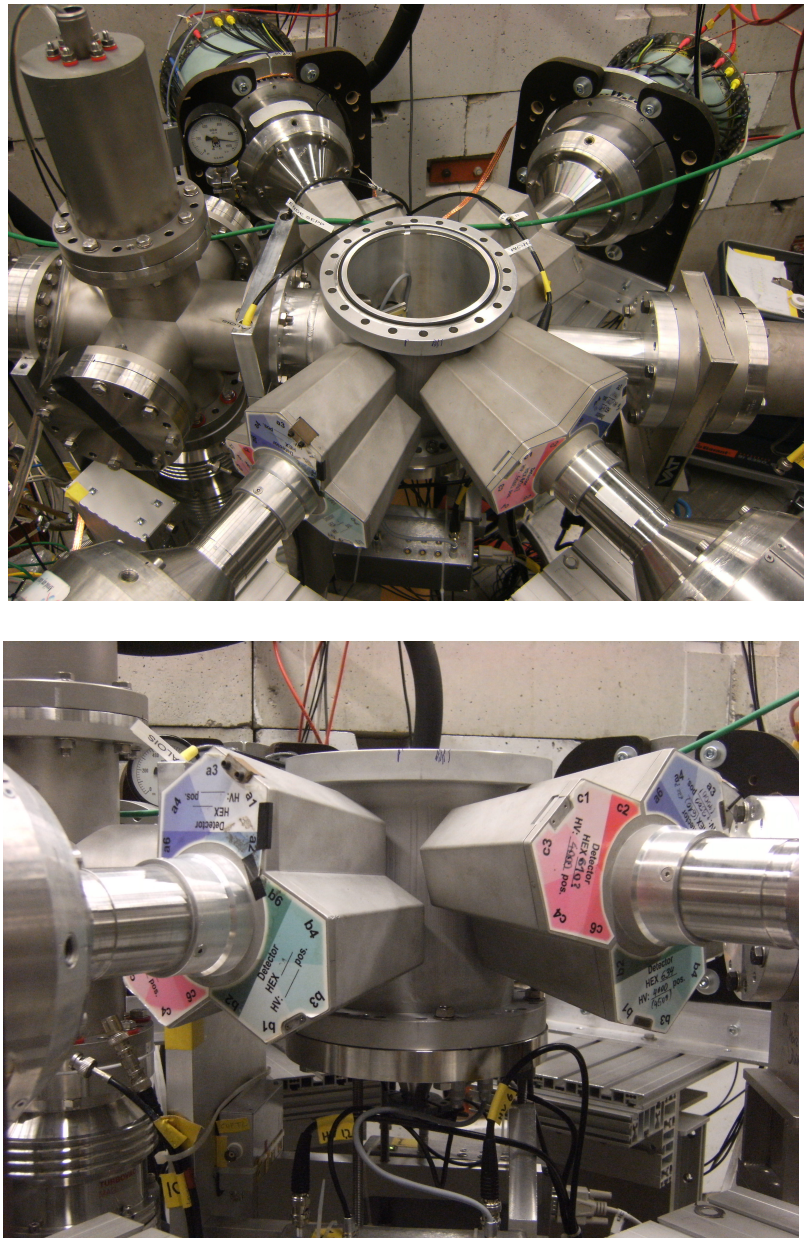

Figure 2.3: View of the detector array (upper panel): The target chamber is surrounded by four MINIBALL-triple detectors and is centred in the beam pipe. The beam direction is from left to right. Detail of two of the clusters is shown (lower panel).

2.1.3 Targets

Two ^{56}Fe targets of different thicknesses (1.1 and 2.1 mg/cm^2) were used. Figure 2.5 shows a detail of the 2.1 mg/cm^2 ^{56}Fe target and the aluminium frame used in the experiment.

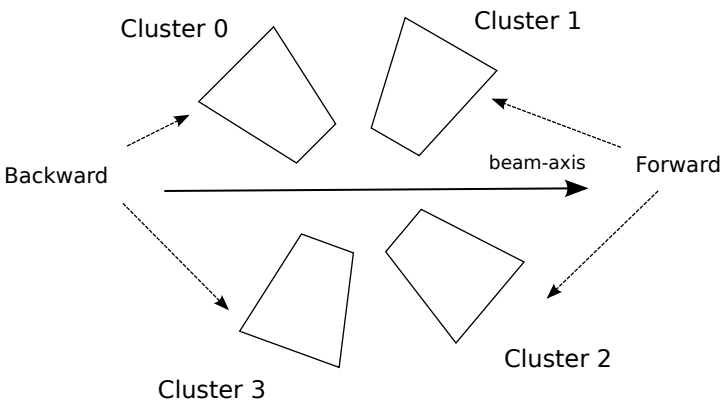

Figure 2.4: A schematic drawing of the experimental setup is shown. Clusters 0 and 3 are located backwards with respect to the beam direction; clusters 1 and 2, forwards.

The 2.1 mg/cm^2 ^{56}Fe target was used for 19 hours in the first part of the experiment with a beam of ~ 1 nA at 9 MeV proton energy.

The other target, the 1.1 mg/cm^2 one, was used during the second part of the experiment. It was irradiated for 5 days + 22 hours approximately (88% of the total beam-time) with a proton beam of $\sim 2-3$ nA, at 12 MeV for the first 25 hours and at 10 MeV the rest of the time. As we will see in section 2.2.2 this target was used as one of the sources for the energy calibration of the detectors.

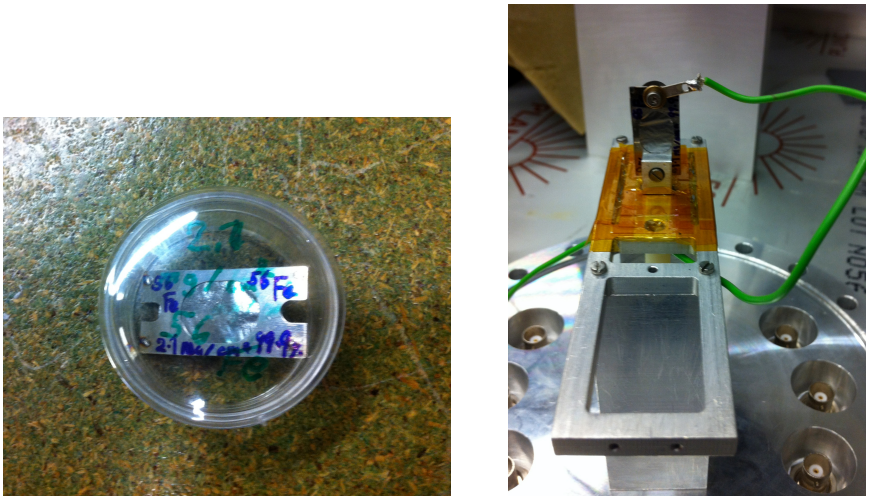

Figure 2.5: Detail of the 2.1 mg/cm^2 ^{56}Fe target (left) and the same target mounted on its frame (right).

2.1.4 MARABOU software

The electronics and data acquisition system used in this experiment were mainly developed at the Technische Universität München (TUM). MARaBOU [35] is a system for data acquisition and evaluation developed at the Tandem Accelerator Laboratory of the University of Munich. It consists of a front-end system for the data readout, event building, and data transport based on the Multi Branch System (MBS) developed at GSI (Darmstadt, Germany) and a back-end system responsible for setup, run control, histogramming, data analysis and data storage written within the ROOT framework (see Fig. 2.6). The ROOT part includes a GUI to control the MBS front-end, a histogram presenter to visualize the data, and class libraries to describe the experiment. MARABOU was established as the common data acquisition system at the Tandem Accelerator Laboratory.

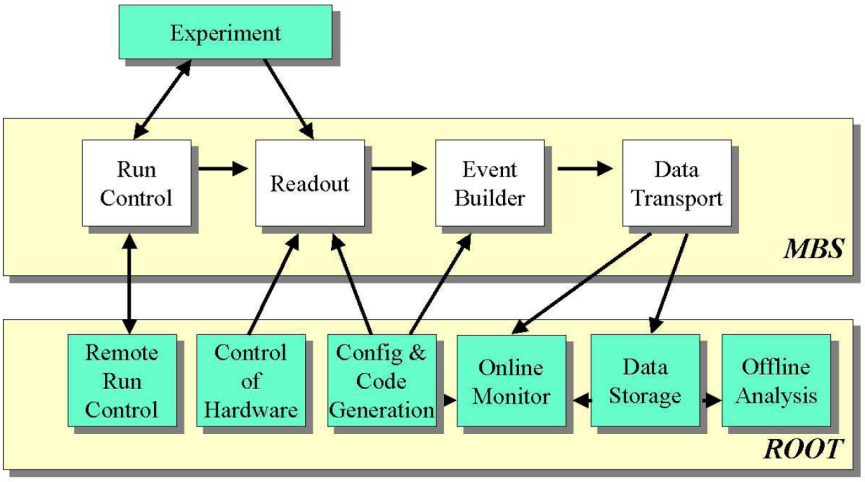

Figure 2.6: MARABOU tasks.

2.1.5 Electronic setup

As previously mentioned, four MINIBALL-triple detectors were used. From now on we will use the term either triple detector or cluster to describe one of these four detectors. Each single detector (crystal) has a central electrode (also known as core) and an outer electrode, which is cut into six segments. The signal on the core electrode indicates the full energy. On the other hand, by looking at the signals in the segments, one can determine what fraction of that full energy was lost in each segment and thereby obtain the segment in which the interaction with the highest energy deposition (main interaction) occurred. By making the assumption that the main interaction is at the same position as the first interaction, this information can

be used to refine the Doppler correction. However, in our experiment the crystals were used without segmentation because the Doppler broadening was not too severe (see sec. 2.2.5).

In the present experiment, the energy resolution of the cores extended from 3.1 to 4.0 keV at 1.238-MeV photon energy, a line in ^{56}Fe coming from the ^{56}Co radioactivity (see later). The segments show a worse energy resolution, with values between 7.0 and 8.9 keV at 1.238 MeV. The high capacity between the detector surface and the capsule wall causes a deterioration in the resolution of the segments.

The electronics was based on standard Mesytec modules [36]. The electronics setup was split into four identical chains, one for each cluster. A pre-amplifier is integrated after all cores and segments (see Fig. 2.7). The core signals are split into slow and fast branches by the MSCF-16[1]. The MSCF-16 module is a shaping/timing filter amplifier with constant fraction discriminator and multiplicity trigger. The incoming signal from the pre-amplifier has a fast increasing slope and a slow exponential decay. Because of the tail, pile-up effects occur when multiple signals come in rapid succession.

The fast branch (time signal) carries the time information and acts as a trigger. Whenever any one of the three crystals of a cluster fires, this fast signal opens a gate in the MADC-32[2] large enough that the energy signal of both the cores and the associated segments are enclosed. The MADC-32 module itself sets the length and delay of the gate. In our experiment the gate was expanded to 10 μs. This module also assigns a time stamp (t.s.) to each signal with a resolution of 16 MHz (i.e. 62.5 ns). To get a global clock, the four MADCs were synchronized in time. If the MADC receives a trigger signal while it is busy, this trigger is held back.

From the slow branch of the core signal one extracts the energy deposited by the γ-ray. The MSCF-16 module provides a new Gaussian-shape signal and magnifies the input amplitude. This branch is then put into the MADC-32 which converts the analogue signal into a digital one.

Due to their worse energy resolution (see above), the segments were used only for time information. The segments were plugged into the STM-16+[3] before being put into the MADC. The STM-16+ module differs from the MSCF-16 mainly because the latter has more individual operational functions such as Pole Zero and threshold settings.

[1]MSCF-16: 16-Channel Shaper with Constant Fraction Discriminator from Mesytec
[2]MADC-32: 32 Channel Peak sensing ADC (Analogue to Digital Converter) from Mesytec
[3]STM-16: 16-fold shaping/timing filter amplifier from Mesytec

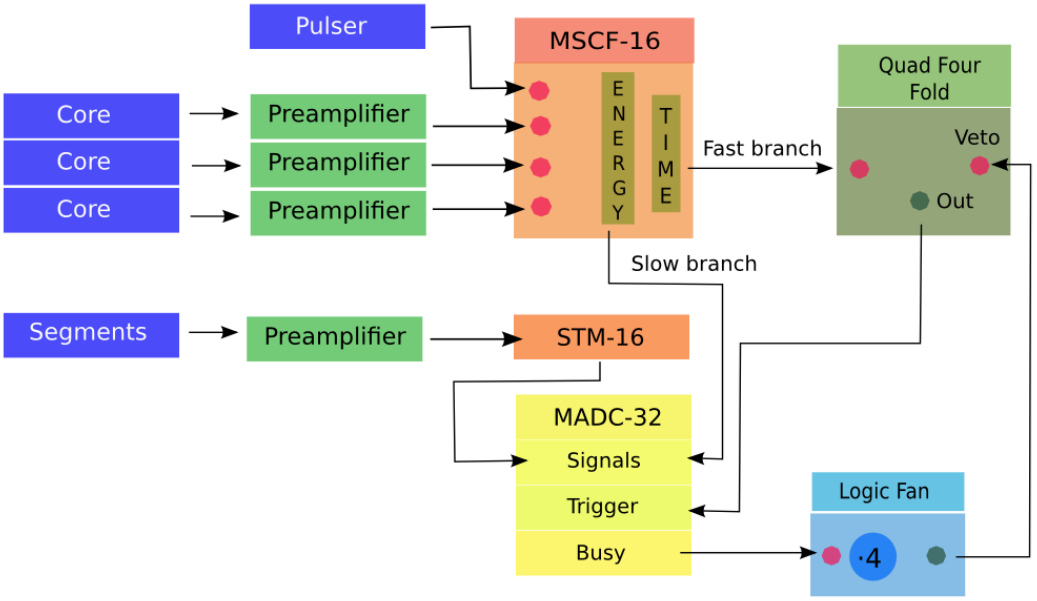

Figure 2.7: Electronics setup of the experiment for one cluster. The label ·4 means that the signals of all four clusters were plugged in.

2.1.6 Data Flow Overview and Event Building

After the readout, the list mode (MED) files are unpacked and data are coded in a specific format defined by the *Event Builder* to make up the "event structure". An event is defined by all clusters that have fired within a coincidence window of 6.25 μs (i.e. 100 t.s.) (see Fig. 2.8). Hence, one event contains all real coincidences between particles and γ-rays but also random coincidences. In Chapter 2.3.1 we will see how we deal with this when searching for γ-γ coincidences.

Each event contains information about which Ge-crystals have fired and which are the parameter values (Energy, Time, etc). The data are then written in a sequential mode, event-by-event, and arranged in files, called *runs*, for easy handling in the off-line analysis. A logbook was used to record the specific details such as the length in time of the run, current intensity of the beam, etc.

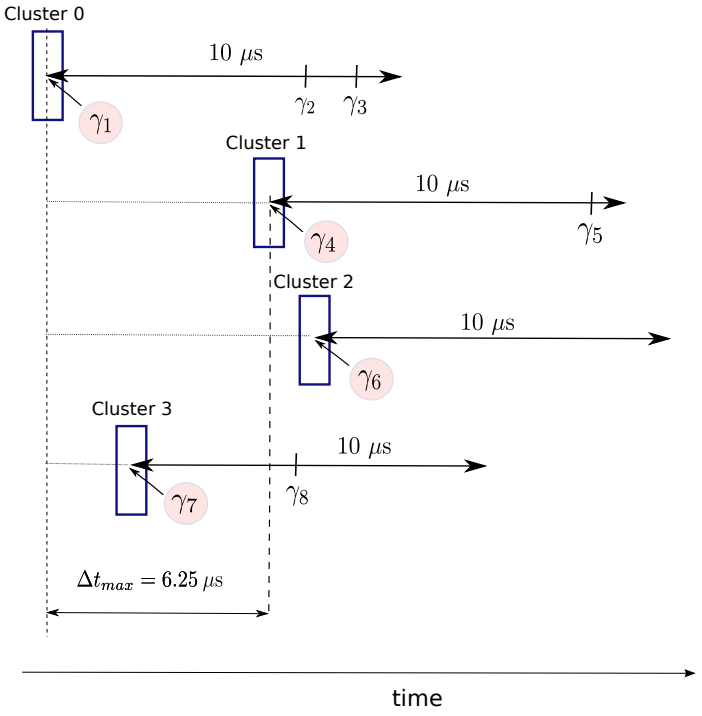

Figure 2.8: Graphical scheme of the *event structure*. In this picture γ_1 acts as trigger of the cluster 0, γ_4 as trigger of cluster 1, γ_6 of cluster 2 and γ_7 of cluster 3. Each cluster then opens a time gate of 10 μs. An event is defined by all clusters that have fired within a coincidence window of 6.25 μs (i.e. 100 time stamps). In the example above all γ-rays but γ_6 would belong to the same event.

2.2 Calibrations and treatment of the data

In this section the calibration processes and treatment of the experimental data will be described. The processes of alignment, energy calibration and efficiency calibration of the γ-spectra are explained in detail.

2.2.1 Alignment of the runs

During the running period, minor instabilities in the electronics might produce slight gain shifts in the spectra. Several factors can lead to these instabilities, e.g., variations in temperature and counting rates. Consequently, this slight drift in spectra must be corrected in order to obtain the best energy resolution when adding all the statistics. This process is known as gain matching or alignment.

At first, we proceeded to align all the runs for each crystal. This alignment was made using the position of two peaks in the spectra with energies 158.4 and 3448.0 keV taking as a reference the run closest to the calibration source measurements. A linear gain-shift correction was used. Figure 2.9 illustrates the quality of the alignment process.

After the crystal-by-crystal alignment, we added all the statistics for each crystal in all the runs at 10 MeV and proceeded to the energy calibration.

We assumed that the gain shift that eventually could have occurred between the run taken as reference for the alignment and the measurements with calibration sources is negligible due to the small gap in time between them. This assumption was made in order to proceed with energy and efficiency calibrations.

2.2.2 Energy Calibration

The energy calibration of all the detectors was performed crystal-by-crystal, once their alignment had been carried out, as explained in the previous section.

Energy calibration was a complicated point in this thesis. In the first step, we used only ^{152}Eu as a calibration source. The ^{152}Eu provides a rich γ-ray decay spectrum with peaks between 122 and 1408 keV. The dominant γ-ray peaks were fitted. However the resulting calibration was not satisfactory at energies higher than the last calibration point at 1.4 MeV. As a second step, we decided to use the 1.1 mg/cm^2 activated ^{56}Fe target itself, i.e., the ^{56}Fe target with some amount of ^{56}Co, which decays in turn to ^{56}Fe again ($t_{1/2} = 77.236 \pm 0.026$ days), as an internal energy calibration source. We will call these ^{56}Fe γ-lines coming from the ^{56}Co decay *radioactivity lines*. The most intense radioactivity lines comprise an energy range

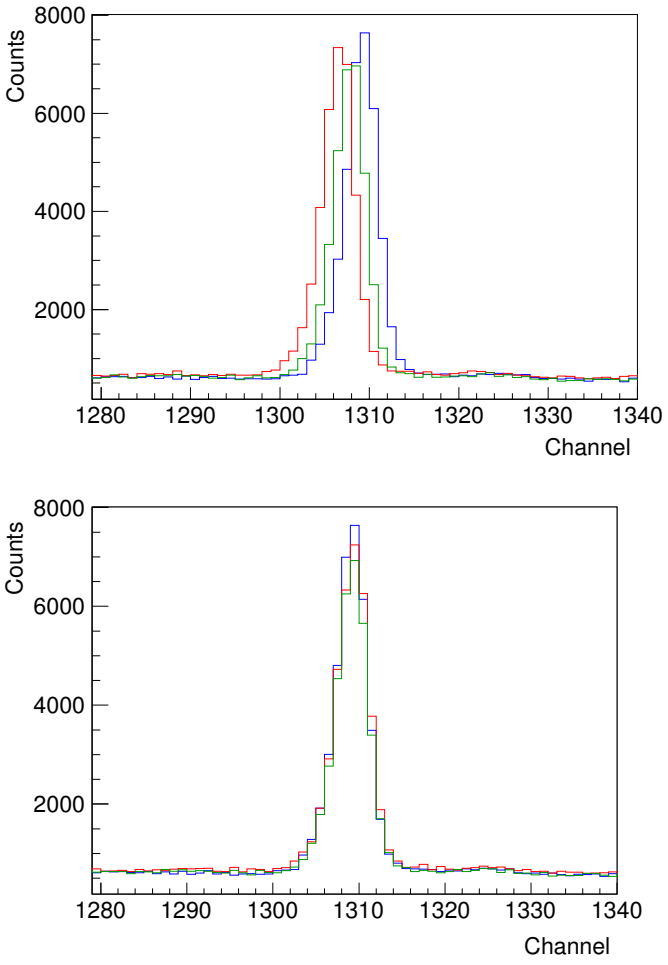

Figure 2.9: Superposition of several runs, i.e., measurements at different times, of the same crystal before (upper panel) and after (lower panel) the gain-shift correction. The quality of the alignment process can be seen.

from 846 up to 3273 keV. The calibration using only ^{56}Fe γ-lines was not satisfactory either.

Then we performed a calibration using both the ^{152}Eu source and the activated ^{56}Fe target. To improve calibration at even higher energies, we identified a peak at 6128.63 keV in the in-beam runs that we think originates from ^{16}O, and its single-escape peak (at 5617.63 keV). The ^{16}O occurs because it covers the surface of the ^{56}Fe target due to oxidation processes.

At this point it can be useful to explain the Doppler shift observed very frequently in γ-lines from our spectra. A γ-ray suffers from Doppler shift when it is emitted by an in-flight nucleus. Then, if the excited state from which the γ-transition takes place has a half-life $t_{1/2}$ shorter than the time the emitting nucleus spends to stop in the medium, the observed γ-ray will suffer from Doppler shift. On the contrary, if

the γ-ray is emitted once the nucleus is stopped, no Doppler shift will be observed. This is why the radioactivity lines will never suffer from this effect, because the emitting nucleus, ^{56}Fe, is stopped (remember: the ^{56}Co has $t_{1/2} = 77.236 \pm 0.026$ days). The Doppler shift will be used to determine the MINIBALL-detectors angles, as will be explained in detail in sec. 2.2.4.

The previously mentioned ^{16}O lines did not suffer from Doppler shifts so they were included in the calibration. The 6128.63-keV γ-transition in ^{16}O de-excites an excited state with $t_{1/2} = 18.4$ ps which is consistent with not observing any Doppler shift (see sec. 2.2.6).

The crystal-by-crystal energy calibration was performed in sections. The first section corresponds to the ^{152}Eu points up to the 778.9-keV line, where second order effects are more pronounced. Second section comprises the radioactivity lines (beginning at 846 keV) and the 6128.63-keV line in ^{16}O together with its single-escape peak. The junction point of the two sections was left as a free parameter in the fit. Continuity and differentiability were required in the joining point of the two parts. While the first section was best fitted with a second order calibration, both linear and second order calibrations were tested for the second section.

In both cases the self-consistency, i.e., the difference between the energy value from the literature and the calibration fit result, was worse around the area of the junction of the two sections. We identified this problem as an effect arising from the different counting rates between the ^{152}Eu run ($\sim 2.4 \cdot 10^3$ Hz per crystal) and the ^{56}Co radioactivity runs ($\sim$150 Hz per crystal). Counting rates of in-beam runs were similar to the former ($\sim 3.5 \cdot 10^3$ Hz per crystal).

A higher counting rate produces an underestimation of the height of the pulses. The reason is that due to the high frequency of incoming signals the preamplifier detects a new signal before the base line has recovered, with the consequent lowering of the height of the pulse. This underestimation of the pulse height corresponds to a displacement of the peak to lower energies in the spectrum. Thus the ^{56}Co radioactivity peak channels were corrected to lower values in order to obtain improved calibration fit parameters.

Final energy calibration

Finally, the best self-consistency was obtained using a second order fit in both sections. A representative example of the energy calibration of one crystal is shown in Fig. 2.10. The self-consistency, point by point, is shown in the lower panel. It can be observed that these differences are less than 0.4 keV in absolute terms.

Once calibrated in energy, we will call each of the individual-crystal energy spectra the *crystal Singles spectrum*. Analogously, the addition of the 3 *crystal Singles* spectra belonging to the same cluster will be called the *cluster Singles spectrum*.

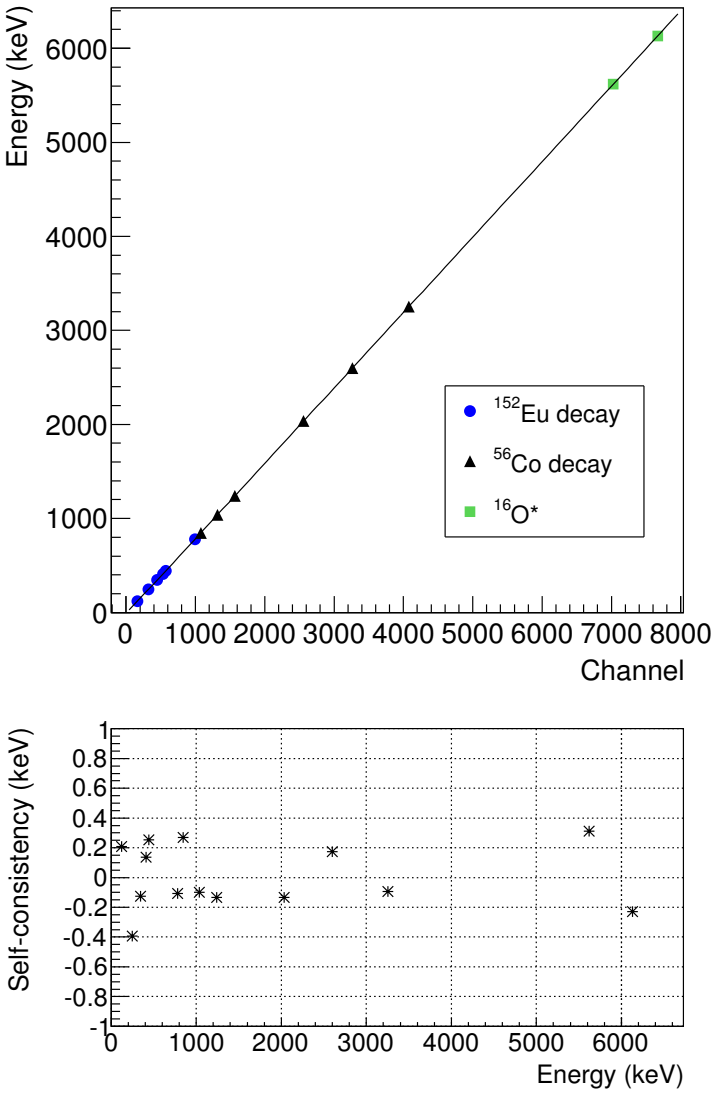

Figure 2.10: An example of the energy calibration of one single crystal is presented in the upper panel. The ^{152}Eu points, ^{56}Co radioactivity lines and the peak at 6128.63 keV from ^{16}O together with its single-escape peak were used. The calibration was carried out using a second order function fit in two sections, leaving the junction as a free parameter, set initially at 800 keV. Self-consistency, i.e., the difference between the energy value from the literature and the fit result after the calibration, is shown in the lower panel.

At that point we observed that two crystals (Cl0Cr2 and Cl0Cr2) presented undesirable features. Crystal Cl0Cr2 had unidentified contamination peaks present during most of the time of the experiment while crystal Cl1Cr2 had tails on the right side of the peaks in the spectra, probably due to instabilities in its electronics. For these reasons they were discarded and not used in the analysis.

Thus only the spectra of 10 crystals were added up. This E_γ-spectrum with all the statistics measured at 10 MeV and "all" crystals will be called the *total Singles spectrum*.

As mentioned before, the energy calibration and its self-consistency shown in Fig. 2.10 are only referred to one given crystal. In order to check the quality of the final energy calibration we proceed to calculate the deviations from the expected values in the most intense γ-lines. We used the main ^{56}Fe and ^{56}Co lines together with the γ-ray peak at 6128.63 keV in ^{16}O and its single-escape peak, in the in-beam *total Singles* spectrum, and the main ^{152}Eu lines from the calibration measurement made after the beam-time (see Fig. 2.11).

It can be seen from Fig. 2.11 that the low energy region is the critical part, with an unpredictable behaviour and higher energy deviations. Precision at low energies is especially important in order to rely on new excited state values, since most of the time these level energies are determined from the sum of consecutive de-excitations which go through the first excited states, for instance the 158.4-keV state in our case.

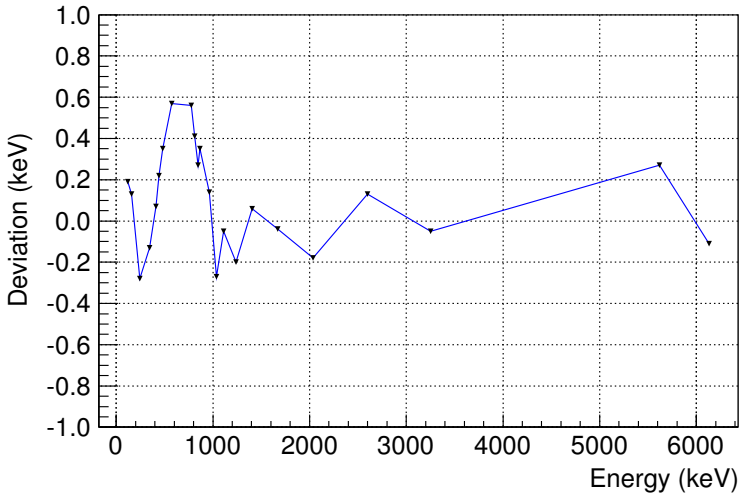

Figure 2.11: The energy deviations of several intense γ-lines after the calibration are shown in the plot. The main ^{56}Fe and ^{56}Co lines together with the peak at 6128.63 keV in ^{16}O and its single-escape peak, in the in-beam *Singles* spectrum, and the main ^{152}Eu lines from the calibration measurement made after the beam-time, were used for this checking. The line connecting points is meant to guide the eye.

We used a polynomial function of degree 6 to fit the deviations up to the 1037.8-keV peak in ^{56}Fe (see Fig. 2.12). This correction was then applied to the experimental E_γ values up to 1 MeV in order to improve the energy precision in that region. No correction was applied to higher energies. To be conservative, despite

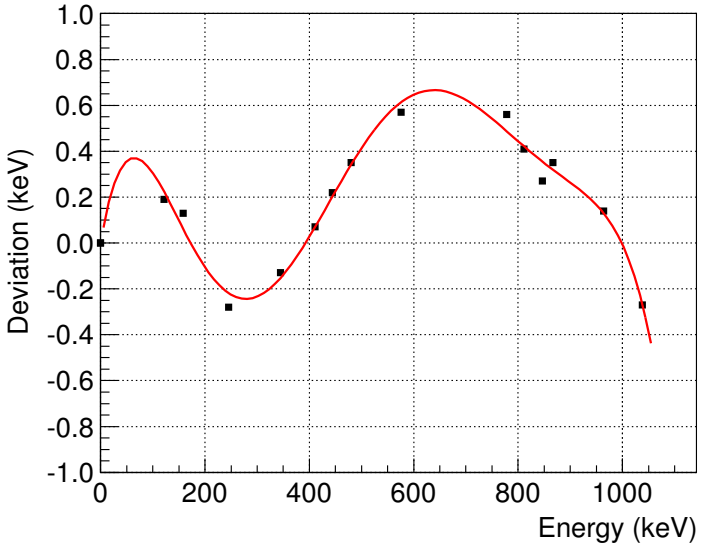

Figure 2.12: Fit of the energy deviations after calibration up to the 1037.8-keV peak in ^{56}Fe. The ^{56}Fe γ-lines used are fitted in the in-beam total *Singles* spectrum. A polynomial function of degree 6 was used. This fit was used to perform a correction to the experimental E_γ values up to 1 MeV.

the correction we decided to associate a calibration error of 0.2 keV to energies up to 1 MeV. A 0.3-keV calibration error was associated with $E_\gamma > 1$ MeV. As usual, calibration errors were quadratically added to statistical ones in order to obtain the final energy errors, as will be explained in detail in Chapter 3.

In-beam γ-spectra

To give an overall idea of the complexity of the experiment, it can be useful to look at the comparison of the E_γ-spectra of different clusters. As it was seen earlier, two clusters were located backwards with respect to the beam direction and the others two, forwards. Figure 2.13 shows the high-energy region of the four *cluster Singles* spectra. Doppler shift effects stand out in contrast with some clear lines which do not suffer from Doppler shifts. They are the 6128.63-keV peak in ^{16}O and its single-escape peak at 5617.63 keV. This is a good way to check the correction of the calibration process, made crystal-by-crystal as explained in the previous section. The quality of the energy calibration can be seen. On the other hand Doppler shift effects are very obvious. So the necessity of performing Doppler shift correction becomes evident when studying γ de-excitations from short-lived excited states. The comparison of one individual crystal (blue) and the total (red) *Singles* spectra is shown in Fig. 2.14. Remember that the latter is the sum of 10 crystals. It can be seen that the energy resolution is preserved in the summing.

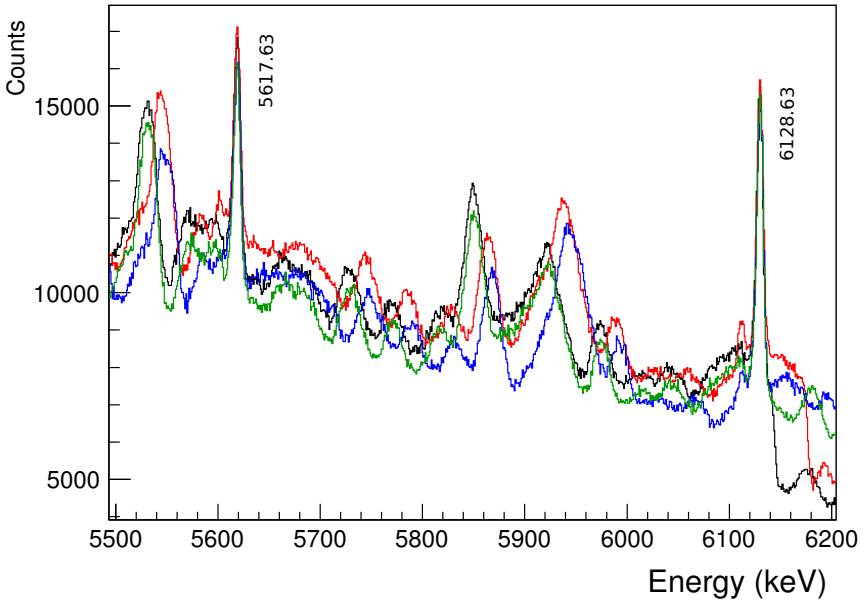

Figure 2.13: The comparison of the four *cluster Singles* spectra is shown. Doppler shift effects stand out due to the different orientation of the clusters, in contrast with the peak at 6128.63 keV from the de-excitation of ^{16}O, and its single-escape peak, which do not suffer from Doppler shift.

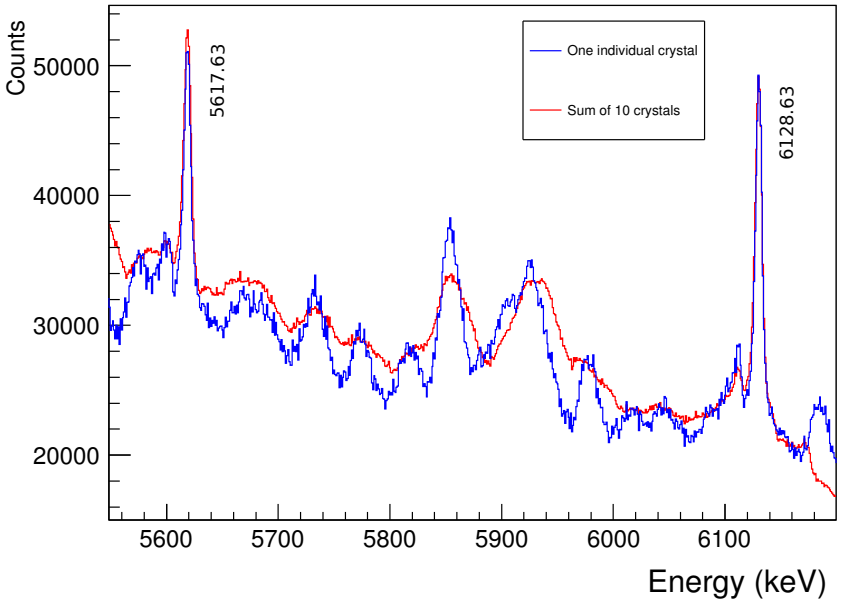

Figure 2.14: One individual crystal (blue) and the total (red) *Singles* spectra are shown. The blue spectrum is normalised to the red one. The peak at 6128.63 keV from the de-excitation of ^{16}O, together with its single-escape peak, are labelled.

2.2.3 Efficiency Calibration

A precise knowledge of the photopeak efficiency of the detection system allows one to calculate the γ-ray yields (intensities). The intensity I_γ of a certain γ-ray of energy E_γ is calculated with the following equation:

$$I_\gamma = \frac{Area}{\epsilon(E_\gamma)} \tag{2.1}$$

where $Area$ is the number of counts in the γ-ray peak and $\epsilon(E_\gamma)$ is the photopeak efficiency at the energy E_γ.

The efficiency of the Ge detectors has a strong dependence on the γ-ray energy. Thus, one has to determine the efficiency curve as a function of E_γ. The energy-dependent photopeak efficiency $\epsilon(E_\gamma)$ is defined as:

$$\epsilon(E_\gamma) = \frac{\text{Counts in the photopeak with energy } E_\gamma}{\text{Total number of emitted } \gamma\text{-rays with energy } E_\gamma} \tag{2.2}$$

The efficiency is calculated using radioactive standard sources located at the position of the target in the reaction. The peaks corresponding to the radioactive decays of the source were analysed in the following way. The counts in the photopeak were determined via a Gaussian fit to the peak and assuming a superposition of a linear function and a step function as a background model. The total number of emitted γ-rays with energy E_γ was calculated as $\text{Yield}_\gamma \cdot t_{live} \cdot Act$, where Yield_γ is the total probability of emission of the γ-ray per decay (values taken from reference [37]), the t_{live} is the time length of the calibration measurement and Act is the source activity at the time of the measurement. The magnitude t_{live} should be corrected for the dead time in order to obtain absolute efficiency values. However, the dead time could not be measured in our experiment due to some technical problems and therefore the efficiency values we will present in this work are *relative* efficiencies. The dates of fabrication of the calibration sources are taken from the specifications of the sources in order to calculate their activities.

The efficiency values were calculated for the strongest photopeaks for each source. As efficiency calibration sources, we used ^{152}Eu (DW540 Amersham) [38], ^{133}Ba (LU838 Amersham) [39] and ^{60}Co (PTB number 418-81) [40] standard sources and the activated ^{56}Fe target itself, i.e., ^{56}Co decay source. After the end of the beam-time, the sources were mounted at the target position. The activities of each standard source were 142 ± 5 kBq, 227 ± 7 kBq and 201 ± 2 Bq, respectively, at the time of the measurement. Nevertheless, the ^{56}Co decay source activity was unknown.

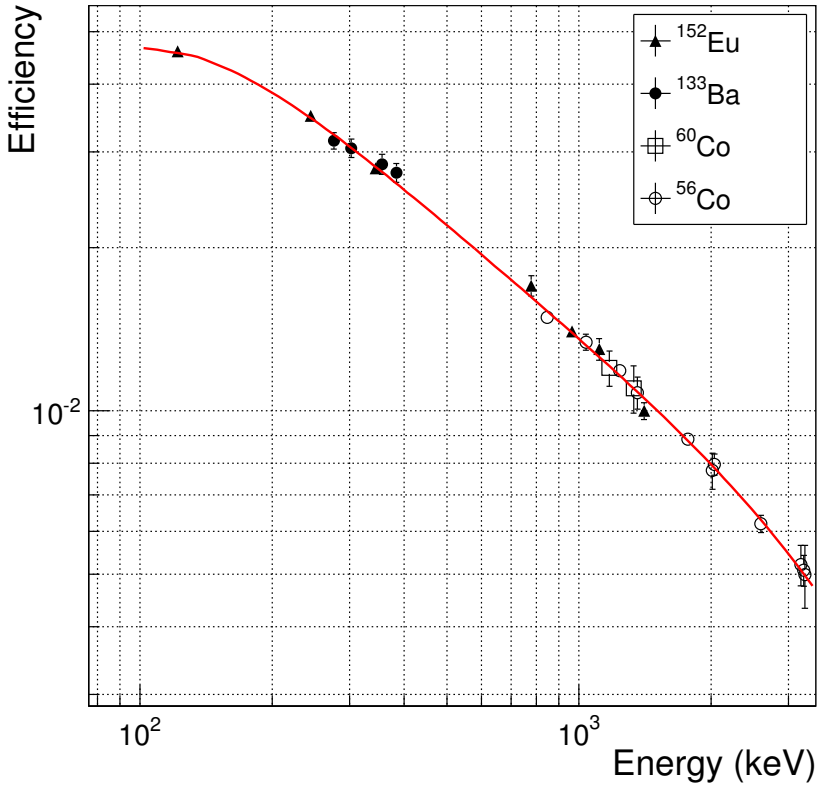

Figure 2.15: Relative efficiency curve of the detection system. The experimental points with their error bars are fitted with the *Jäckel* function as a continuous curve.

The fit to the experimental points was made with the function proposed by Jäckel et al. [41] for the Ge detectors:

$$ln\epsilon(E_\gamma) + 25 = (b_1 + b_2 x + b_3 x^2)\frac{2}{\pi}\arctan(exp(b_4 + b_5 x + b_6 x^2)) \qquad (2.3)$$

where $x = lnE_\gamma$.

At first, we used only the ^{152}Eu, ^{133}Ba and ^{60}Co sources to calculate the efficiency curve. However, some disagreement between the three sets of points was observed: taking as a reference the best fit of the ^{152}Eu points, we observed displacements of ^{133}Ba and ^{60}Co with respect to that fit of around 4%, which agreed with the nominal error in the activity of the sources.

Then points from ^{133}Ba and ^{60}Co were displaced to the curve determined by the ^{152}Eu points, and a new fit was made. Finally the set of points from the ^{56}Co radioactivity had to be displaced to the curve determined by the remainder of the

points, in order to calculate the relative photopeak efficiency curve at higher energies. Once it was done, a new fit was made to the full set of points.

Figure 2.15 shows the relative photopeak efficiency curve of the detection system. Error bars take into account the uncertainty in the source activities and the statistical error of the photopeak areas. The 80.99-keV peak from the ^{133}Ba source was not included in the fit because it reduced its quality and we did not need that low energy range. In order to take into account the effect on the final fit parameters of the displacement applied to the ^{56}Co relative efficiency values we estimated a 3% error with the calculated efficiency values for energies up to 3.5 MeV, and a 5% error with higher values.

2.2.4 Determination of the MINIBALL θ-angles

After the energy calibration of the MINIBALL detectors, the determination of their angles relative to the beam direction was essential to allow an accurate Doppler correction. For this purpose a calibration reaction was performed in inverse kinematics. The reaction used was the transfer reaction d(^{32}S,pγ)^{33}S. The main idea of this method is to obtain the detector angles that best describe the Doppler shift of well known γ-rays emitted in flight, i.e., with a short enough $t_{1/2}$, by the ejectile.

The Doppler-corrected energy E_{rest} of the detected γ-ray with E_{lab} is given by the expression:

$$E_{rest} = \frac{E_{lab}}{\sqrt{1-\beta^2}}(1 - \beta\cos\alpha) \tag{2.4}$$

where α is the angle between the ejectile emitting the γ-ray (the ^{33}S nucleus in this case) and the γ-ray itself and $\beta = v/c$ is related to the ejectile velocity v. The MINIBALL detectors are defined by their azimuthal (ϕ) and polar (θ) angles, defined with respect to the beam along the z-axis (see Fig. 2.16). Then, the α angle can be defined as a function of the ϕ and θ angles of the ejectile and the γ-ray as follows:

$$\cos\alpha = \sin\theta_\gamma \sin\theta_{eject} \cos(\phi_{eject} - \phi_\gamma) + \cos\theta_{eject}\cos\theta_\gamma \tag{2.5}$$

We used a high intensity, stable ^{32}S beam of 75 MeV energy which impinged on a deuterated Ti target (dTi) of $\Delta\xi = 0.5$ mg/cm^2 thickness, equivalent to $\Delta x = 1.106$ μm. The ^{32}S can undergo several reactions with the deuterium d of the target. The transfer channel with the highest cross section and its most dominant γ-ray are d(^{32}S,p)^{33}S with an 840.9-keV line. This γ-ray de-excites the low-lying state in ^{33}S of the same energy with $t_{1/2} = 1.15$ ps.

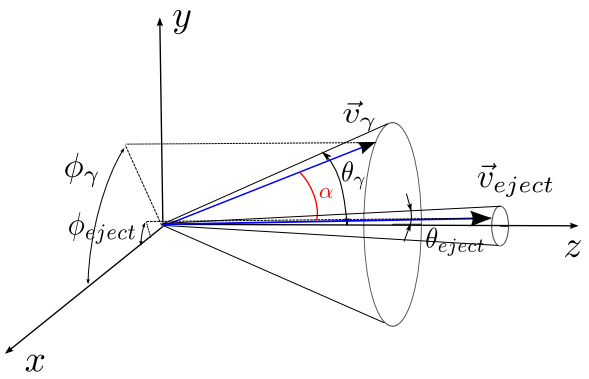

Figure 2.16: The azimuthal (ϕ) and polar (θ) angles, defined with respect to the beam along the z-axis, of the ejectile emitting the γ-ray (the ^{33}S nucleus) and the γ-ray itself. The α is the angle between the ejectile and the γ-ray.

Due to the features of the reaction in inverse kinematics, the ejectile (^{33}S) has small opening angles θ_{eject} with respect to the beam. Thus, it can be assumed to good approximation that $\theta_{eject} \simeq 0$, with the corresponding simplification of Eq. 2.5 giving $\cos\alpha = cos\theta_\gamma$. Then, for the present work the equation 2.4 can be rewritten as:

$$E_{rest} = \frac{E_{lab}}{\sqrt{1-\beta^2}}(1 - \beta\cos\theta_\gamma) \tag{2.6}$$

By means of the SRIM (The Stopping and Range of Ions in Matter) software [42] and the relativistic kinematics programme Catkin [43], we calculated the energy losses of the projectile and ejectile while passing through the target. Assuming that the reaction takes place in the middle of the target ($\Delta\xi = 0.25$ mg/cm^2) the beam energy at that point is $E_{^{32}S} = 71.8$ MeV and the corresponding ^{33}S ejectile produced has energy values $E_{^{33}S} = 74.976$ MeV (at mid target) and $E_{^{33}S} = 71.8$ MeV (at the end of the target). Their corresponding beta values are $\beta = 0.0697$ and $\beta = 0.0682$, respectively.

Knowing E_{rest} (literature) and E_{lab} (present measurement), from Eq. 2.6 one can deduce the θ_γ with respect to the beam direction, which is equivalent to the θ for each detector. Table 2.1 shows MINIBALL detector angles obtained using the d(^{32}S,p)^{33}S reaction. We present θ average values using the two slightly different β values obtained as explained in the previous paragraph.

Figure 2.17 shows the γ-spectra measured from one forward and one backward crystal. Apart from the intense 840.9-keV γ-ray from the d(^{32}S,pγ)^{33}S reaction (in pink), many other γ-transitions from other reactions were identified in the spec-

Table 2.1: MINIBALL-crystal θ angles.

Crystal	$\theta(^\circ) \pm 1.5^\circ$
Cl0Cr0	101.0
Cl0Cr1	125.3
Cl0Cr2	127.3
Cl1Cr0	43.0
Cl1Cr1	66.3
Cl1Cr2	69.7
Cl2Cr0	41.8
Cl2Cr1	45.9
Cl2Cr2	61.4
Cl3Cr0	116.0
Cl3Cr1	101.9
Cl3Cr2	128.9

tra. The most dominant ones were identified as lines coming from the fusion-evaporation reaction ^{16}O(^{32}S,2pγ)^{46}Ti (in orange). Some other γ-transitions from the fusion-evaporation reaction ^{16}O(^{32}S,npγ)^{46}V and from the inelastic scattering ^{48}Ti(^{32}S,^{32}Sγ)^{48}Ti were also identified (^{48}Ti is the main component of natural Ti with 73.7% abundance). The 801.5-keV γ-ray from the former and the 983.5-keV γ-ray from the latter are labelled in Fig. 2.17. These lines do not suffer from Doppler shifts and are a good indication of the correct alignment of the different crystals.

The reaction ^{16}O(^{32}S,2pγ)^{46}Ti is not strictly an inverse-kinematics type and the ejectile emerging cone of $\theta_{eject} \simeq 0^\circ$ approximation is not really valid. This fact would lower the energy resolution of the peak, but anyhow these γ-lines can be used as a useful cross-check of our determination using the 840.9-keV γ-ray. Moreover, in some crystals in which this Doppler-shifted 840.9-keV γ-line was superposed on the 801.5-keV peak or had a shape difficult to fit, the 889.3-keV γ-ray from the ^{16}O(^{32}S,2pγ)^{46}Ti reaction was used for the angle determination instead. Two other intense γ-lines at 1120.5 and 1289.1 keV from the same reaction were used as cross-checks, and gave compatible values.

2.2.5 Doppler-shift correction of the in-beam γ-spectra

As explained earlier, there exists a dependence of the Doppler shift with the θ angle and the β parameter of the γ-emitting nucleus (see Eq. 2.4). Then, the next step after the determination of the MINIBALL θ-angles is the determination of the recoiling ^{56}Co velocity, in order to obtain the β. However, the β determination was not trivial, as we will see in the following discussion.

Once the detector θ-angles and the β of the emitting nucleus are estimated, the

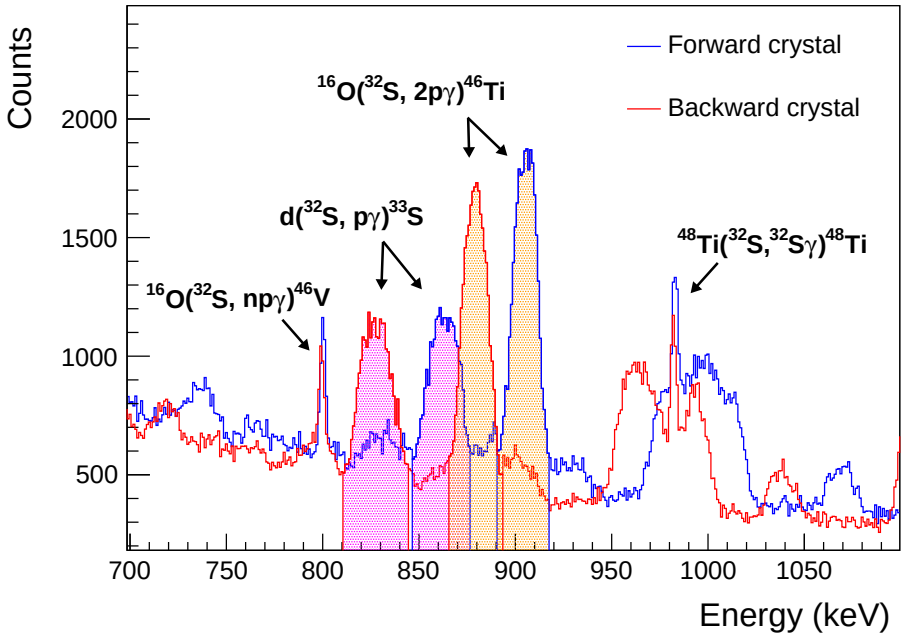

Figure 2.17: The comparison of the γ-spectra from one forward and one backward crystal from the angle calibration reaction is presented. Several γ-transitions from different reactions were identified: the 840.9-keV peak from the d(^{32}S,pγ)^{33}Si reaction (pink dashed area) and the 889.3-keV line from the ^{16}O(^{32}S, 2pγ)^{46}Ti reaction (orange dashed area) are shown. The Doppler shifts are clearly observed. The 801.5-keV γ-ray coming from the ^{16}O(^{32}S,npγ)^{46}V reaction and the 983.5-keV γ-ray from the ^{48}Ti(^{32}S, γ)^{48}Ti reaction, are also indicated in the spectra. See main text for details.

corrected E_{rest} will be obtained from Eq. 2.4. After the correction is made, the optimum way to check the Doppler shift correction in the E_γ-spectra is done testing the ^{56}Co peaks in E_γ-spectra that are emitted in flight and suffer from Doppler shifts. Comparing the energies of these γ-rays in the forward and backward clusters they should have the same energy. High energy transitions have a greater sensitivity to this checking because the Doppler shifts are larger at these energies. However, our E_γ-spectra showed very intense ^{56}Fe transitions in the high-energy region, but no known ^{56}Co ones. In order to use ^{56}Fe peaks for this correction we had to make sure that the recoiling ^{56}Fe kinetic energy distribution was similar to the ^{56}Co one. Due to the similar mass and charge of both ^{56}Fe and ^{56}Co nuclei, one would expect similar kinematics for the recoil, i.e., similar β values. This is the reason why it was important to study the energy distribution of the recoiling ^{56}Fe. In the next section we will estimate the β values of both ^{56}Co and ^{56}Fe after the reaction using TALYS.

The β determination using TALYS and SRIM calculations

The study of the (p,p') and (p,n) channels is essential for the interpretation of the different γ-emission spectra. The TALYS software [32] was used to study the different channels of the p + ^{56}Fe reaction and determine the recoil-energy spectra of both the ^{56}Co and ^{56}Fe nuclei (see the Appendix C for a more detailed study). Calculations with the SRIM software showed that protons lose very little energy while passing through the target, i.e., an incident proton of $E_p = 10$ MeV arrives at the final target edge with $E_p = 9.97$ MeV. Thus for simplicity we will assume that the p + ^{56}Fe reaction always take place at 10-MeV proton-beam energy.

For each channel, one has a spread in the kinetic energy of the recoil (E_{recoil}). Looking at Fig. 2.18 we see that the two kinetic-energy distributions are quite different, especially at low energies. These distributions are studied in detail in Appendix C. In the ^{56}Co recoil case, this distribution has a maximum cross-section at $E_{recoil} = 0.166$ MeV (see left panel of Fig. 2.18). This E_{recoil} is equivalent to a value of $\beta = 0.0025$ ($v = 0.076$ cm/ns).

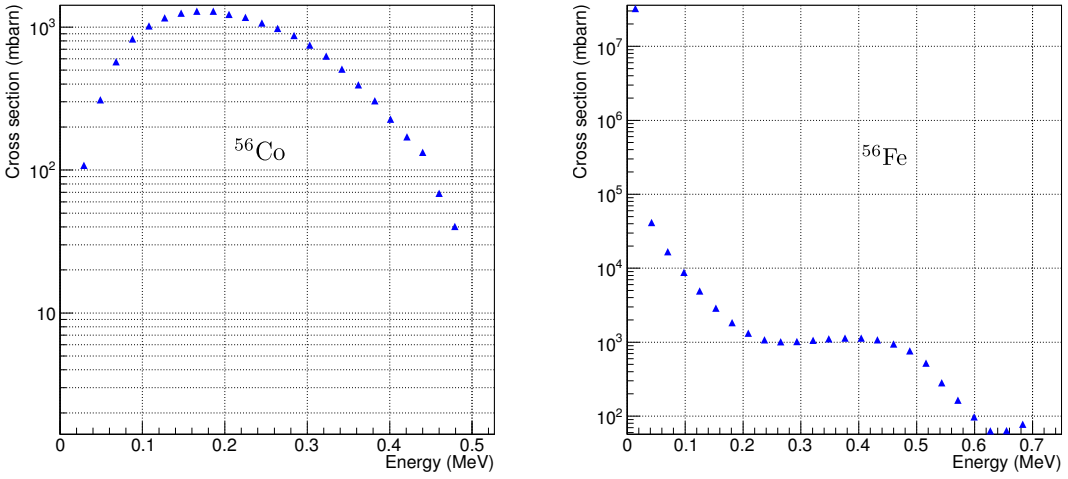

Figure 2.18: The kinetic-energy distributions of the recoiling ^{56}Co (left) and ^{56}Fe (right) following the p + ^{56}Fe reaction at $E_p = 10$ MeV, calculated with the TALYS software.

The kinetic-energy distribution of the recoiling ^{56}Fe is more complicated (see right panel of Fig. 2.18). It is strongly peaked at low energies and has a hump around 0.4 MeV. Taking extreme values of the energy range, $E_{recoil} = 0.05$ MeV would imply $\beta = 0.0014$, while $E_{recoil} = 0.5$ MeV is equivalent to $\beta = 0.0044$.

As one can see, the initial assumption that the velocities of the recoiling ^{56}Co and ^{56}Fe were very similar was not correct. The ^{56}Fe nucleus will have more or less

velocity depending on whether it has been produced either in a compound nucleus reaction (fusion-evaporation) or in a direct reaction. It will also depend on which excited state is populated after the reaction.

Thus the theoretical determination of the β value was very complex and finally we had to proceed with an empirical determination. Even though we concluded that we have a spread of β values in the recoiling ^{56}Co and ^{56}Fe and the comparison between them can be very complex, we proceeded with the checking of the Doppler correction using ^{56}Fe peaks at high energies. We also used a known ^{56}Co peak (at 1625.2 keV), the only clean case and at high enough energy which suffers from the Doppler shift.

Thus, we chose the peaks at 3448 and 3548 keV, coming mainly from the γ-de-excitation of the 3448.41-keV ($t_{1/2} = 8 \pm 3$ fs) and 4394.3-keV ($t_{1/2} = 35 \pm 17$ fs) excited states, respectively, in ^{56}Fe, to check the β value validity chosen for the Doppler shift correction. Figure 2.19 shows both peaks in the x-projection of the γ-γ coincidence matrix (for forward and backward clusters) before and after the Doppler shift correction (see later in section 2.3.1 about the γ-γ coincidence matrices construction). The correction was made using $\beta = 0.0017$, for which we obtained the best superposition in both the 3448- and 3548-keV peaks.

These coincidence matrices are constructed only with coincident γ-rays between crystals of either forward clusters or backward clusters, respectively. Forward clusters (in blue) and backward clusters (in red) are compared in each plot. The quality of the correction can be observed. As one can see this β value is lower than the estimates obtained with TALYS, but it is at least of the same order-of-magnitude.

As previously said, the only good case to check the Doppler shift correction in ^{56}Co transitions, clean and at energy high enough to see clearly the shift, is the 1625.2-keV γ-ray from the de-excitation of the 3075.7-keV level ($t_{1/2} = 22 + 8 - 6$ fs). Figure 2.20 shows again the x-projection of the γ-γ coincidence matrix before (upper panel) and after (lower panel) Doppler shift correction using $\beta = 0.0017$. Again the quality of the correction can be seen. In the same plot a peak at 1670.8 keV is observed. This peak comes mainly from the de-excitation of the 3755.6-keV excited state in ^{56}Fe ($t_{1/2} = 130 \pm 20$ fs) from the (p,p') inelastic scattering process. It can be observed that this peak is well aligned before the correction, because it is emitted once the recoiling ^{56}Fe is already stopped.

2.2.6 Half-life estimate for ^{56}Co excited states

An average range $\bar{r} = 0.0545$ μm of the recoiling nucleus ^{56}Co of $E_{recoil} = 0.166$ MeV in the ^{56}Fe target is obtained using the SRIM package. This value represents only 5% of the target width (Note: $\Delta x = 1.106$ μm). This means that the ^{56}Co recoils are practically all stopped inside the target. Assuming that the ^{56}Co recoil energy is constant during this average range (which is not true), it would take 72 fs

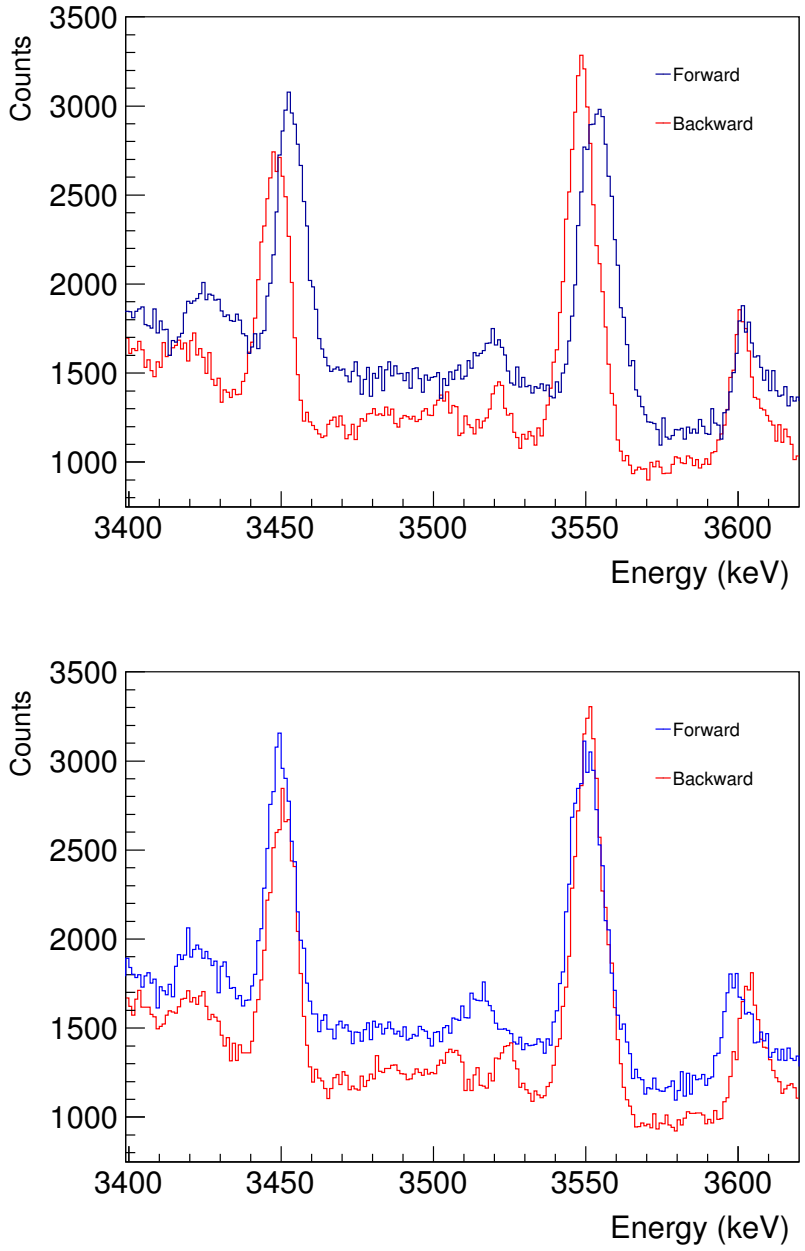

Figure 2.19: Peaks at 3448 and 3548 keV (coming mainly from the γ-de-excitation of the 3448.41-keV ($t_{1/2} = 8 \pm 3$ fs) and 4394.3-keV ($t_{1/2} = 35 \pm 17$ fs) excited states, respectively, of ^{56}Fe) in the x-projection of the γ-γ coincidence matrix (for forward and backward clusters) before (upper panel) and after (lower panel) the Doppler shift correction using $\beta = 0.0017$.

until it is completely stopped. Thus we can get an estimated maximum threshold for the $t_{1/2}$ that a ^{56}Co excited state must have in order to observe Doppler shift in its γ-de-excitations, which is the previous value: 72 fs. Higher $t_{1/2}$ values would imply that the γ-rays are emitted from a nucleus which is at rest. Actually the

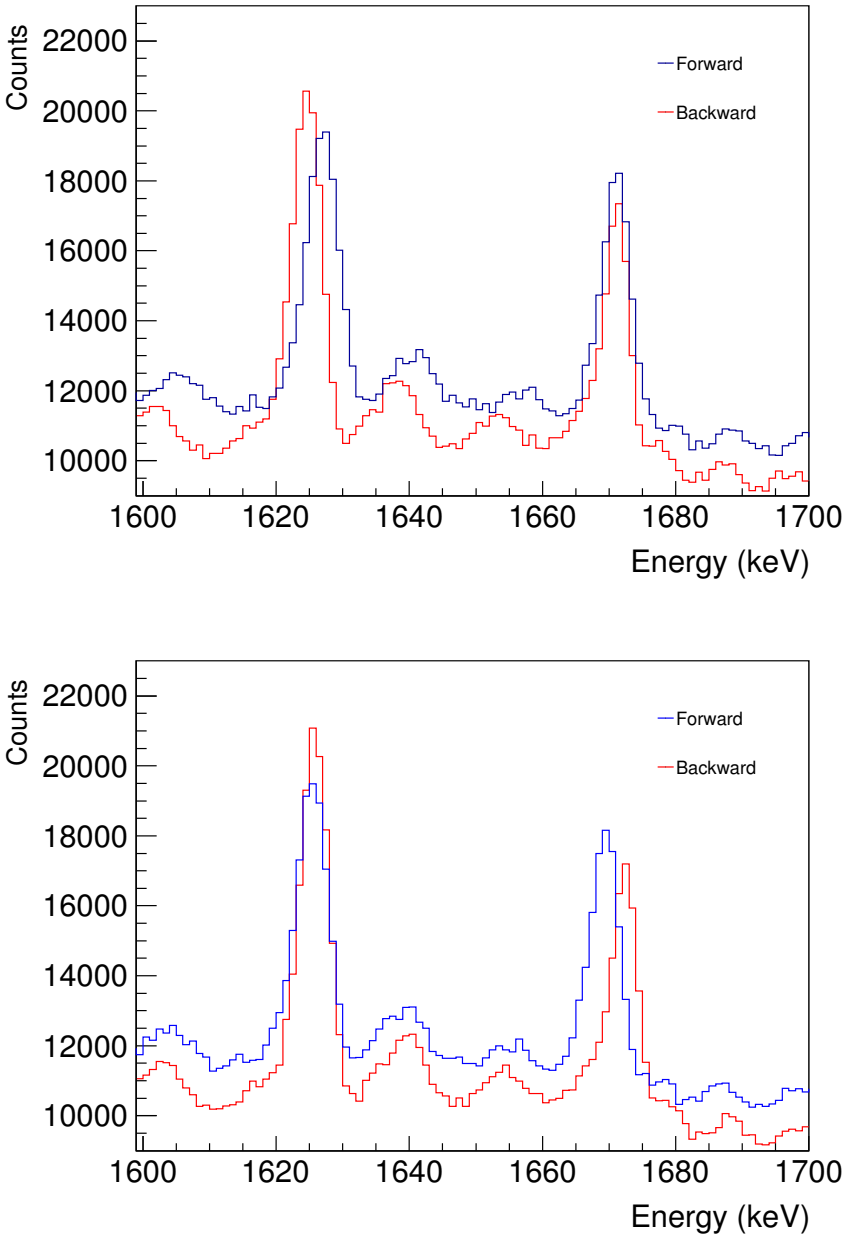

Figure 2.20: Peak at 1625.2 keV from the de-excitation of the 3075.7-keV level ($t_{1/2} = 22 + 8 - 6$ fs) in ^{56}Co in the x-projection of the γ-γ coincidence matrix before (upper panel) and after (lower panel) the Doppler shift correction using $\beta = 0.0017$. The 1670.8-keV peak, coming mainly from the de-excitation of the 3755.6-keV excited state in ^{56}Fe ($t_{1/2} = 130 \pm 20$ fs), is also observed. This line, contrary to the 1625.2-keV peak, does not suffer from the Doppler shift (see main text).

recoil spends a slightly higher time until stopping, because its velocity is smoothly decreasing until it becomes zero. This can be used in the opposite sense: if one

observe a Doppler shift for a γ-transition of ^{56}Co then we can rest assured that the excited state from which the γ-decay is emitted has $t_{1/2} \leq 72$ fs, and vice versa.

2.3 The analysis procedure

In the following section the procedure followed in the analysis of the experimental data will be described. The construction of several two-dimensional γ-γ coincidence matrices in order to establish the complex level scheme of ^{56}Co and determine the γ-transition intensities I_γ is explained. We will also describe how are they used to obtain the angular distributions of the γ-ray transitions.

2.3.1 Matrices

In the sorting procedure the calibrated data can be re-arranged in one-, two- or three-dimensional histograms, i.e., single histograms, matrices and cubes, respectively.

As explained in Chapter 1, γ-γ coincidence measurements are needed for different purposes. Thus the construction of γ-γ coincidence matrices is required. These matrices have to be made off-line, with subroutines that decode the event structure and construct the 2D-histograms with the desired conditions. In order to look for the coincidences, some time condition has to be set to decide when two γ-rays are "coincident", which is called the *coincidence window*. This condition is established making use of the time stamps (t.s.). The statistics were not sufficient to build reasonable three-dimensional γ-γ-γ coincidences matrices. This is partially due to the low multiplicity of the γ-cascades.

As detailed in section 2.1.5, every time a cluster fires, its ADC assigns a time stamp to that signal and opens a 10 μs gate. This implies that one cluster can detect two γ-rays separated by that temporal gap but recorded by the DAQ system as having the same "time" (i.e., same time stamp). Besides, the event builder groups clusters that have fired within a coincidence window of 100 t.s. (i.e., 6.25 μs) (see sec. 2.1.6). This means that the real time difference between two γ-rays belonging to the same event but detected by different clusters can be as big as 16.25 μs (See Fig. 2.8); actually one should also add the resolution of the time stamp itself (62.5 ns) to that difference. This enormous time difference can be a problem when constructing the γ-γ coincidence matrix, because it will introduce many "false" coincidence transitions (random coincidences), i.e., signals that satisfy the "coincidence" condition but do not have physical meaning. To reduce this effect, in the analysis we asked for crystal multiplicity equal to 1 in each cluster (i.e., only one crystal firing per cluster). This condition will imply that demanding that two clusters have the same time stamp will mean that the two γ-rays from those clusters are separated at most by 62.5 ns. Sorting event-by-event, one takes one γ-ray detected in one cluster and look for any other γ-ray detected by a different

cluster. After several tests with different time conditions we imposed that the time difference between both γ-rays, in absolute terms, was equal to or smaller than 2 time stamps, i.e., $\mid t_{diff} \mid \leq 2$ t.s. This *coincidence window* implies that the two γ-rays can be separated at most by 312.5 ns. This condition instead of the *same* time stamp condition was preferred because the statistics improved by almost a factor of 3 with respect to the latter and the ratio between real and random coincidences does not change significantly. In order to perform background subtraction, signals with time condition such that 20 t.s $< \mid t_{diff} \mid \leq 40$ t.s were subtracted from the real coincidences matrix, weighted as a function of the time condition width (i.e., 5/40 t.s.).

γ-γ coincidence matrices variety

Different γ-γ coincidence matrices were built fulfilling different requirements: one *total*, one *forward*, one *backward* and 12 *conditioned* γ-γ coincidence matrices. A summary is provided in Table 2.2.

In the cases of the *total*, *forward* and *backward* γ-γ coincidence matrices, Doppler shift corrected (DC) versions were also built. Forward detectors are those belonging to clusters 1 and 2; backward detectors, those from clusters 0 and 3 (see Fig. 2.4). They were used in the level scheme construction (see the next section).

Conditioned γ-γ coincidence matrices of one detector at a particular angle versus all the others were used to obtain the angular distributions of γ-transitions (12 detector angles were studied, see sec. 2.3.3). (Due to the fact that the main purpose here was getting statistics and not precise peak centroids, Doppler shift corrected versions were not constructed for these matrices.)

2.3.2 Level scheme and Intensities

As mentioned above, a two-dimensional γ-γ coincidence matrix is needed in order to construct the level scheme of ^{56}Co, since the determination of coincidence relationships between γ-ray transitions forms the basis for their placement in it.

After building up the γ-γ coincidence matrix with the desired conditions, the appropriate tools of γ-spectroscopy analysis were used to extract the information. As a first step, x and y projections of the 2D-matrix were obtained. Because we made symmetrical matrices, both projections are identical. Secondly, the Tv package [44], a γ-spectroscopy analysis tool developed at the Institut für Kernphysik (Nuclear Physics Institute) of Universität zu Köln, was used to look for γ-transition sequences.

The procedure is the following: one selects a certain region of the 1D-projection (x or y), and as many background regions as one desires. This combination of regions

Table 2.2: Different γ-γ coincidence matrices constructed in the data sorting. In all cases coincidences were restricted to be between detectors in different clusters. By forward detectors we mean detectors in clusters 1 and 2; by backward detectors, those in clusters 0 and 3.

Total γ-γ coincidence matrix
(10 detectors)$\otimes$(10 detectors) 1 matrix
Forward-Backward γ-γ coincidence matrices
(Forward detectors)$\otimes$(Forward detectors) 1 matrix (Backward detectors)$\otimes$(Backward detectors) 1 matrix
Conditioned γ-γ coincidence matrices
(one detector)$\otimes$(the other detectors) 12 matrices

is called *gate*. Afterwards one obtains the "gated" spectrum, i.e., the spectrum of all γ-rays detected in *coincidence* with the selected main region after background subtraction. If we observe a peak in this spectrum we can say that the gating transition and the transition corresponding to this peak are in coincidence. However, one must ensure that the coincidence is real, i.e., the coincidence is true also in the reverse direction. For that, a new gate in the candidate transition is set. The comparison of the projections of Doppler shift corrected (DC) and non DC *total* γ-γ coincidence matrices, as well as the comparison of the projections of the *forward* and *backward* matrices, were used to determine whether a γ-transition suffers from Doppler shift or not. For most of the transitions, which are not intense enough to be observed in the projections or are obscured by a stronger transition, this comparison was made looking at the "gated" spectra. When we conclude that a particular γ-ray *is* Doppler shifted, the DC *total* γ-γ coincidence matrix is used to determine both the energy value and the intensity of the transition. In the opposite case, the non Doppler-corrected version is used.

Low energy γ-rays are a special case. They are located in the region most strongly affected by the Compton background (see sec. 2.3.4 for the explanation). For these

transitions one has to look for, if possible, a gate in which the peak is not distorted by the characteristic hollows produced by the Compton scattering.

The previous procedure allowed us to check the level scheme known from previous work and to place most of the new transitions observed in ^{56}Co. Sometimes intensity arguments were used to decide the gamma de-excitation sequence. We will present the complex level scheme obtained in this work in Chapter 3.

The complexity of the level scheme of ^{56}Co required a careful combination of methods in order to deduce the γ-transition intensities, I_γ. The areas of the peaks have to be corrected by the corresponding photopeak efficiency value in order to deduce the intensity (see sec. 2.2.3). Whenever possible, these areas are extracted directly from the total *Singles* spectra. The Doppler- or non Doppler-corrected *Singles* spectrum is used according to whether the half-life value of the level from which the γ-ray originates is higher or lower than 72 fs. This threshold was obtained using the TALYS and SRIM software, as explained in sections 2.2.5 and 2.2.6.

The areas of weak transitions or members of unresolved multiplets have been extracted from the γ-γ matrices. In the majority of cases, the areas are obtained using a gate set on a transition de-exciting the level fed by the γ-ray of interest. Whenever possible, the one with the largest statistics in the projection is used. If the γ-transition under study has a γ-ray of similar energy in coincidence with this gate, another gate is used. The γ-intensities obtained in this way are proportional to the intensities in the total *Singles* spectrum but require a normalisation. Thus, for a given gate, all intensities from the γ-transitions in coincidence are normalised to one of them for which the intensity could be determined in the *Singles* spectrum. We will call these values *normalised* intensities.

All the intensities were normalised so that $I_{158\,keV} = 100$. The γ-transition at 158 keV is the most intense line observed in the de-excitation of ^{56}Co and corresponds to the de-excitation from the first excited state to the ground state (see later).

When neither direct extraction from the *Singles* spectrum nor extraction from a gate from a transition below in the γ-γ matrices are possible, a gate on a transition feeding the de-exciting level is used and the intensities are extracted from the branching ratios. Again one has to know the intensity in the *Singles* spectrum of at least one of the peaks de-exciting the level in order to scale the others to it.

In a few cases, none of the previous methods was available and the I_γ of the transition could not be obtained or only a relative value within the gate was determined.

In order to obtain the level energies and intensity balance of the level scheme, the *Eleven* code was used [45]. The code is explained in detail in Appendix D and summarised in the following lines. The input consists of the level scheme and the E_γ and I_γ of the transitions. On one hand, *Eleven* provides the optimal level energies, E_{level}, based on the experimental γ-ray energies, E_γ. On the other hand, the intensity balance is made calculating the difference between the intensity de-exciting and

feeding each level from upper levels. This is done level by level. This difference corresponds to the direct feeding to a certain excited state in the reaction and cannot be negative. This condition was always checked and, as said earlier, it was taken into consideration to place new γ-rays in the level scheme and check the intensity balance.

Internal conversion (IC) is possible whenever gamma decay is possible, except in the case where the atom is fully ionised. However it is favoured whenever the energy available for a gamma transition is small, and it is also the primary mode of decay for $0^+ \rightarrow 0^+$ transitions, where the de-excitation cannot take place by emitting a γ-ray since it would violate conservation of angular momentum. The competition between internal conversion and gamma decay is quantified in the form of the *internal conversion coefficient* which is defined as $\alpha_{\mathrm{TOT}} = I_e/I_\gamma$, where I_e is the rate of conversion electrons and I_γ is the rate of gamma-ray emission observed in the decay of an excited state.

The internal conversion coefficient has to be taken into account in order to obtain a correct intensity balance. In the present experiment conversion electrons were not measured and the α_{TOT} values were obtained from [46]. For mixed multipolarity transitions, the mixing parameter δ (see sec. 1.6.2 for definition) was needed to calculate α_{TOT}. The δ values were taken from [47].

2.3.3 Angular Distributions of γ-transitions

One can obtain the angular distribution of a certain γ-transition by measuring its intensity at different angles with respect to the beam direction. The intensity of the γ-ray is obtained from the area of the photopeak in the γ-spectrum for the specific angle, after correction for the detector efficiency.

In principle, the intensities of the γ-transitions are determined in the *Singles* spectrum, angle by angle. However, in order to allow weak transitions or members of unresolved multiplets to be investigated, one can study the γ-γ coincidence measurements in a particular way. In the present work we built up γ-γ coincidences matrices for one detector at a particular angle versus all the others. We called them *conditioned* γ-γ coincidence matrices (see sec. 2.3.1).

We sorted a group of twelve matrices corresponding to the twelve detector angles. These matrices were filled with the coincidences cases between one γ-ray detected at a specific angle (i.e., by a detector located at this angle) with any γ-ray detected at any other angle (i.e., any other detector), fulfilling the condition that belongs to a different cluster. Afterwards, by selecting a gate in the axis corresponding to these *other* detectors (E_{all}-axis) we obtained the gated γ-spectrum at a certain angle. Then the photopeak of interest was fitted in the spectrum.

The photopeak area had to be corrected by the respective detector efficiencies (both

the intrinsic and the geometrical ones). As we mentioned earlier, MINIBALL detectors were positioned at slightly different distances and therefore the geometrical correction factors are different. These factors can be estimated by using a known γ-transition with known angular distribution. In our case we deduced these values using the 480.5-keV γ-ray angular distribution, which should be flat because it de-excites a 0^+ level and hence has no angular distribution. We followed this procedure on the assumption that the shape of the individual efficiency curves of all the detectors was very similar.

In the following section we will explain the procedure used to normalise all the angular distributions studied.

Normalization to the 480.5 keV γ-ray angular distribution

When studying the 480.5 keV γ-ray distribution as a function of the θ angle, we observed that its shape depends on the gate choice. This was partially due to the fact that the assumption about the similarity of the efficiency-curve shapes might not be totally correct. Therefore, we used four different gates (peaks at 158.4, 811.9, 269.4 and 1184.6 keV) and normalised each of the distributions to the 811.9-keV one. We chose that gate due to its good statistics and cleanliness. To do that we looked for the factor f which minimized the following χ^2 function:

$$\chi^2 = \sum_i \frac{(A_i - fB_i)^2}{\sigma_{A_i}^2 + \sigma_{B_i}^2} \tag{2.7}$$

where $i = 1, ..., 12$ is the crystal index and:

- $A_i \equiv$ Photopeak area detected in crystal i obtained with gate 811.9 keV
- $B_i \equiv$ Photopeak area detected in crystal i obtained with another of the 3 gates

All individual points have associated statistical errors. Once the optimum factor was applied to one distribution,

$$\tilde{B}_i = fB_i \tag{2.8}$$

the new values had an associated error equal to the quadratic sum of the statistical error and the error associated with the factor itself σ_f:

$$\sigma_{\tilde{B}_i} = \sqrt{\left(\frac{\sigma_f}{f}\right)^2 + \left(\frac{\sigma_{B_i}}{B_i}\right)^2} \cdot \tilde{B}_i \tag{2.9}$$

Then we calculated the weighted average of the four values at each angle. These final values represent the *average* angular distribution of the 480.5-keV γ-transition

and were normalised to 1. From this process we extracted the geometrical factors to correct the other angular distributions studied.

Once corrected by their geometrical factor, all the angular distributions were normalised to 1 at 102.1° (which corresponds to the detector Cl3Cr1).

Finally, the angular distributions $W(\theta_\gamma)$ were fitted to the expression given in Chapter 1.6.2,

$$W(\theta_\gamma) = A_0 + A_2^* P_2(cos(\theta_\gamma)) + A_4^* P_4(cos(\theta_\gamma)) \tag{2.10}$$

where A_0 is a normalization factor and $A_2 = A_2^*/A_0$ and $A_4 = A_4^*/A_0$, the angular distribution coefficients. We present the A_2 values from this work in Table 3.2. The precision was not accurate enough to obtain the A_4. This coefficient was fixed to 0 in the fit.

The A_2 coefficient is related to the attenuation coefficient α_2 and the A_2^{max} coefficient as follows (see Equation 1.5),

$$A_2 = \alpha_2 \, A_2^{max} \tag{2.11}$$

Pure-multipole transitions provide a clean way to estimate α_2 since the coefficient A_2^{max} is known in these cases.

2.3.4 General aspects of the analysis

Add-back procedure

In some cases it can occur that the γ-ray scatters from one crystal to another. The full incident γ-ray energy can be recovered by summing the energy deposited in the neighbouring detectors leading to an increase in the photopeak efficiency. This procedure is called "add-back". In our case, comparison between cluster add-back and the sum of three single crystals showed an increase (in the former) not only in the sum-peak detection efficiency, where by sum-peak we mean a peak due to the sum of two transitions in the same γ cascade, but also in the random sum efficiency. By random summing peaks we mean the peaks corresponding to the sum of two γ-transition energies detected apparently in coincidence which in reality do not belong to the same cascade. This increase in efficiency for undesired events is due to the combination of the increase in solid angle but specially due to the 10 μs time gate opened by the ADC every time a cluster fires. This dramatically increased the number of random coincidences and hence the random summing peaks. For that reason we decided not to use the add-back procedure.

The Compton scattering problem

The interaction process of Compton scattering takes place between the incident γ-ray photon and an electron in the absorbing material, i.e., the Ge detector in our case. It is most often the predominant interaction mechanism for gamma-ray energies typical of radioisotope sources. The Compton scattering is the process by which a photon scatters from a nearly free atomic electron, resulting in a less energetic photon and a scattered electron carrying the energy lost by the photon. If we assume as a good approximation that the electron is free and at rest then conservation of linear momentum and total energy gives the Compton-scattering formula

$$E'_\gamma = \frac{E_\gamma}{1 + (E_\gamma/mc^2)(1 - cos\theta)} \tag{2.12}$$

where E'_γ is the energy of the scattered photon and θ is the scattering angle. Because all angles of scattering are possible, the energy transferred to the electron can vary from zero for $\theta = 0^\circ$ (forward scattering, corresponding with no interaction) to a large fraction of the gamma-ray energy for $\theta = \pi$.

Due to our experimental geometry, both the scattered electron and scattered photon were often detected simultaneously in different crystals. This fact produces an undesirable effect in the γ-γ coincidence matrices, especially when selecting a gate at low energies. Figure 2.21 shows the γ-spectrum gated at the 480-keV peak in the total γ-γ coincidence matrices. The A, B and C labelled areas correspond to the energies such that summed up to those of the background subtraction areas ("Bck") give as a result a value which coincides with some of the strongest transitions observed in the reaction. In the example shown in Fig. 2.21, these sums are the numbers 671, 812 and 847, which correspond to the γ-rays at 668.9-671.2 keV and 811.9 keV in ^{56}Co and the 846.8-keV γ-transition in ^{56}Fe.

This effect is well understood and generally recognisable in the gated spectra. However, in some cases it could disturb the observation of "true" coincidences happening in the same energy interval.

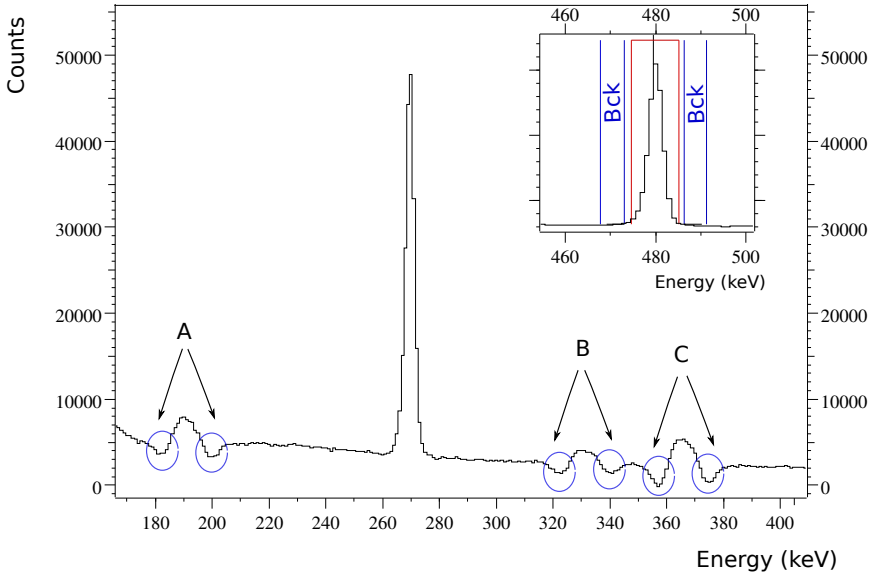

Figure 2.21: Compton scattering effect observed in the γ-spectrum gated on the 480-keV peak in the total γ-γ coincidence matrix. The A, B and C labelled areas correspond to the energies such that summed with those of the background subtraction areas ("Bck") give as a result a value which coincides with some of the strongest transitions observed in the reaction. In the example it is shown here, these sums are the numbers 671, 812 and 847, which correspond to the γ-rays at 668.9-671.2 and 811.9 keV in ^{56}Co and the 846.8-keV γ-transition in ^{56}Fe.

Chapter 3

Experimental results

In this chapter we will present the experimental results obtained on the ^{56}Fe(p,nγ)^{56}Co reaction at E_p = 10 MeV analysed in the present work. In section 3.1 the level scheme of ^{56}Co, as well as the main γ-transition information regarding the de-excitation of its excited states, will be presented. Section 3.2 is focused on the information extracted from the angular distributions of γ-transitions measured in this work.

3.1 The ^{56}Co level scheme

In this section we will present all the information regarding the level scheme of the ^{56}Co nucleus obtained in this work, as well as some measured γ-ray spectra from the reaction.

The total *Singles* spectrum is shown in Fig. 3.1, up to 1.5 MeV. On the other hand, the full projection spectrum is presented in Fig. 3.2, first up to 1.5 MeV, and then in steps of 500 keV. The experimental results are presented ordered by level energy (E_{level}) in Table 3.1 and by γ-transition energy (E_γ) in Table 3.2.

A first inspection of the *Singles* spectrum, as well as of the projection spectra, shows that in the present experiment two primary reaction channels were open: the (p,p') channel populating excited states in ^{56}Fe and the (p,n) channel populating excited states in ^{56}Co. As already mentioned in Chapter 1, calculations using the TALYS software were made to study in detail the p + ^{56}Fe reaction at E_p = 10 MeV (see Appendix C). These calculations anticipated that both channels are strong and make up a large fraction of the cross-section in this reaction at this bombarding energy. Since there is significant knowledge in the literature of the properties of both ^{56}Co and ^{56}Fe, it was relatively easy to identify the most intense peaks in the spectra.

Apart from the greater statistics in the *Singles* spectrum, as expected, when it is compared with the projection spectra one observes that the ratio of the ^{56}Co and the ^{56}Fe peak intensities increases in the projection spectra. As an example, one can compare the intensities of the peaks at 811.9 and 846.8 keV, coming from the de-excitation of excited states in ^{56}Co and ^{56}Fe, respectively.

In our experiment other peaks corresponding to the γ-de-excitation of several other nuclei were also identified. As explained in section 2.2.2, a high-energy peak from the de-excitation of the ^{16}O nucleus (at 6.1 MeV) together with its single-escape peak were used in the energy calibration process. The ^{16}O probably occurred because it covered the surface of the ^{56}Fe target due to oxidation processes, and the inelastic scattering channel ^{16}O(p,p')^{16}O was opened. On the other hand, several identified γ-transitions from the de-excitation of the stable isotopes ^{72}Ge (27.5 % of natural abundance) and ^{74}Ge (36.5 %) were identified and are labelled in the projection spectra (see Fig. 3.2). The germanium is the material the detectors are made of and the neutron-induced inelastic scattering ^{72}Ge(n,n')^{72}Ge and ^{74}Ge(n,n')^{74}Ge reactions took place, following the ^{56}Fe(p,nγ)^{56}Co reaction.

The construction of the ^{56}Co level scheme was mainly based on the analysis of the γ-γ coincidence matrices, as was explained in detail in Chapter 2.3. The first step in the analysis was to check that our data confirmed the level scheme known from previous work [47]. After gating on all previously known γ-transitions, following an ascending order in their placement in the level scheme, the reported levels were confirmed. In the process, a large number of new γ-rays, i.e., γ-transitions that were previously unknown, were observed. Then by gating on these new transitions we did a carefully study in order to place them in the level scheme. This process is explained in detail in section 2.3.2. Following this procedure, several new excited states were also found.

In the present work, a large amount of new information has been obtained. In the following lines we summarise the experimental results:

- A total of 223 γ-transitions have been observed and placed in the level scheme, of which 169 were previously unobserved.

- A much higher sensitivity level for the γ-de-excitation for excited states in ^{56}Co than reported in the literature has been reached for spins between 0 and 6. A total of 77 excited states have been observed, 37 of which were previously known states for which no gamma de-excitation had been observed. In 42 cases the energy precision of the levels has been improved. In this work, 14 excited states have been observed for the first time.

- The angular distributions of 53 γ-transitions have been measured, obtaining the corresponding angular coefficients A_2. These A_2 values were taken into consideration for the J^π assignments (see next section). 36 new J^π assignments have been made, 10 corrections to previous J^π assignments have been suggested and in 4 cases J^π assignment ambiguities have been resolved. For the remaining states, the previous J^π assignments have been confirmed.

As mentioned above, the experimental levels observed in this work, ordered by increasing excitation energy value, are presented in Table 3.1, together with their γ-transitions. The criteria followed in order to associate an uncertainty with the

E_{level} will be explained in sec. 3.1.1. The E_{level} value is presented together with the level energy from previous work, taken from [47]. In the case of levels observed for the first time in this work, the word "New" is shown, instead. The relative photon branchings BR from each level are presented, normalised to 100 for the strongest branch. The spin and parity of the level (J^π) is shown, together with the previous assignment (if available) taken from [47]. The spin-parity assignments are explained in detail in Appendix E. The direct level-feeding in the reaction was obtained from the level-scheme intensity balance using the *Eleven* code (see sec.2.3.2).

In order to have a negative-parity state in ^{56}Co the unpaired neutron above the $1f_{7/2}$ shell must be promoted to the $1g_{9/2}$ orbital at least. The first $J^\pi = (9/2)^+$ excited state in the ^{57}Ni nucleus (whose structure is simply one neutron outside the $1f_{7/2}$ shell with respect to the doubly magic nucleus $^{56}_{28}$Ni$_{28}$) is located at an excitation energy of 3.009 MeV. Based on this value we assumed that the first negative-parity state in ^{56}Co will lie above $\sim$ 3 MeV. Then no negative-parity levels were considered below 3 MeV in this work. Note that the first candidate to have negative parity was proposed at 3.3 MeV (see Table 3.1).

On the other hand, Table 3.2 shows the γ-ray energies observed in this work, ordered by increasing value. The intensities were normalised to 100 for the 158.4-keV γ-ray intensity. This γ-transition is the most intense line observed in the de-excitation of ^{56}Co (see Fig. 3.2) and corresponds to the de-excitation from the first excited state to the ground state. The angular coefficient A_2, excitation energy of the initial state E^i_{level}, spin and parity of the initial and final states (J^π_i and J^π_f) and multipolarity of the transition are shown. In some cases, the multipolarity is clear from the initial and final J^π involved. In other cases it can be deduced from the A_2 value, even if J^π_i and J^π_f are ambiguous. No multipolarity assignment was made in the remainder of the cases. In section 3.2 we will discuss the angular distribution results in more detail.

The γ-spectrum gated on the 480-keV peak is shown in Fig. 3.3. It should be noted that by gating on this transition all the γ-rays de-exciting the two 0^+ states whose study was the main motivation of this work are seen. However their relative intensities can only be compared with the real ones in pairs, corresponding to the γ-transitions de-exciting to the same level: the 1806.1 and 1877.9 keV, the 797.2 and 868.6 keV, and the 891.5 and 969.9 keV peaks. The gated γ-spectra chosen to properly observe these γ-transitions are shown in section 4.2.

Due to the complexity of the ^{56}Co level scheme, we present a simplified diagram where only the most intense γ-transitions are shown, i.e., the γ-transitions such that $I_\gamma > 1.5$ (see Fig. 3.5). Note that for completeness the first 6^+ and 7^+ observed excited states are also presented in the level scheme, as are the two 0^+ states of interest, which are the 3526.4- and 3597.9-keV states. However, the intensities of the γ-de-excitations from the previous four states are below the threshold chosen for Fig. 3.5 and therefore no γ-transitions de-exciting these states are shown. The intensities of the 1806.1 and 1877.9 keV γ-rays, the most intense γ-transitions that de-excite the 3526.4- and 3597.9-keV states, respectively, are $I_{1806.1\,keV} = 1.13(12)$

and $I_{1877.9\,keV} = 0.74(5)$. Again, for further details of the γ-decay of these two 0^+-states see section 4.2.

Figure 3.6 shows all the excited states in ^{56}Co observed in the present thesis and their corresponding spin-parity values assigned in this work. The states are arranged in columns ordered by increasing spin value. As can be observed most of them are new J^π assignments with respect to the previous knowledge of ^{56}Co. As mentioned earlier, these assignments are explained in detail in Appendix E.

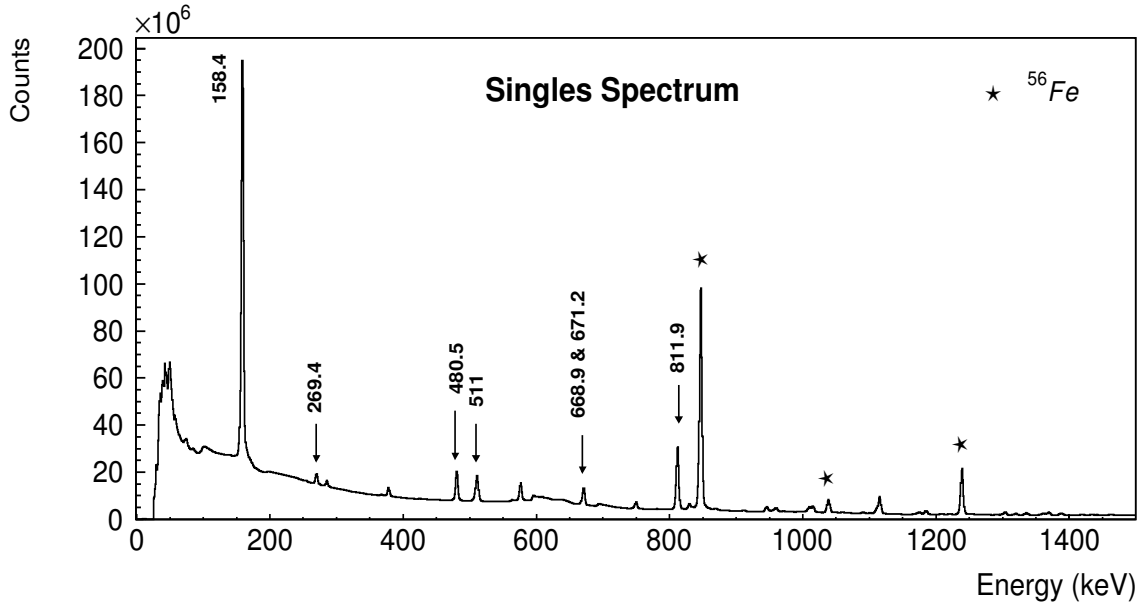

Figure 3.1: The in-beam *Singles* spectrum from the ^{56}Fe(p,nγ)^{56}Co reaction at $E_p =$ 10 MeV is shown up to 1.5 MeV. The most intense γ-transitions in ^{56}Co are labelled. Note that the peaks coming from the de-excitation of ^{56}Fe are indicated with a symbol $\star$.

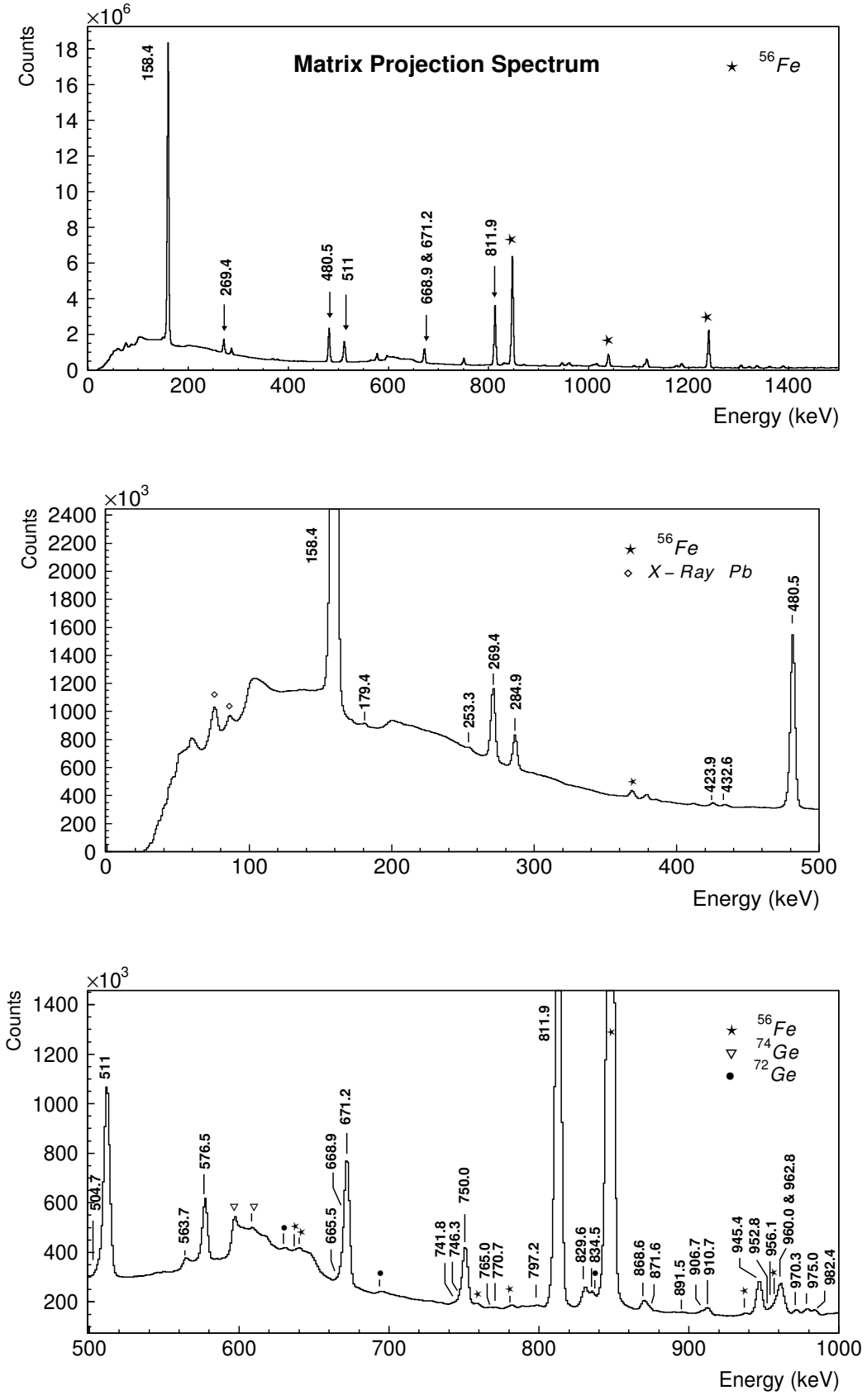

Figure 3.2: The γ-γ coincidence matrix projection spectrum in ranges of 500 keV, except the spectrum at the top in the 0-1500 keV range, is shown. All the γ-rays observed in this work are labelled.

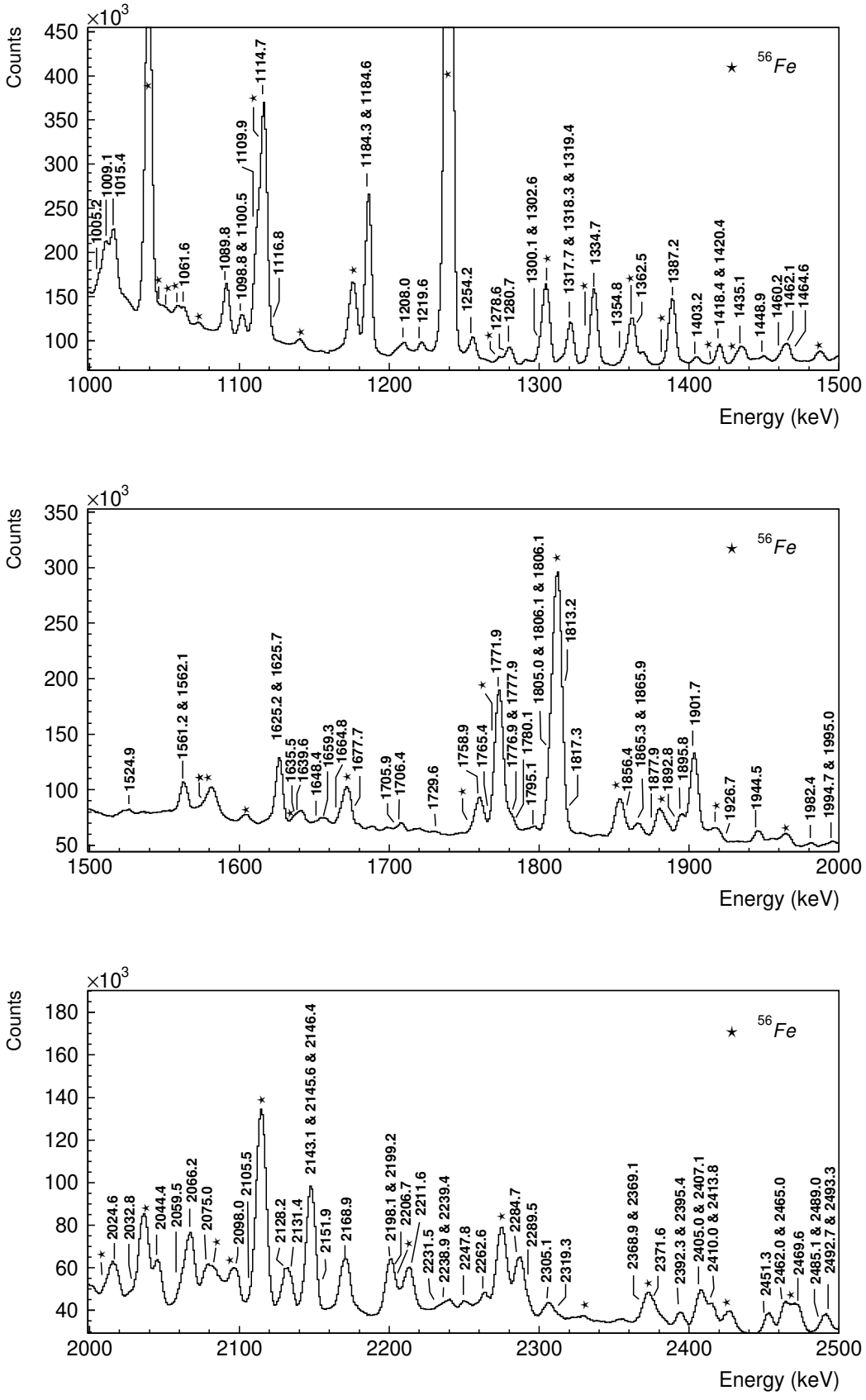

Figure 3.2: *(continued)* The γ-γ coincidence matrix projection spectrum is shown, in ranges of 500 keV. All the γ-rays observed in this work are labelled.

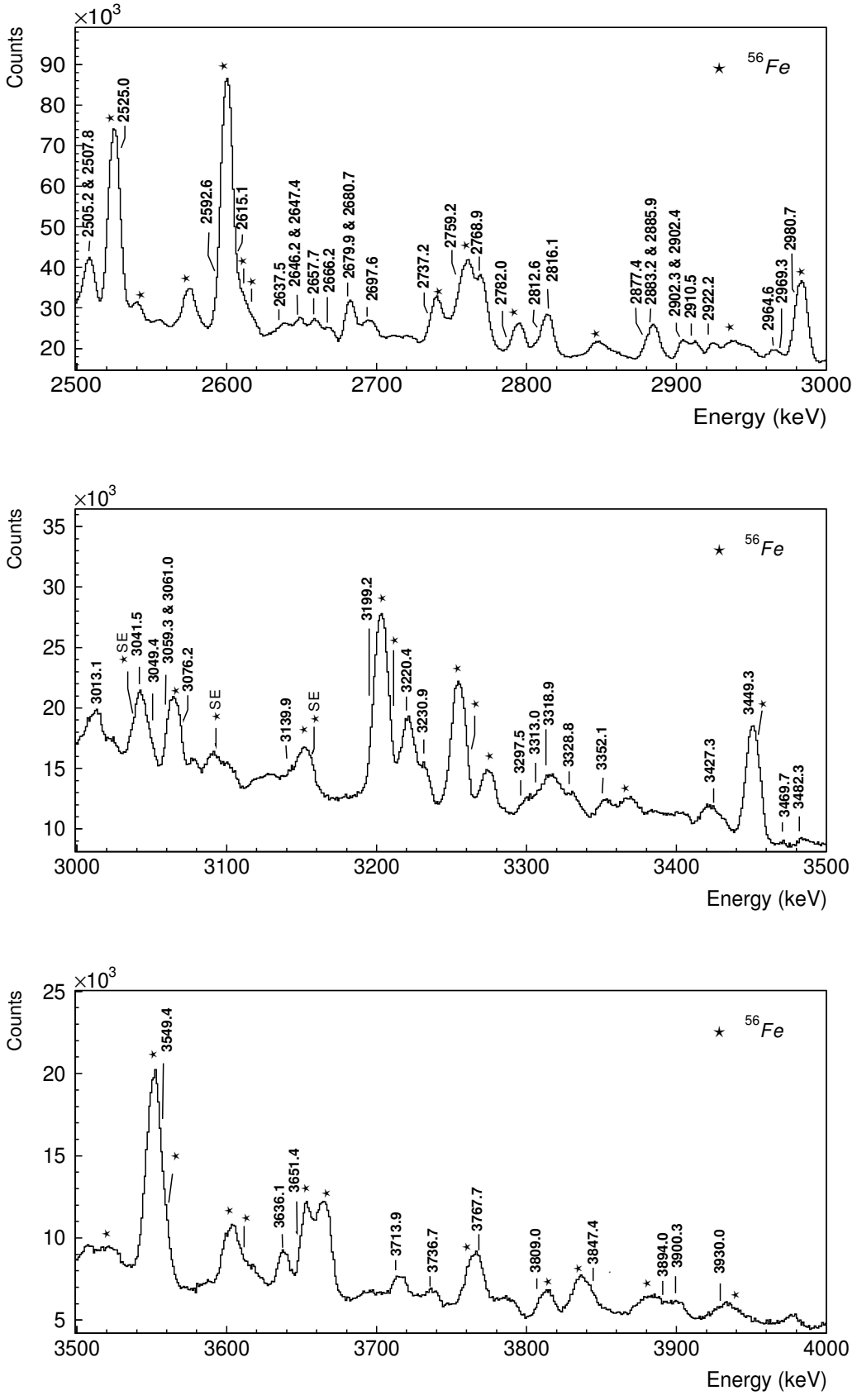

Figure 3.2: *(continued)* The γ-γ coincidence matrix projection spectrum is shown, in ranges of 500 keV. All the γ-rays observed in this work are labelled. SE stands for "Single Escape" peak.

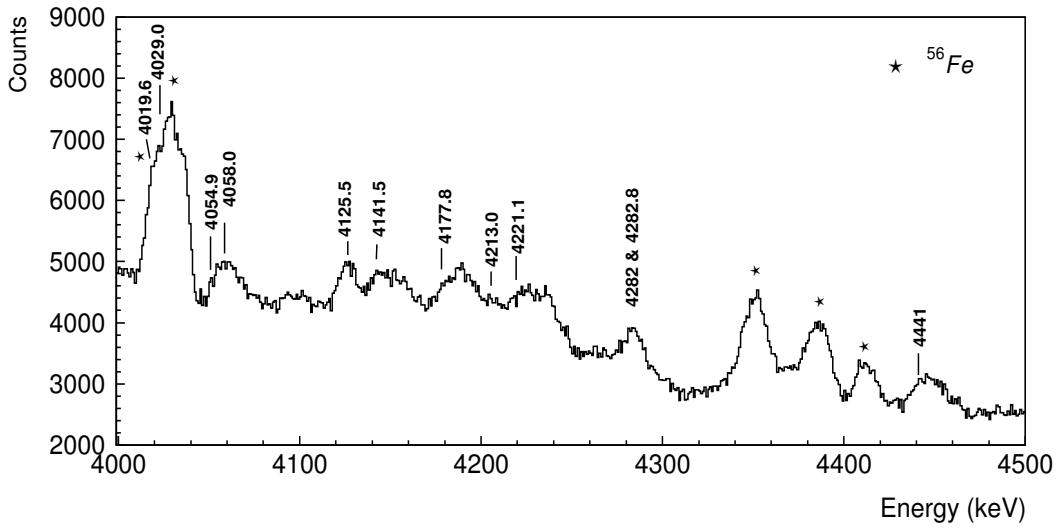

Figure 3.2: *(continued)* The γ-γ coincidence matrix projection spectrum is shown, in ranges of 500 keV. All the γ-rays observed in this work are labelled.

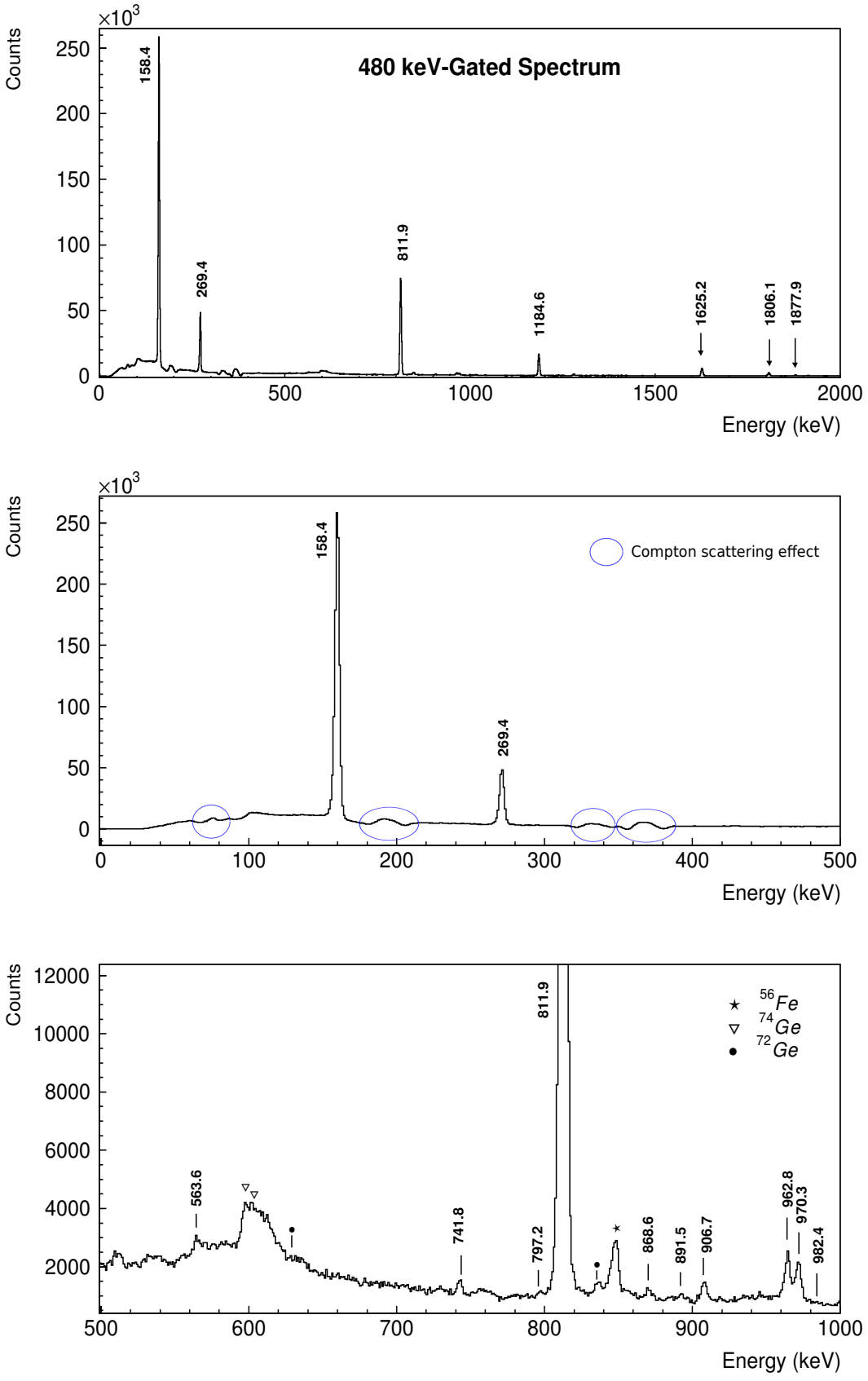

Figure 3.3: The 480 keV-gated spectrum in ranges of 500 keV, except for the spectrum at the top which covers 0-2000 keV, is shown. All the γ-rays observed in this work are labelled. See sec. 2.3.4 for details about the Compton scattering effect when gating at low energies peaks.

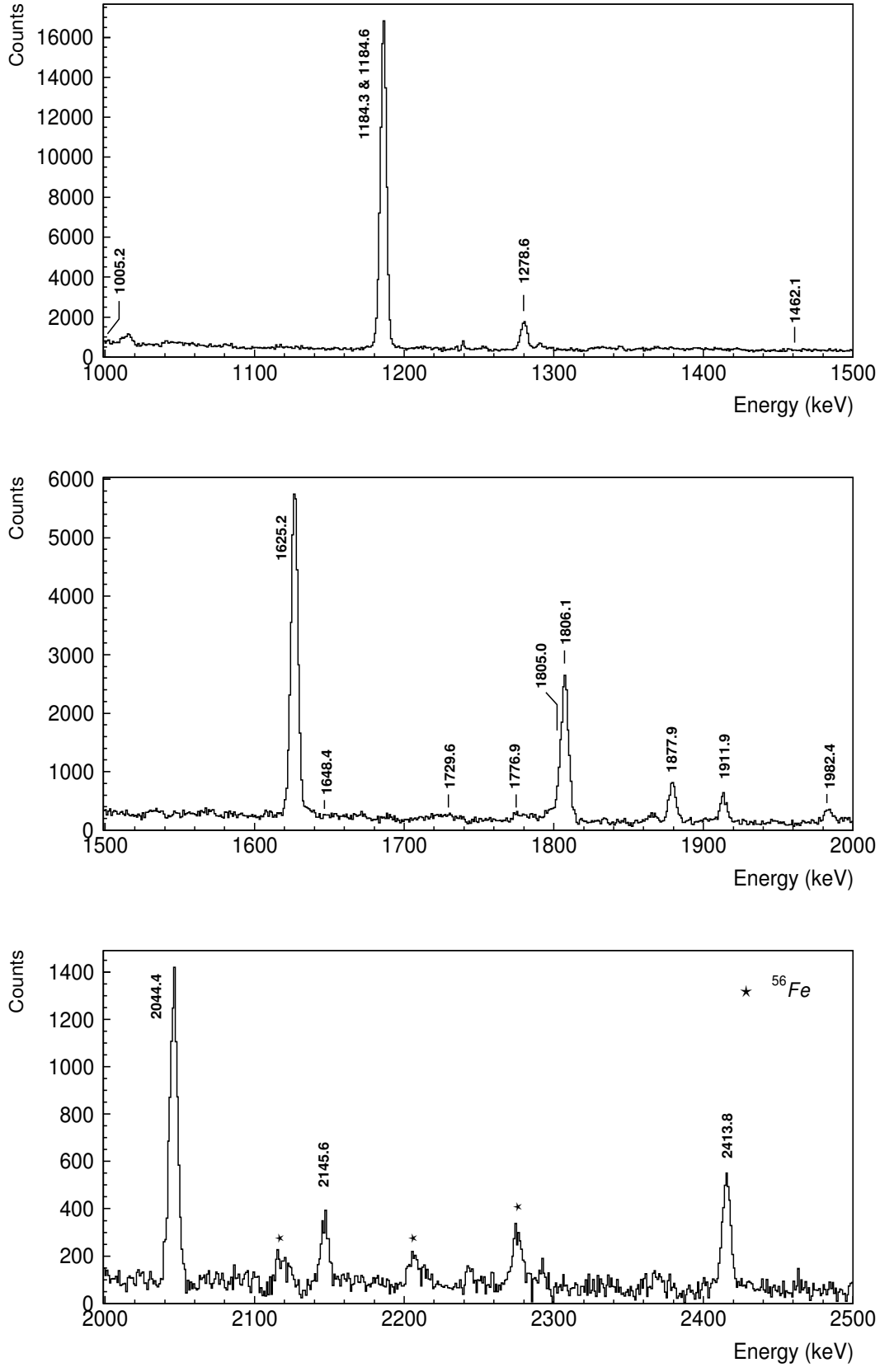

Figure 3.3: *(continued)* The 480 keV-gated spectrum in ranges of 500 keV is shown. All the γ-rays observed in this work are labelled.

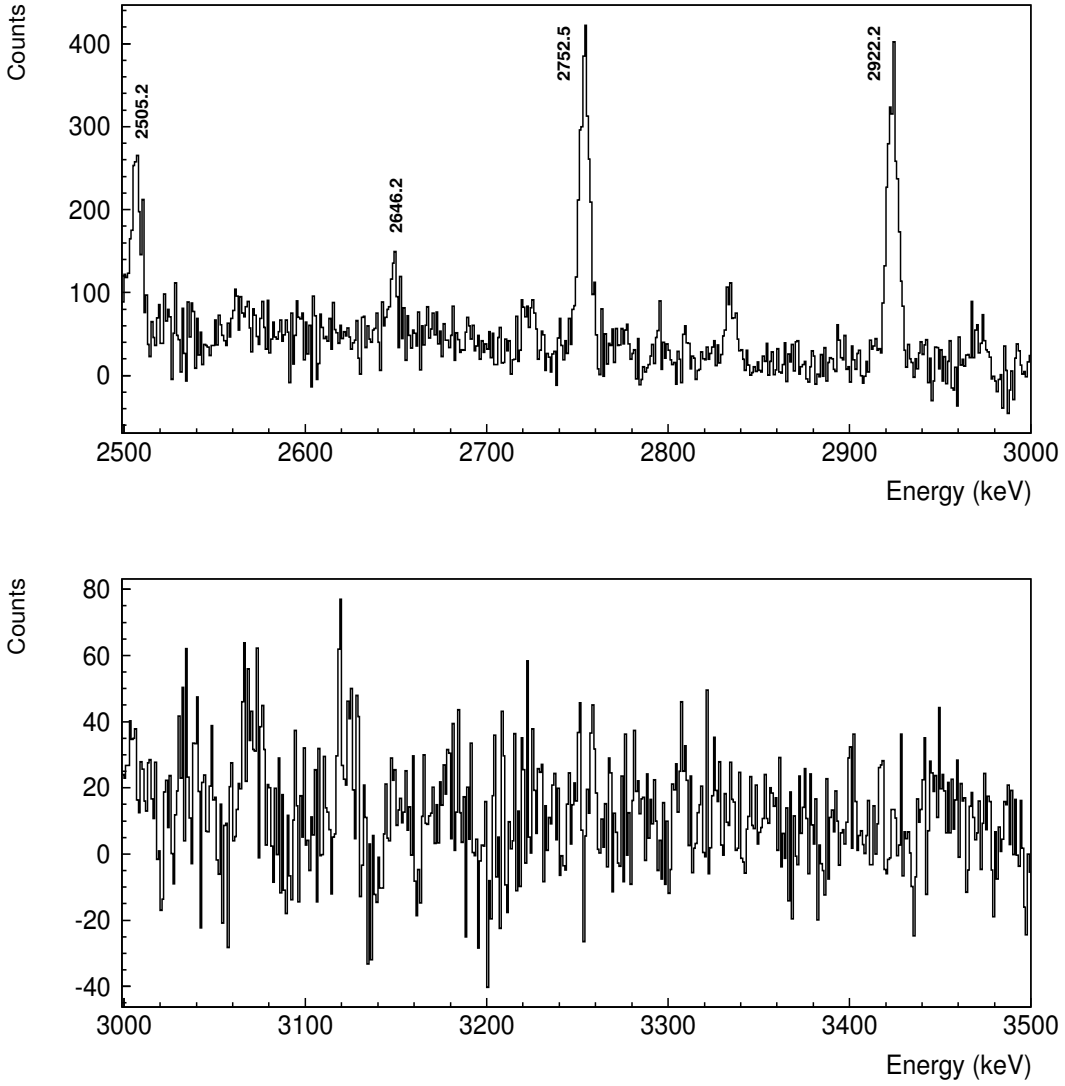

Figure 3.3: *(continued)* The 480 keV-gated spectrum in ranges of 500 keV is shown. All the γ-rays observed in this work are labelled.

Table 3.1: Excited states observed in ^{56}Co in the ^{56}Fe(p,nγ)^{56}Co reaction at $E_p = 10$ MeV ordered by increasing E_{level} value. The E_{level} and J^π values from previous work are taken from reference [47]. The relative photon branching BR from each level is presented, renormalised to 100 for the strongest branch. Preferred J^π values are shown without parenthesis. Direct feeding in the reaction to each level is obtained from the level-scheme intensity balance using the *Eleven* code.

E_{level}(keV)	E_{level}(keV) Lit.	E_γ(keV)	BR	J^π Lit.	J^π	Feeding
158.4(2)	158.38(3)	158.4(2)	100	3^+	3^+	1(5)
576.4(2)	576.50(7)	576.5(2)	100	5^+	5^+	4.8(4)
829.7(2)	829.61(5)	253.3(3)	7.7(11)	4^+	4^+	6.6(8)
		671.2(2)	100(7)			
		829.6(2)	35(2)			
970.3(2)	970.23(4)	811.9(2)	100(3)	2^+	2^+	1.7(15)
		970.3(2)	2.41(13)			
1009.1(2)	1009.13(7)	179.4(8)	3(2)	5^+	5^+	1.4(7)
		432.6(2)	9.0(3)			
		1009.1(3)	100(23)			
1114.6(2)	1114.51(5)	284.9(2)	11.5(3)	3^+	3^+	7.6(8)
		956.1(2)	6.4(14)			
		1114.7(3)	100			
1450.6(2)	1450.68(4)	480.5(2)	100	0^+	0^+	2.9(5)
1720.2(2)	1720.18(4)	269.4(2)	74(2)	1^+	1^+	4.9(2)
		750.0(2)	100(4)			
		1562.1(3)	27(2)			
1930.3(2)	1930.36(16)	960.0(2)	81(4)	3^+	3^+	7.7(5)
		1100.5(3)	13.9(9)			
		1771.9(3)	100(12)			
2060.1(2)	2060.00(15)	945.4(2)	78(5)	2^+	2^+	8.0(7)
		1089.8(3)	24(1)			
		1901.7(3)	100(5)			
2224.5(3)	2224.87(15)	1109.9(3)	100(10)	2^+	2^+	6.1(5)
		1254.2(3)	22(3)			
		2066.2(3)	60(3)			
2282.3(3)	2282.63(12)	1705.9(3)	100	7^+	7^+	0.29(2)
2289.7(3)	2290.1(3?)	1319.4(3)	68.7(4)	?	3^+	6.8(2)

[a] Clear γ de-excitation to the g.s. deduced from Singles.
[b] Possible γ de-excitation to the g.s. deduced from Singles.
[c] Intensity determination not possible.
[d] Only intensity relative to the gate (Not normalised intensity).
[e] Impossibility of feeding determination because γ de-excitation intensity is unknown.

Table 3.1 (Continued): Excited states observed in ^{56}Co in the ^{56}Fe(p,nγ)^{56}Co reaction at $E_p = 10$ MeV ordered by increasing E_{level} value.

E_{level}(keV)	E_{level}(keV) Lit.	E_γ(keV)	BR	J^π Lit.	J^π	Feeding
		1460.2(3)	14.2(11)			
		2131.4(3)	72.4(4)			
		2289.5(3)	100(7)			
2305.1(3)	2306.13(21)	1334.7(3)	37.7(2)	$(2)^+$	$2^+(3^+)$	6.5(5)
		2146.4(3)	100.0(6)			
		2305.1(4)	44.5(6)			
2357.3(3)	2357.4(3)	906.7(2)	4.9(4)	1^+	1^+	5.3(2)
		1387.2(3)	99.6(5)			
		2199.2(3)	100(5)			
2371.5(3)	2371.83(20)	1362.5(3)	53(8)	6^+	6^+	1.24(11)
		1795.1(3)	96(6)			
		2371.6(5) [a]	100(20)			
2469.3(3)	2469.6(6)	1354.8(3)	4.4(4)	?	$4^+(3^+,5^+)$	2.31(12)
		1639.6(4)	8.8(10)			
		1892.8(3)	100(6)			
		2469.6(5) [a]	c			
2609.7(3)	2609.5(7)	1780.1(3)	34(2)	3^+	3^+	1.58(9)
		2451.3(3)	100(5)			
2635.1(3)	2635.64(19)	1184.6(3)	100.0(5)	1^+	1^+	4.02(19)
		1664.8(3)	10.9(8)			
2647.3(3)	2647.2(7)	1817.3(4)	15.6(2)	$(0^+,1^+)$	$4^+(2^+)$	2.58(7)
		2489.0(3)	85.9(5)			
		2647.4(3) [a]	100(3)			
2666.2(3)	2665.1(7)	2507.8(3)	100(5)	(3^+)	3^+	3.88(13)
		2666.2(3) [a]	92.1(3)			
2729.1(3)	2729.89(15)	423.9(2)	24.3(9)	1^+	1^+	2.2(5)
		504.7(2)	25.5(9)			
		668.9(2)	72.1(27)			
		1278.6(3)	24.2(9)			
		1758.9(3)	100.0(36)			
2774.3(3)	2770(5)	1659.3(4)	5.7(5)	?	$4^+(3^+,5^+)$	1.24(6)
		1765.4(4)	36(5)			
		1944.5(3)	100(5)			
		2198.1(4)	26(3)			

[a] Clear γ de-excitation to the g.s. deduced from Singles.
[b] Possible γ de-excitation to the g.s. deduced from Singles.
[c] Intensity determination not possible.
[d] Only intensity relative to the gate (Not normalised intensity).
[e] Impossibility of feeding determination because γ de-excitation intensity is unknown.

Table 3.1 (Continued): Excited states observed in ^{56}Co in the ^{56}Fe(p,nγ)^{56}Co reaction at $E_p = 10$ MeV ordered by increasing E_{level} value.

E_{level}(keV)	E_{level}(keV) Lit.	E_γ(keV)	BR	J^π Lit.	J^π	Feeding
2835.7(4)	New	1865.3(4)	100	?	$2^+(1^+,3^+)$	0.19(2)
2927.5(3)	2926(5)	1813.2(4)	3.5(3)	(2^+)	$4^+(2^+)$	2.62(13)
		2098.0(6)	5.8(8)			
		2768.9(3)	100(5)			
2970.7(3)	2969(5)	665.5(3)	10.0(12)	2^+	2^+	3.1(2)
		746.3(2)	19(7)			
		910.7(2)	24(9)			
		1856.4(3)	5.3(5)			
		2000.2(3)	22(2)			
		2812.6(3)	100(5)			
3041.5(3)	3048(5)	1926.7(4)	1.8(2)	$3^+,4^+,5^+$	$3^+,5^+(4^+)$	3.21(11)
		2032.8(5)	9(2)			
		2211.6(3)	60(3)			
		2465.0(4)	14.4(11)			
		2883.2(3)	100(5)			
		3042.0(10)[b]	c			
3061.0(3)	3060(5)	2231.5(4)	40(3)	5^+	$3^+(5^+)$	1.12(11)
		2485.1(5)	47(4)			
		2902.4(3)	100(15)			
		3061.0(10)[b]	30(27)			
3068.8(3)	New	2059.5(3)	46(7)	?	$3^+,4^+$	1.47(12)
		2238.9(4)	21(2)			
		2492.7(4)	38(3)			
		2910.5(3)	100(15)			
3075.7(3)	3075.91(22)	770.7(4)	3.6(7)	1^+	1^+	2.7(2)
		1015.4(3)	29(10)			
		1625.2(3)	100(5)			
		2105.5(4)	13.0(11)			
3139.2(3)	3140(5)	834.5(4)	6.7(10)	3^+	3^+	4.35(16)
		2024.6(4)	2.0(2)			
		2168.9(3)	99(5)			
		2980.7(3)	100(5)			
3176.8(3)	3180(5)	871.6(2)	62(4)	$1^+,3^+$	$1^+,3^+$	2.0(3)
		952.8(5)	51(19)			
		1116.8(3)	100(36)			

[a] Clear γ de-excitation to the g.s. deduced from Singles.
[b] Possible γ de-excitation to the g.s. deduced from Singles.
[c] Intensity determination not possible.
[d] Only intensity relative to the gate (Not normalised intensity).
[e] Impossibility of feeding determination because γ de-excitation intensity is unknown.

Table 3.1 (Continued): Excited states observed in ^{56}Co in the ^{56}Fe(p,nγ)^{56}Co reaction at $E_p = 10$ MeV ordered by increasing E_{level} value.

E_{level}(keV)	E_{level}(keV) Lit.	E_γ(keV)	BR	J^π Lit.	J^π	Feeding
		2206.7(4)	71(4)			
3234.4(3)	3234(5)	765.0(5)	d	(0^+)	$4^+(3^+)$	1.58(5)
		2405.0(3)	100(5)			
		2657.7(3)	38(3)			
		3076.2(3)	63(4)			
3255.1(3)	3255(5)	1805.0(10)	22(2)	?	$1^-(1^+)$	2.69(13)
		2284.7(3)	100(5)			
3298.2(3)	3297(5)	3139.9(3)	92(5)	4^+	4^+	0.73(4)
		3297.5(10)[a]	100(24)			
3339.6(3)	New	982.4(2)	d	?	2^+	0.49(3)
		2368.9(3)	100			
3362.5(3)	3366(5)	1005.2(3)	d	(-)	2^+	0.86(4)
		1911.9(3)	26.5(18)			
		2247.8(3)	10.5(10)			
		2392.3(3)	100(6)			
3377.2(3)	3378(10)	741.8(3)	d	1^+	2^+	1.35(7)
		1317.7(5)	7(3)			
		2262.6(3)	25(2)			
		2407.1(3)	100(6)			
3379.0(3)	New	1448.9(3)	d	?	3^+	1.06(6)
		3220.4(3)	100			
3432.5(3)	3436(5)	1208.0(3)	23(8)	$0^+, 1^+$	1^+	1.65(12)
		1982.4(4)	11.5(9)			
		2462.0(3)	100(6)			
3495.2(3)	3493(5)	1435.1(3)	56(19)	?	1^+	1.32(12)
		2044.4(3)	100(5)			
		2525.0(3)	75(5)			
3510.3(3)	3510(11)	2395.4(5)	3.4(3)	(0^+)	$4^+(3^+)$	1.14(5)
		2680.7(3)	100(6)			
		3352.1(3)	24(2)			
3524.6(3)	New	1219.6(3)	46(5)	?		1.3(3)
					$2^+, 3^+, 4^+(2^-, 3^-, 1^+)$	
		1300.1(3)	48(17)			
		1464.6(3)	100(35)			

[a] Clear γ de-excitation to the g.s. deduced from Singles.
[b] Possible γ de-excitation to the g.s. deduced from Singles.
[c] Intensity determination not possible.
[d] Only intensity relative to the gate (Not normalised intensity).
[e] Impossibility of feeding determination because γ de-excitation intensity is unknown.

Table 3.1 (Continued): Excited states observed in ^{56}Co in the ^{56}Fe(p,nγ)^{56}Co reaction at $E_p = 10$ MeV ordered by increasing E_{level} value.

E_{level}(keV)	E_{level}(keV) Lit.	E_γ(keV)	BR	J^π Lit.	J^π	Feeding
		2410.0(4)	4.2(5)			
3526.4(3)	3526.6(5)	797.2(5)	10(2)	0^+	0^+	1.25(12)
		891.5(4)	d			
		1806.1(3)	100(11)			
3545.7(5)	3544(11)	2969.3(5)	100	7^+	7^+	0.110(10)
3585.4(3)	3570(?)	975.0(5)	22(9)	?	2^+	0.69(5)
		1280.7(5)	40(6)			
		1524.9(4)	49(18)			
		2615.1(4)	100(9)			
		3427.3(3)	98(7)			
3589.4(3)	New	2759.2(5)	32(3)	?	$5^+, 4^+(5^-, 4^-)$	0.89(4)
		3013.1(3)	100(6)			
3597.9(3)	3598.64(23)	868.6(2)	62(3)	0^+	0^+	1.21(5)
		962.8(2)	d			
		1877.9(3)	100(7)			
3607.8(3)	3610(5)	1302.6(3)	42(3)	?	$3^+(2^+)$	1.16(4)
		1318.3(5)	2(2)			
		1677.7(4)	2(2)			
		2493.3(4)	3.1(5)			
		2637.5(4)	47(3)			
		3449.3(3)	100(5)			
3707.0(3)	New	2592.6(3)	27(2)	?	$3^+(5^+)$	0.49(4)
		2697.6(3)	100(15)			
		2877.4(4)	63(6)			
3708.0(3)	3717(5)	1098.8(5)	14(4)	(-)	$2^+, 3^+$	2.49(10)
		1403.2(3)	21(2)			
		1418.4(3)	d			
		2737.2(3)	100(5)			
		1777.9(4)	d			
		3549.4(3)	88(6)			
3791.7(4)	3798(11)	1420.4(4)	d	(+)	$6^+, 6^-$	0.080(10)
		2782.0(7)	100(14)			
3794.4(3)	New	2679.9(3)	14.5(13)	?	$3^+, 3^-(4^+)$	1.31(6)
		2964.6(3)	34(2)			

[a] Clear γ de-excitation to the g.s. deduced from Singles.
[b] Possible γ de-excitation to the g.s. deduced from Singles.
[c] Intensity determination not possible.
[d] Only intensity relative to the gate (Not normalised intensity).
[e] Impossibility of feeding determination because γ de-excitation intensity is unknown.

Table 3.1 (Continued): Excited states observed in ^{56}Co in the ^{56}Fe(p,nγ)^{56}Co reaction at $E_p = 10$ MeV ordered by increasing E_{level} value.

E_{level}(keV)	E_{level}(keV) Lit.	E_γ(keV)	BR	J^π Lit.	J^π	Feeding
		3636.1(3)	100(7)			
3809.7(3)	3807(10)	3651.4(3)	100(7)	$1^+, 2^+, 3^+$	$4^+(3^+, 2^+)$	1.80(12)
		3809.0(10)[b]	11(3)			
3819.3(3)	New	563.6(4)	d	?	$0^+(1^+)$	0.03(2)
		1184.3(3)	d			
		1462.1(3)	d			
3866.1(3)	3863(12)	1561.2(3)	100(9)	?	$1^+, 2^+(3^+)$	1.00(8)
		1806.1(6)	34(14)			
		2145.6(4)	93(9)			
3872.6(3)	3876(12)	2902.3(3)	100(7)	(+)	$3^+(2^+)$	0.90(5)
		3713.9(4)	45(3)			
		3873.0(10)[b]	55(9)			
3895.1(3)	3900(12)	2885.9(3)	56(8)	?	$4^+, 5^+(3^+, 4^-)$	1.09(6)
		3318.9(3)	100(6)			
		3736.7(3)	78(6)			
		3894.0(10)[a]	69(11)			
3925.4(3)	New	1635.5(5)	d	?	$2^+, 3^+$	0.51(7)
		1865.9(6)	d			
		1995.0(5)	58(23)			
		3767.7(3)	100(6)			
3930.7(3)	3935(12)	1625.7(4)	100(18)	?	$3^+, 2^+, 4^+$	0.16(2)
		2816.1(5)	39(5)			
		3930(2)[a]	c			
4005.5(3)	4011(12)	1648.4(9)	d	$3^+, 4^+, 5^+$	3^+	0.21(2)
		2075.0(3)	100			
		3847.4(4)	d			
4011.6(3)	4019(12)	1706.4(3)	82(8)	?	$2^+(1^+, 3^+)$	0.71(4)
		3041.5(3)	100(5)			
4029.3(3)	4032(10)	3059.3(4)	100(9)	$1^+, 2^+, 3^+$	2^+	0.31(3)
		3199.2(6)	38(6)			
		4029.0(10)[b]	c			
4058.6(3)	4062(12)	2128.2(5)	d	?	$4^+(4^-, 5^+, 3^+)$	0.80(6)
		3049.4(4)	59(11)			
		3482.3(3)	100(7)			

[a] Clear γ de-excitation to the g.s. deduced from Singles.
[b] Possible γ de-excitation to the g.s. deduced from Singles.
[c] Intensity determination not possible.
[d] Only intensity relative to the gate (Not normalised intensity).
[e] Impossibility of feeding determination because γ de-excitation intensity is unknown.

Table 3.1 (Continued): Excited states observed in ^{56}Co in the ^{56}Fe(p,nγ)^{56}Co reaction at $E_p = 10$ MeV ordered by increasing E_{level} value.

E_{level}(keV)	E_{level}(keV) Lit.	E_γ(keV)	BR	J^π Lit.	J^π	Feeding
		3900.3(3)	60(5)			
		4058.0(10)[b]	74(19)			
4086.9(4)	4094(12)	1729.6(4)	d	?	$1^+, 0^+, 2^+$	e
4134.1(3)	New	1776.9(5)	d	?	$1^+, 2^+$	0.76(5)
		2413.8(3)	100(7)			
4177.9(3)	4183(10)	4019.6(4)	27(3)	(+)	$4^+(3^+, 4^-, 3^-)$	0.56(8)
		4177.8(5)[a]	100(18)			
4201.1(3)	4209(13) or New	1061.6(3)	58(8)	?	$2^+, 1^+, 3^+$	1.12(5)
		1895.8(6)	58(6)			
		3230.9(3)	100(2)			
4203.2(4)	4209(13) or New	2143.1(4)	90(30)	?	$2^+, 1^+, 1^-$	0.44(8)
		2752.5(3)	100(7)			
4213.2(4)	4209(13) or New	4054.9(4)	100	?	$4^+(3^+, 4^-, 3^-)$	0.140(10)
		4213.0(10)[a]	c			
4225.4(3)	4222(13)	2505.2(3)	100	?	$1^+, 0^+, 2^+$	0.36(3)
4283.7(3)	4281(13)	1994.7(8)	d	?	$3^+(4^+, 2^+, 3^-)$	0.59(6)
		3313.0(4)	59(5)			
		4125.5(3)	100(9)			
		4282(2) [b]	96(22)			
4299.4(3)	4293(13)	2239.4(5)	60(23)	?	$3^+(2^+, 4^+, 3^-)$	0.28(4)
		2369.1(4)	c			
		3328.8(4)	58(6)			
		3469.7(6)	38(5)			
		4141.5(4)	100(7)			
4366.4(5)	New	2646.2(5)	100	?	$1^+, 0^+, 2^+$	0.11(2)
4372.9(3)	4372(3)	2922.2(3)	100	1^+	1^+	0.24(2)
4379.4(5)	4388(13)	2319.3(12)	100(42)	$1^+, 2^+, 3^+$	$2^+, 3^+(4^+)$	0.22(5)
		4221.1(5)	83(8)			
4441.2(5)	4441(13)	2151.9(10)	d	7^+	$3^+(4^+)$	0.21(2)
		4282.8(5)	100			
		4441(2) [b]	c			

[a] Clear γ de-excitation to the g.s. deduced from Singles.
[b] Possible γ de-excitation to the g.s. deduced from Singles.
[c] Intensity determination not possible.
[d] Only intensity relative to the gate (Not normalised intensity).
[e] Impossibility of feeding determination because γ de-excitation intensity is unknown.

Table 3.2: γ-transitions observed in ^{56}Co in the ^{56}Fe(p,nγ)^{56}Co reaction at $E_p = 10$ MeV ordered by increasing E_γ value. The intensity I_γ is normalised to 100 for the intensity of the 158.4-keV transition. The angular coefficient A_2, excitation energy of the initial state E^i_{level}, spin-parity of the initial and the final states (J^π_i and J^π_f) and multipolarity are shown.

E_γ(keV)	I_γ	A_2	E^i_{level} (keV)	$J^\pi_i \rightarrow J^\pi_f$	Mult.
158.4(2)	100(5)		158.4(2)	$3^+ \rightarrow 4^+$	
179.4(8) [c]	0.08(6)		1009.1(2)	$5^+ \rightarrow 4^+$	
253.3(3) [c]	0.81(12)		829.7(2)	$4^+ \rightarrow 5^+$	
269.4(2)	3.06(9)	−0.07(3)	1720.2(2)	$1^+ \rightarrow 0^+$	M1
284.9(2)	1.70(5)		1114.6(2)	$3^+ \rightarrow 4^+$	
423.9(2) [a]	0.27(10)		2729.1(3)	$1^+ \rightarrow 2^+(3^+)$	
432.6(2)	0.253(8)		1009.1(2)	$5^+ \rightarrow 5^+$	
480.5(2)	13.4(4)		1450.6(2)	$0^+ \rightarrow 2^+$	E2
504.7(2) [a]	0.29(10)		2729.1(3)	$1^+ \rightarrow 2^+$	
563.6(4) [cN]	e		3819.3(3)	$0^+(1^+) \rightarrow 1^-(1^+)$	
576.5(2)	11.3(4)		576.4(2)	$5^+ \rightarrow 4^+$	
665.5(3) [N]	0.17(2)		2970.7(3)	$2^+ \rightarrow 2^+(3^+)$	
668.9(2) [c]	0.8(3)		2729.1(3)	$1^+ \rightarrow 2^+$	
671.2(2)	10.5(7)		829.7(2)	$4^+ \rightarrow 3^+$	
741.8(3) [aN]	e		3377.2(3)	$2^+ \rightarrow 1^+$	
746.3(2) [N]	0.32(12)		2970.7(3)	$2^+ \rightarrow 2^+$	
750.0(2)	4.14(15)		1720.2(2)	$1^+ \rightarrow 2^+$	
765.0(5) [aN]	e		3234.4(3)	$4^+(3^+) \rightarrow 4^+(3^+, 5^+)$	
770.7(4) [aN]	0.066(12)		3075.7(3)	$1^+ \rightarrow 2^+(3^+)$	
797.2(5) [aN]	0.11(2)		3526.4(3)	$0^+ \rightarrow 1^+$	
811.9(2)	44.8(13)		970.3(2)	$2^+ \rightarrow 3^+$	
829.6(2)	3.7(2)		829.7(2)	$4^+ \rightarrow 4^+$	
834.5(4) [N]	0.14(2)		3139.2(3)	$3^+ \rightarrow 2^+(3^+)$	
868.6(2) [a]	0.46(2)		3597.9(3)	$0^+ \rightarrow 1^+$	

[a] γ-ray with Doppler shift.
[b] γ-ray possibly with Doppler shift.
[c] Not possible to determine whether the γ-ray suffer from Doppler effect or not.
[d] Impossible intensity determination.
[e] Only intensity relative to the gate (Not normalised intensity).
[N] γ-ray observed for the first time in this work.

Table 3.2 (Continued): γ-transitions observed in ^{56}Co in the ^{56}Fe(p,nγ)^{56}Co reaction at $E_p = 10$ MeV ordered by increasing E_γ value.

E_γ(keV)	I_γ	A_2	E^i_{level} (keV)	$J^\pi_i \rightarrow J^\pi_f$	Mult.
871.6(2) [bN]	0.43(3)	−0.21(12)	3176.8(3)	$1^+, 3^+ \rightarrow 2^+(3^+)$	
891.5(4) [aN]	e		3526.4(3)	$0^+ \rightarrow 1^+$	
906.7(2) [aN]	0.128(10)		2357.3(3)	$1^+ \rightarrow 0^+$	
910.7(2) [N]	0.41(15)		2970.7(3)	$2^+ \rightarrow 2^+$	
945.4(2) [a]	4.7(3)		2060.1(2)	$2^+ \rightarrow 3^+$	
952.8(5) [aN]	0.35(13)		3176.8(3)	$1^+, 3^+ \rightarrow 2^+$	
956.1(2) [c]	0.95(20)		1114.6(2)	$3^+ \rightarrow 3^+$	
960.0(2) [a]	3.41(17)		1930.3(2)	$3^+ \rightarrow 2^+$	
962.8(2) [a]	e		3597.9(3)	$0^+ \rightarrow 1^+$	
970.3(2)	1.08(6)		970.3(2)	$2^+ \rightarrow 4^+$	E2
975.0(5) [aN]	0.05(2)		3585.4(3)	$2^+ \rightarrow 3^+$	
982.4(2) [aN]	e	−0.25(12)	3339.6(3)	$2^+ \rightarrow 1^+$	M1/E2
1005.2(3) [aN]	e		3362.5(3)	$2^+ \rightarrow 1^+$	
1009.1(3)	2.8(6)		1009.1(2)	$5^+ \rightarrow 4^+$	
1015.4(3) [a]	0.53(19)		3075.7(3)	$1^+ \rightarrow 2^+$	
1061.6(3) [aN]	0.30(4)		4201.0(3)	$2^+, 1^+, 3^+ \rightarrow 3^+$	
1089.8(3) [a]	1.45(8)		2060.1(2)	$2^+ \rightarrow 2^+$	
1098.8(5) [aN]	0.15(4)		3708.0(3)	$2^+, 3^+ \rightarrow 3^+$	
1100.5(3) [a]	0.65(4)		1930.3(2)	$3^+ \rightarrow 4^+$	
1109.9(3) [a]	4.2(4)		2224.5(3)	$2^+ \rightarrow 3^+$	
1114.7(3)	14.8(6)		1114.6(2)	$3^+ \rightarrow 4^+$	
1116.8(3) [aN]	0.7(3)	−0.05(13)	3176.8(3)	$1^+, 3^+ \rightarrow 2^+$	M1/E2
1184.3(3) [aN]	e		3819.3(3)	$0^+(1^+) \rightarrow 1^+$	
1184.6(3) [a]	3.67(19)	−0.33(3)	2635.1(3)	$1^+ \rightarrow 0^+$	M1
1208.0(3) [aN]	0.28(10)		3432.5(3)	$1^+ \rightarrow 2^+$	
1219.6(3) [aN]	0.30(3)		3524.6(3)	$2^+, 3^+, 4^+(2^-, 3^-, 1^+) \rightarrow 2^+(3^+)$	

[a] γ-ray with Doppler shift.
[b] γ-ray possibly with Doppler shift.
[c] Not possible to determine whether the γ-ray suffer from Doppler effect or not.
[d] Impossible intensity determination.
[e] Only intensity relative to the gate (Not normalised intensity).
[N] γ-ray observed for the first time in this work.

Table 3.2 (Continued): γ-transitions observed in ^{56}Co in the ^{56}Fe(p,nγ)^{56}Co reaction at $E_p = 10$ MeV ordered by increasing E_γ value.

E_γ(keV)	I_γ	A_2	E^i_{level} (keV)	$J^\pi_i \rightarrow J^\pi_f$	Mult.
1254.2(3) [a]	0.94(11)		2224.5(3)	$2^+ \rightarrow 2^+$	
1278.6(3) [a]	0.27(10)	−0.08(8)	2729.1(3)	$1^+ \rightarrow 0^+$	M1
1280.7(5) [aN]	0.090(14)		3585.4(3)	$2^+ \rightarrow 2^+(3^+)$	
1300.1(3) [aN]	0.31(11)		3524.6(3)	$2^+, 3^+, 4^+(2^-, 3^-, 1^+) \rightarrow 2^+$	
1302.6(3) [aN]	0.25(2)	0.29(18)	3607.8(3)	$3^+(2^+) \rightarrow 2^+(3^+)$	M1/E2
1317.7(5) [aN]	0.07(3)		3377.2(3)	$2^+ \rightarrow 2^+$	
1318.3(5) [aN]	e		3607.8(3)	$3^+(2^+) \rightarrow 3^+$	
1319.4(3) [b]	1.84(10)	0.02(4)	2289.7(3)	$3^+ \rightarrow 2^+$	M1/E2
1334.7(3) [a]	2.00(11)	0.08(4)	2305.1(3)	$2^+(3^+) \rightarrow 2^+$	M1/E2
1354.8(3) [aN]	0.089(8)		2469.3(3)	$4^+(3^+, 5^+) \rightarrow 3^+$	
1362.5(3) [a]	0.27(4)		2371.5(3)	$6^+ \rightarrow 5^+$	
1387.2(3) [a]	2.60(14)		2357.3(3)	$1^+ \rightarrow 2^+$	
1403.2(3) [aN]	0.23(2)	−0.1(2)	3708.0(3)	$2^+, 3^+ \rightarrow 2^+(3^+)$	
1418.4(3) [aN]	e		3708.0(3)	$2^+, 3^+ \rightarrow 3^+$	
1420.4(4) [aN]	e		3791.7(4)	$6^+, 6^- \rightarrow 6^+$	
1435.1(3) [aN]	0.32(11)		3495.2(3)	$1^+ \rightarrow 2^+$	
1448.9(3) [aN]	e		3379.0(3)	$3^+ \rightarrow 3^+$	
1460.2(3) [N]	0.38(3)		2289.7(3)	$3^+ \rightarrow 4^+$	
1462.1(3) [aN]	e		3819.3(3)	$0^+(1^+) \rightarrow 1^+$	
1464.6(3) [aN]	0.7(3)		3524.6(3)	$2^+, 3^+, 4^+(2^-, 3^-, 1^+) \rightarrow 2^+$	
1524.9(4) [aN]	0.11(4)		3585.4(3)	$2^+ \rightarrow 2^+$	
1561.2(3) [aN]	0.44(4)		3866.1(3)	$1^+, 2^+(3^+) \rightarrow 2^+(3^+)$	
1562.1(3)	1.13(7)	0.05(4)	1720.2(2)	$1^+ \rightarrow 3^+$	E2
1625.2(3) [a]	1.84(10)	−0.42(4)	3075.7(3)	$1^+ \rightarrow 0^+$	M1
1625.7(4) [aN]	0.11(2)		3930.7(3)	$3^+, 2^+, 4^+ \rightarrow 2^+(3^+)$	

[a] γ-ray with Doppler shift.
[b] γ-ray possibly with Doppler shift.
[c] Not possible to determine whether the γ-ray suffer from Doppler effect or not.
[d] Impossible intensity determination.
[e] Only intensity relative to the gate (Not normalised intensity).
[N] γ-ray observed for the first time in this work.

Table 3.2 (Continued): γ-transitions observed in ^{56}Co in the ^{56}Fe(p,nγ)^{56}Co reaction at $E_p = 10$ MeV ordered by increasing E_γ value.

E_γ(keV)	I_γ	A_2	E^i_{level} (keV)	$J^\pi_i \rightarrow J^\pi_f$	Mult.
1635.5(5) [aN]	e		3925.4(3)	$2^+, 3^+ \rightarrow 3^+$	
1639.6(4) [aN]	0.18(2)		2469.3(3)	$4^+(3^+, 5^+) \rightarrow 4^+$	
1648.4(9) [bN]	e		4005.5(3)	$3^+ \rightarrow 1^+$	E2
1659.3(4) [aN]	0.042(4)		2774.3(3)	$4^+(3^+, 5^+) \rightarrow 3^+$	
1664.8(3) [aN]	0.40(3)		2635.1(3)	$1^+ \rightarrow 2^+$	
1677.7(4) [aN]	e	−1.2(3)	3607.8(3)	$3^+(2^+) \rightarrow 3^+$	M1/E2
1705.9(3)	0.287(18)		2282.3(3)	$7^+ \rightarrow 5^+$	E2
1706.4(3) [aN]	0.32(3)	−0.17(17)	4011.6(3)	$2^+(1^+, 3^+) \rightarrow 2^+(3^+)$	M1/E2
1729.6(4) [aN]	e		4086.9(4)	$(1^+, 0^+, 2^+) \rightarrow 1^+$	
1758.9(3) [a]	1.1(4)		2729.1(3)	$1^+ \rightarrow 2^+$	
1765.4(4) [aN]	0.27(4)		2774.3(3)	$4^+(3^+, 5^+) \rightarrow 5^+$	
1771.9(3) [a]	4.2(5)		1930.3(2)	$3^+ \rightarrow 3^+$	
1776.9(5) [aN]	e		4134.1(3)	$1^+, 2^+ \rightarrow 1^+$	
1777.9(4) [aN]	e		3708.0(3)	$2^+, 3^+ \rightarrow 3^+$	
1780.1(3) [aN]	0.45(3)		2609.7(3)	$3^+ \rightarrow 4^+$	
1795.1(3) [a]	0.48(3)		2371.5(3)	$6^+ \rightarrow 5^+$	
1805.0(10) [aN]	0.48(4)	−0.11(7)	3255.1(3)	$1^-(1^+) \rightarrow 0^+$	E1 or M1
1806.1(3) [a]	1.13(12)		3526.4(3)	$0^+ \rightarrow 1^+$	
1806.1(6) [aN]	0.15(6)		3866.1(3)	$1^+, 2^+(3^+) \rightarrow 2^+$	
1813.2(4) [aN]	0.084(8)	−0.5(2)	2927.5(3)	$4^+(2^+) \rightarrow 3^+$	M1/E2
1817.3(4) [aN]	0.20(2)		2647.3(3)	$4^+(2^+) \rightarrow 4^+$	
1856.4(3) [N]	0.090(8)		2970.7(3)	$2^+ \rightarrow 3^+$	
1865.3(4) [aN]	0.19(2)		2835.7(4)	$2^+(1^+, 3^+) \rightarrow 2^+$	
1865.9(6) [aN]	e		3925.4(3)	$2^+, 3^+ \rightarrow 2^+$	
1877.9(3) [a]	0.74(5)		3597.9(3)	$0^+ \rightarrow 1^+$	
1892.8(3) [a]	2.04(12)		2469.3(3)	$4^+(3^+, 5^+) \rightarrow 5^+$	

[a] γ-ray with Doppler shift.
[b] γ-ray possibly with Doppler shift.
[c] Not possible to determine whether the γ-ray suffer from Doppler effect or not.
[d] Impossible intensity determination.
[e] Only intensity relative to the gate (Not normalised intensity).
[N] γ-ray observed for the first time in this work.

Table 3.2 (Continued): γ-transitions observed in ^{56}Co in the ^{56}Fe(p,nγ)^{56}Co reaction at $E_p = 10$ MeV ordered by increasing E_γ value.

E_γ(keV)	I_γ	A_2	E^i_{level} (keV)	$J^\pi_i \rightarrow J^\pi_f$	Mult.
1895.8(6) [aN]	0.30(3)		4201.0(3)	$2^+, 1^+, 3^+ \rightarrow 2^+(3^+)$	
1901.7(3) [a]	6.0(3)		2060.1(2)	$2^+ \rightarrow 3^+$	
1911.9(3) [aN]	0.164(11)		3362.5(3)	$2^+ \rightarrow 0^+$	E2
1926.7(4) [aN]	0.031(3)		3041.5(3)	$3^+, 5^+(4^+) \rightarrow 3^+$	
1944.5(3) [aN]	0.74(4)		2774.3(3)	$4^+(3^+, 5^+) \rightarrow 4^+$	
1982.4(4) [aN]	0.142(11)	−0.6(3)	3432.5(3)	$1^+ \rightarrow 0^+$	M1
1994.7(8) [aN]	e		4283.7(3)	$3^+(4^+, 2^+, 3-) \rightarrow 3^+$	
1995.0(5) [aN]	0.18(7)		3925.4(3)	$2^+, 3^+ \rightarrow 3^+$	
2000.2(3) [N]	0.38(3)		2970.7(3)	$2^+ \rightarrow 2^+$	
2024.6(4) [N]	0.041(4)		3139.2(3)	$3^+ \rightarrow 3^+$	
2032.8(5) [aN]	0.15(3)		3041.5(3)	$3^+, 5^+(4^+) \rightarrow 5^+$	
2044.4(3) [aN]	0.57(3)	−0.61(9)	3495.2(3)	$1^+ \rightarrow 0^+$	M1
2059.5(3) [bN]	0.33(5)		3068.8(3)	$3^+, 4^+ \rightarrow 5^+$	
2066.2(3) [a]	2.50(13)		2224.5(3)	$2^+ \rightarrow 3^+$	
2075.0(3) [N]	e		4005.5(3)	$3^+ \rightarrow 3^+$	
2098.0(6) [aN]	0.14(2)		2927.5(3)	$4^+(2^+) \rightarrow 4^+$	
2105.5(4) [a]	0.24(2)		3075.7(3)	$1^+ \rightarrow 2^+$	
2128.2(5) [aN]	e		4058.6(3)	$4^+(4^-, 5^+, 3^+) \rightarrow 3^+$	
2131.4(3)	1.94(10)	0.22(4)	2289.7(3)	$3^+ \rightarrow 3^+$	M1/E2
2143.1(4) [aN]	0.21(8)		4203.2(4)	$2^+, 1^+, 1^- \rightarrow 2^+$	
2145.6(4) [aN]	0.41(4)		3866.1(3)	$1^+, 2^+(3^+) \rightarrow 1^+$	
2146.4(3) [a]	5.3(3)	0.07(3)	2305.1(3)	$2^+(3^+) \rightarrow 3^+$	M1/E2
2151.9(10) [bN]	e		4441.2(5)	$3^+(4^+) \rightarrow 3^+$	
2168.9(3) [N]	2.07(11)	0.19(4)	3139.2(3)	$3^+ \rightarrow 2^+$	M1/E2
2198.1(4) [a]	0.19(2)		2774.3(3)	$4^+(3^+, 5^+) \rightarrow 5^+$	
2199.2(3) [a]	2.61(14)		2357.3(3)	$1^+ \rightarrow 3^+$	E2

[a] γ-ray with Doppler shift.
[b] γ-ray possibly with Doppler shift.
[c] Not possible to determine whether the γ-ray suffer from Doppler effect or not.
[d] Impossible intensity determination.
[e] Only intensity relative to the gate (Not normalised intensity).
[N] γ-ray observed for the first time in this work.

Table 3.2 (Continued): γ-transitions observed in ^{56}Co in the ^{56}Fe(p,nγ)^{56}Co reaction at $E_p = 10$ MeV ordered by increasing E_γ value.

E_γ(keV)	I_γ	A_2	E^i_{level} (keV)	$J^\pi_i \rightarrow J^\pi_f$	Mult.
2206.7(4) [bN]	0.49(3)		3176.8(3)	$1^+, 3^+ \rightarrow 2^+$	
2211.6(3) [aN]	1.04(6)		3041.5(3)	$3^+, 5^+(4^+) \rightarrow 4^+$	
2231.5(4) [aN]	0.181(15)		3061.0(3)	$3^+(5^+) \rightarrow 4^+$	
2238.9(4) [bN]	0.154(14)		3068.8(3)	$3^+, 4^+ \rightarrow 4^+$	
2239.4(5) [aN]	0.10(4)		4299.4(3)	$3^+(2^+, 4^+, 3-) \rightarrow 2^+$	
2247.8(3) [aN]	0.065(6)	0.14(12)	3362.5(3)	$2^+ \rightarrow 3^+$	M1/E2
2262.6(3) [aN]	0.25(2)	−0.37(7)	3377.2(3)	$2^+ \rightarrow 3^+$	M1/E2
2284.7(3) [aN]	2.21(12)	−0.17(5)	3255.1(3)	$1^-(1^+) \rightarrow 2^+$	E1 or M1/E2
2289.5(3) [c]	2.68(19)		2289.7(3)	$3^+ \rightarrow 4^+$	
2305.1(4) [b]	2.4(3)		2305.1(3)	$2^+(3^+) \rightarrow 4^+$	
2319.3(12) [aN]	0.12(5)		4379.4(5)	$2^+, 3^+(4^+) \rightarrow 2^+$	
2368.9(3) [aN]	0.48(3)	0.21(10)	3339.6(3)	$2^+ \rightarrow 2^+$	M1/E2
2369.1(4) [aN]	e	0.0(3)	4299.4(3)	$3^+(2^+, 4^+, 3^-) \rightarrow 3^+$	
2371.6(5) [bN]	0.50(10)		2371.5(3)	$6^+ \rightarrow 4^+$	E2
2392.3(3) [aN]	0.62(4)	−0.06(8)	3362.5(3)	$2^+ \rightarrow 2^+$	M1/E2
2395.4(5) [aN]	0.030(3)		3510.3(3)	$4^+(3^+) \rightarrow 3^+$	
2405.0(3) [aN]	0.78(4)		3234.4(3)	$4^+(3^+) \rightarrow 4^+$	
2407.1(3) [aN]	1.02(6)	0.02(1)	3377.2(3)	$2^+ \rightarrow 2^+$	M1/E2
2410.0(4) [aN]	0.027(3)		3524.6(3)	$2^+, 3^+, 4^+(2-, 3-, 1^+) \rightarrow 3^+$	
2413.8(3) [aN]	0.75(5)	−0.50(15)	4134.1(3)	$1^+, 2^+ \rightarrow 1^+$	
2451.3(3) [a]	1.33(7)	0.10(5)	2609.7(3)	$3^+ \rightarrow 3^+$	M1/E2
2462.0(3) [aN]	1.23(7)		3432.5(3)	$1^+ \rightarrow 2^+$	
2465.0(4) [aN]	0.25(2)		3041.5(3)	$3^+, 5^+(4^+) \rightarrow 5^+$	
2469.6(5) [cN]	d		2469.3(3)	$4^+(3^+, 5^+) \rightarrow 4^+$	
2485.1(5) [aN]	0.155(14)		3061.0(3)	$3^+(5^+) \rightarrow 5^+$	

[a] γ-ray with Doppler shift.
[b] γ-ray possibly with Doppler shift.
[c] Not possible to determine whether the γ-ray suffer from Doppler effect or not.
[d] Impossible intensity determination.
[e] Only intensity relative to the gate (Not normalised intensity).
[N] γ-ray observed for the first time in this work.

Table 3.2 (Continued): γ-transitions observed in ^{56}Co in the ^{56}Fe(p,nγ)^{56}Co reaction at $E_p = 10$ MeV ordered by increasing E_γ value.

E_γ(keV)	I_γ	A_2	E^i_{level} (keV)	$J^\pi_i \rightarrow J^\pi_f$	Mult.
2489.0(3) [a]	1.10(6)	−1.12(8)	2647.3(3)	$4^+(2^+) \rightarrow 3^+$	M1/E2
2492.7(4) [bN]	0.27(2)		3068.8(3)	$3^+, 4^+ \rightarrow 5^+$	
2493.3(4) [aN]	0.018(3)		3607.8(3)	$3^+(2^+) \rightarrow 3^+$	
2505.2(3) [aN]	0.36(3)		4225.4(3)	$(1^+, 0^+, 2^+) \rightarrow 1^+$	
2507.8(3) [a]	2.02(11)	0.22(4)	2666.2(3)	$3^+ \rightarrow 3^+$	M1/E2
2525.0(3) [aN]	0.43(3)		3495.2(3)	$1^+ \rightarrow 2^+$	
2592.6(3) [aN]	0.070(6)	−0.16(17)	3707.0(3)	$3^+(5^+) \rightarrow 3^+$	
2615.1(4) [aN]	0.22(2)		3585.4(3)	$2^+ \rightarrow 2^+$	
2637.5(4) [aN]	0.28(2)		3607.8(3)	$3^+(2^+) \rightarrow 2^+$	
2646.2(5) [aN]	0.106(18)		4366.4(5)	$(1^+, 0^+, 2^+) \rightarrow 1^+$	
2647.4(3) [bN]	1.28(4)		2647.3(3)	$4^+(2^+) \rightarrow 4^+$	
2657.7(3) [aN]	0.30(2)		3234.4(3)	$4^+(3^+) \rightarrow 5^+$	
2666.2(3) [aN]	1.86(6)		2666.2(3)	$3^+ \rightarrow 4^+$	
2679.9(3) [aN]	0.128(11)	0.46(10)	3794.4(3)	$3^+, 3^-(4^+) \rightarrow 3^+$	
2680.7(3) [aN]	0.89(5)		3510.3(3)	$4^+(3^+) \rightarrow 4^+$	
2697.6(3) [aN]	0.26(4)	0.6(2)	3707.0(3)	$3^+(5^+) \rightarrow 5^+$	
2737.2(3) [aN]	1.11(6)		3708.0(3)	$2^+, 3^+ \rightarrow 2^+$	
2752.5(3) [aN]	0.228(15)		4203.2(3)	$2^+, 1^+, 1^- \rightarrow 0^+$	
2759.2(5) [aN]	0.22(2)		3589.4(3)	$5^+, 4^+, (5^-, 4^-) \rightarrow 4^+$	
2768.9(3) [aN]	2.40(13)		2927.5(3)	$4^+(2^+) \rightarrow 3^+$	
2782.0(7) [aN]	0.070(10)		3791.7(3)	$6^+, 6- \rightarrow 5^+$	
2812.6(3) [N]	1.70(9)	0.07(4)	2970.7(3)	$2^+ \rightarrow 3^+$	M1/E2
2816.1(5) [aN]	0.043(5)		3930.7(3)	$3^+, 2^+, 4^+ \rightarrow 3^+$	
2877.4(4) [aN]	0.163(15)		3707.0(3)	$3^+(5^+) \rightarrow 4^+$	
2883.2(3) [aN]	1.74(9)	0.28(5)	3041.5(3)	$3^+, 5^+(4^+) \rightarrow 3^+$	
2885.9(3) [aN]	0.20(3)		3895.1(3)	$4^+, 5^+(3^+, 4^-) \rightarrow 5^+$	

[a] γ-ray with Doppler shift.
[b] γ-ray possibly with Doppler shift.
[c] Not possible to determine whether the γ-ray suffer from Doppler effect or not.
[d] Impossible intensity determination.
[e] Only intensity relative to the gate (Not normalised intensity).
[N] γ-ray observed for the first time in this work.

Table 3.2 (Continued): γ-transitions observed in ^{56}Co in the ^{56}Fe(p,nγ)^{56}Co reaction at $E_p = 10$ MeV ordered by increasing E_γ value.

E_γ(keV)	I_γ	A_2	E^i_{level} (keV)	$J^\pi_i \rightarrow J^\pi_f$	Mult.
2902.3(3) [aN]	0.45(3)	−1.05(15)	3872.6(3)	$3^+(2^+) \rightarrow 2^+$	M1/E2
2902.4(3) [aN]	0.33(5)	−0.13(10)	3061.0(3)	$3^+(5^+) \rightarrow 3^+$	M1/E2
2910.5(3) [bN]	0.72(11)	−0.61(16)	3068.8(3)	$3^+, 4^+ \rightarrow 3^+$	M1/E2
2922.2(3) [aN]	0.236(15)	−0.54(16)	4372.9(3)	$1^+ \rightarrow 0^+$	M1
2964.6(3) [aN]	0.30(2)		3794.4(3)	$3^+, 3^-(4^+) \rightarrow 4^+$	
2969.3(5) [aN]	0.112(12)		3545.7(5)	$7^+ \rightarrow 5^+$	E2
2980.7(3) [N]	2.10(11)	−0.21(4)	3139.2(3)	$3^+ \rightarrow 3^+$	M1/E2
3013.1(3) [aN]	0.68(4)		3589.4(3)	$5^+, 4^+, (5^-, 4^-) \rightarrow 5^+$	
3041.5(3) [aN]	0.39(2)	−0.39(10)	4011.6(3)	$2^+(1^+, 3^+) \rightarrow 2^+$	M1/E2
3042.0(10) [cN]	d		3041.5(3)	$3^+, 5^+(4^+) \rightarrow 4^+$	
3049.4(4) [aN]	0.16(3)		4058.6(3)	$4^+(4^-, 5^+, 3^+) \rightarrow 5^+$	
3059.3(4) [aN]	0.22(2)	0.7(2)	4029.3(3)	$2^+ \rightarrow 2^+$	M1/E2
3061.0(10) [cN]	0.10(9)		3061.0(3)	$3^+(5^+) \rightarrow 4^+$	
3076.2(3) [aN]	0.49(3)	0.09(8)	3234.4(3)	$4^+(3^+) \rightarrow 3^+$	M1/E2
3139.9(3) [aN]	0.35(2)	−0.21(10)	3298.2(3)	$4^+ \rightarrow 3^+$	M1/E2
3199.2(6) [aN]	0.084(14)		4029.3(3)	$2^+(4^+) \rightarrow 4^+$	
3220.4(3) [aN]	1.05(6)	0.41(6)	3379.0(3)	$3^+ \rightarrow 3^+$	M1(+E2)
3230.9(3) [aN]	0.520(10)	0.04(8)	4201.0(3)	$2^+, 1^+, 3^+ \rightarrow 2^+$	M1/E2
3297.5(10) [aN]	0.38(9)		3298.2(3)	$4^+ \rightarrow 4^+$	
3313.0(4) [aN]	0.135(12)		4283.7(3)	$3^+(4^+, 2^+, 3^-) \rightarrow 2^+$	
3318.9(3) [aN]	0.36(2)		3895.1(3)	$4^+, 5^+(3^+, 4^-) \rightarrow 5^+$	
3328.8(4) [aN]	0.100(10)		4299.4(3)	$3^+(2^+, 4^+, 3^-) \rightarrow 2^+$	
3352.1(3) [aN]	0.216(15)	0.96(17)	3510.3(3)	$4^+(3^+) \rightarrow 3^+$	M1/E2
3427.3(3) [aN]	0.220(15)	−1.06(4)	3585.4(3)	$2^+ \rightarrow 3^+$	M1/E2
3449.3(3) [aN]	0.59(3)	−0.11(7)	3607.8(3)	$3^+(2^+) \rightarrow 3^+$	M1/E2
3469.7(6) [aN]	0.065(9)		4299.4(3)	$3^+(2^+, 4^+, 3^-) \rightarrow 4^+$	

[a] γ-ray with Doppler shift.
[b] γ-ray possibly with Doppler shift.
[c] Not possible to determine whether the γ-ray suffer from Doppler effect or not.
[d] Impossible intensity determination.
[e] Only intensity relative to the gate (Not normalised intensity).
[N] γ-ray observed for the first time in this work.

Table 3.2 (Continued): γ-transitions observed in ^{56}Co in the ^{56}Fe(p,nγ)^{56}Co reaction at $E_p = 10$ MeV ordered by increasing E_γ value.

E_γ(keV)	I_γ	A_2	E^i_{level} (keV)	$J^\pi_i \rightarrow J^\pi_f$	Mult.
3482.3(3) [aN]	0.27(2)		4058.6(3)	$4^+(4^-, 5^+, 3^+) \rightarrow 5^+$	
3549.4(3) [aN]	0.98(7)	−0.20(6)	3708.0(3)	$2^+, 3^+ \rightarrow 3^+$	M1/E2
3636.1(3) [aN]	0.88(6)	0.44(5)	3794.4(3)	$3^+, 3^-(4^+) \rightarrow 3^+$	
3651.4(3) [aN]	1.62(11)	−0.16(5)	3809.7(3)	$4^+(3^+, 2^+) \rightarrow 3^+$	M1/E2
3713.9(4) [aN]	0.202(14)		3872.5(3)	$3^+(2^+) \rightarrow 3^+$	
3736.7(3) [aN]	0.28(2)		3895.1(3)	$4^+, 5^+(3^+, 4^-) \rightarrow 3^+$	
3767.7(3) [aN]	0.31(2)		3925.7(3)	$2^+, 3^+ \rightarrow 3^+$	
3809.0(10) [cN]	0.18(5)		3809.7(3)	$4^+(3^+, 2^+) \rightarrow 4^+$	
3847.4(4) [N]	0.19(2)		4005.5(3)	$3^+ \rightarrow 3^+$	
3873.0(10) [cN]	0.25(4)		3872.5(3)	$3^+(2^+) \rightarrow 4^+$	
3894.0(10) [cN]	0.25(4)		3895.1(3)	$4^+, 5^+(3^+, 4^-) \rightarrow 4^+$	
3900.3(3) [aN]	0.163(13)		4058.6(3)	$4^+(4^-, 5^+, 3^+) \rightarrow 3^+$	
3930(2) [cN]	d		3930.7(3)	$3^+, 2^+, 4^+ \rightarrow 4^+$	
4019.6(4) [aN]	0.119(11)		4177.9(3)	$4^+(3^+, 4^-, 3^-) \rightarrow 3^+$	
4029.0(10) [cN]	d		4029.3(3)	$2^+ \rightarrow 4^+$	E2
4054.9(4) [aN]	0.133(11)		4213.2(4)	$4^+(3^+, 4^-, 3^-) \rightarrow 3^+$	
4058.0(10) [cN]	0.20(5)		4058.6(3)	$4^+(4^-, 5^+, 3^+) \rightarrow 4^+$	
4125.5(3) [aN]	0.23(2)		4283.7(3)	$3^+(4^+, 2^+, 3^-) \rightarrow 3^+$	
4141.5(4) [aN]	0.171(12)		4299.42(30)	$3^+(2^+, 4^+, 3^-) \rightarrow 3^+$	
4177.8(5) [aN]	0.44(8)		4177.9(3)	$4^+(3^+, 4^-, 3^-) \rightarrow 4^+$	
4213.0(10) [cN]	d		4213.2(3)	$4^+(3^+, 4^-, 3^-) \rightarrow 4^+$	
4221.1(5) [aN]	0.100(10)		4379.4(5)	$2^+, 3^+(4^+) \rightarrow 3^+$	
4282(2) [cN]	0.22(5)		4283.7(3)	$3^+(4^+, 2^+, 3^-) \rightarrow 4^+$	
4282.8(5) [aN]	0.187(16)		4441.2(5)	$3^+(4^+) \rightarrow 3^+$	
4441(2) [cN]	d		4441.2(5)	$3^+(4^+) \rightarrow 4^+$	

[a] γ-ray with Doppler shift.
[b] γ-ray possibly with Doppler shift.
[c] Not possible to determine whether the γ-ray suffer from Doppler effect or not.
[d] Impossible intensity determination.
[e] Only intensity relative to the gate (Not normalised intensity).
[N] γ-ray observed for the first time in this work.

3.1.1 Determination of the level energy precision

In order to associate an uncertainty with the level energies (E_{level}) obtained with the *Eleven* code (see Appendix D) and presented in Table 3.1, we compared them with the previously reported values in the literature [47]. The differences between the reported value and the experimental E_{level}, as a function of the excitation energy, are shown in Fig. 3.4. The comparison has been made only for those cases with high precision in literature, i.e., one or two decimal digits. The errors presented are the quadratic sum of the level uncertainties from [47] and the ones provided by the *Eleven* code. As can be observed, most of the excited states lie within 0.5 keV of deviation, except some single cases. These cases are analysed below:

- 2305.1-keV state: The level energy from compilation [47] is mainly based on the experiment from Ref. [29]. However we have observed that the γ-ray energies from that work seem to be overestimated. Our results match perfectly with the γ-ray values from Ref. [24].
- 2666.2-keV state: There is only one previously observed γ-transition for this state. In the present work two γ-rays have been observed giving consistent results. We conclude that our result is more reliable.
- 2729.1-keV state: In the present work we have observed the five previously known γ-rays that de-excite this level. They all give a very consistent E_{level} value.
- 3597.9-keV state: The level energy from compilation [47] is based on γ-rays only observed in work [29]. In Ref. [24] this state is not seen. There are no more references to compare with. According to comparisons of energies for other γ-rays, the γ-ray energies seem to be overestimated in Ref. [29].

In the majority of the levels used in the previous comparison, the uncertainties provided by the *Eleven* code are smaller than the ones reported in [47]. In light of the previous discussion and the difference values shown in Fig. 3.4 we decided to associate an uncertainty of 0.2 keV with the level energies up to 2 MeV and an uncertainty of 0.3 keV for higher ones, except in those cases where the *Eleven* code provided a higher error, in which case this value is used.

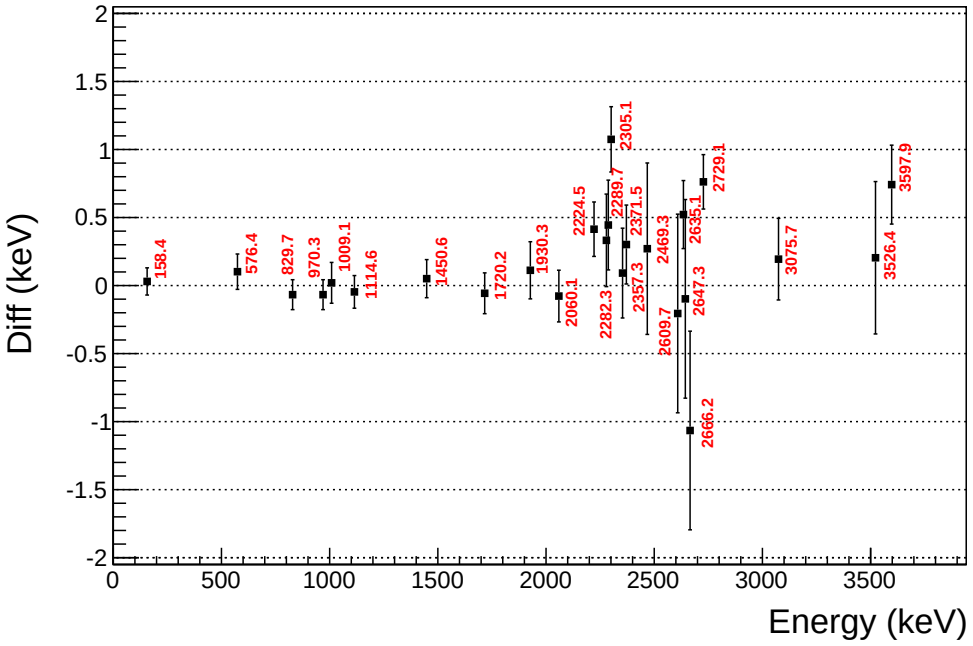

Figure 3.4: The differences between the level energies from Ref. [47] and the experimental E_{level} are shown. These differences are presented with an error which is the quadratic sum of the level uncertainties from [47] and those provided by the *Eleven* code. It can be observed that except for single cases (the states at 2305.1, 2666.2, 2729.1 and 3597.9 keV) the differences shown here lie within 0.5 keV. These single cases are discussed in the main text.

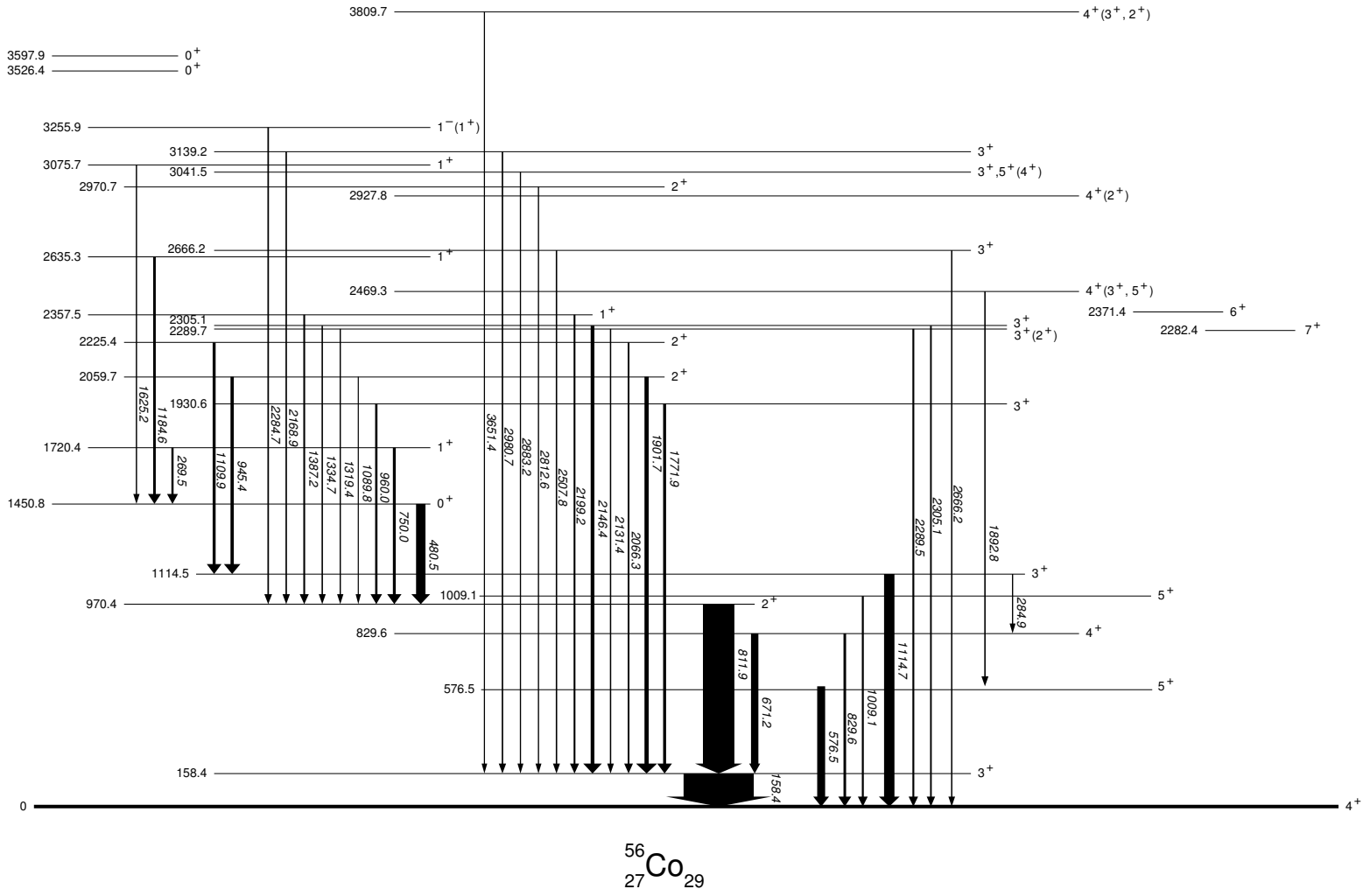

Figure 3.5: The level scheme of ^{56}Co is shown, where only the γ-transitions with $I_\gamma > 1.5\%$ are presented. The γ-rays and level energies are in keV. Note that in the scheme the first 6^+ and 7^+ experimental states are also presented, as are the two 0^+ states of interest (see main text), though their γ-transition intensities are below the threshold chosen in this scheme. This is in order to give an overview of the range of spins covered in the present work.

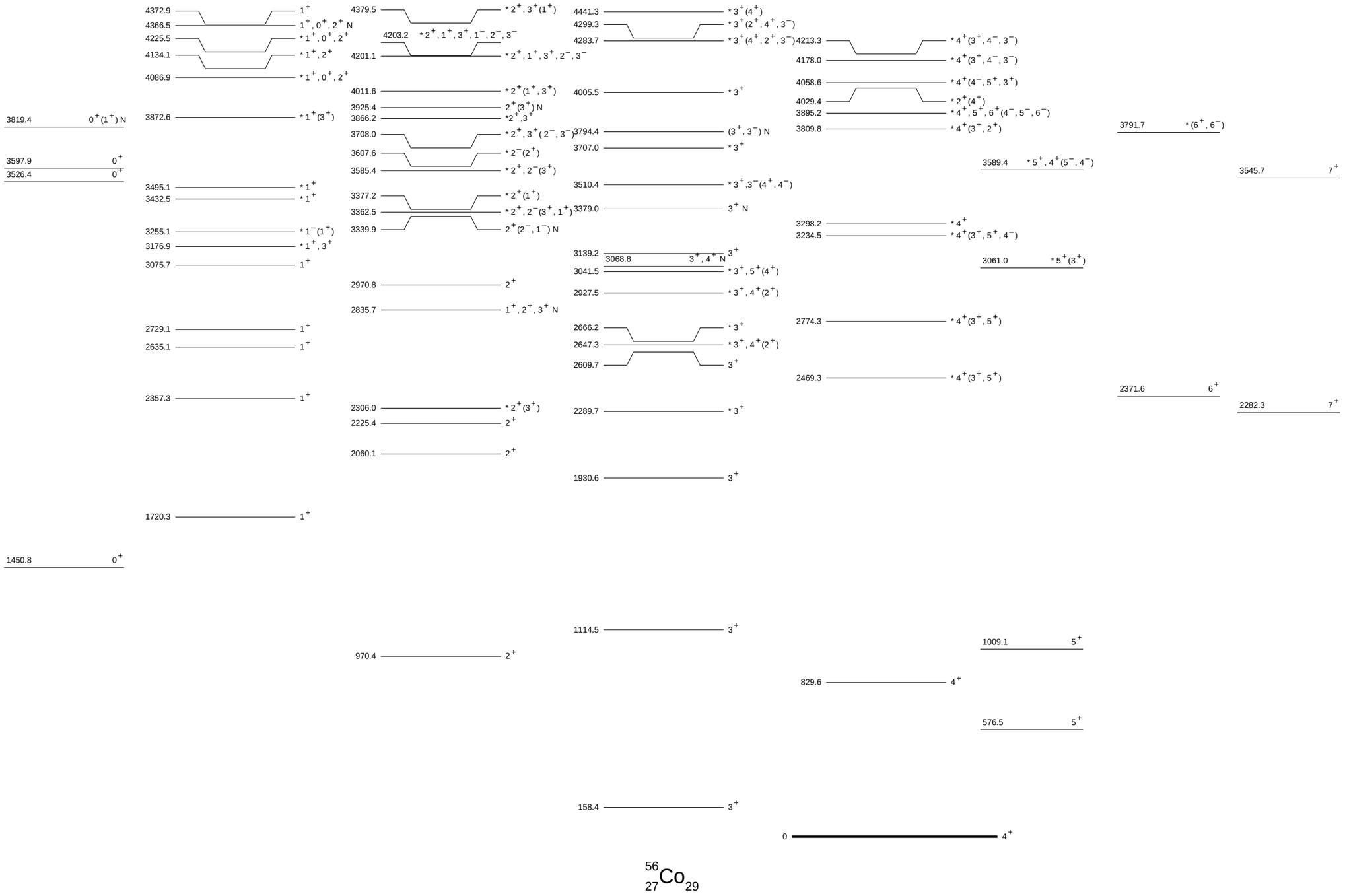

Figure 3.6: The excited nuclear states in ^{56}Co observed in this work and their spin-parity assignments are shown. The states are arranged in columns ordered by increasing spin value. An star (*) indicates new spin-parity assignment to a previously known level or previous ambiguity resolved. The symbol N stands for new level.

3.2 Angular distributions of γ-transitions

In this section we will present the information extracted from the angular distributions of γ-transitions $W(\theta_\gamma)$ obtained in this work. The details of how the angular distributions were obtained are explained in detail in section 2.3.3.

The $W(\theta_\gamma)$ distributions have been obtained for 53 of the γ-ray transitions observed in this work. Of special importance were the γ-transitions de-exciting excited states of unknown spin and parity values, since the angular distribution coefficients can be useful in assigning these quantities. The $W(\theta_\gamma)$ for most of the pure-multipole γ-transitions were also obtained. They constitute excellent cases for estimating the attenuation coefficient α_2 when the alignment of the excited state is incomplete, as in our case, since the coefficient A_2^{max} is known in these cases (see section 1.6.2).

The angular coefficients A_2 were obtained by fitting the $W(\theta_\gamma)$ functions to the expression given by Eq. 2.10, and were already presented in Table 3.2. As mentioned in section 2.3.3, the precision of the angular distributions was not accurate enough to obtain the A_4 coefficient. This was due to a combination of small alignment in the reaction together with the relatively large solid angle covered and some ambiguities introduced by the normalization procedure.

The multipolarity of the γ-transitions was deduced whenever possible. First, when the spins of the initial and final states (J_i and J_f) indicate a pure-multipole transition. A summary of the pure-multipole γ-transitions for which $W(\theta_\gamma)$ was obtained in this work is presented in Table 3.3. As mentioned above, the A_2^{max} is known in these cases and therefore the α_2 can be deduced for each partially-aligned excited state. The A_2^{max} values used to calculate the α_2 in the particular transitions presented in Table 3.3 are extracted from [48] and given below:

$J_i \rightarrow J_f$	A_2^{max}
$1 \rightarrow 0$	-1
$1 \rightarrow 3$	0.14286

On the other hand, in some other cases the multipolarity of the γ-transition could be deduced from the A_2 value, even if the J_i^π and J_f^π were ambiguous. In these cases the A_2 values obtained indicated that the γ-transitions have mixed multipolarity, though the parameter δ is unknown (see definition given by Eq. 1.6). These results were already presented in Table 3.2. The tabulated A_2 coefficients as a function of δ used to draw the previous conclusions were consulted in [49].

Due to the positive parity of most of the excited states observed, and according to the selection rules presented in section 1.6.1, most of the γ-transitions are pure M1 or E2 radiation, or a mixture of both (see Table 3.2).

We measured the angular distribution of 53 γ-transitions in the present work. In Fig. 3.7 we present the 30 most accurate ones, ordered by increasing γ-transition energy. Of special interest are the angular distributions of the 1184.6-keV (de-exciting the 2635.1-keV state) and 1625.2-keV (de-exciting the 3075.7-keV state) γ-rays. As presented in Chapter 1, one of the motivations of the present work was the study of the 2635.1- and 3075.7-keV states, for which doubts existed about the previously reported $J^\pi = 1^+$ value [2]. These two γ-rays correspond to transitions to the firm 1450.6-keV 0^+ level. In both cases we measured a clear $A_2 < 0$ angular coefficient, which confirms the M1 character of the transition and hence the $J^\pi = 1^+$ value of both initial states.

Table 3.3: The pure-multipole γ-transitions in ^{56}Co for which the angular distributions $W(\theta_\gamma)$ were obtained in this work. The angular coefficient A_2 of each transition and attenuation coefficient α_2 of the corresponding level are shown. The spin-parities of the initial and final states (J_i^π and J_f^π) and the corresponding multipolarity are presented.

E_{level} (keV)	E_γ (keV)	A_2	α_2	$J_i^\pi \rightarrow J_f^\pi$	Multipolarity
1720.2(2)	269.4(2)	−0.07(3)	0.07(3)	$1^+ \rightarrow 0^+$	M1
1720.2(2)	1562.1(3)	0.05(4)	0.4(3)	$1^+ \rightarrow 3^+$	E2
2635.1(3)	1184.6(3) [a]	−0.33(3)	0.33(3)	$1^+ \rightarrow 0^+$	M1
3075.7(3)	1625.2(3) [a]	−0.42(4)	0.42(4)	$1^+ \rightarrow 0^+$	M1
3255.1(3)	1805.0(10) [aN]	−0.11(7)	0.11(7)	$1^-(1^+) \rightarrow 0^+$	E1 or M1
3432.5(3)	1982.4(4) [aN]	−0.6(3)	0.6(3)	$1^+ \rightarrow 0^+$	M1
3495.2(3)	2044.4(3) [aN]	−0.61(9)	0.61(9)	$1^+ \rightarrow 0^+$	M1
4372.9(3)	2922.2(3) [aN]	−0.54(16)	0.54(16)	$1^+ \rightarrow 0^+$	M1

[a] γ-ray with Doppler shift.
[N] γ-ray observed for the first time in this work.

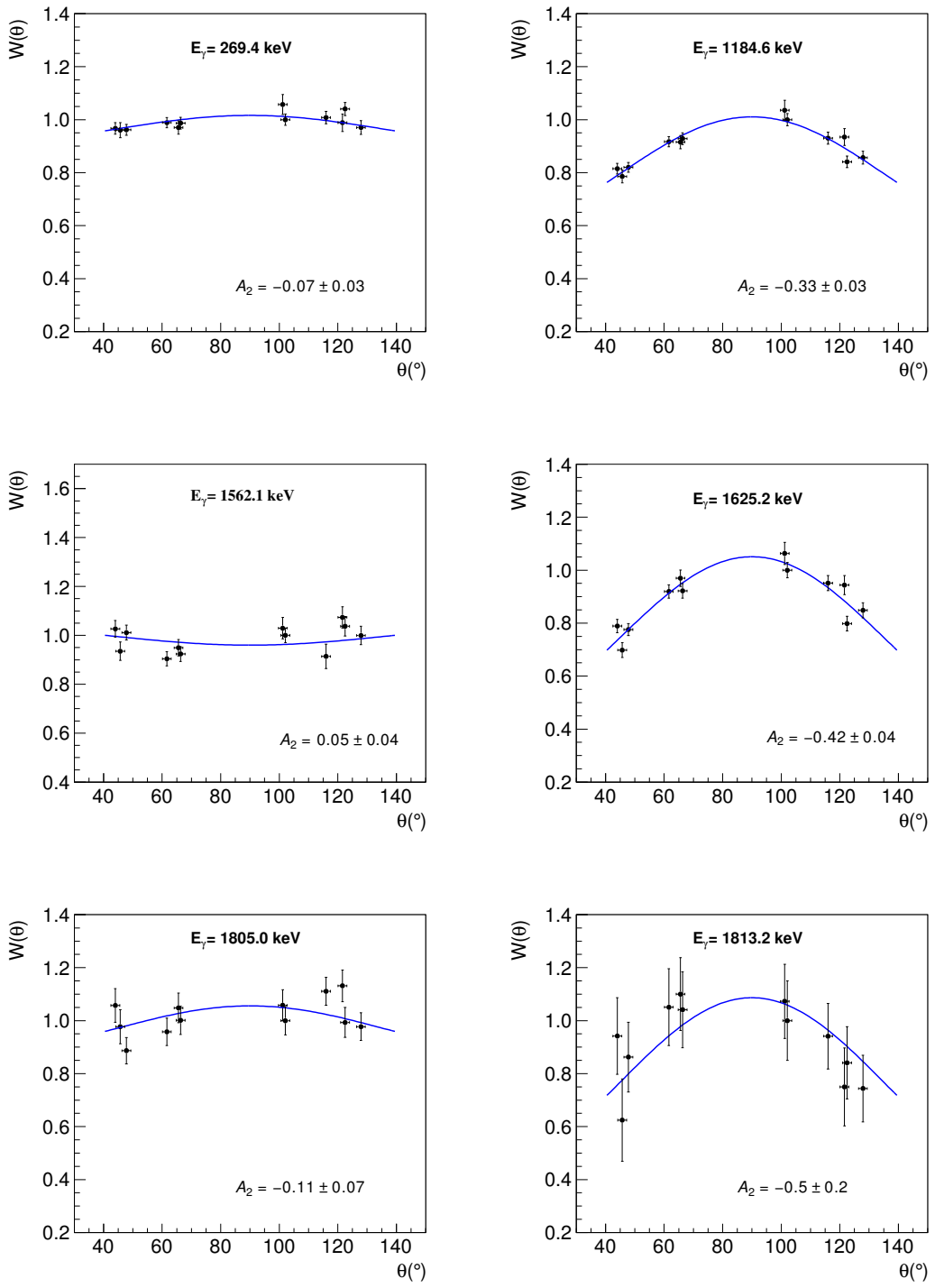

Figure 3.7: Angular distributions $W(\theta)$ of γ-rays depopulating excited states in ^{56}Co. The experimental points are fitted to the expression given by Eq. 2.10 (see main text). The $W(\theta)$ have been normalised to 1 at 102°. The angular coefficients A_2 are presented.

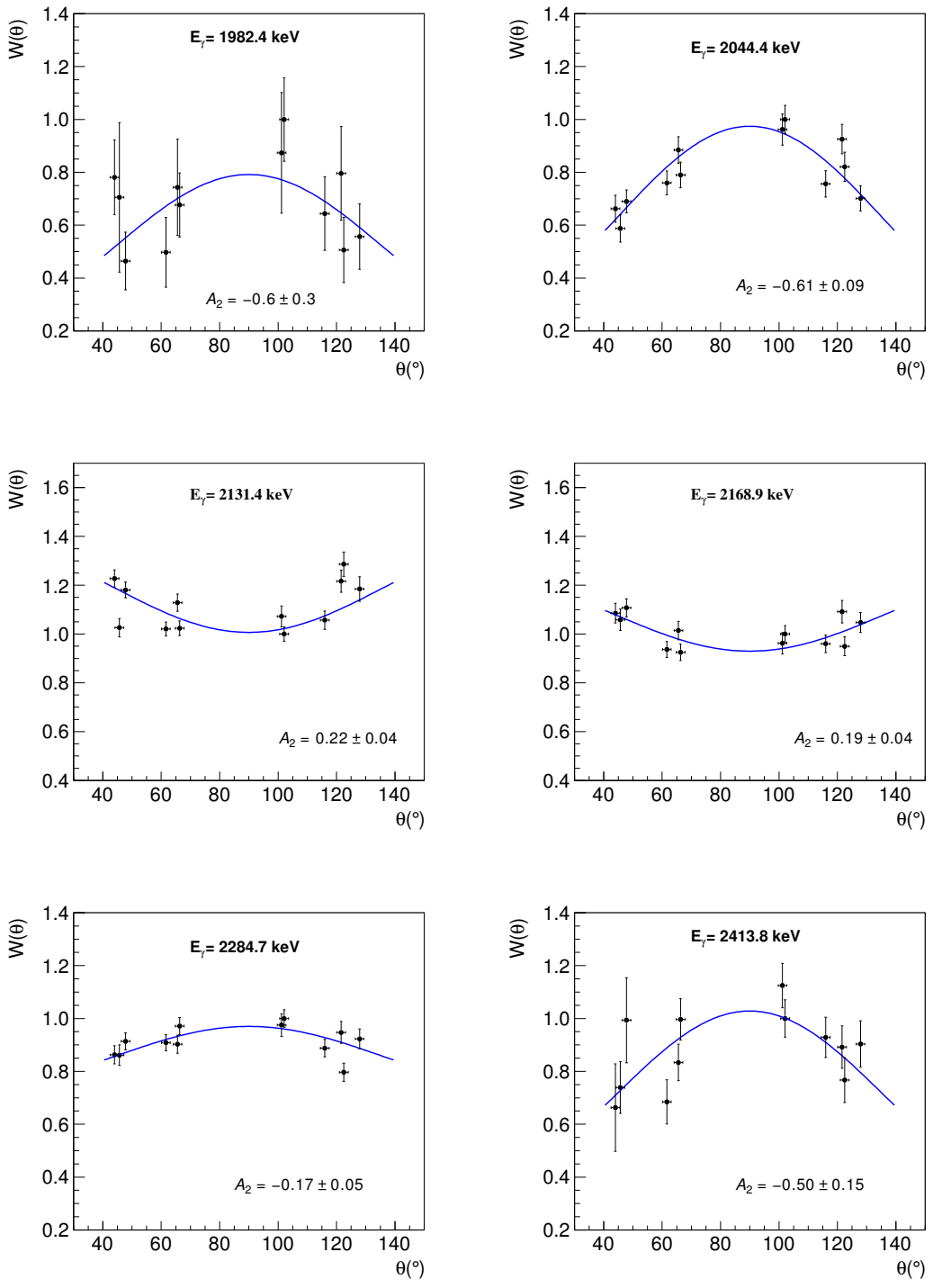

Figure 3.7: *(continued)* Angular distributions $W(\theta)$ of γ-rays depopulating excited states in ^{56}Co.

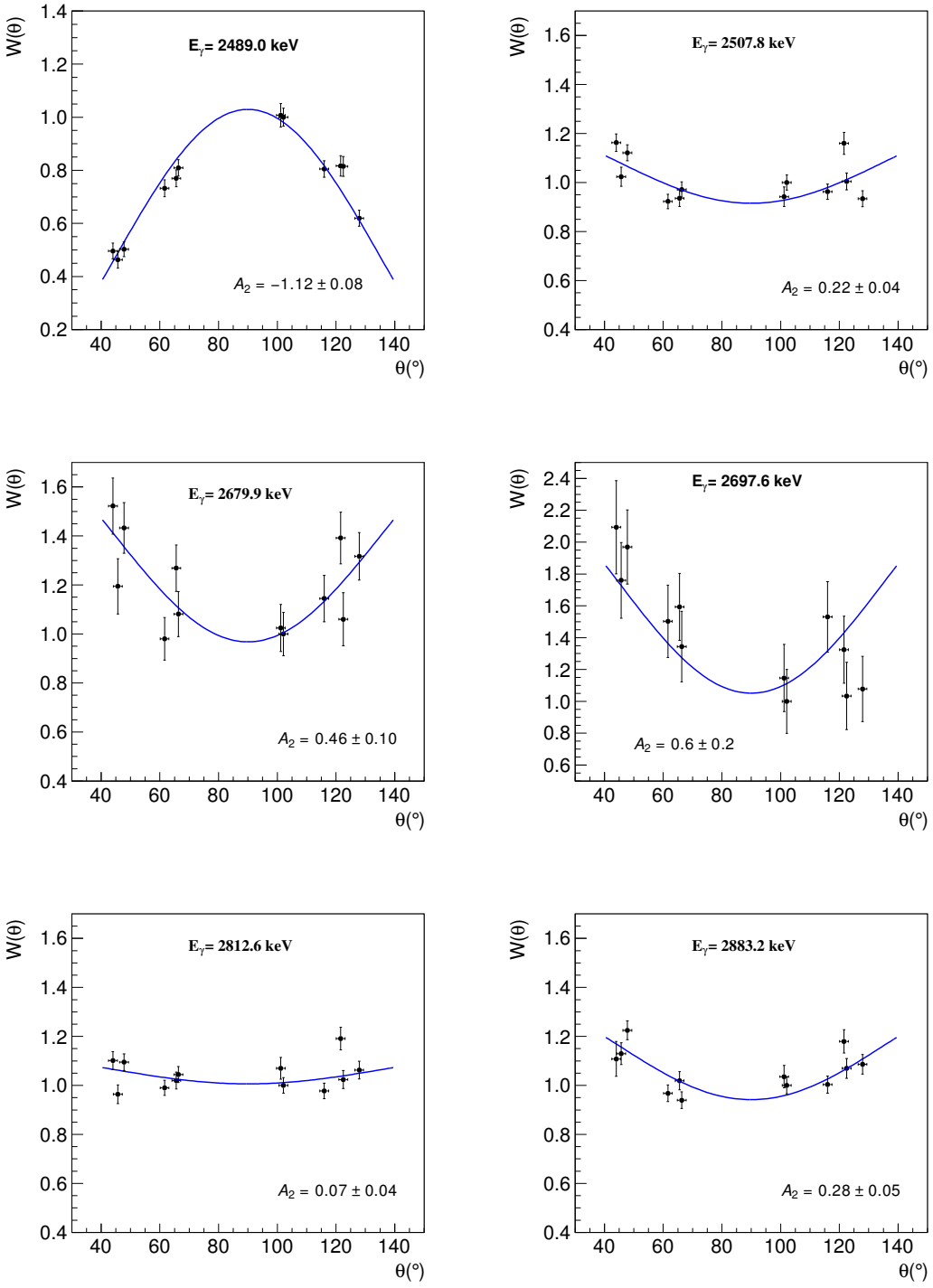

Figure 3.7: *(continued)* Angular distributions $W(\theta)$ of γ-rays depopulating excited states in ^{56}Co.

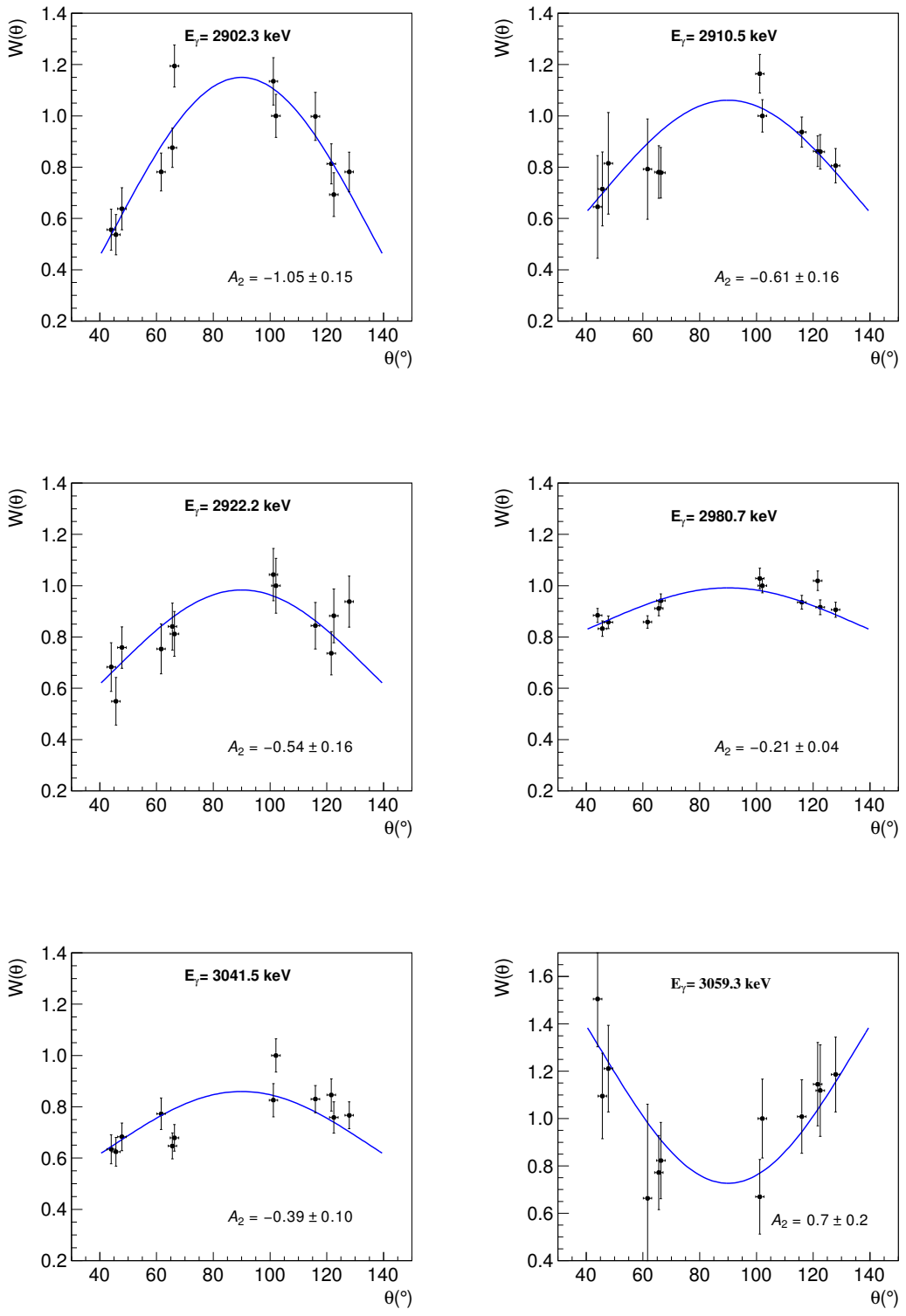

Figure 3.7: *(continued)* Angular distributions $W(\theta)$ of γ-rays depopulating excited states in ^{56}Co.

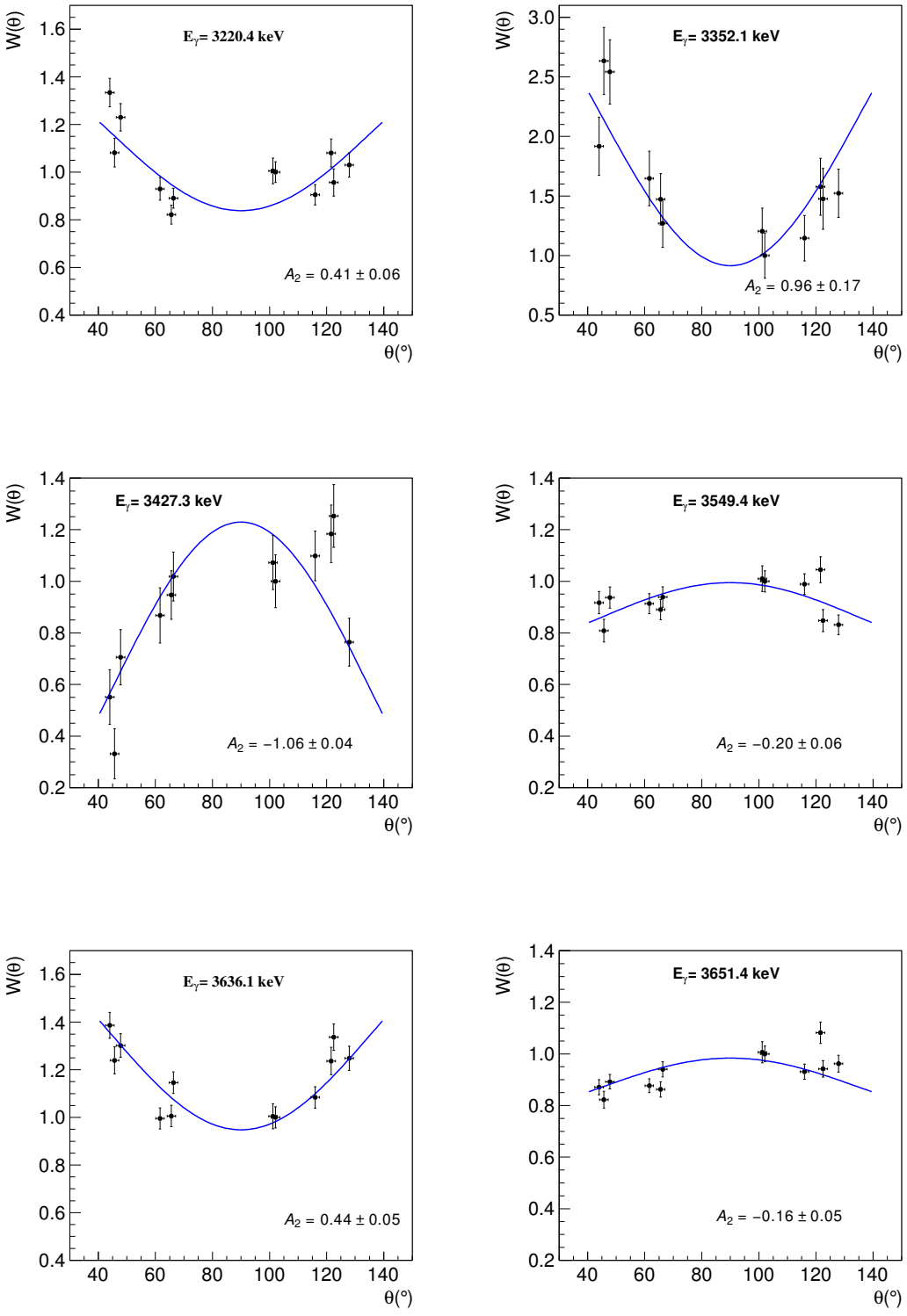

Figure 3.7: *(continued)* Angular distributions $W(\theta)$ of γ-rays depopulating excited states in ^{56}Co.

Chapter 4

Theoretical interpretation

4.1 Shell-model and excited states in ^{56}Co

4.1.1 Isospin symmetry

Symmetries are intimately related to conservation laws and to conserved quantities which, in quantum mechanics, translate into *good* quantum numbers. Isospin symmetry is one of the fundamental symmetries in nuclear physics and is related to the identical behaviour of protons and neutrons in a nuclear field. It is a consequence of the almost perfect charge independence and charge symmetry of the attractive strong nucleon-nucleon interaction. Obviously isospin symmetry is broken by the Coulomb force acting between protons. However additional isospin non-conserving (INC) forces exist although in general they are smaller than the Coulomb terms. These isospin-breaking terms are, apart from the Coulomb multipole contributions (V_{CM}), the electromagnetic spin-orbit coupling (V_{Cls}), isovector matrix elements (V_{BM}), strong charge-asymmetry and charge-independence-breaking interactions, amongst others [50, 51]. The isospin breaking induces impurities in the wave functions that affect the β decay [52, 53] and the properties of the isobaric analogue state [54].

In the present section we will present the shell-model calculations performed to interpret the results of this work. First we will discuss the low-lying states. In section 4.2 we will focus on the study of the γ-decay of the two isospin-mixed 0^+ states in ^{56}Co which were one of the main motivations of the present work, and we will compare the experimental results with the predictions.

4.1.2 Shell-model calculations and effective interactions

The experimental results can be compared with theoretical predictions in order to interpret the results and/or check the theoretical descriptions. In the present case we will use the Shell Model as the main theoretical approach to interpreting the results. The theoretical shell-model calculations provide us with energy spectra, electromagnetic transitions and moments of the individual states.

Shell-model calculations in a truncated *fp*-shell valence space were carried out. A variety of effective interactions have been, and continue to be, developed to describe different mass regions in the table of isotopes. They are intimately related to the choice of the valence space. The $1f_{7/2}$ shell, between the doubly magic nuclei ^{40}Ca and ^{56}Ni, constitutes a very special case, as it can be considered to be an isolated shell. This simplistic approximation allows straightforward predictions to be made. However, it is clear that the $1f_{7/2}$ shell-model space is not sufficient to describe the spectroscopy of the nuclei of this region with good accuracy and that the *fp* orbitals $2p_{3/2}, 1f_{5/2}$ and $2p_{1/2}$ have to be taken into account in the calculations [50].

Since the magic numbers of Z and N (=28) provide a good core for ^{56}Ni, the majority of low-lying states in ^{56}Co can be described in terms of the one-particle-one-hole (1p-1h) configurations, i.e., $(1f_{7/2})^{-1}_{\pi} \times (2p_{3/2}, 1f_{5/2}, 2p_{1/2})^{1}_{\nu}$ (see Fig. 4.1). Indeed, this configuration space yields the $T = 1$ (the minimum T value in the $T_z = +1$ ^{56}Co nucleus), $J^{\pi} = 1^+, ..., 6^+$ states, and gives a good description for the low-lying states in ^{56}Co below E_x=1.5 MeV [55][56][57]. Meanwhile, core-excited configurations such as two-particle-two-holes (2p-2h) should be included to describe the 0^+ states in ^{56}Co. For this purpose, two-body effective interactions have to be used.

The most reliable two-body effective interactions in the full *fp* valence space for the descriptions of the $1f_{7/2}$-shell nuclei are FPD6 [58] and KB3G [59]. Another interaction, GXPF1a [60], which includes in part empirically adjusted two-body matrix elements, is also used to describe nuclei in the whole *fp* main shell. We hoped that these effective interactions will also work for ^{56}Co, just above the $1f_{7/2}$-shell. The core used in the calculations was the doubly magic $Z = N = 20$ ^{40}Ca nucleus.

For the present discussion large-scale shell-model calculations in a truncated *fp*-shell valence space have been performed using the NuShellX@MSU [61] and ANTOINE [62] shell-model codes with the effective interactions KB3G and GXPF1a. Neither KB3G nor GXPF1a interactions contain isospin-nonconserving terms in the nuclear interaction. In consequence, isospin mixing has to be introduced "a posteriori". Both effective interactions are *fp*-shell interactions, which implies that they exclude the $1g_{9/2}$ orbital. Thus negative parity states cannot be obtained in the calculations.

In the next section we will discuss the description of the low-lying states in ^{56}Co. Section 4.2 focuses on the discussion of the isospin-mixed 0^+ states and their γ-decay. For that purpose an improved version of the KB3G effective interaction, the KB3GR [63], was also used in the shell-model calculations.

4.1.3 Low-lying states in ^{56}Co

Large-scale shell-model calculations in a truncated *fp*-shell valence space have recently been performed by Edward Simpson [64] (Department of Nuclear Physics, Australian National University) using the NuShellX@MSU code and the effective

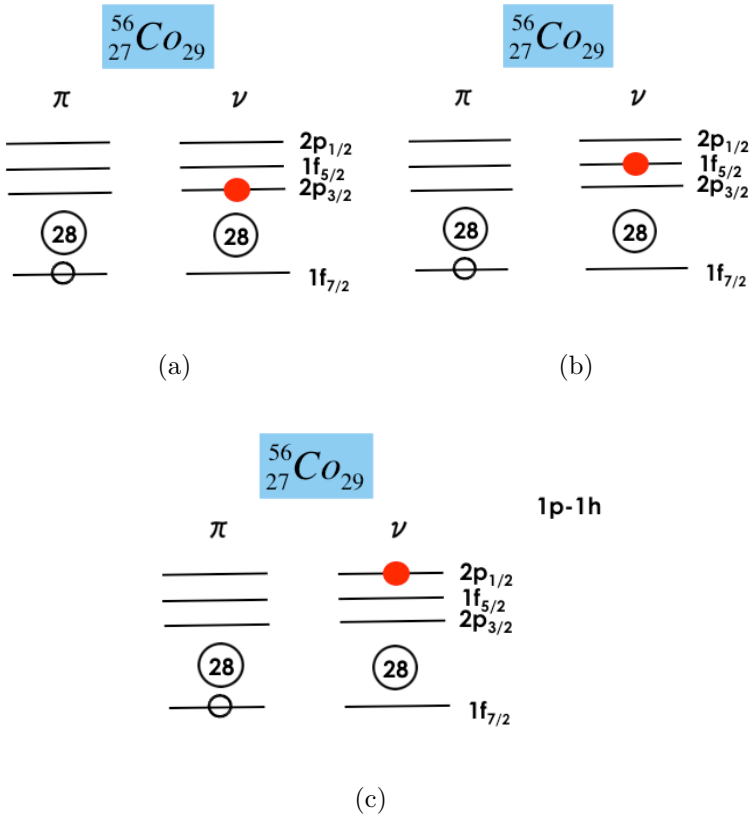

Figure 4.1: 1p-1h configurations in the *fp*-shell valence space, i.e., $(1f_{7/2})^{-1}_{\pi} \times (2p_{3/2}, 1f_{5/2}, 2p_{1/2})^{1}_{\nu}$ ((a), (b) and (c), respectively), that constitute the majority of low-lying states in ^{56}Co. This configuration space yields the $T = 1$, $J^{\pi} = 1^{+}, ..., 6^{+}$ states.

interactions KB3G and GXPF1a. A valence space of $q = 2$ (q is the minimum number of protons and neutrons that remain in the $1f_{7/2}$ shell) was used. Figure 4.3 shows the comparison between experimental levels and theoretical calculations. It can be observed that the KB3G predictions seem to be on an expanded scale with respect to experiment, while the GXPF1a interaction shows the opposite behaviour if we look above 1.5 MeV, i.e., the predicted levels are compressed in energy.

The identification of a state seen in the experiment with its theoretical counterpart is initially based on the energy and J^{π} values. To confirm this assignment a comparison of the observed and predicted γ-decay pattern and branching ratios was made. We have observed that there is a good agreement between the experimental γ-deexcitation of the low-lying states and the theoretical predictions up to approximately 2.5 MeV for spins J=3,4,5,6,7. However for 1^{+} and 2^{+} states the comparison begins to be difficult due to the increasing level density and the consequent possible mixing with neighbouring states, which is not taken into account in the calculations. This will be better understood when we discuss multiplet assignments (in next section). From 2.5 up to 3 MeV the tentative identifications were based exclusively on J^{π}

values. It should be noted that only 6 levels per spin were calculated. Thus, for energies higher than 3 MeV, any attempt at identification becomes impossible.

Multiplets

Shell-model calculations provide the final description of each individual state in terms of wave functions (or configurations). Then each state can be expressed as a linear combination of different configurations, with a certain probability for each.

In turn, in a same configuration the unpaired protons and neutrons (or eventually holes in the proton or in the neutron orbitals) can be coupled in different ways giving different final J^π values. Traditionally, the word "multiplet" is used to describe these states of different spin corresponding to the same configuration.

As explained previously in this chapter, low-lying states in ^{56}Co can be described by the 1p-1h configurations, i.e., $(1f_{7/2})^{-1}_\pi \times (2p_{3/2}, 1f_{5/2}, 2p_{1/2})^1_\nu$. In these cases, it is easy to identify which configuration should be dominant in the description of each state. Then we can identify the different J^π members of a certain multiplet considering the dominant configuration in the description of a given state. Figure 4.2(a) shows the experimental states which we identify as the main components of the three multiplets: $(1f_{7/2})^{-1}_\pi(2p_{3/2})^1_\nu$ (in red), $(1f_{7/2})^{-1}_\pi(1f_{5/2})^1_\nu$ (in green) and $(1f_{7/2})^{-1}_\pi(2p_{1/2})^1_\nu$ (in blue). It also shows the contribution of the calculated main configuration in each member of the multiplet and the comparison of the experimental energies with the shell-model calculations using the above mentioned KB3G and GXPF1a effective interactions (see Fig. 4.2(b)). A more detailed description of Fig. 4.2 is given below:

- Multiplet $(1f_{7/2})^{-1}_\pi(2p_{3/2})^1_\nu$: This multiplet is relatively pure.

- Multiplet $(1f_{7/2})^{-1}_\pi(1f_{5/2})^1_\nu$: A stronger fragmentation in terms of configuration mixing begins to occur when one goes up in energy. Then the main configuration becomes less dominant. In the case of the 1^+ states this fragmentation is evident and we find a small component of this multiplet distributed over a wide range of states. Table 4.1 shows how the 1^+ member of the $(1f_{7/2})^{-1}_\pi(1f_{5/2})^1_\nu$ multiplet fragments over the different 1^+ states. Notice how strongly this fragmentation depends on the interaction used. Then the experimental identification of the main 1^+ member of this multiplet is not possible. Column E^{exp}_{level} shows the experimental excited state identified with the corresponding 1^+_n level from calculations. This identification is based on the ordering of the observed 1^+ states and comparison between the γ-decay pattern of the theoretical and the experimental levels. Above 3 MeV, the identification becomes more difficult due to the increase in the level density, because there is a larger probability of mixing between individual states not taken into account in the calculations. Besides that, the branching ratio values from theoretical calculations are very sensitive to the effective interaction used.

- Multiplet $(1f_{7/2})^{-1}_\pi(2p_{1/2})^1_\nu$: Clear identification of the correspondence between

experimental and theoretical states. Purity remains high specially with the KB3G interaction.

Table 4.1: Fragmentation of the 1^+ member of the $(1f_{7/2})^{-1}_{\pi}(1f_{5/2})^{1}_{\nu}$ multiplet over the different predicted 1^+ states in the shell-model calculations using the NuShellX@MSU code with GXPF1a and KB3G effective interactions and truncation $q = 2$, where q is the minimum number of protons and neutrons that remain in the $1f_{7/2}$ shell. The identification with the corresponding experimental states is made.

	%		
J^{π}_{n}	GXPF1a	KB3G	$E^{\mathrm{exp}}_{\mathrm{level}}$ (keV)
1^+_1	0.0	1.7	1720.3
1^+_2	0.1	1.4	2357.3
1^+_3	0.0	5.2	2635.1
1^+_4	0.2	28.5	2729.1
1^+_5	0.0	4.9	3075.7
1^+_6	8.0	5.7	[a]

[a] Difficult identification between the theoretical 1^+_n state and the corresponding experimental excited state. The increase in the level density enhances the probability of mixing between individual states which is not taken into account in the calculations.

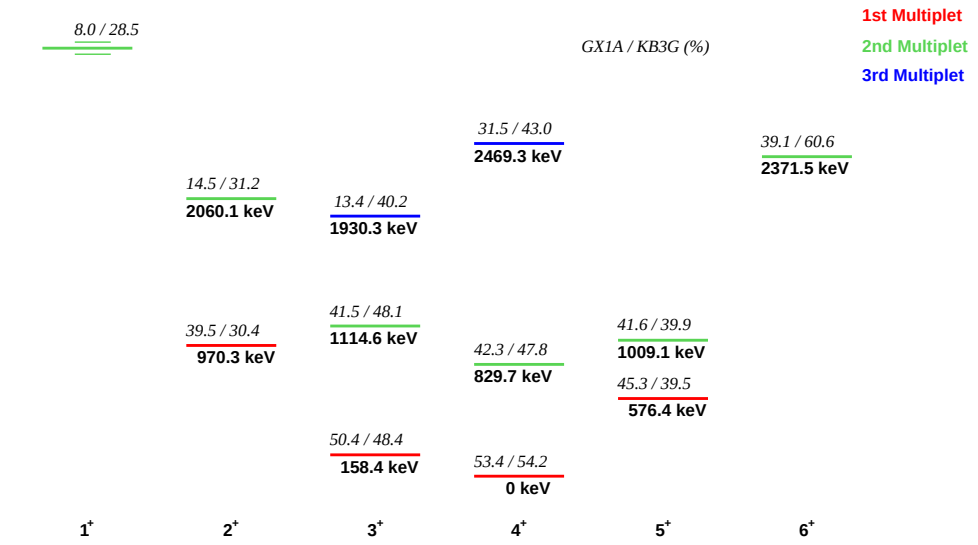

(a)

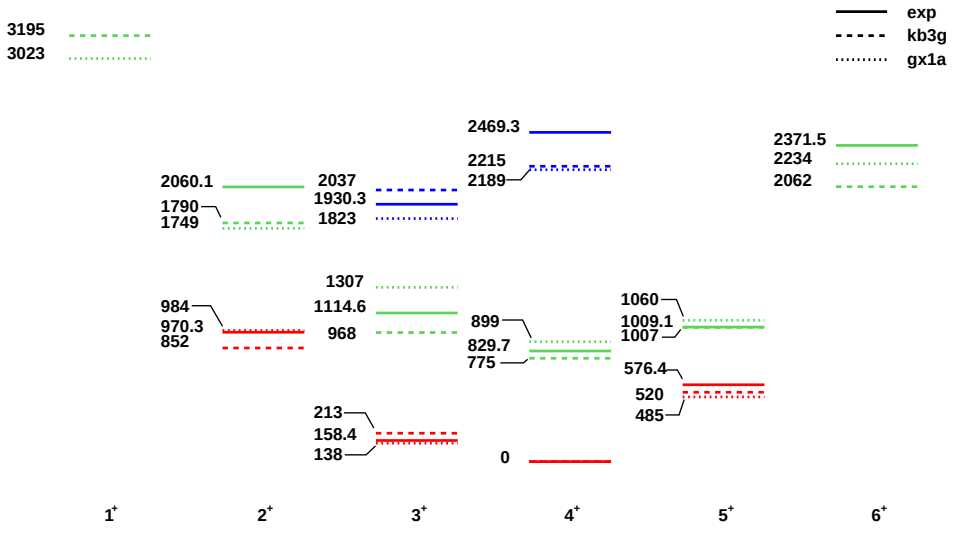

(b)

Figure 4.2: (a) Experimental states identified as the main components of the 1p-1h multiplets: $(1f_{7/2})^{-1}_{\pi}(2p_{3/2})^{1}_{\nu}$ (in red), $(1f_{7/2})^{-1}_{\pi}(1f_{5/2})^{1}_{\nu}$ (in green) and $(1f_{7/2})^{-1}_{\pi}(2p_{1/2})^{1}_{\nu}$ (in blue), with excitation energies in keV. In italics, the percentage of the calculated dominant configuration are presented, using the NuShellX code with the KB3G and GXPF1a effective interactions and truncation $q = 2$. (b) The same experimental levels (solid lines) are compared with the predicted energies using the two previously mentioned effective interactions. The experimental identification of the main 1^+ member of the second multiplet was not possible (see main text).

Valence space comparison

As mentioned above, the calculations presented in the previous section were performed in a truncated *fp*-shell valence space characterized by a truncation $q = 2$. It is also interesting to compare the predictions as a function of the valence space. It is worth remembering that q is the minimum number of protons and neutrons that remain in the $1f_{7/2}$ shell. This means that the lower the q the bigger the valence space. Comparison of shell-model calculations using q =2, 4 and 6 for both KB3G (Fig. 4.4) and GXPF1a (Fig. 4.5) are presented. Both figures show six levels per spin $J = 1, 2, 3, 4, 5$ and 6, the first two 7 states and the first 8 state. As noted earlier, only positive parity states are calculated because both KB3G and GXPF1a are *fp*-shell interactions, which means that they exclude the $1g_{9/2}$ orbital.

It can be observed that the most restricted space (i.e. $q = 6$) shows a more expanded level scheme compared with the other spaces, for both effective interactions used. The evolution from $q = 4$ to $q = 2$ towards the convergence of the results is evident.

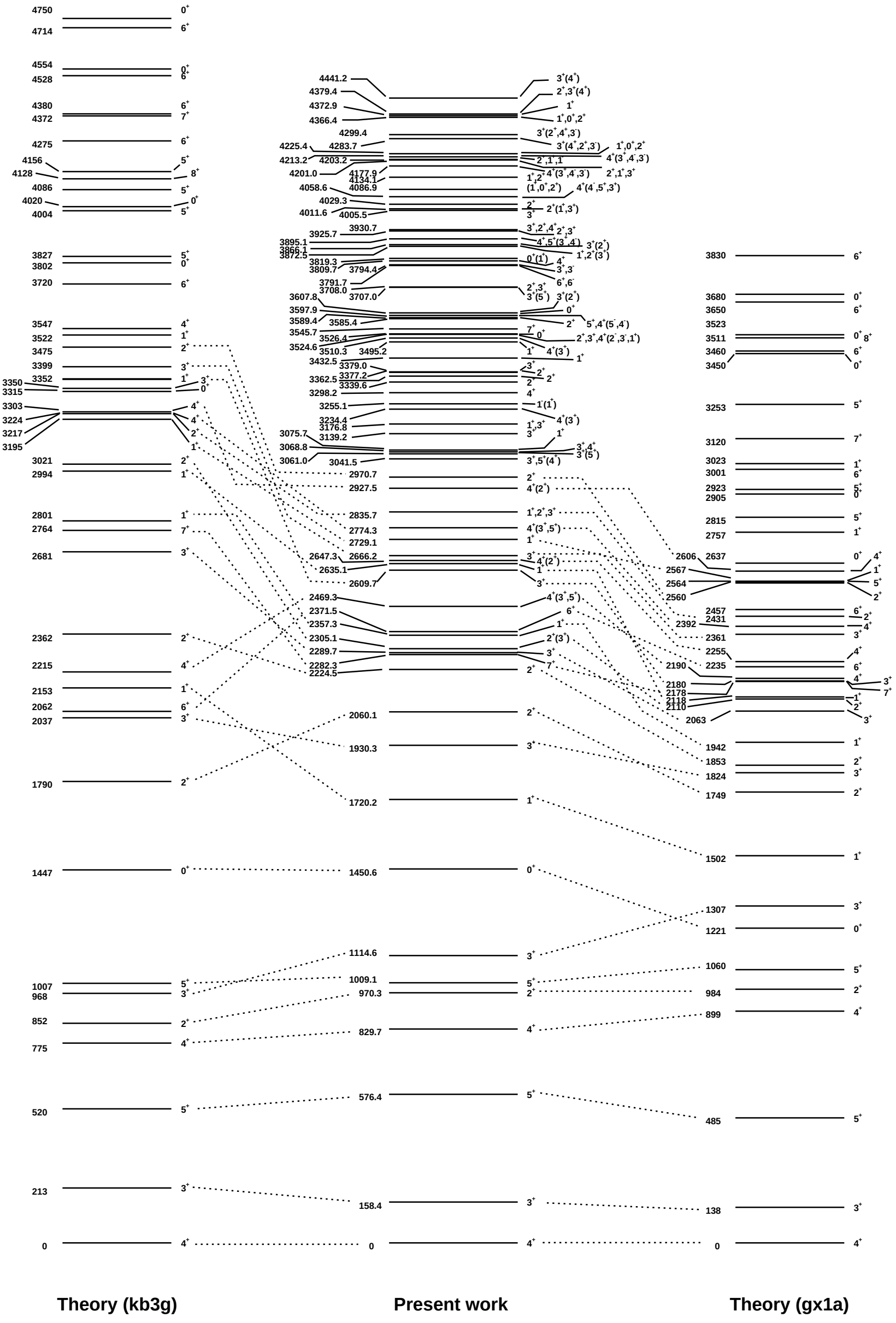

Figure 4.3: Graphical comparison of the results of the present work with theoretical predictions using the NuShellX code with the KB3G (left) and GXPF1a (right) effective interactions and a truncation $q = 2$, where q is the minimum number of protons and neutrons that remain in the $1f_{7/2}$ shell. Energy (in keV) and spin-parity assignments are presented. Tentative identification between experimental levels and theoretical calculations have been made up to 3 MeV. It should be noted that this scheme should not be taken as a level density comparison with predictions since only six levels per spin were calculated. The first two predicted 7^+ states and the first 8^+ state are shown.

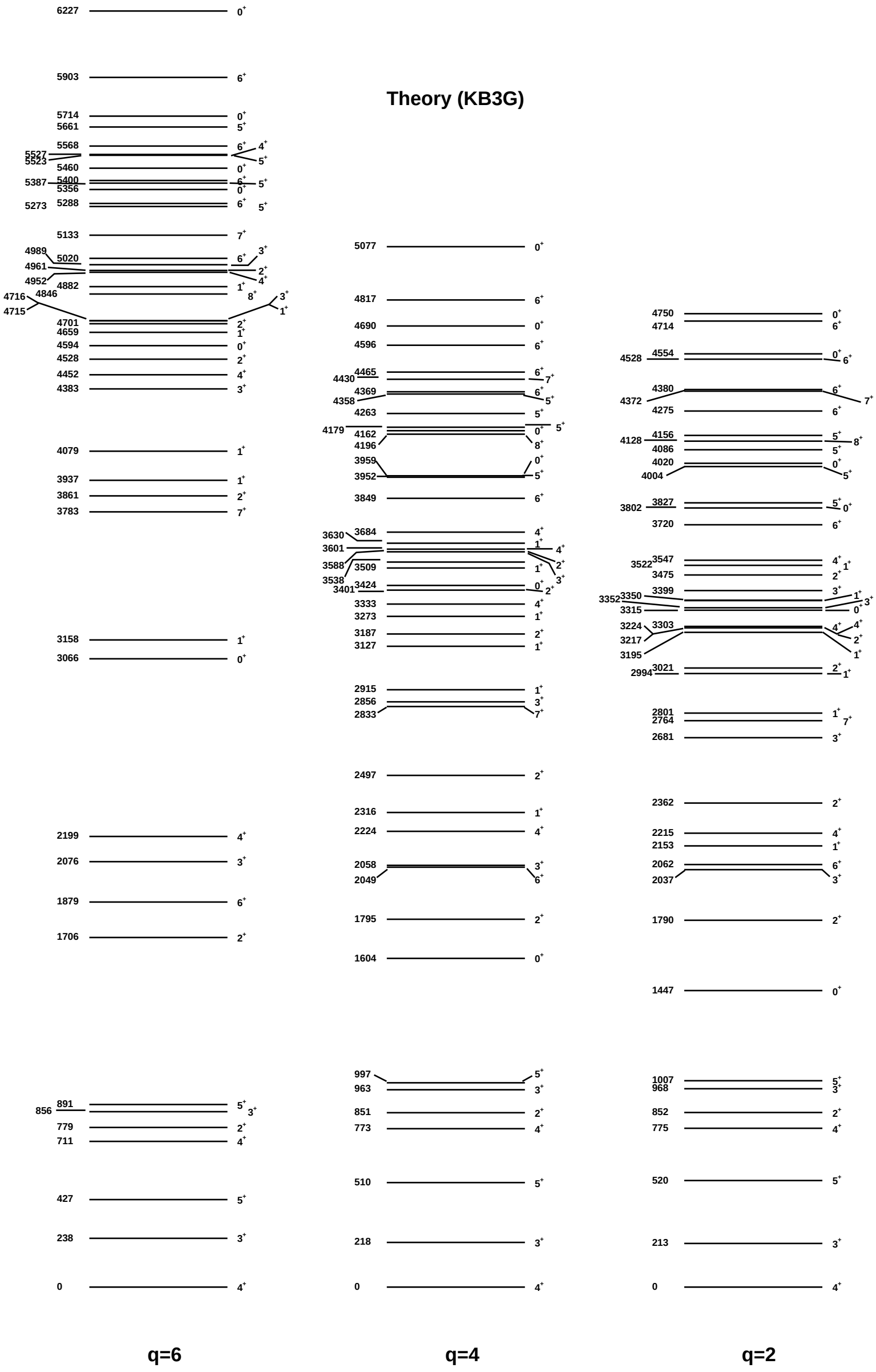

Figure 4.4: Graphical comparison of shell-model calculations in a truncated *fp*-shell valence space using the NuShellX code with the KB3G effective interaction as a function of the truncation q (where q is the minimum number of protons and neutrons that remain in the $1f_{7/2}$ shell). Valence spaces of $q = 2$, 4 and 6 were used.

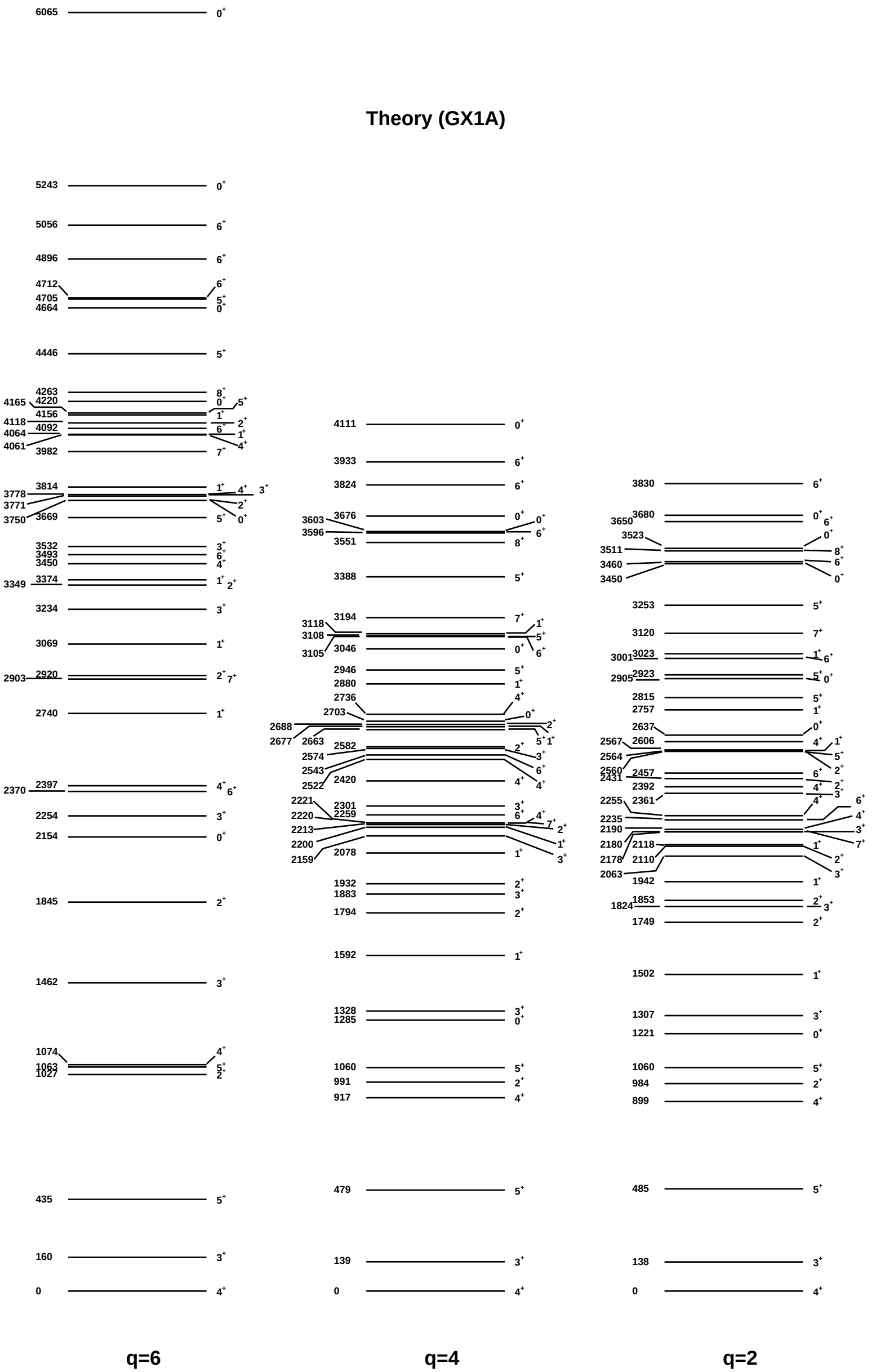

Figure 4.5: Graphical comparison of shell-model calculations in a truncated *fp*-shell valence space using the NuShellX code with the GXPF1a effective interaction as a function of the truncation q (where q is the minimum number of protons and neutrons that remain in the $1f_{7/2}$ shell). Valence spaces of $q = 2$, 4 and 6 were used.

4.2 The 0^+ states

The study of the splitting of the isobaric analogue state (IAS) in ^{56}Co was one of the main purposes of the experiment presented here. In the following section the results obtained in this work regarding the γ-decay of the two isospin-mixed 0^+ states will be presented. In section 4.2.2 the comparison with the theoretical predictions will be discussed.

4.2.1 Experimental results

As explained in section 1.4, the reaction and beam energy were carefully chosen in order to guarantee that the 0^+ states in ^{56}Co were populated up to 3.6 MeV excitation energy.

Experimentally, the first observed 0^+ state is located at an excitation energy of 1450.6 keV (see Table 3.1). On the other hand, the 3526.4- and 3597.9-keV states correspond to the two strongly isospin-mixed 0^+ states and both have a component of the IAS, as demonstrated in several works [2, 7, 8]. These two states correspond to the second and third observed 0^+ states (see Table 3.1).

Several 0^+ candidates had previously been reported in the ^{56}Co nucleus between 3 and 3.6 MeV [47]. However, apart from the 3526.4- and 3597.9-keV states, our experimental results do not agree with the previous 0^+ assignments to the remainder of the candidate states (see Appendix E for a detailed description of the J^π assignments made in this work), and we believe that there are no other 0^+ states in that region. We have observed a possible candidate for a 0^+ state at 3819.4 keV.

A summary of the γ-decay of the two 0^+ states of interest is shown in Table 4.2. A drawing of the same results is presented in Fig. 4.6. Besides the previously known γ-transitions de-exciting these states, two new γ-decays were observed for the first time in this work de-exciting the lower-lying level. Thus we concluded that both states decay to the 1^+ states at 1720.3, 2635.1 and 2729.1 keV. It can be observed that the two levels decay in a clearly different way, contrary to our first naive thinking. It should be noted that the γ-ray energies (E_γ), branching ratios (BR) and intensities (I_γ) of the decay of those 0^+ states were already presented in Tables 3.1 and 3.2. Only I_γ values relative to a γ-transition in coincidence with them could be obtained for the 962.8- and 891.5-keV γ-decays in this work. In order to be able to compare the experimental results with theoretical calculations we used the 962.8-keV branching ratio from reference [29] and that value together with the intensity ratio $I_{891.5}/I_{962.8} = 0.083$ (with 22% error) obtained in this work using a gate on a γ-transition below the 2635.1-keV level, to calculate the I_γ and branching ratio of the 891.5-keV γ-transition.

According to the theoretical B(M1) calculations, the γ-decay from the upper 0^+ state to the 2357.3-keV 1^+ state should also occur (see sec. 4.2.3). Since the energy

Table 4.2: Summary of the γ-decay of the 0^+ states at 3526.4 and 3597.9 keV. The experimental γ-energies and branching ratios (BR) are shown for each level. The $t_{1/2}$ values are taken from Ref. [29]. Note that all decays are transitions to 1^+ states.

E_{level}(keV)	$t_{1/2}$ (fs)	E_γ(keV)	$J_i^\pi \rightarrow J_f^\pi$	I_γ	BR	Comments
3526.4	6(5)	797.2(5)	$0^+ \rightarrow 1^+$	0.11(2)	10(2)	[N]
		891.5(4)	$0^+ \rightarrow 1^+$	c	1.8(5)	[aN]
		1806.1(3)	$0^+ \rightarrow 1^+$	1.13(12)	100(11)	
3597.9	18(5)	868.6(2)	$0^+ \rightarrow 1^+$	0.46(2)	62(3)	
		962.8(2)	$0^+ \rightarrow 1^+$	c	33(6)	[b]
		1877.9(3)	$0^+ \rightarrow 1^+$	0.74(5)	100(7)	

[N] γ-transition observed for the first time in this work.

[a] BR value obtained using the BR value from the 962.8-keV γ-ray and the ratio of relative intensities $I_{891.5}/I_{962.8}$ obtained using a gate on a γ-transition in coincidence (see main text).

[b] BR value obtained from reference [29].

[c] Only intensity relative to the gate (Not normalised intensity)

of this hypothetical decay is very close to an intense γ-peak in ^{56}Fe, we can neither confirm nor deny the existence of this transition.

The gated γ-spectra showing the γ-transitions de-exciting the 0^+ states at 3526.4 and 3597.9 keV are presented in Fig. 4.7: the peaks at 1806.1 and 1877.9 keV de-exciting to the 1720.3-keV level (a), 891.5 and 962.9 keV de-exciting to the 2635.1-keV level (b), and 797.2 and 868.6 keV de-exciting to the 2729.1-keV level (c) are shown. These γ-ray spectra have been obtained using the Doppler-shift corrected (DC) *total* γ-γ coincidence matrix gating on a suitable γ-transition (or γ-transitions) from below: the 750.0-keV transition to obtain the spectrum in (a), the 480.5- and 1184.6-keV transitions and summing their corresponding statistics to obtain the spectrum in (b) and the 1758.9-keV transition to obtain the spectrum in (c).

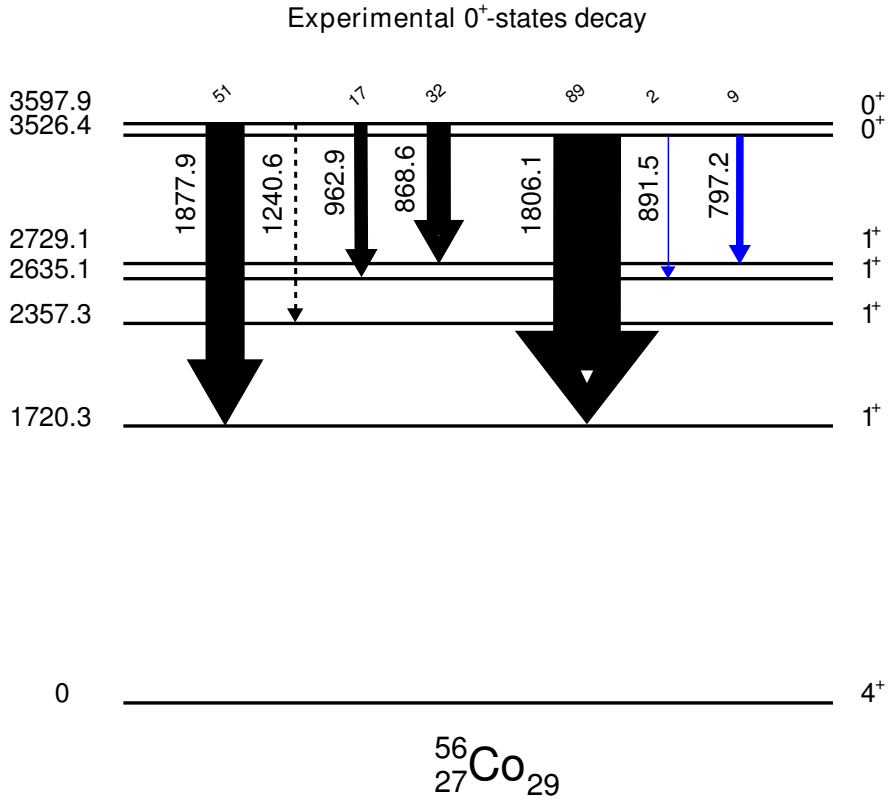

Figure 4.6: Scheme of the experimental γ-decay of the 0^+ states at 3526.4 and 3597.9 keV measured in this work. The arrow widths are proportional to the intensity and the branching ratios from each level are indicated above the arrows. Solid black arrows indicate γ-rays already known in the literature. Solid blue arrows indicate γ-transitions observed for the first time in this work. The dashed arrow shows a possible but unconfirmed γ-transition. Level and γ-transition energies are in keV.

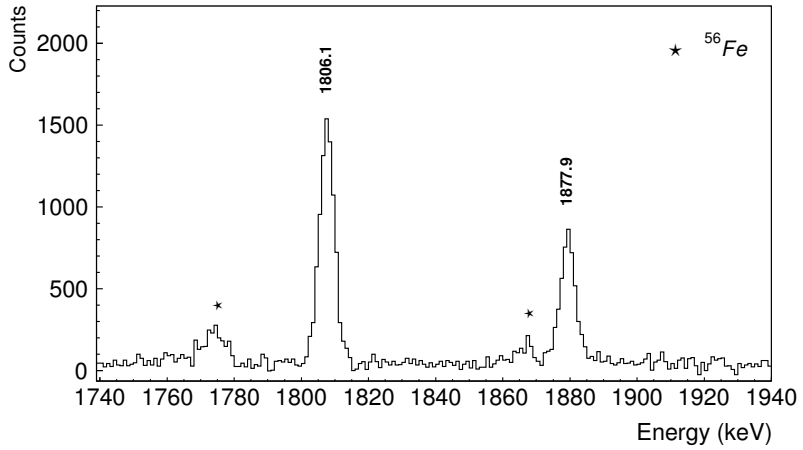

(a)

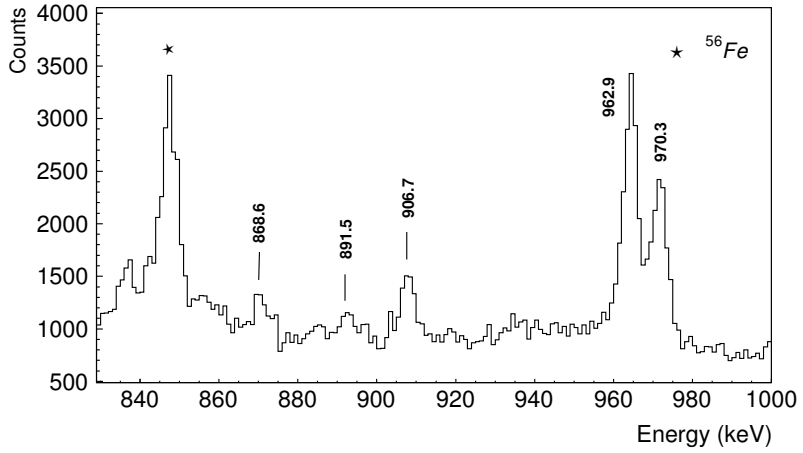

(b)

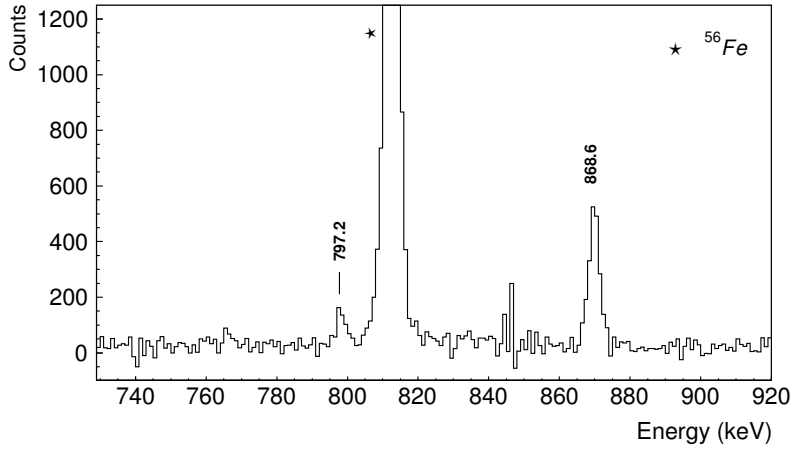

(c)

Figure 4.7: The panels show the γ-transitions de-exciting the 0^+ states at 3526.4 and 3597.9 keV: the peaks at 1806.1 and 1877.9 keV (a), 891.5 and 962.9 keV (b), and 797.2 and 868.6 keV (c) are shown. These γ-spectra were obtained from the Doppler-shift corrected *total* γ-γ coincidence matrix gating on suitable γ-transitions from below (see main text).

4.2.2 Theoretical calculations

A special effort was made to perform calculations to describe the 0^+ states properties. Besides the KB3G and GXPF1a effective interactions, shell-model calculations in a truncated *fp*-shell valence space with the ANTOINE code were made by Alfredo Poves [65] (Department of Theoretical Physics, Universidad Autónoma de Madrid). The effective interaction used was the KB3GR [63], an updated version of the KB3G interaction which improves the spectroscopy near and beyond $N = Z = 28$ nuclei. The results we will present here were obtained with a truncation $t = 7$, i.e., imposing a final configuration where 7 nucleons can be outside the $1f_{7/2}$ orbital. These calculations were only made for 0^+ and 1^+ states.

Identification of the IAS and the AAS in ^{56}Co

As explained at the beginning of this chapter, core-excited configurations such as two-particle-two-holes (2p-2h) have to be included in the calculations in order to describe the 0^+ states in ^{56}Co.

The ^{56}Fe ground state has quantum numbers $T = 2$ and $J^\pi = 0^+$. It is expected to be mainly described by the configuration $(1f_{7/2})^{-2}_\pi (2p_{3/2})^2_\nu$ (see Fig. 4.8(a)). Thus its IAS in ^{56}Co will be mainly a mixture of the configurations $(1f_{7/2})^{-2}_\pi (2p_{3/2})^1_\pi (2p_{3/2})^1_\nu$ (Fig. 4.8(b)) and $(1f_{7/2})^{-1}_\pi (1f_{7/2})^{-1}_\nu (2p_{3/2})^2_\nu$ (Fig. 4.8(c)) and will have $T = 2$. These configurations correspond to the transformation of a neutron in the $(2p_{3/2})_\nu$ orbital into a proton in the $(2p_{3/2})_\pi$ orbital or a neutron in the $(1f_{7/2})_\nu$ orbital into a proton in the $(1f_{7/2})_\pi$ orbital with respect to the $^{56}\mathrm{Fe}_{gs}$ configuration. In this specific case, these two configurations can also be combined in a way that they form a $T = 1$ state. By definition, this state will be the *anti-isobaric analogue state* (AAS) to the ^{56}Fe ground state in ^{56}Co, which has the same configuration (i.e., same wave function and quantum number J^π) as the IAS but an isospin different by one unit. Due to its $T = 1$ value, the AAS will have a lower excitation energy than the IAS.

The identification of the IAS and the AAS in the theoretical calculations can be made by analysing the description of the different 0^+ states in terms of the possible configurations. Let us call the configuration $(1f_{7/2})^{-2}_\pi (2p_{3/2})^1_\pi (2p_{3/2})^1_\nu$ A and configuration $(1f_{7/2})^{-1}_\pi (1f_{7/2})^{-1}_\nu (2p_{3/2})^2_\nu$ B. We will identify the AAS as the lowest 0^+ state with dominant contribution of the configurations A and B. Actually, it came out to be the first 0^+ state in all calculations. The IAS will be then identified as the state with the highest percentage of (again) configurations A and B of the remainder of 0^+ states. It came out that the contributions of both configurations are practically identical, and in turn these probabilities are almost the same in both the AAS and the IAS. These values are around 15-18% each, depending on the effective interaction and valence space used. Finally, the identification of the state which mixes with the IAS is not trivial. The mixing will be favoured if this state and the IAS are not too far apart in energy.

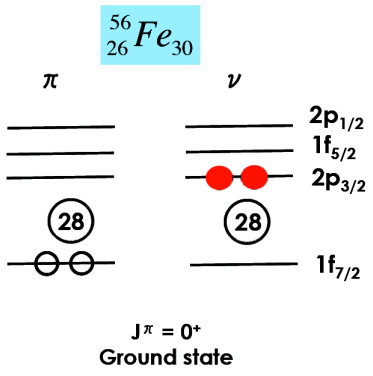

(a)

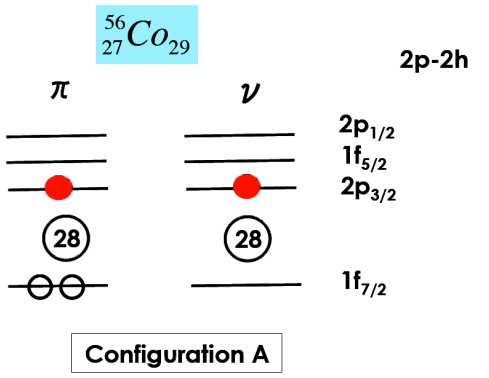

(b)

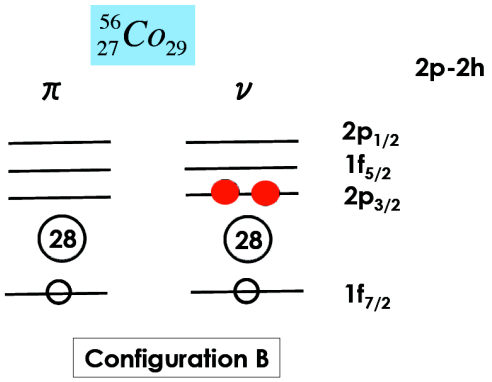

(c)

Figure 4.8: The main configuration of the ground state of ^{56}Fe is shown in (a)). Its isobaric analogue state (IAS) and anti-isobaric analogue state (AAS) in ^{56}Co are mainly a mixture of the configurations A and B (subfigs. (b) and (c)) (see main text).

The predicted excitation energies E^* of the six lowest 0^+ states in ^{56}Co are summarised in Table 4.3. The calculations have been carried out with the KB3G and GXPF1a effective interactions with the NuShellX code and different valence spaces (q=2 and 4) and the KB3GR effective interaction with the ANTOINE code and truncation $t = 7$. It is worth remembering that q is the minimum number of protons and neutrons that remain in the $1f_{7/2}$ shell, while t is the number of nucleons that can be outside the $1f_{7/2}$ shell.

As mentioned above, the AAS comes out to be the first 0^+ state in all calculations. The predicted states identified as the IAS are shown in bold in Table 4.3. As can be observed, the IAS comes out to be a different 0^+ state in terms of relative position with respect to the other 0^+ states depending on the interaction used and the valence space chosen. In the next section we will compare these calculations with the experimental relative position of the two isospin-mixed 0^+ states.

Table 4.3: Predicted excitation energies E^* of the six lowest 0^+ states in ^{56}Co. The calculations were obtained with the KB3G and GXPF1a effective interactions with the NuShellX code and truncations $q = 2$ and 4 and KB3GR effective interaction with the ANTOINE code and truncation $t = 7$. The parameter q is the minimum number of protons and neutrons that remain in the $1f_{7/2}$ shell, while t is the number of nucleons that can be outside the $1f_{7/2}$ shell. The states identified as the IAS are shown in bold.

State	E^* (MeV)				
	KB3G		GXPF1a		KB3GR
	q=2	q=4	q=2	q=4	t=7
0_1^+	1.447	1.604	1.221	1.285	1.330
0_2^+	3.315	3.424	2.637	2.736	2.650
0_3^+	**3.802**	**3.959**	2.905	3.046	2.890
0_4^+	4.020	4.179	3.450	**3.603**	3.190
0_5^+	4.554	4.690	**3.523**	3.676	3.390
0_6^+	4.750	5.077	3.680	4.111	**3.460**

4.2.3 Isospin-mixed 0^+ states

As mentioned above, neither the KB3G nor GXPF1a interactions contain isospin non-conserving (INC) terms. This means that isospin is a good quantum number and the calculated individual states have pure isospin values T. Then if one wants to calculate isospin mixing between two individual states additional INC terms have either to be included in the interaction or it has to be done *manually* once the states of pure isospin have been calculated. In this work we did the latter.

Let us describe our two isospin-mixed 0^+ states of interest, $|0^+_{upper}\rangle$ and $|0^+_{lower}\rangle$, as a linear combination:

$$|0^+_{upper}\rangle = \beta|\Phi_a\rangle \pm \alpha|\Phi_b\rangle \tag{4.1a}$$
$$|0^+_{lower}\rangle = \mp\ \alpha|\Phi_a\rangle + \beta|\Phi_b\rangle \tag{4.1b}$$

where $|\Phi_a\rangle$ and $|\Phi_b\rangle$ are the unperturbed states with good quantum numbers $T = 2$ and $T = 1$, respectively (see Appendix B). The parameter α specifies the amount of isospin impurity and, as usual, α and β must fulfill the condition $\alpha^2 + \beta^2 = 1$.

Therefore, as explained at the beginning of this chapter, the 3526.4- and 3597.9-keV states would correspond to the $|0^+_{lower}\rangle$ and $|0^+_{upper}\rangle$ states, respectively.

The 3597.9-keV state is mainly $T = 2$ and therefore carries the major part of the wave function of the IAS. Its observed position, third lowest 0^+ state, is only consistent with the theoretical calculations performed with the KB3G effective interaction, where the IAS comes out to be the 0^+_3 (see Table 4.3). The GXPF1a and KB3GR effective interactions provide a larger number of 0^+ states at excitation energies below the IAS. Why this is so is a question that still puzzles us and has not been understood.

As mentioned at the beginning of this section, the KB3GR effective interaction is known to improve the spectroscopy near and beyond the $N = Z = 28$ nucleus. As can be seen in Table 4.3, in the calculations using this effective interaction the 0^+_6 state at 3.460 MeV is identified as the IAS. Even though the number of 0^+ states below the IAS obtained in these calculations is higher than the number observed experimentally, the neighbouring 0^+_5 state at 3.390 MeV is only 70 keV away from the predicted excitation energy of the IAS. This separation energy reproduces very well the experimental results obtained for the two 0^+ states of interest. Therefore in what follows only comparisons with the shell-model calculations using the KB3GR effective interaction will be presented.

Reduced transition probabilities

As explained above, in this section we will only use the shell-model calculations performed using the ANTOINE code with the KB3GR effective interaction for the interpretation of the experimental results concerning the two isospin-mixed 0^+ states. The 0^+_6 and 0^+_5 states obtained in these calculations were associated with the isospin-pure states $|\Phi_a\rangle$ ($T = 2$) and $|\Phi_b\rangle$ ($T = 1$) of the previous section, respectively. In these calculations five 1^+ levels below 4-MeV excitation energy were obtained. We are concerned here exclusively with the M1 transition operator since we are dealing with $0^+ \rightarrow 1^+$ transitions. The theoretical calculations provided *reduced transition probabilities* B(M1), also called *transition strengths*, for the various $1^+_i \rightarrow 0^+_n$ transitions (see Table 4.4).

J_i^π	J_f^π	B(M1:$J_i^\pi \rightarrow J_f^\pi$)($\mu_N^2$))
1_1^+	0_6^+	0.0506
	0_5^+	0.0033
1_2^+	0_6^+	0.0380
	0_5^+	0.0006
1_3^+	0_6^+	0.0167
	0_5^+	0.0271
1_4^+	0_6^+	0.3820
	0_5^+	0.0510
1_5^+	0_6^+	0.1680
	0_5^+	0.0521

Table 4.4: Theoretical B(M1) values from shell-model calculations performed in a truncated *fp*-shell valence space using the ANTOINE code with the KB3GR effective interaction and a truncation $t = 7$, where t is the number of nucleons that can be outside the $1f_{7/2}$ shell. Note that the B(M1) values are given for the $1^+ \rightarrow 0^+$ transition, while experimentally we measure the transition $0^+ \rightarrow 1^+$.

It should be noted that the values presented in Table 4.4 are obtained for the inverse direction ($1^+ \rightarrow 0^+$) to the γ-decays from the 0^+ states. Applying Eq. 1.11 one obtains the relation:

$$B(M1 : 0^+ \rightarrow 1^+) = 3 \ B(M1 : 1^+ \rightarrow 0^+) \tag{4.2}$$

which relates the reduced matrix elements of the same transition in opposite directions.

As mentioned above, the theoretical calculations provide B(M1) values for the transitions between individual unperturbed states. Thus, in order to calculate the B(M1) values for the de-excitations from the isospin-mixed $|0^+_{upper}\rangle$ and $|0^+_{lower}\rangle$ states, equations 4.1a and 4.1b have to be used. Then they will be functions of the B(M1) values obtained for the individual states $|\Phi_a\rangle$ and $|\Phi_b\rangle$, here $|0_6^+\rangle$ and $|0_5^+\rangle$ for the case under study.

As already explained in Chapter 1, an isospin impurity of $\alpha^2 = 28(1)\%$ was found in the charge exchange ^{56}Fe(^{3}He,t)^{56}Co reaction of [2]. Due to the fact that the signs of α and β in Eqs. 4.1a and 4.1b are unknown, there is an ambiguity in the results for the calculation of the B(M1). Due to the orthogonality of the isospin-mixed states, a constructive solution for the $|0^+_{upper}\rangle$ state (i.e., using the sign "+" in Eq. 4.1a) is only compatible with a destructive solution for the $|0^+_{lower}\rangle$ state (i.e., using the sign "-" in Eq. 4.1b), and vice versa. This has to be taken into account when comparing

the predictions with the experimental values. Combining the previously mentioned equations with Eq. 1.10, one obtains the following pair of expressions:

$$B(M1, 0^+_{upper} \rightarrow 1^+_i) = |\langle 1^+_i|M1|0^+_{upper}\rangle|^2 = (\beta\langle 1^+_i|M1|0^+_6\rangle \pm \alpha\langle 1^+_i|M1|0^+_5\rangle)^2 \tag{4.3a}$$

$$B(M1, 0^+_{lower} \rightarrow 1^+_i) = |\langle 1^+_i|M1|0^+_{lower}\rangle|^2 = (\mp\alpha\langle 1^+_i|M1|0^+_6\rangle + \beta\langle 1^+_i|M1|0^+_5\rangle)^2 \tag{4.3b}$$

where the different terms,

$|\langle 1^+_i|M1|0^+_n\rangle| = \sqrt{B(M1 : 0^+_n \rightarrow 1^+_i)}$ (with i=1,2,3,4 and n=5,6)

can be obtained from Table 4.4 and using Eq. 4.2.

On the other hand, the B(M1) strength and the total transition probability T(M1) are related through the expression (see Eq. 1.8):

$$T(M1) = 1.779 \times 10^{13} E^3_\gamma \, B(M1) \tag{4.4}$$

for lifetimes in units of seconds and E_γ in MeV. The magnetic matrix elements $B(M1)$ have units of μ^2_N where,

$$\mu_N = \frac{e\hbar}{2m_p c} \tag{4.5}$$

is the nuclear magneton and m_p is the single nucleon mass. It is worth remembering the relation between the total transition probability T and the partial mean lifetime $\tau_{partial}$ and its definition:

$$T = \frac{1}{\tau_{partial}} = \frac{ln(2)}{t^{partial}_{1/2}} \tag{4.6}$$

where

$$t^{partial}_{1/2} = \frac{t_{1/2}}{BR} \tag{4.7}$$

Then, the experimental B(M1) values can be deduced using Eq. 4.4 if the partial half-life $t^{partial}_{1/2}$ of the initial state is known. Thus, as can be observed above, the branching ratios have to be taken into consideration.

Figure 4.9 shows a drawing of the experimental and theoretical B(M1) values for the observed transitions connecting the two isospin-mixed 0^+ states of interest with the various low-lying 1^+ states. On the other hand, a comparison of these values is shown in Fig. 4.10. The predicted values have been calculated using constructive/destructive options in the calculation of the B(M1) corresponding to the transitions from the $|0^+_{upper}\rangle$ state (using Eq. 4.3a), with the complementary option in the calculation of the B(M1) for the transitions from the $|0^+_{lower}\rangle$ state (using Eq. 4.3b). It has to be taken into account that the previously known half-lives for the 0^+ states of interest have large uncertainties [29], the 3597.9-keV state has $t_{1/2} = 18 \pm 5$ fs, and the nearby 3526.4-keV state, 6 ± 5 fs. Therefore the experimental B(M1) uncertainties are large, especially those corresponding to the lower-lying state. However, if we look at the de-excitation of the upper level, where the error bar is smaller, the constructive option is clearly favoured.

Another motivation for this work was the comparison of the γ-de-excitation of ^{56}Co with its mirror nucleus ^{56}Cu, as already discussed in Chapter 1. As mentioned at the beginning of this chapter, the shell-model calculations using the KB3GR effective interaction does not include either Coulomb force or any additional isospin non-conserving forces. This implies an identical behaviour of protons and neutrons in the calculations, and therefore the theoretical B(M1) values discussed previously are also valid for the ^{56}Cu discussion. On the other hand, the experimental B(M1) values cannot be calculated for ^{56}Cu since the $t_{1/2}$ values of its isospin-mixed 0^+ states are unknown. However, the non-observation of one of the γ-transitions from the upper isospin-mixed 0^+ state in ^{56}Cu as compared with its counterpart level in ^{56}Co (one of the puzzling results in the ^{56}Zn decay experiment of [1], and marked as a dashed line in Fig. 1.3) could be explained by the destructive solution presented in Fig. 4.10. The explanation for the non-observation of γ-ray decays from the lower isospin-mixed 0^+ state in ^{56}Cu is more difficult because in this case the main factor which contributes is the $t_{1/2}$ of the level (unknown) and its competition with the proton decay as well as the limited statistics obtained in the measurement.

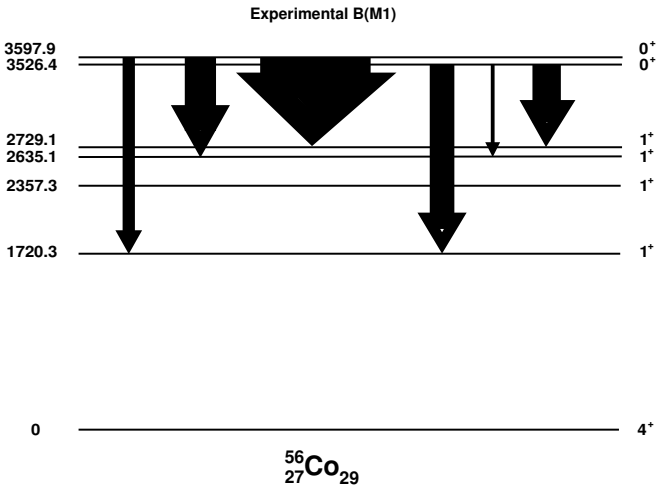

(a)

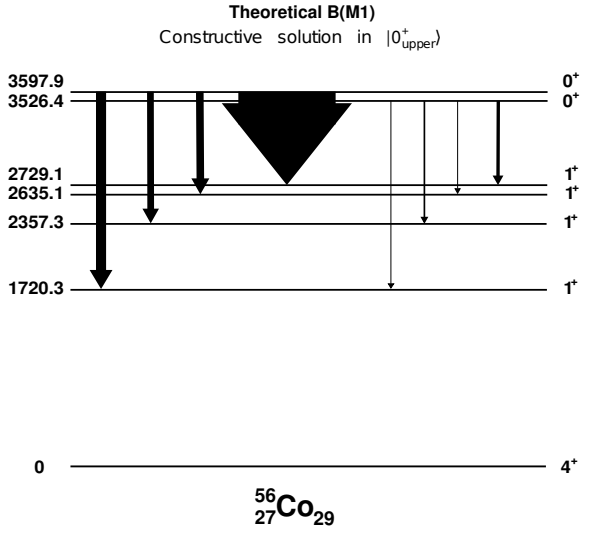

(b)

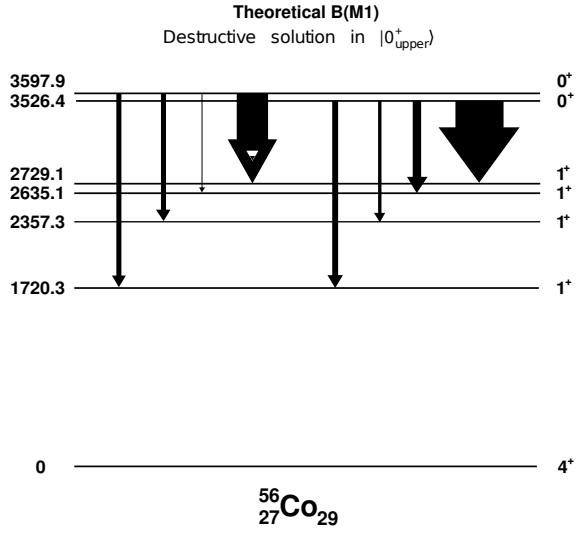

(c)

Figure 4.9: Schematic diagram showing the experimental (a) and theoretical B(M1) values for the observed transitions connecting the two isospin-mixed 0^+ states ($|0^+_{upper}\rangle$ and $|0^+_{lower}\rangle$) with the different 1^+ states. These values are large-scale shell-model calculations in a truncated *fp*-shell valence space using the ANTOINE code with the KB3GR effective interaction. A truncation $t = 7$ was used, where t is the number of nucleons that can be outside the $1f_{7/2}$ shell. The constructive (b) and destructive (c) options in the calculation of the B(M1) from the $|0^+_{upper}\rangle$ state (Eq. 4.3a), with the complementary option for the B(M1) from the $|0^+_{lower}\rangle$ state (Eq. 4.3b), are shown.

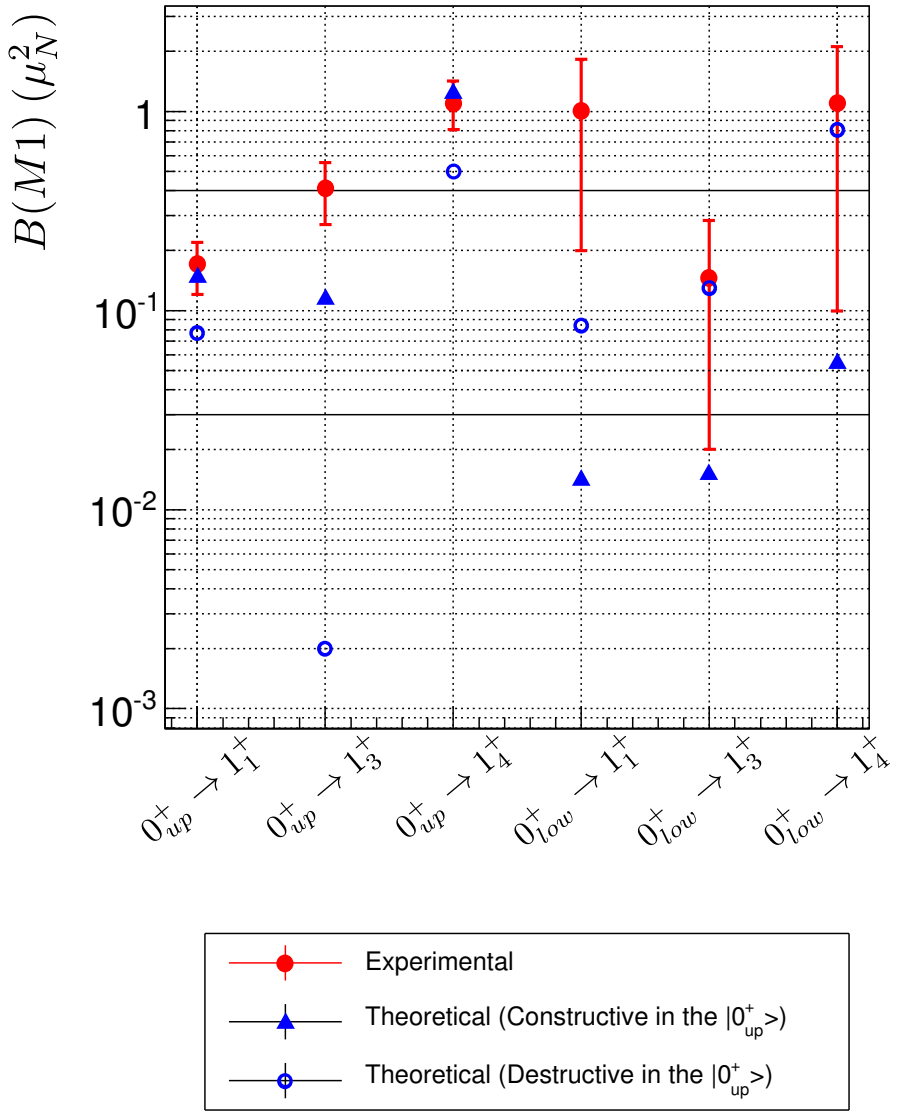

Figure 4.10: Comparison of the experimental B(M1) values with shell-model calculations in a truncated *fp*-shell valence space using the ANTOINE code with the KB3GR effective interaction. A truncation $t = 7$ was used, where t is the number of nucleons that can be outside the $1f_{7/2}$ shell. The constructive and destructive options in the calculation of the B(M1) from the $|0^+_{upper}\rangle$ state (Eq. 4.3a), with the complementary option for the B(M1) from the $|0^+_{lower}\rangle$ state (Eq. 4.3b), are shown. Note that the experimental B(M1) uncertainties come mainly from the large uncertainty of the half-lives of both states.

Chapter 5

Conclusions

In the present work we have studied the (mainly) fusion-evaporation reaction ^{56}Fe(p,nγ)^{56}Co at $E_p = 10$ MeV. The γ-rays emitted in the de-excitation of the ^{56}Co excited states were measured in-beam with four high-resolution MINIBALL-triple Ge detectors, at the Maier-Leibnitz-Laboratory (MLL) of the Technische Universität München (TUM, Munich, Germany).

Despite the extensive work previously done studying the ^{56}Co nucleus, the experiment analysed in this work has resulted in a large improvement in the knowledge of its structure. In summary, the following experimental results have been obtained:

- A total of 223 γ-transitions have been observed and placed in the level scheme, of which 169 were previously unobserved.
- A much higher sensitivity level for the γ-de-excitation for excited states in ^{56}Co than reported in the literature has been reached for spins between 0 and 6. A total of 77 excited states have been observed, 37 of which were previously known states for which no gamma de-excitation had been observed. In 42 cases the energy precision of the levels has been improved. In this work, 14 excited states have been observed for the first time.
- 36 new J^π assignments have been made, 10 corrections to previous J^π assignments have been suggested and in 4 cases J^π-assignment ambiguities have been resolved. For the remaining states, the previous J^π assignments have been confirmed.

A topic of interest was the spin-parity (J^π) assignment of the 2635.1- and 3075.7-keV states, for which doubts about the previously reported $J^\pi = 1^+$ value existed [2]. In the angular distributions of the 1184.6-keV (de-exciting the 2635.1-keV state) and 1625.2-keV (de-exciting the 3075.7-keV state) γ-rays to the firm 1450.6-keV 0^+ level we have measured clear $A_2 < 0$ angular coefficients, which confirms the M1 character of the transitions and the corresponding initial $J^\pi = 1^+$ assignments for both states. Other γ-transitions de-exciting these two levels are also compatible with the 1^+ assignment.

Low-lying levels in ^{56}Co are expected to have relatively pure configurations and one-particle-one-hole character. In our experiment we could identify almost all the

members of the $(1f_{7/2})^{-1}_{\pi} \times (2p_{3/2}, 1f_{5/2}, 2p_{1/2})^{1}_{\nu}$ multiplets which we have compared with shell-model predictions. Large-scale shell-model calculations in a truncated *fp*-shell valence space were performed, using the NuShellX@MSU code with the KB3G and GXPF1a effective interactions. We have observed that there is a good agreement between the excitation energies and γ-de-excitation of the low-lying states and the theoretical predictions up to approximately 2.5 MeV for spins J=3,4,5,6,7. However, at those energies for 1^+ and 2^+ states, and above 2.5 MeV for the remainder of spins, the comparison begins to be difficult due to the increasing level density, making more questionable any further identification with the predicted states.

On the other hand, the study of the two isospin-mixed 0^+ states, which both have a component of the IAS of the ^{56}Fe ground state in ^{56}Co, was one of the main motivations of the present thesis. It has been proved that both states, at excitation energies of 3526.4 and 3597.9 keV, were strongly populated in the reaction, despite the difficulty of populating 0^+ states at such incident-proton energies (E_p = 10 MeV), where the fusion-evaporation mechanism dominates over the direct reaction.

Besides the previously known γ-transitions de-exciting the two 0^+ states, we have observed two new γ-rays depopulating the lower level. The measured intensities indicate that the two states clearly decay in a different way, contrary to our first thinking.

In the study of the two isospin-mixed 0^+ states, besides the previous calculations using the KB3G and GXPF1a effective interactions, shell-model calculations in a truncated *fp*-shell valence space using the ANTOINE code with the KB3GR effective interaction were performed. We observed that the predicted relative position of the IAS in ^{56}Co with respect to the other 0^+ states is very sensitive to the effective interaction used. This is a question that puzzled us and it has not been understood yet.

Using the ANTOINE calculations and mixing the two 0^+ states we calculated the reduced transition strength B(M1) values of the transitions de-exciting these levels. The comparison between the experimental and predicted B(M1) values clearly favours the constructive mixing scheme in ^{56}Co. Moreover, because the shell-model calculations were performed without using either Coulomb force or any additional isospin non-conserving forces, they can be also used for the discussion of the mirror nucleus ^{56}Cu. Thus, the destructive solution of the calculated B(M1) values presented in this work could explain the non-observation of one of the possible gamma branches in the decay of the upper isospin-mixed 0^+ state in ^{56}Cu, populated in the ^{56}Zn decay experiment, as compared with the mirror level in ^{56}Co. On the other hand, the non-observation of γ-rays de-exciting the lower-lying 0^+ state in ^{56}Cu is more difficult to discuss because the $t_{1/2}$ value of this level is unknown and its competition with proton decay is a main factor in the γ-de-excitation. Besides, the intensity of these hypothetical decays could have been below the gamma-sensitivity threshold of the decay experiment. Therefore more experimental data on ^{56}Cu would be valuable for future discussions.

Appendix A
Astrophysical interest of ^{56}Co

The ^{56}Ni nucleus is the most abundantly produced isotope in the silicon burning stage of a $\geqslant 10$ solar-mass star. After this stage, the energy from fusion of light nuclei is exhausted, and the star undergoes gravitational collapse resulting in a shock wave and supernova explosion. The light output from the supernova remnant is largely due to the energy from the radioactive decay of the ^{56}Ni and its daughter ^{56}Co ($t_{1/2} = 77.236 \pm 0.026$ days). This prediction was corroborated by the observation of the 77.1-day exponential decay of the light output from Type II supernova (SN) 1987A [66]. In Type Ia supernovae, the ejected material is proceeded through nuclear statistical equilibrium. This favours the production of $N = Z$ nuclei and, in particular, ^{56}Ni, meaning $N = Z = 28$. The ^{56}Ni nucleus is produced in high abundance both because 28 is a magic nucleon number and because even-even $N = Z$ nuclei have an additional binding energy, commonly known as 'Wigner energy'. Therefore the ^{56}Ni and ^{56}Co nuclei play an important role in the radioactive power of most supernovae.

A wider knowledge of the properties of ^{56}Co is also important for nuclear astrophysics, more generally. Binary neutron stars (BNS) mergers produce rapidly evolving optical and infrared transients accompanied by the radiation of gravitational waves. Radioactive materials synthesized in the rapid neutron capture process (r-process) are ejected during the merger. The decay of these radioactive materials results in optical and infrared emission with a typical duration of a day to a week, and a peak luminosity that is about a few thousand times that of a typical nova. Such transient objects in the optical are given the name kilonovae (or macronovae). In contrast to binary black hole mergers, where there is no consensus on the detectability of electromagnetic radiation after the merger, kilonovae were expected to be detectable in both GW and optical/IR bands.

On August 17, 2017, the LIGO-Virgo gravitational wave (GW) detector network observed a GW signal from a BNS merger, referred to as GW170817 [67]. The detection of a kilo/macronova electromagnetic counterpart (AT 2017gfo) of the GW170817 has confirmed the occurrence of r-process nucleosynthesis in this kind of event [68]. The blue and red components of AT 2017gfo have been interpreted as the signature of multi-component ejecta in the merger dynamics.

The brightness and time evolution of this optical transient associated with GW170817 are broadly consistent with the predictions of models involving merging binary neutron stars. In particular, the first calculations of the radioactive powered transients

from the compact object mergers, i.e., binary neutron star(NS)/black hole systems, computed by Metzger, Martínez-Pinedo, et al. [69], had self-consistently determined the radioactive heating by means of a nuclear reaction network. Using this heating rate, they had modelled the light curve with a one-dimensional Monte Carlo radiation transfer calculation. Since NS merger transient peaked at a luminosity that was a factor of $\sim 10^3$ higher than a typical nova, they proposed naming these event 'kilo-novae'.

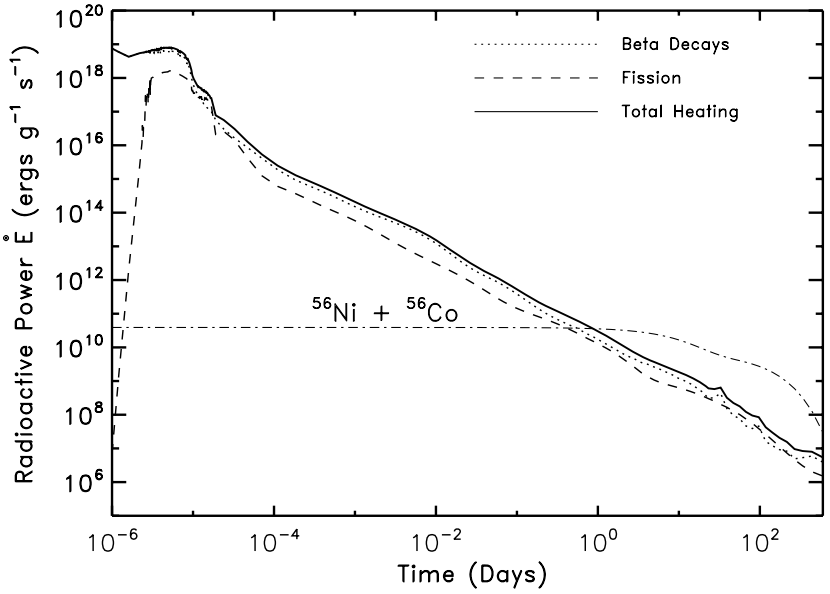

Figure A.1: Radioactive heating rate per unit mass $\dot{E}$ in NS merger ejecta due to r-process material, calculated for an ejecta trajectory from [70] and [71]. The total heating rate is shown with a solid line and is divided into contributions from β-decays (dotted line) and fission (dashed line). For comparison the heating rate per unit mass produced by the decay chain ^{56}Ni $\rightarrow^{56}$ Co $\rightarrow^{56}$ Fe is also shown (dot-dashed line).

In this work they calculated the total radioactive power $\dot{E}$ with time (see Fig. A.1). On the time-scales of interest the radioactive power can be divided into two contributions: fission and β-decays. The large heating rate at very early times is due to the r-process, which ends when neutrons are exhausted at $t \sim 1\text{s} \sim 10^{-5}$ days. The heating on longer time-scales results from the synthesized isotopes decaying back to stability. On the time-scales of interest for powering EM emission ($t \sim$ hours-days) fission and β-decays make similar contributions to the total r-process heating. In addition, the r-process and the decay-chain ^{56}Ni $\rightarrow^{56}$ Co $\rightarrow^{56}$ Fe heating shown for comparison are similar. Even if ^{56}Ni is not produced during the r-process, a small abundance of ^{56}Ni may be produced in accretion disc outflows from compact object mergers.

Also related with the astrophysical motivations, a measurement of the ^{56}Ni cosmic ray abundance has been recently discussed as a possible tool to determine the acceleration time scale of relativistic particles in cosmic rays [72]. At the high temperature at which ^{56}Ni is produced, atoms are fully ionized and, consequently, ^{56}Ni cannot decay to ^{56}Co by atomic electron capture but only by higher-order forbidden transitions. The halflife of totally ionized ^{56}Ni has been calculated within large-scale shell model calculations in order to investigate if ^{56}Ni can serve as a chronometer for cosmic rays. They concluded that the calculated halflife is significantly shorter than the time relativistic particles need to escape from our galaxy ($> 10^7$ years). Thus, even ^{56}Ni, originally accelerated from a supernova remnant into the cosmic rays, will be depleted too fast to serve as cosmic ray chronometer.

Appendix B

Isospin mixing matrix element

The splitting of the Fermi transition strength is caused by the isospin mixing between states having nominally different values of isospin T. Such mixing is caused by the off-diagonal matrix element of the charge-dependent part of the Hamiltonian, which we will denote as $\langle \mathcal{H}_c \rangle$ [2, 8].

Let the nuclear Hamiltonian be written as $\mathcal{H} = \mathcal{H}_0 + \mathcal{H}_C$ where $\mathcal{H}_0$ is the charge-independent part of the Hamiltonian and $\mathcal{H}_C$ includes any charge-dependent term. Then all eigenfunctions of $\mathcal{H}_0$ have isospin as a good quantum number. Thus, two eigenstates $|\Phi_a\rangle$ and $|\Phi_b\rangle$ of H_0, having isospin values T and $T_< = T - 1$, satisfy

$$H_0\Phi_a = e_a\Phi_a, \tag{B.1a}$$
$$H_0\Phi_b = e_b\Phi_b, \tag{B.1b}$$

where e_a and e_b are the unperturbed energies of the two states.

On the other hand, the charge-dependent part $\mathcal{H}_C$ can mix different eigenstates of $\mathcal{H}_0$ by the off-diagonal matrix elements. The energies of the observed states, E_a and E_b, are eigenvalues of the total Hamiltonian $\mathcal{H}$ and satisfy the relations,

$$(\mathcal{H}_0 + \mathcal{H}_C)|\Psi_a\rangle = E_a|\Psi_a\rangle, \tag{B.2a}$$
$$(\mathcal{H}_0 + \mathcal{H}_C)|\Psi_b\rangle = E_b|\Psi_b\rangle, \tag{B.2b}$$

where $|\Psi_a\rangle$ and $|\Psi_b\rangle$ are the two isospin-mixed states and can be written as a linear combination of the unperturbed states $|\Phi_a\rangle$ and $|\Phi_b\rangle$ of good quantum numbers T and $T_<$:

$$|\Psi_a\rangle = \beta|\Phi_a\rangle \pm \alpha|\Phi_b\rangle \tag{B.3a}$$
$$|\Psi_b\rangle = \mp\ \alpha|\Phi_a\rangle + \beta|\Phi_b\rangle. \tag{B.3b}$$

The parameter α specifies the amount of isospin impurity, and α and β must accomplish the condition

$$\alpha^2 + \beta^2 = 1. \tag{B.4}$$

By using these relationships, it can be deduced that the off-diagonal matrix elements of $\mathcal{H}_C$ can be written as:

$$\langle \mathcal{H}_c \rangle = \langle \Phi_a | \mathcal{H}_c | \Phi_b \rangle = \alpha\beta(E_a - E_b) \tag{B.5}$$

Studying the particular case of the present work, $|\Phi_a\rangle$ and $|\Phi_b\rangle$ are the unperturbed 0^+ states with good quantum numbers T=2 and T=1, respectively, and $|\Psi_a\rangle$ and $|\Psi_b\rangle$ are the observed isospin-mixed 0^+ states at 3526.4 and 3597.9 keV, respectively, in ^{56}Co. In order to avoid confusion, from now on we will specify the third component of isospin $T_z = (N-Z)/2$ of these unperturbed states in ^{56}Co, e.g., $|\Phi_a\rangle = |\Phi_a(T_z = +1)\rangle$.

In the $|T_z| = 2$ parent nuclei, i.e., ^{56}Fe ($T_z = +2$) or ^{56}Zn ($T_z = -2$), an isospin mixing with a $T = 1$ state cannot happen because they can never have such isospin value states. Thus, the initial ^{56}Fe or ^{56}Zn ground state is expected to be described by the eigenstate $|\Phi_a\rangle$ of good quantum number $T = 2$ of its isobaric analogue state (IAS) in the $|T_z| = 1$ nuclei except for the different T_z value. Thus we will use the following nomenclature: $|^{56}Fe_{g.s.}\rangle = |\Phi_a(T_z = +2)\rangle$.

Therefore, when isospin mixing exists and the Fermi transition strength is splitted, the ratio of the two Fermi-transition cross sections, in the particular case of the (p, n)-type CE reaction on ^{56}Fe, can be expressed as follows:

$$\begin{aligned}
\frac{d\sigma_b}{d\Omega} \Big/ \frac{d\sigma_a}{d\Omega} &= \frac{B(F)_b}{B(F)_a} \\
&= \frac{|\langle \Psi_b | \tau_- | ^{56}Fe_{g.s.} \rangle|^2}{|\langle \Psi_a | \tau_- | ^{56}Fe_{g.s.} \rangle|^2} \\
&= \frac{|\langle \Psi_b | \tau_- | \phi_a(T_z = +2) \rangle|^2}{|\langle \Psi_a | \tau_- | \phi_a(T_z = +2) \rangle|^2} \\
&= \frac{|\langle \Psi_b | \phi_a(T_z = +1) \rangle|^2}{|\langle \Psi_a | \phi_a(T_z = +1) \rangle|^2} \\
&= \left(\frac{\alpha}{\beta}\right)^2
\end{aligned} \tag{B.6}$$

where we have used the fact that the τ_- operator reduces the quantum number T_z in one unit. An analogue reasoning can be applied to the ^{56}Zn $\rightarrow^{56}$ Cu decay, which was also discussed in Chapter 1. Consequently, the isospin impurity α^2 can be deduced using Eqs. B.4 and B.6 if the ratio of the Fermi-transition cross sections can been measured. Then the off-diagonal matrix element $\langle \mathcal{H}_c \rangle$ is deduced using Eq. B.5.

Appendix C

TALYS software

TALYS is a software package for the simulation of nuclear reactions [32].

This package incorporates modern nuclear models for the optical model, level densities, direct reactions, compound (or fusion-evaporation) reactions, pre-equilibrium reactions, fission reactions and a large nuclear structure database. It calculates total and partial cross sections, energy spectrum angular distributions, residual production cross sections and recoils.

A particle incident on a target nucleus will induce several *binary* reactions which are described by various competing reaction mechanisms. The end products of a binary reaction are the emitted particle and the corresponding recoiling residual nucleus.

A common classification of the reaction mechanisms is made in terms of time scales: short reaction times are associated with direct reactions and long reaction times with compound nucleus processes. At intermediate time scales, pre-equilibrium processes occur. An alternative classification can be given with the number of intranuclear collisions, which is one or two for direct reactions, a few for pre-equilibrium reactions and many for compound reactions, respectively.

Inelastic scattering to discrete levels has a compound and a direct component. The former is described by the compound nucleus theory, while the latter is described by the Distorted Wave Born Approximation (DWBA) for spherical nuclei and by coupled-channels equations for deformed nuclei. At higher incident energies, inelastic cross sections to both discrete states and the continuum are possible. Like reactions to discrete states, reactions to the continuum also have a compound and a direct-like component. The latter are usually described by pre-equilibrium reactions which, by definition, include direct reactions to the continuum.

Compound versus pre-equilibrium reactions

The term compound reaction (or fusion-evaporation reaction) is mainly used for the process of the capture of the projectile in the target nucleus to form a compound nucleus, which subsequently emits a particle or a gamma. It is imagined that the incident particle step-by-step creates more complex states in the compound system

and gradually loses its memory of the initial energy and direction. Pre-equilibrium reactions embody both direct- and compound-like features. For instance, they are memory-preserving, which is a characteristic from the direct reactions. This type of reaction is not discussed in the present thesis, but it is useful to know its definition in order to understand the TALYS cross-section classification, presented in the following section.

C.0.1 TALYS cross section calculations

The TALYS software was used to study in detail the ^{56}Fe(p,n)^{56}Co reaction. We simulated a 10 MeV proton beam impinging on an ^{56}Fe target, i.e., p +^{56}Fe at $E_p = 10$ MeV.

TALYS uses the term non-elastic to refer to inelastic processes. We will use both the terms *non-elastic* and *inelastic* from now on. Total (binary) cross sections (in mb) are listed below:

- Reaction = 831.79
  - Compound elastic = 4.48
  - Non-elastic= 827.32
    - Direct=39.34
    - Pre-equilibrium=27.44
    - Giant resonance=3.17
    - Compound non-elastic=757.37

From the previous list it can be observed that inelastic reactions are clearly dominant, and in particular compound non-elastic is strongly the main mechanism.

In terms of the residual production, cross sections are shown in Table C.1 listed by isotope.

Table C.1: Residual-production cross section, calculating with the TALYS software, for the p +^{56}Fe reaction at $E_p = 10$ MeV, ordered by isotope.

Z	A	Nuclide	Total cross section
27	57	^{57}Co	0.42
27	56	^{56}Co	321.00
26	56	^{56}Fe	489.75
25	53	^{53}Mn	16.15

The ^{56}Fe(p,n)^{56}Co reaction

Studying the channel of interest, i.e., the (p,n) channel, we found that the compound reaction contribution represents more than 85% of the total cross section for all discrete levels up to 3.6 MeV (except, for two cases), and normally this percentage is higher than 96%.

We explained in section 2.2.5 that this information is important in order to choose appropriate peaks to check the Doppler shift correction. In that section we presented the reasons why in our experiment the ^{56}Fe peaks were chosen instead of ^{56}Co ones. We started from the assumption that due to the similar masses of both ^{56}Fe and ^{56}Co nuclei, one would expect a similar kinematics for the recoil in those cases, i.e., similar β value. If, tocheck the Doppler shift correction, we use ^{56}Fe peaks coming from the de-excitation of excited states that have been populated through the same reaction processes (and not radioactivity) than those in ^{56}Co we are interested in, the recoiling ^{56}Fe nucleus is expected to have a β value very similar to the recoiling ^{56}Co. Then we used two γ-rays de-exciting two different excited levels in ^{56}Fe that are strongly populated through compound reaction according to TALYS, as our 0^+ levels of interest in ^{56}Co are.

C.0.2 Recoiling ^{56}Co and ^{56}Fe kinetic-energy distributions

As already seen in subsection 2.2.5, the TALYS software was used to determine the recoil-energy spectrum of the ^{56}Co and ^{56}Fe nuclei after the p + ^{56}Fe reaction. The main aim was to justify and study the possibility of using ^{56}Fe peaks to check the Doppler shift correction. For each channel, one has a spread in the kinetic energies of the recoil. Looking at Fig. 2.18 we observe that the two recoil-kinetic-energy distributions are quite different, especially at low energies.

In the ^{56}Co case, this distribution has a maximum cross-section at $E_{recoil} = 0.166$ MeV (see left panel of Fig. 2.18).

The recoiling ^{56}Fe kinetic-energy distribution is more complicated (see right panel of Fig. 2.18). The cross-section as function of the ^{56}Fe kinetic energy is strongly peaked at low energies and has a hump around 0.4 MeV.

The recoiling ^{56}Fe nucleus will have more or less velocity depending on whether it has been produced either by a compound reaction or by a direct reaction. In direct reactions the outgoing particle keeps more energy and a lesser amount of the projectile momentum is transferred to the recoil. Thus the large cross-section values at low energies in the ^{56}Fe plot are probably associated with the direct component of the reaction populating low excited levels. So, why is this so in ^{56}Fe and not in ^{56}Co? Even though ^{56}Co and ^{56}Fe excited states are mostly populated via compound reaction processes (according to TALYS calculations), the first ^{56}Fe excited state, at 846.8 keV, has a dominant direct reaction component and large cross section

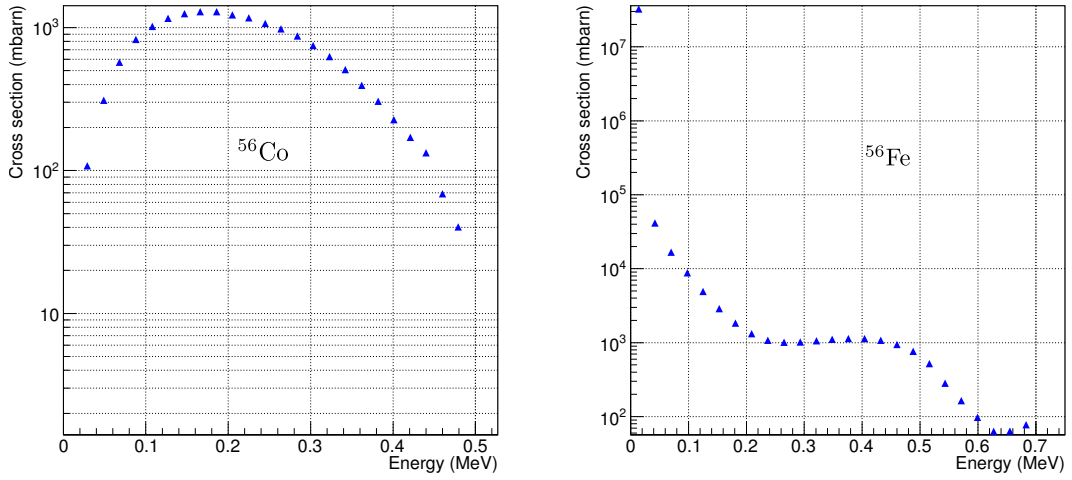

Figure C.1: The kinetic-energy distributions of the recoiling ^{56}Co (left) and ^{56}Fe (right) nuclei following the p + ^{56}Fe reaction at $E_p = 10$ MeV, calculated using the TALYS software.

(15% of the total cross-section up to 4.9-MeV excited levels). Also the direct-like components in the rest of the levels, even though small, are of direct origin, instead of pre-equilibrium origin as for ^{56}Co. Another result supporting the assumption that less energy is transferred to the recoiling ^{56}Fe nucleus than to the recoiling ^{56}Co nucleus is that the outgoing particle in the (p,p') channel, i.e., the proton, has an energy E_{out} around a factor of 3 larger than the outgoing particle of the (p,n) channel, i.e., the neutron, for the same excitation energy. Previous comments could partly explain the enormous cross-section values at low recoiling energies in the ^{56}Fe(p,p')^{56}Fe reaction.

Thus, summarising, we found out that, using an incident proton-beam of E_p =10 MeV:

- The ^{56}Fe(p,p')^{56}Fe reaction has a very important direct-component contribution, especially in the population of low excited states of the residual nucleus.
- In the ^{56}Fe(p,n)^{56}Co case, compound reactions are favoured and the direct reaction process (which is the *charge exchange* reaction) appears to be less likely. Thus the fusion-evaporation process seems to be favoured compared with the charge-exchange mechanism.

As a conclusion, we can claim that the reactions ^{56}Fe(p,p')^{56}Fe and ^{56}Fe(p,n)^{56}Co at an incident proton beam of 10 MeV show very different characteristics.

Appendix D

The *Eleven* code

The *Eleven* program is a code written in the FORTRAN programming language and developed by J. Gulyás at the Institute for Nuclear Research (Debrecen, Hungary) [45]. This code was created in order to obtain the level energies and intensity balance of a level scheme, specially necessary when handling with a large amount of information.

The code input is the experimental γ-transition information de-exciting each level, i.e., the transition energy and its uncertainty (E_γ and ΔE_γ), the transition intensity and its uncertainty (I_γ and ΔI_γ) and the internal conversion coefficient α_{TOT}.

The output provides the optimal level energies, E_{level}, based on the input information, accompanied by two different errors, and the balance of intensities feeding and de-exciting each level, which corresponds to the direct level-feeding. The code uses two standard methods for calculating the errors of the fitted parameters (i.e., E_{level}) from the input data (i.e., all E_γ provided). In the first method, the fitted parameter errors are the diagonal element square roots of the Least Squares fitting procedure matrix divided by the degree of freedom (i.e., number of input data minus number of fitted parameters). In the second method, the level energy errors come directly from the γ-transition energy errors, obtained by error propagation. Both values mean an error of one sigma. In the present work, the largest of the two errors was used.

The deviation of the new E_γ with respect to the input value is also provided in the output.

Appendix E

Spin-parity assignments

A detailed study of the spin-parity (J^π) assignments made in this work, level by level, is presented in this section. The J^π values suggested by us were already presented in Table 3.1.

The J^π assignments were mainly based on the γ-decay pattern observed in this work for a given level, and the selection rules presented in section 1.6.1. When previous J^π values existed in the literature for a given level, they were taken into account. Whenever possible, the angular coefficients A_2 obtained in the angular distributions $W(\theta_\gamma)$ of the γ-rays de-exciting the level in this work were taken into consideration. These values were compared with the tabulated values from Ref. [49]. For that purpose the Tables of the A_2 for mixed-multipolarity γ-rays as a function of the parameter δ (see the definition given in sec. 1.6.2) were used. The way of using these tables is the following: one looks for the spin (or spins) of the initial excited state J_i and the different options provided in the tables for the final spin J_f choosing the one which provides an A_2 value closer to our experimental value. From this comparison one can deduce if the transition had dipole (M1, E1), quadrupole (E2) or mixed character (M1/E2) (see 3.2). The A_2 coefficients measured in this work were already presented in Table 3.2.

Based on the different points discussed above, a definitive J^π value or several tentative options for each excited state were proposed by us. When different J^π values are suggested, the preferred ones are presented without parenthesis.

The levels discussed below are those for which there existed ambiguities or no previous J^π values were available in the literature. For the remainder of states, the γ-transitions observed in this work agreed with the previously reported J^π assignments.

A discussion of the J^π assignments, level by level, follows below:

2289.7-keV level

The J^π value of this level was previously unknown.

The γ-decays observed in this work suggest possible $J^\pi = 3^+(2^+, 4^+)$ values.

From previous work, we find the following information:

- No J^π assignment was made to this level in the ^{54}Fe(^{3}He,p)^{56}Co reaction [29]. They observed γ-transitions de-exciting to 2^+, 3^+ and 4^+ excited states.
- A $\Delta L = 2$+6 was assigned to the doublet 2281 + 2289 keV in the ^{56}Fe(^{3}He,t)^{56}Co experiment of [9]. The 2281 keV state corresponds to the 7^+ state at 2282.3 keV, which is in agreement with the $\Delta L = 6$ value. Therefore we could associate the $\Delta L = 2$ with the level under discussion, which is compatible with any of our previously mentioned J^π values.

From the angular distributions in this work we find:

- An $A_2 \sim 0$ for the W(θ_γ) of the 1319.4 keV γ-ray transition de-exciting to the firm 2^+ excited state at 970.3 keV. This result is not conclusive due to the large associated error but rules out the E2 character for the transition and hence the 4^+ possible J^π value of the level.
- An $A_2 > 0$ for the W(θ_γ) of the 2131.4 keV γ-ray transition de-exciting to the firm 3^+ excited state at 158.4 keV. This A_2 value is compatible with $3^+ \rightarrow 3^+$ or $4^+ \rightarrow 3^+$ mixed M1/E2 transitions, but makes the transition from $2^+ \rightarrow 3^+$ very unlikely.

Thus according to the previous discussion we propose $J^\pi = 3^+$ for this state.

2305.1-keV level

An uncertain $J^\pi = (2^+)$ assignment was previously reported [47].

Previous work provided the following information:

- An uncertain ΔL=2 was measured in the ^{58}Ni(d,α)^{56}Co reaction of [11]. They proposed $(2^+, 3^+)$.
- A possible natural parity from the tensor analysing powers, T_{20}, was deduced in the ^{58}Ni($\vec{d}, \alpha$)^{56}Co reaction at detection angles near 0° [18].

From the γ-decays observed in this work, this level would be compatible with $J^\pi = 2^+$ and 3^+. The angular distributions W(θ_γ) of the 1334.7 keV and 2146.4 keV γ-rays do not provide conclusive results. Nevertheless, the de-excitations from above can provide some clue about its spin-parity. The W(θ_γ) of the 871.6 keV de-exciting the 3176.8 keV level shows mixed M1/E2 character. Because of that we can affirm

that if the 3176.8-keV level (with $1^+, 3^+$ assignments from this work) was a 1^+, the 2305.1-keV level could not be 3^+.

From the previous results we suggest $J^\pi = 2^+(3^+)$ values, with the remark that if the 3176.8-keV level is actually a 1^+, the 2305.1-keV level could not be 3^+.

The comparison with the shell-model predictions in a truncated pf-shell valence space using KB3G and GX1A effective interactions with a truncation $q = 2$ suggest that this state is actually a 2^+ (see Fig. 4.3).

2469.3-keV level

The J^π value of this level was previously unknown.

The γ-decays observed in this work suggest a probable 4^+, but 3^+, 5^+ are also possible. Then we propose $J^\pi = 4^+(3^+, 5^+)$ for this state.

The comparison with the shell-model predictions in a truncated pf-shell valence space using the KB3G and GX1A effective interactions with a truncation $q = 2$ suggest that this state is actually a 4^+ (see Fig. 4.3).

2635.1-keV level

A $J^\pi = 1^+$ value was reported for this level in the literature [47].

The reported information about this level is the following:

- An uncertain $\Delta L = (0)$ was assigned in the ^{58}Ni$(d, \alpha)^{56}$Co and ^{54}Fe(^{3}He,p)^{56}Co reactions in [11]. In this reference they assigned $J^\pi = (1^+)$ to this level.
- A $\Delta L = 2$ in the ^{58}Ni(p,^{3}He)^{56}Co reaction of [23] was assigned to a state at 2.626 MeV. In this reference they assigned $J^\pi = 2^+, 3^+$.
- An unnatural parity from the tensor analysing powers, T_{20}, was deduced in the ^{58}Ni$(\vec{d}, \alpha)^{56}$Co reaction at detection angles near 0° of [18].
- This level was observed in the favoured $\Delta L = 0$ high-resolution ^{56}Fe(^{3}He,t)^{56}Co experiment of [2]. However, in this work they claimed that there exist serious doubts about the $J^\pi = 1^+$ value of this level.

From the angular distribution W(θ_γ) of the de-exciting 1184.6-keV γ-ray to the firm 1450.6-keV 0^+ level we obtain a clear negative A_2 value ($A_2 = -0.33 \pm 0.03$), totally in agreement with a pure M1 transition corresponding to a $J^\pi = 1^+$ value of the initial state.

Our measured γ-ray transitions de-exciting this level and the previous angular distributions results corroborate the previous $J^\pi = 1^+$ assignment.

2647.3-keV level

Uncertain assignments $J^\pi = (0^+, 1^+)$ to this state were previously reported in [47]. However we do not agree with this spin-parity value.

From previous work, the following information is available:

- No determination of natural or unnatural parity from the tensor analysing power, T_{20}, was made in the ^{58}Ni$(\vec{d}, \alpha)^{56}$Co reaction at detection angles near 0° [18].
- A ΔL=0 was assigned in the ^{58}Ni(d,α)^{56}Co reaction of [11]. This is the evidence used in the compilation [47] to make the assignment $(0^+, 1^+)$. However an examination of their results suggest that ΔL=2 or 3 is a better match, which agrees with our results.

Our γ-transitions suggest $J^\pi = 3^+, 4^+(2^+)$. The angular distributions from this work result in an $A_2 = -1.12(8)$ from W(θ_γ) of the 2489.0-keV γ-ray transition to the firm 3^+ level at 158.4 keV. This result is compatible with a mixed M1/E2 $4^+ \rightarrow 3^+$ or $2^+ \rightarrow 3^+$ transition, but it is *too negative* to be a $3^+ \rightarrow 3^+$ decay.

Therefore we suggest $J^\pi = 4^+(2^+)$ values.

The comparison with the shell-model predictions in a truncated *pf*-shell valence space using the KB3G and GX1A effective interactions with a truncation $q = 2$ suggest that this state is actually a 4^+ (see Fig. 4.3).

2666.2-keV level

An uncertain $J^\pi = (3^+)$ assignment to this level was reported in [47].

The previously reported information is presented here:

- An unnatural parity from the tensor analysing powers, T_{20}, was deduced in the ^{58}Ni$(\vec{d}, \alpha)^{56}$Co reaction at detection angles near 0° [18]. They suggested 3^+.
- A possible ΔL=(2) was measured in the ^{58}Ni(d,α)^{56}Co reaction of [11]. They suggested $2^+, 3^+$.

The angular distributions from this work results in an $A_2 > 0$ for W(θ_γ) of the 2507.8-keV γ-ray transition to the firm 158.4-keV 3^+ level. This result is compatible with a $3^+ \rightarrow 3^+$ mixed M1/E2 transition.

According to the previously known information and the results from this work we support the $J^\pi = 3^+$ value.

2729.1-keV level

A firm $J^\pi = 1^+$ assignment to this level was reported in reference [**Nds2100**].

The following information from previous work was reported:

- An unnatural parity from the tensor analysing powers, T_{20}, was deduced in the ^{58}Ni($\vec{d}, \alpha$)^{56}Co reaction at detection angles near 0° [18].
- A ΔL=0 was assigned to this level in the ^{58}Ni(d,α)^{56}Co reaction of [11]. They suggested 1^+.
- A ΔL=0+2 was measured in the ^{56}Fe(^{3}He,t)^{56}Co experiment of [9]. They suggested $1^+(2^+)$.
- This level was observed in the favoured $\Delta L = 0$ high-resolution ^{56}Fe(^{3}He,t)^{56}Co experiment of [2].

No angular distributions have been obtained in this work. Based on the γ-ray transitions observed in the present work, we agree with the previous assignment of $J^\pi = 1^+$.

2774.3-keV level

The J^π value of this level was previously unknown.

From the γ-ray transitions observed in the present work, we suggest $J^\pi = 4^+(3^+, 5^+)$ values.

The comparison with the shell-model predictions in a truncated *pf*-shell valence space using the KB3G and GX1A effective interactions with a truncation $q = 2$ suggest that this state is actually a 4^+ (see Fig. 4.3).

2835.7-keV level

This level has been observed in this work for the first time.

The clear γ-ray transition to the firm 970.3-keV 2^+ state suggest $J^\pi = 1^+, 2^+, 3^+$ as probable values for this state. No angular distributions have been made in this work for γ-transitions de-exciting this level.

The comparison with the shell-model predictions in a truncated *pf*-shell valence space using the KB3G and GX1A effective interactions with a truncation $q = 2$ suggest that this state is actually a 2^+ (see Fig. 4.3).

We propose then $J^\pi = 2^+(1^+, 3^+)$ values.

2927.5-keV level

An uncertain $J^\pi = (2^+)$ value was reported to this level in [47].

Our γ-transitions suggest $J^\pi = 3^+, 4^+(2^+)$. This level was studied in most of the previous experiments as part of the doublet with the 2970.7 keV state due to a deficient resolution. We have the following information from the previous work:

- $\Delta L = 2$ was measured in a (^{3}He,p) reaction from reference [73].
- An uncertain ΔL=(2) was measured in the ^{58}Ni(d,α)^{56}Co reaction of [11]. The experimental data from that work look more compatible with ΔL=3 or 4. They assigned ΔL=(4) to its partner in the doublet, the 2970 keV level.
- Very clear natural parity from the tensor analysing powers, T_{20}, was deduced in the ^{58}Ni($\vec{d}, \alpha$)^{56}Co reaction at detection angles near 0° [18]. They suggested a possible (2^+) value for this level, because they assigned a clear 2^+ to its partner in the doublet, the state at 2969 keV.

From the angular distributions in this work we find a clear $A_2 < 0$ from W(θ_γ) of 1813.2 keV γ-ray transition to the firm 1114.6-keV 3^+ level. This value and the previous information are compatible with the $2^+ \rightarrow 3^+$ and $4^+ \rightarrow 3^+$ mixed M1/E2 transitions.

We suggest $J^\pi = 4^+(2^+)$ values for this state.

The comparison with the shell-model predictions in a truncated *pf*-shell valence space using the KB3G and GX1A effective interactions with a truncation $q = 2$ suggest that this state is actually a 4^+ (see Fig. 4.3).

2970.7-keV level

A $J^\pi = 2^+$ value was previously assigned to this level in [47].

Our γ-transitions suggest $J^\pi = 3^+, 4^+(2^+)$. This level was studied in most of the previous works as part of the doublet with the 2927.5 keV state due to a deficient resolution. We have the following information from the previous work:

- A possible ΔL=(4) was assigned in the ^{58}Ni(d,α)^{56}Co reaction of [11]. No spin-parity assignment was made to this level in this work.

- A ΔL=2 was measured in the ^{56}Fe(^{3}He,t)^{56}Co experiment of [9]. They suggested $1^+, 2^+$.

- Very clear natural parity from the tensor analysing powers, T_{20}, was deduced in the ^{58}Ni($\vec{d}, \alpha$)^{56}Co reaction at detection angles near 0° [18]. They assigned a clear 2^+.

From the angular distributions in this work we find an slightly $A_2 > 0$ from W(θ_γ) of the 2812.6-keV γ-ray transition to the firm 158.4-keV 3^+ level. Relying on this result and on the previous information this transition is compatible with a $2^+ \rightarrow 3^+$ mixed M1/E2 transition.

Therefore we agree with the $J^\pi = 2^+$ previous assignment.

3041.5-keV level

Possible values $J^\pi = 3^+, 4^+, 5^+$ were assigned to this level according to compilation [47].

The previously reported information is presented:

- An uncertain $\Delta L = (4)$ was measured in the ^{58}Ni(p,^{3}He)^{56}Co reaction of [23].

- An unnatural parity from the tensor analysing powers, T_{20}, was deduced in the ^{58}Ni($\vec{d}, \alpha$)^{56}Co reaction at detection angles near 0° [18]. This would favour only 3+ and 5+ options.

- Possible ΔL=5 or 6 were assigned in the ^{58}Ni(d,α)^{56}Co reaction of [11].

From the angular distributions in this work we find an $A_2 > 0$ for the W(θ_γ) of the 2883-keV γ-ray transition to the firm 158.4-keV 3^+ level which is compatible with $5^+ \rightarrow 3^+$ (E2) or $3^+ \rightarrow 3^+$ (non-stretch M1) transitions.

Our measured γ-transitions de-exciting this level and the positive A_2 value found in the angular distributions support the $J^\pi = 3^+, 5^+$ assignments.

3061.0-keV level

A firm $J^\pi = 5^+$ was assigned to this level in reference [47].

From previous work the following information is available:

- $\Delta L = 4$ was measured in the ^{58}Ni$(d,\alpha)^{56}$Co reaction of [11]. In this reference they assigned $J^\pi = 4^+(5^+)$ but do not provide reasons to reject the 3^+ option.
- An unnatural parity from the tensor analysing powers, T_{20}, was deduced in the ^{58}Ni$(\vec{d},\alpha)^{56}$Co reaction at detection angles near 0° [18].
- A doublet $L = 2 + 4$ was seen in the ^{56}Fe(^{3}He,t)^{56}Co reaction of [9] at the excitation energy of this state.

From the angular distributions in this work we find an slightly $A_2 < 0$ for the W(θ_γ) of the de-exciting 2902.4-keV γ-ray to the firm 158.4-keV 3^+ level. This result is not compatible with $5^+ \rightarrow 3^+$ (E2 transition), but $3^+ \rightarrow 3^+$ mixed M1/E2 would be possible.

From our γ-transitions de-exciting this level and from the angular distribution discussion made in the previous paragraph we propose $J^\pi = 3^+(5^+)$ values.

3068.8-keV level

This level has been observed for the first time in the present work.

Our γ-transitions suggest $J^\pi = 3^+, 4^+, 5^+$. A clear $A_2 << 0$ for the W(θ_γ) of the de-exciting 2910.5-keV γ-ray to the firm 158.4-keV 3^+ level is compatible with $3^+ \rightarrow 3^+$ and $4^+ \rightarrow 3^+$ mixed M1/E2 transitions.

Then the options $J^\pi = 3^+$,4^+ are proposed for this level.

3075.7-keV level

A $J^\pi = 1^+$ value was assigned to this level from previous work [47].

The reported information about this level is the following:

- A $\Delta L = 2$ was measured in ^{58}Ni$(d,\alpha)^{56}$Co reaction of [11]. In this reference they assigned $J^\pi = (1^+), 2^+, 3^+$.
- An unnatural parity from the tensor analysing powers, T_{20}, was deduced in the ^{58}Ni$(\vec{d},\alpha)^{56}$Co reaction at detection angles near 0° [18]. They proposed $J^\pi = 1^+, 3^+$.

- A $J^\pi = 1^+$ assignment was made from the angular distributions measured in the ^{58}Ni$(d, \alpha\gamma)^{56}$Co reaction of [31].

- This level was observed in the favoured $\Delta L = 0$ high-resolution ^{56}Fe(^{3}He,t)^{56}Co experiment of [2]. However, in this work they claimed that there exist serious doubts about the $J^\pi = 1^+$ value of this level.

From the angular distributions in this work we find a clear negative A_2 value ($A_2 = -0.42 \pm 0.04$) for the W(θ_γ) of the de-exciting 1625.2-keV γ-ray to the firm 1450.6-keV 0^+ level, totally in agreement with a pure M1 transition corresponding to a $J^\pi = 1^+$ value of the initial state.

Our measured γ-ray transitions de-exciting this level and the previous angular distributions results corroborate the previous $J^\pi = 1^+$ assignment.

3139.2-keV level

A firm $J^\pi = 3^+$ was assigned to this level from previous work [47].

Previous work provided the following information:

- A possible $\Delta L = 2 + 4$ was measured in the ^{58}Ni(p,^{3}He)^{56}Co reaction of [23]. They proposed an uncertain $J^\pi = 3^+$.

- $\Delta L = 2$ was measured in the ^{58}Ni$(d, \alpha)^{56}$Co reaction of [11]. In this reference they suggested $J^\pi = 3^+, (2^+)$.

- An unnatural parity was deduced from the tensor analysing powers, T_{20}, in the ^{58}Ni$(\vec{d}, \alpha)^{56}$Co reaction at detection angles near 0° [18].

The γ-ray transitions observed at the present work de-exciting this level agree with the previous $J^\pi = 3^+$ assignment. The information extracted from the angular distributions is not conclusive but is compatible with that value. Nevertheless, some multipolarity discussion can be made:

- An slightly $A_2 < 0$ for the W(θ_γ) of the de-exciting 2980.7-keV transition to the firm 158.4-keV 3^+ indicates that this $3^+ \rightarrow 3^+$ transition is a mixture M1/E2 .

- An slightly $A_2 > 0$ for the W(θ_γ) of the de-exciting 2168.9-keV transition to the firm 970.3-keV 2^+ indicates that this $3^+ \rightarrow 2^+$ transition is a mixture M1/E2.

3176.9-keV level

The values $J^\pi = 1^+, 3^+$ were proposed for this level in literature [47].

The information already reported in the literature is presented:

- A $\Delta L = 2$ was assigned in the ^{54}Fe(^{3}He, p)^{56}Co reaction from reference [73]. Their work suggested $J^\pi = 1^+, 2^+, 3^+$.
- A possible $\Delta L = (2)$ was assigned in the ^{58}Ni(d, α)^{56}Co reaction of [11]. No spin-parity tentative assignments were made to this level.
- A doublet $\Delta L = 0 + 4$ was seen in the ^{56}Fe(^{3}He,t)^{56}Co for this level in [9].
- An unnatural parity from the tensor analysing powers, T_{20}, was deduced in the ^{58}Ni($\vec{d}, \alpha$)^{56}Co reaction at detection angles near 0° [18].

From the angular distributions in this work we find:

- Uncertain $A_2 \leq 0$ for the W(θ_γ) of the de-exciting 1116.8-keV transition to the well-known 2060.1-keV 2^+ level. Without being conclusive, this value is compatible with both $1^+ \rightarrow 2^+$ and $3^+ \rightarrow 2^+$ transitions.
- An slightly $A_2 < 0$ for the W(θ_γ) of the 871.6-keV γ-ray transition to the 2305.1-keV level (of spin-parity values $J^\pi = 2^+(3^+)$ proposed at the present work). Option $1^+ \rightarrow 3^+$ (E2 transition) would show a positive A_2 behaviour. This argument was presented in the 2305.1-keV level discussion to justify the preference of the $J^\pi = 2^+$ assignment to that level. If the actual initial spin-parity was 3^+, the $3^+ \rightarrow 3^+$ transition would be clearly a mixture M1/E2. For the present level, both $1^+ \rightarrow 2^+$ and $3^+ \rightarrow 2^+$ would be compatible with the measured A_2 value.

We conclude that both options $J^\pi = 1^+, 3^+$ are compatible with our experimental information.

3234.5-keV level

A $J^\pi = (0^+)$ was assigned to this level in reference [47]. However we do not agree with this spin-parity value.

From previous work, the reported information is the following:

- This level was suggested to be a $J^\pi = 0$ value due to a $\Delta L = 2$ observed in the ^{58}Ni(d, α)^{56}Co experiment of [11]. Nevertheless, an examination of their results suggests that a transfer of $\Delta L = 4$ is also possible.

- An unnatural parity from the tensor analysing powers, T_{20}, was deduced in the ^{58}Ni$(\vec{d},\alpha)^{56}$Co reaction at detection angles near 0° [18].

Our measured γ-ray transitions indicate that the following J^π values would be possible: $4^+(3^+,5^+,4^-)$. From the angular distributions in this work we find an $A_2 \geq 0$ value for the W(θ_γ) of the de-exciting 3076.0-keV γ-ray to the 158-keV 3^+ level. This value excludes E2 ($5^+ \rightarrow 3^+$) and E1 ($4^- \rightarrow 3^+$) transitions. For the remaining of the options, the transition would be in any case a mixture M1/E2.

We suggest the spin-parity values $J^\pi = 4^+(3^+)$ for this level.

3255.1-keV level

The J^π value of this level was previously unknown.

This level is not seen in the favoured $\Delta L = 0$ high-resolution ^{56}Fe(^{3}He,t)^{56}Co experiment measured at 0° [2]. This fact relegates 1^+ value from a preferential option.

Our measured γ-ray transitions are compatible with $J^\pi = 1^+, 1^-, 2^+$. From the angular distributions in this work we find:

- Very uncertain $A_2 < 0$ for the W(θ_γ) of the de-exciting 1805.0-keV γ-ray to the firm 1450.6-keV 0^+ state. This result implies a very attenuated but pure M1 transition, favouring initial spins $J^\pi = 1^+, 1^-$.

- An $A_2 < 0$ value for the W(θ_γ) of the de-exciting 2284.7-keV γ-ray to the firm 970.3-keV 2^+ level, which is compatible with the J^π values comptabile with our measured γ-ray transitions. Within the error this A_2 implies a pure E1 or an almost pure M1 transition.

We propose $J^\pi = 1^-(1^+)$ values according to the previous discussion.

3298.2-keV level

A firm $J^\pi = 4^+$ was reported in literature for this state [47] due to the following evidences:

- A $\Delta L = 4$ was assigned in the ^{58}Ni$(d,\alpha)^{56}$Co reaction of [11]. They assigned $J^\pi = 4^+, 5^+$.

- Natural parity from the tensor analysing powers, T_{20}, was deduced in the ^{58}Ni$(\vec{d},\alpha)^{56}$Co reaction at detection angles near 0° [18].

From the angular distributions in this work we find:

- An $A_2 < 0$ for the W(θ_γ) of the de-exciting 3139.9-keV γ-ray to the firm 158.4-keV 3^+ level which would be compatible with a mixed $4^+ \rightarrow 3^+$ M1/E2 transition.

Our experimental results are not conclusive but they are compatible with the previous spin-parity assignment $J^\pi = 4^+$.

3339.6-keV level

This level has been observed in this work for the first time.

Our measured γ-ray transitions suggest possible values $J^\pi = 1^+, 1^-, 2^+, 2^-, 3^+$.

Because this level was not seen in the favoured $\Delta L = 0$ high-resolution ^{56}Fe(^{3}He,t)^{56}Co experiment measured at 0° [2], we discard 1^+ value as a preferential option.

From the angular distributions in this work we find:

- An $A_2 < 0$ for the W(θ_γ) of the de-exciting 982.4-keV γ-ray to the firm 2357.3-keV 1^+ level compatible with $2^+ \rightarrow 1^+$ mixed M1/E2 transition. This result excludes an $1^- \rightarrow 1^+$ E1 transition, but a $2^- \rightarrow 1^+$ E1 transition would be possible within the error. Clearly it is not an E2 transition, then we also discard 3^+.

- An $A_2 > 0$ for the W(θ_γ) of the de-exciting 2368.9-keV γ-ray to the firm 970.3-keV 2^+ level which is also compatible with a $2^+ \rightarrow 2^+$ mixed M1/E2 transition. However $2^- \rightarrow 2^+$ E1 transition looks very unlikely according to that A_2 value.

Taking all this into account our best value for this state is $J^\pi = 2^+$.

3362.5-keV level

This state is probably the 3366(5)-keV level from reference [47], for which a possible negative parity was proposed.

Our measured γ-ray transitions suggest $J^\pi = 2^+(1^+)$ values. However the 1^-,2^- and 3^- options are excluded, so not negative parity options are proposed.

The previously reported information is the following:

- An uncertain $\Delta L = (3)$? assignment in the ^{58}Ni$(d,\alpha)^{56}$Co reaction of [11] was made. No spin-parity assignment was made for this state.
- An unnatural parity from the tensor analysing powers, T_{20}, was deduced in the ^{58}Ni$(\vec{d},\alpha)^{56}$Co reaction at detection angles near 0° [18].
- Because this level was not seen in the favoured $\Delta L = 0$ high-resolution ^{56}Fe(^{3}He,t)^{56}Co experiment measured at 0° [2], we discard 1^+ value as a preferential option.

From the angular distributions in this work we find:

- An uncertain $A_2 \gtrsim 0$ for the W(θ_γ) of the de-exciting 2247.8-keV γ-ray to the firm 1114.6-keV 3^+ level. It is not a conclusive information but it makes the $1^+ \rightarrow 3^+$ E2 transition very unlikely.
- An uncertain $A_2 \lesssim 0$ for the W(θ_γ) of the de-exciting 2392.3-keV γ-ray to the firm 970.3-keV 2^+ level. Not conclusive.

Therefore we do not propose any negative parity option and relying on the previous information presented here we suggest $J^\pi = 2^+$ for this level.

3377.2-keV level

A $J^\pi = 1^+$ value was assigned to this level in [47]. However we do not agree with this assignment.

The previous information in literature about this state looks ambiguous. This ambiguity is probably due to the presence of an unresolved doublet (from this work we have obtain a neighbouring level at 3379.2 keV (see next case)):

- A $\Delta L = 0 + 2$ was assigned to a 3379-keV state from a (^{3}He,p) reaction in compilation [73].
- In the ^{58}Ni$(d,\alpha)^{56}$Co reaction of [11] a 2284-keV state was seen and associated to an unknown ΔL.
- A 3374-keV level was observed in the favoured $\Delta L = 0$ high-resolution ^{56}Fe(^{3}He,t)^{56}Co experiment measured at 0° [2], and associated to a possible $\Delta L = (0)$.

From the angular distributions in this work we find:

- A clear $A_2 < 0$ for the W(θ_γ) of the de-exciting 2262.6-keV γ-ray to the firm 1114.6-keV 3^+ level. This result excludes the possibility of an $1^+ \rightarrow 3^+$ E2 transition.

- An uncertain $A_2 \simeq 0$ for the W(θ_γ) of the de-exciting 2407.1-keV γ-ray to the firm 970.3-keV 2^+ level. This information is not conclusive but it is compatible with a $2^+ \rightarrow 3^+$ mixed M1/E2 transition.

Based on the γ-transitions observed in this work and according to the angular distribution results we propose $J^\pi = 2^+$ for this state.

3379.0-keV level

This level has been observed in this work for the first time.

The angular distributions of the present work shows a clear $A_2 > 0$ for the W(θ_γ) of the de-exciting 3220.4-keV γ-ray to the firm 158.4-keV 3^+ level. The γ-de-excitations and the previous result shows that this level is probably a $J^\pi = 3^+$. In that case the 3220.4-keV transition would be a pure non-stretched $3^+ \rightarrow 3^+$ M1 transition.

We propose a $J^\pi = 3^+$ value for this state.

3432.5-keV level

This level was associated with the possible $J^\pi = 0^+, 1^+$ values in [47]. Our γ-decays suggest $1^+(1^-, 2^+)$, discarding the 0^+ option.

The following information from previous works is available:

- $\Delta L = 1$ assignment was made in the ^{58}Ni$(d, \alpha)^{56}$Co reaction of [11]. They assigned a $J^\pi = 1^+$ value to the level.

- An unnatural parity from the tensor analysing powers, T_{20}, was deduced in the ^{58}Ni$(\vec{d}, \alpha)^{56}$Co reaction at detection angles near 0° [18]. They associated $J^\pi = 1^+$.

- This level was observed in the favoured $\Delta L = 0$ high-resolution ^{56}Fe(^{3}He,t)^{56}Co experiment measured at 0° [2]. They assigned a clear $\Delta L = 0$ to this state.

From the angular distributions in this work we find a clear $A_2 < 0$ for the W(θ_γ) of the de-exciting 1982.4-keV γ-ray to the firm 1450.6-keV 0^+ level. This result shows a pure L=1 transition. Relying on the unnatural parity from [18] we can affirm that the state has $J^\pi = 1^+$ and therefore the 1982.4-keV γ-decay is a pure M1 transition.

We propose a firm $J^\pi = 1^+$ value.

3495.2-keV level

The J^π value of this level was previously unknown.

This state has very similar features to the previous case (see the 3432.5-keV level). Our γ-decays suggest $1^+(1^-, 2^+)$.

The following results were obtained in previous work:

- An unnatural parity from the tensor analysing powers, T_{20}, was deduced in the ^{58}Ni($\vec{d}, \alpha$)^{56}Co reaction at detection angles near 0° [18]. No spin-parity assignment was made to this level in this work.
- This level was observed in the favoured $\Delta L = 0$ high-resolution ^{56}Fe(^{3}He,t)^{56}Co experiment measured at 0° [2]. They make the clear assignment to a $\Delta L = 0$.

The angular distributions in this work shows a clear $A_2 < 0$ for the W(θ_γ) of the de-exciting 2044.4-keV γ-ray to the firm 1450.6-keV 0^+ level. This result shows a pure L=1 transition. Relying on the unnatural parity from [18] we can affirm that the state has $J^\pi = 1^+$ and the 2044.4-keV γ-decay is a pure M1 transition.

We propose a firm $J^\pi = 1^+$ value for this state.

3510.3-keV level

A $J^\pi = (0^+)$ was assigned to this level from previous work [47]. However we do not agree with this spin-parity value.

The previously reported information about this level is presented:

- $\Delta L = 0$ was assigned to a state at 3511-keV excitation energy in the ^{56}Fe(^{3}He,t)^{56}Co experiment from reference [9]. However, the state that they observed was the 3526.6-keV 0^+ state.
- In the ^{58}Ni(p,^{3}He)^{56}Co reaction in [23], they assigned $\Delta L = 0$ to a 3501-keV state. As the previous comment, we strongly believe that the state which was observed was the 3526.6-keV 0^+ state.

From the angular distributions in this work we find a clear positive A_2 value ($A_2 = 0.96(17)$) in the W(θ_γ) of the 3352.1-keV γ-ray to the firm 158.4-keV 3^+ state. This value is not compatible either with $(3^-, 4^-) \rightarrow 3^+$ E1 transitions or with a pure $3^+ \rightarrow 3^+$ non-stretch M1 transition. However, it is compatible with $3^+ \rightarrow 3^+$ or $4^+ \rightarrow 3^+$ mixed M1/E2 decays. The A_2^{max} coefficient from Ref. [**Mateosian**] reaches values as high as our experimental A_2 in the latter transition. This suggests that $J^\pi = 4^+$ is slightly more probable than the $J^\pi = 3^+$.

Taking all this into account we propose $J^\pi = 4^+(3^+)$ values for this state.

3524.6-keV level

This level has been observed in this work for the first time.

The γ-de-excitations from this work suggest $J^\pi = 2^+, 3^+, 4^+(2^-, 3^-, 1^+)$. No angular distributions for the γ-transitions de-exciting this level have been obtained in the present work.

3526.4-keV level

This level was previously reported as $J^\pi = 0^+$ in [47]. This state is one of the 0^+ states which study was one of the main motivations to perform the experiment that we present in this work.

From previous work, the following information is available:

- A $\Delta L = 0$ value was assigned to a state at 3522(9)-keV excitation energy identified as the IAS in the ^{56}Fe(^{3}He,t)^{56}Co experiment from reference [8].
- In the ^{54}Fe(^{3}He,p)^{56}Co reaction in [29], they assigned $J^\pi = 0^+, 1^+$ values to this level due to its γ-decay pattern.
- Natural parity from the tensor analysing powers, T_{20}, was deduced in the ^{58}Ni($\vec{d}, \alpha$)^{56}Co reaction at detection angles near 0° [18].
- A $\Delta L = 0$ was assigned to this level in the favoured $\Delta L = 0$ high-resolution ^{56}Fe(^{3}He,t)^{56}Co experiment measured at 0° [2]. They identified the state as a clear 0^+.

The γ-decays observed in this work corroborate this assignment. No angular distributions have been made in this work for γ-transitions de-exciting this level. The statistics of the new γ-transitions is not sufficient to obtain reasonable W(θ_γ) distributions.

Taking all this into account we agree with the $J^\pi = 0^+$ assignment for this state.

3545.7-keV level

A $J^\pi = 7^+$ value was reported in literature for this level [47].

From previously reported information, we have the following items:

- An unnatural parity from the tensor analysing powers, T_{20}, was deduced in the ^{58}Ni$(\vec{d},\alpha)^{56}$Co reaction at detection angles near 0° [18]. They suggested $J^\pi = 7^+$.
- In the ^{58}Ni$(d,\alpha)^{56}$Co reaction of [**Nann**], a $\Delta L = 6$ transfer was deduced.

No angular distributions have been made in this work for the γ-transitions de-exciting this level. The γ-decay observed in this work is in agreement with the previous spin-parity assignment.

Thus we agree with the $J^\pi = 7^+$ value.

3585.4-keV level

This level probably corresponds to the unknown spin-parity state at 3570(?)keV excitation energy.

From the γ-decays observed in this work, possible values are $J^\pi = 2^+(2^-, 3^+, 1^+)$.

Previous work provided the following information:

- This level was not observed in the favoured $\Delta L = 0$ high-resolution ^{56}Fe(^{3}He,t)^{56}Co experiment measured at 0° [2]. Then we exclude 1^+ as a preferential option.
- From the angular distributions in this work we find a clear negative A_2 value ($A_2 = -1.06(4)$) in the W(θ_γ) of the 3427.3-keV γ-ray to the firm 158.4-keV 3^+ state. This value is not compatible either with a $2^- \rightarrow 3^+$ E1 transition or with a $3^+ \rightarrow 3^+$ transition. It would be compatible with a $2^+ \rightarrow 3^+$ mixed M1/E2 transition.

Then we suggest $J^\pi = 2^+$ for this level.

3589.4-keV level

This level has been observed in this work for the first time.

No angular distributions have been made in this work for the γ-transitions de-exciting this level. From the γ-transitions observed in this work $J^\pi = 5^+, 4^+(4^-, 5^-)$ values are possible.

3597.9-keV level

This state is the well known 0^+ isobaric analogue state (IAS) of the 0^+ g.s. in ^{56}Fe (see reference [47]).

The following information is reported in the literature:

- A $\Delta L = 0$ value was assigned to the state at 3592(9)-keV excitation energy identified as the IAS in the ^{56}Fe(^{3}He,t)^{56}Co experiment from reference [8].

- In the ^{54}Fe(^{3}He,p)^{56}Co reaction in [29] they assigned a $J^\pi = 0^+$ value.

- A $\Delta L = 0$ was measured in the favoured $\Delta L = 0$ high-resolution ^{56}Fe(^{3}He,t)^{56}Co experiment measured at 0° [2]. They identified the state as a clear 0^+.

The γ-decays observed in this work corroborate this assignment. No angular distributions have been made in this work for the γ-transitions de-exciting this level.

According to the information presented here we agree with the previously assigned $J^\pi = 0^+$ value for this state.

3607.8-keV level

The J^π value of this level was previously unknown.

From our γ-transitions this state is compatible with $J^\pi = 3^+, 3^-, 2^+, 2^-$.

From previous work [18], an unnatural parity from the the tensor analysing powers, T_{20}, was deduced in the ^{58}Ni($\vec{d}, \alpha$)^{56}Co reaction at detection angles near 0°. No spin-parity assignments were made to this level.

From the angular distributions in this work we find:

- A clear $A_2 > 0$ for the W(θ_γ) of the de-exciting 1302.6-keV γ-ray to the $2^+(3^+)$ state at 2305.1-keV excitation energy.

- Uncertain but clear negative $A_2 << 0$ value from W(θ_γ) of the 1677.7-keV γ-ray to the firm 1930.3-keV 3^+ state. This result would exclude the $(2^-, 3^-) \rightarrow 3^+$ E1 transitions.

- An slightly $A_2 < 0$ for the W(θ_γ) of the de-exciting 3449.3-keV ray to the firm 158.4-keV 3^+ state. This value is compatible with the $(2^+, 3^+) \rightarrow 3^+$ mixed M1/E2 transitions.

According to the previous results we suggest $J^\pi = 3^+(2^+)$ for this level.

3707.0-keV level

This level has been observed in this work for the first time.

From the γ-transitions observed in this work $J^\pi = 3^+, 4^+, 4^-, 5^+$ values are possible.

From the angular distributions in this work we find:

- A clear $A_2 >> 0$ ($A_2 = 0.6(2)$) for the W(θ_γ) of the de-exciting 2697.6-keV γ-ray to the firm 1009.1-KeV 5^+ state. This result would be favoured by $J^\pi = 3^+, 5^+$ values of the state under discussion. However, using the theoretical $A_2^{max} = 0.238$ for a $3^+ \rightarrow 5^+$ transition, one obtains a nonsense attenuation coefficient for this level.

- An slightly $A_2 < 0$ value from the W(θ_γ) of the 2592.6-keV γ-ray to the firm 1114.6-keV 3^+ state, though a large uncertainty is associated. This value would discard an E2 $5^+ \rightarrow 3^+$ transition.

Previous angular distribution results are contradictory. However, the $J^\pi = 3^+$ value seems to be slightly more probable. Then we suggest $J^\pi = 3^+(5^+)$ values.

3708.0-keV level

There exists a previously known state at 3717(5)-keV excitation energy of negative parity reported in [47]. The γ-de-excitations observed in this work suggest $J^\pi = 2^+, 3^+(2^-, 3^-)$ values.

We present here the information previously reported in the literature:

- $\Delta L = (3)$ in the ^{58}Ni$(d, \alpha)^{56}$Co reaction from [11] assigned to a 3711-keV state. No spin-parity conclusions are obtained.

- An unnatural parity of a 3717-keV state from the tensor analysing powers, T_{20}, was deduced in the ^{58}Ni$(\vec{d}, \alpha)^{56}$Co reaction at detection angles near 0° [18]. No spin-parity assignments were made to this level in this work.

From the angular distributions in this work we find:

- An uncertain $A_2 < 0$ for the W(θ_γ) of the de-exciting 1403.2-keV γ-ray to the 2305.1-keV $2^+(3^+)$ state.

- Uncertain $A_2 \simeq 0$ value from the W(θ_γ) of the 2737.2-keV γ-ray to the firm 970.3-keV 2^+ state. This result excludes the $2^- \rightarrow 2^+$ E1 transition.

- Clear $A_2 < 0$ value from the W(θ_γ) of the 3549.4 keV γ-ray to the firm 158.4 keV 3^+ state. This result excludes the $3^- \rightarrow 3^+$ E1 transition.

From the γ-transitions observed in this work and the angular distribution results shown above, we propose $J^\pi = 2^+, 3^+$ values for this level.

3791.7-keV level

There is a previously known level at 3798(11) keV reported in [47], with positive parity assignment.

A $\Delta L = (6)$ in the ^{58}Ni$(d, \alpha)^{56}$Co reaction from [11] was determined, though no spin-parity assignments were made.

Our γ-de-excitations suggest $J^\pi = 6^+, 6^-$. Option $J^\pi = 5^+$ does not look so likely because the transition to the 576-keV 5^+ state is not seen. No angular distributions have been made in this work for the γ-transitions de-exciting this level.

Therefore we propose $J^\pi = 6^+, 6^-$ values.

3794.4-keV level

This level has been observed in this work for the first time.

The γ-de-excitations observed in the present work suggest $J^\pi = 3^+, 4^+, 2^+, 3^-, 4^-$ as possible values.

From the angular distributions in this work we find:

- A clear $A_2 >> 0$ for the W(θ_γ) of the de-exciting 2679.9-keV γ-ray to the firm 1114.5-keV 3^+ state. Pure $(3^+, 3^-) \rightarrow 3^+$ L=1 transitions (M1 or E1 respectively) are compatible with this result. A mixed $4^+ \rightarrow 3^+$ M1/E2 transition is also possible. The $4^- \rightarrow 3^+$ decay (E1 transition) is excluded.

- A clear $A_2 >> 0$ for the W(θ_γ) of the de-exciting 3636.1-keV γ-ray to the firm 158.4-keV 3^+ state. Same comments from previous item.

- Not conclusive information from an uncertain A_2 value from the W(θ_γ) of the 2964.6-keV γ-ray.

We strongly suggest $J^\pi = 3^+, 3^-(4^+)$ values.

3809.8-keV level

The spin-parity assignments $J^\pi = 1^+, 2^+, 3^+$ to this state are reported in [47].

We discard the 1^+ option due to γ-de-excitations observed in the present work. The possible values are $J^\pi = 2^+, 3^+, 4^+, 3^-, 4^-$.

From previous work, the following information is reported:

- In [11] an uncertain $\Delta L = (2)$ from the ^{58}Ni$(d,\alpha)^{56}$Co and $\Delta L = (4)$ from the ^{54}Fe(^{3}He,p)^{56}Co are assigned to the level under discussion.
- The level was not observed in the favoured $\Delta L = 0$ high-resolution ^{56}Fe(^{3}He,t)^{56}Co experiment measured at 0° [2], excluding 1^+ as a preferential option.

From the angular distributions in this work we find an $A_2 < 0$ value from the W(θ_γ) of the de-exciting 3651.4.1-keV γ-ray to the firm 158.4-keV 3^+ state. This result excludes the $3^- \rightarrow 3^+$ and $4^- \rightarrow 3^+$ E1 transitions. It is compatible with a mixed M1/E2 transition from any of the remaining J^π proposed values.

The γ-de-excitation to the ground state (4^+) looks probable from the experimental data. Therefore, based on the γ-de-excitations seen in this work and from the negative angular distribution, we propose as most probable the $J^\pi = 4^+(3^+, 2^+)$ values.

3819.4-keV level

This level has been observed in this work for the first time.

No angular distributions have been made in this work for the γ-transitions de-exciting this level. The γ-transitions observed by us would suggest that this state is $J^\pi = 0^+(1^+)$.

3866.2-keV level

The J^π value of this level was previously unknown.

Previously reported information is presented here:

- A 3.870-MeV state was observed in the favoured $\Delta L = 0$ high-resolution ^{56}Fe(^{3}He,t)^{56}Co experiment measured at 0° [2]. They associated this level to the previously known state at 3863(12) keV and assigned a $\Delta L = 0$ and $J^\pi = 1^+$.

- $\Delta L = (3, 4)$ in the ^{58}Ni$(d, \alpha)^{56}$Co reaction from [11]. No spin-parity conclusions were obtained.

The previous information is contradictory. No angular distributions have been obtained in this work.

From the γ-transitions observed by us we suggest $J^\pi = 1^+, 2^+(3^+)$ values .

3872.6-keV level

A previously positive parity was assigned to this level in [47].

The γ-de-excitation to the ground state looks possible from our *Singles* spectrum. According to the γ-de-excitations observed depopulating this level it could be $J^\pi = 2^+, 3^+, 4^+, 3^-$.

From previous work, we have the following information:

- Very uncertain $\Delta L = (2)$ in the ^{58}Ni$(d, \alpha)^{56}$Co reaction from [11]. No spin-parity conclusions were deduced.

- A 3.870-MeV state was observed in the favoured $\Delta L = 0$ high-resolution ^{56}Fe(^{3}He,t)^{56}Co experiment measured at 0° [2]. They assigned $\Delta L = 0$ and $J^\pi = 1^+$. However they associated this level to the previously known state at 3863(12)keV.

From the angular distributions in this work we find a clear $A_2 << 0$ ($A_2 = -1.05$) for the W(θ_γ) of the de-exciting 2902.3-keV γ-ray to the firm 970.4-keV 2^+ state. This value excludes the E1 ($3^- \rightarrow 2^+$) and E2 ($4^+ \rightarrow 2^+$) transitions. In turn, it is more compatible with a $3^+ \rightarrow 2^+$ mixed M1/E2 transition than with a $2^+ \rightarrow 2^+$ transition due to its *very negative* value.

We propose then the $J^\pi = 3^+(2^+)$ values for this state.

3895.2-keV level

The J^π value of this level was previously unknown.

No angular distributions have been obtained in this work. From the γ-transitions observed in this work from this level we suggest $J^\pi = 4^+, 5^+(3^+, 4^-)$ values.

3925.4-keV level

This level has been observed in this work for the first time.

No angular distributions have been made in this work for the γ-transitions de-exciting this level. We propose $J^\pi = 2^+, 3^+$ values for this state based on the γ-transitions seen in this work.

3930.7-keV level

The J^π value of this level was previously unknown.

In [11] a state at 3935(12)-keV excitation energy in the ^{58}Ni$(d,\alpha)^{56}$Co reaction was observed. No spin-parity assignments were made.

No angular distributions have been made in this work for the γ-transitions de-exciting this level. From the γ-transitions observed by us we propose $J^\pi = 3^+, 2^+, 4^+$.

4005.5-keV level

The values $J^\pi = 3^+, 4^+, 5^+$ were assigned to a 4011(12)-keV state in [47]. The assignment was based on the $\Delta L = 4$ measured in the ^{58}Ni(d,α)^{56}Co reaction of reference [11].

No angular distributions have been made in this work for the γ-transitions de-exciting this level. Due to a clear γ-de-excitation to the 2357.3-keV state (firm 1^+) observed in this work, and relying on the convincing $\Delta L = 4$ from the previous reference, we propose the $J^\pi = 3^+$ as the most probable spin-parity value.

4011.6-keV level

This excited state is compatible in energy with the 4011(12)-keV state in [47] from reference [11] (see the previous level case). However, from our γ-de-excitations we believe it is another level, probably the 4019(12)-keV state observed in [11]. Apart from that, a 4019-keV state was observed in the favoured $\Delta L = 0$ high-resolution ^{56}Fe(^{3}He,t)^{56}Co experiment measured at 0° [2]. No spin-parity assignments were made.

From the angular distributions in this work we find:

- An slightly $A_2 < 0$ for the W(θ_γ) of the de-exciting 3041.5-keV γ-ray to the firm 970.4-keV 2^+ state.

- A very uncertain $A_2 < 0$ for the W(θ_γ) of the de-exciting 1706.4-keV γ-ray to the 2306.0-keV $2^+(3^+)$ state. This result is not conclusive.

- Both results would be compatible with mixed M1/E2 transitions.

Based on γ-de-excitations and the previous angular distribution results we propose $J^\pi = 2^+(1^+, 3^+)$ values.

4029.4-keV level

$J^\pi = 1^+, 2^+, 3^+$ values were assigned to a state at 4032(12) keV in [47].

From previous work, the following information is available:

- A 4032(12)-keV state with uncertain $\Delta L = (3)$ in the ^{58}Ni(d,α)^{56}Co reaction from [11].

- The $L(^3$He,p) = 2 presented in reference [47] about this level is not found in the cited references.

Our γ-transitions are compatible with 2^+ and 4^+ options. From the angular distributions in this work we find:

- A clear $A_2 >> 0$ ($A_2 = 0.7(2)$) for the W(θ_γ) of the de-exciting 3059.3-keV γ-ray to the firm 970.4-keV 2^+ state. This value is not compatible with a $4^+ \rightarrow 2^+$ E2 transition (which would have $A_2 < 0$). Moreover, it implies that the $2^+ \rightarrow 2^+$ decay is probably a mixture M1/E2.

- Not enough statistics to obtain the W(θ_γ) of the de-exciting 3199.2-keV γ-ray.

Therefore we propose $J^\pi = 2^+$ value for this level.

4058.6-keV level

The J^π value of this level was previously unknown.

The following information was already reported in the literature:

- An 4062(12)-keV state with uncertain $\Delta L = (3)$? in the ^{58}Ni(d,α)^{56}Co reaction and $\Delta L = (4)$ in the ^{54}Fe(^{3}He,p)^{56}Co reaction from [11]. No spin-parity assignments were made.

No angular distributions have been made in this work for the γ-transitions de-exciting this level.

Based on the γ-transitions obtained in the present work we propose $J^\pi = 4^+(4^-, 5^+, 3^+)$ values.

4086.9-keV level

The J^π value of this level was previously unknown.

Previously reported information is presented:

- A 4094(12)-keV state was presented in [11] with neither L value nor spin-parity assignments.
- A 4093-keV state was seen in the favoured $\Delta L = 0$ high-resolution ^{56}Fe(^{3}He,t)^{56}Co experiment measured at 0° [2]. No spin-parity assigned were made to this level.

Only one (but clear) γ-transition is observed in this work de-exciting this state. This little information impedes a definite assignment. No angular distributions have been made in this work for the γ-transitions de-exciting this level. Our best guesses are $J^\pi = 1^+, 0^+, 2^+$.

4134.1-keV level

The values $J^\pi = (3^+, 4^+, 5^+)$ were associated to the 4139(12)-keV state observed in [11]. They assigned a clear $\Delta L = 4$ in the ^{58}Ni(d,α)^{56}Co reaction.

From the γ-de-excitations observed in the present work (to two 1^+ states) we believe that the 4134.1-keV state is not that previously known level.

From the angular distributions in this work we find an $A_2 < 0$ for the W(θ_γ) of the de-exciting 2413.8-keV γ-ray to the firm 1720.3-keV 1^+ state.

Therefore this state is suggested to be $J^\pi = 1^+, 2^+$.

4177.9-keV level

This level is a positive-parity state according to [47].

There is a 4185(10)-keV state with an uncertain $\Delta L = (2)$? associated in the ^{58}Ni(d,α)^{56}Co reaction from [11]. No spin-parity assignment were made . Due to γ-transitions observed in this work we propose $J^\pi = 4^+(3^+, 4^-, 3^-)$ values.

4201.1-keV level

This level is a level observed for the first time in this work or the previously known 4209(12)-keV state in compilation [47] taken from reference [11].

Previously reported information is presented here:

- The 4209(12)-keV state from reference [11] has neither L value nor spin-parity assignments.
- In the favoured $\Delta L = 0$ high-resolution ^{56}Fe(^{3}He,t)^{56}Co experiment measured at 0° [2] a 4210-keV state was observed. No spin-parity assignment were made.

From the angular distributions in this work we find:

- Uncertain $A_2 \geq 0$ value from the W(θ_γ) of the de-exciting 3230.9-keV γ-ray to the firm 970.4-keV 2^+ state. This value excludes the E1 transitions $2^- \rightarrow 2^+$ and $3^- \rightarrow 2^+$.
- There is not enough statistics from our data to obtain the W(θ_γ) of the other γ-rays.

Based on our γ-de-excitations and according to the angular distributions values from above we propose $J^\pi = 2^+, 1^+, 3^+$ values.

4203.2-keV level

This level is a level observed for the first time in this work or the previously known 4209(12)-keV state in compilation [47] from reference [11]. Despite the closeness in energy to 4201.1keV level (see the previous level case) due to the γ-de-excitations pattern we consider it is a different level. Then the same observations can be made:

- The 4209(12)-keV state from reference [11] has neither L value nor spin-parity assignments.
- In the favoured $\Delta L = 0$ high-resolution ^{56}Fe(^{3}He,t)^{56}Co experiment measured at 0° [2] a 4210-keV state was observed. No spin-parity assignment.

No angular distributions have been obtained in this work. Based on the experimental γ-de-excitations we propose $J^\pi = 2^+, 1^+, 1^-$ values.

4213.3-keV level

This level is a level observed for the first time in this work or the previously known 4209(12)-keV state in compilation [47] taken from work [11]. The same observations than the two previous cases (see 4201.1 and 4203.2keV states) can be made:

- The 4209(12)-keV state from reference [11] has neither L value nor spin-parity assignments.
- In the favoured $\Delta L = 0$ high-resolution ^{56}Fe(^{3}He,t)^{56}Co experiment measured at 0° [2] a 4210-keV state was observed. No spin-parity assignment were made.

No angular distributions have been made in this work for the γ-transitions de-exciting this level.

Due to γ-transitions observed in the present thesis we propose $J^{\pi} = 4^{+}(3^{+}, 4^{-}, 3^{-})$ values.

4225.5-keV level

The J^{π} value of this level was previously unknown.

From previous work, the following information is available:

- The state at 4222(13)keV observed in reference [11] has neither L value nor spin-parity values assigned to it.
- No state close to that energy was observed in the favoured $\Delta L = 0$ high-resolution ^{56}Fe(^{3}He,t)^{56}Co experiment measured at 0° [2].

Only one (but clear) γ-transition observed de-exciting this state in this work. This little information impedes making a definite assignment. No angular distributions were made for the transitions de-exciting this level in the present work.

Our best guesses are $J^{\pi} = 1^{+}, 0^{+}, 2^{+}$.

4283.7-keV level

The J^{π} value of this level was previously unknown.

The previously reported information is presented:

- The state at 4281(13) keV from reference [11] has neither L value nor spin-parity values assigned to it.
- In the favoured $\Delta L = 0$ high-resolution ^{56}Fe(^{3}He,t)^{56}Co experiment measured at 0° [2] a 4284-keV state was observed. No spin-parity assignments were made to this level in this work.

From the angular distributions in this work we find:

- An $A_2 < 0$ for the W(θ_γ) of the de-exciting 4125.5-keV γ-ray to the firm 158.4-keV 4^+ state.
- Not enough statistics to obtain the W(θ_γ) of the de-exciting 1994.7- and 3313.0-keV γ-rays.

Based on the γ-transitions observed in this work and on the previous information, this level is suggested to be $J^\pi = 3^+(4^+, 2^+, 3^-)$.

4299.3-keV level

The J^π value of this level was previously unknown.

From previously reported work, a state at 4293(13)keV was observed in [11] with neither L value nor spin-parity assigned to it.

No angular distributions were made for the transitions de-exciting this level in the present work.

Based on the γ-transitions observed in this work we propose $J^\pi = 3^+(2^+, 4^+, 3^-)$ values.

4366.5-keV level

This level has been observed in this work for the first time.

No state close to that energy was observed in the favoured $\Delta L = 0$ high-resolution ^{56}Fe(^{3}He,t)^{56}Co experiment measured at 0° [2].

No angular distributions were made for the transitions de-exciting this level in the present work.

Only one (but clear) γ-transition observed de-exciting this state in this work. This little information impedes making a definite assignment. No angular distributions have been obtained in the present work. Our best guesses are $J^\pi = 1^+, 0^+, 2^+$.

4372.9-keV level

This level is a $J^\pi = 1^+$ state according to compilation [47].

The following information was already reported in the literature:

- $\Delta L = 0{+}2$ in the ^{54,56,58}Fe(^{3}He,p)^{56}Co reaction in [12]. They assigned $J^\pi = 1^+$.
- In the ^{54}Fe(^{3}He,p)^{56}Co reaction from [29], $J^\pi = (1^+, 2^+)$ values are assigned to this level due to its γ-decay.
- A 4387-keV state was observed in the favoured $\Delta L = 0$ high-resolution ^{56}Fe(^{3}He,t)^{56}Co experiment measured at 0° [2]. No spin-parity assignments were made. It could correspond to the 4372.9-keV state (the one under discussion) or to the 4379.5-keV state (see next level).

From the angular distributions in this work we find a clear $A_2 << 0$ for the W(θ_γ) of the de-exciting 2922.2-keV γ-ray to the firm 1450.8-keV 0^+ stat. Therefore the transition corresponds to a pure M1 decay, and there is no ambiguity about the spin of the de-exciting state, $J = 1$.

Then based on the γ-transition de-exciting the state and the A_2 value obtained in this work we are in fully agreement with the previous $J^\pi = 1^+$ assignment.

4379.5-keV level

The possible values $J^\pi = 1^+, 2^+, 3^+$ were assigned to this state in the reference [47].

From previous works, the following information is reported:

- A state at 4388(13) keV seen in [11]. They assigned a clear $\Delta L = 2$ in the ^{58}Ni(d,α)^{56}Co reaction. Therefore $J^\pi = 2^+, 3^+(1^+)$ values.
- A 4387-keV state observed in the favoured $\Delta L = 0$ high-resolution ^{56}Fe(^{3}He,t)^{56}Co experiment measured at 0° [2]. No spin-parity assignments were made. It could correspond to the 4372.9-keV state (see the previous level) or to the 4379.5-keV state (the one under discussion).

No angular distributions were made for the transitions de-exciting this level in the present work.

According to the γ-de-excitations observed in this work and to the previous information we propose $J^\pi = 2^+, 3^+(1^+)$ values.

4441.3-keV level

A $J^\pi = 7^+$ value was assigned to this state in [47]. However we do not agree with this spin-parity value.

From previously reported works, the following information is available:

- A 4439-keV state was observed in the ^{54,56,58}Fe(^{3}He,p)^{56}Co reaction in [12]. However no L value was assigned.
- In the ^{58}Ni(p,^{3}He)^{56}Co reaction in [23], a $\Delta L = 2$ value was assigned to a 4.432-MeV state.
- A 4.451-MeV state was seen in the ^{54}Fe(^{3}He,p)^{56}Co reaction from [74], where a $\Delta L = 2$ value was assigned.
- A 4441-keV level was observed in the ^{58}Ni(d,α)^{56}Co reaction from [11] for which a $\Delta L = 6(+4)$ value was assigned. The $J^\pi = 7^+$ value in [47] is probably taken from this work. We strongly believe that our state is not this one.

No angular distributions were made for the transitions de-exciting this level in the present work.

From the γ-transitions observed in the present work we suggest $J^\pi = 3^+(4^+, 4^-)$ values.

Appendix F

Resum del treball

F.1 Introducció i motivació de l'experiment

La investigació del nucli imparell-imparell ^{56}Co és interessant per una sèrie de raons. Des del punt de vista del model de capes, a l'anàlisi més simple el ^{56}Co ($Z = 27$, $N = 29$) té només un protó menys (també vist com un forat als protons) i un neutró més que el nucli doblement màgic ^{56}Ni ($N = Z = 28$). Idealment, l'espectroscopia del ^{56}Co hauria de proporcionar directament informació sobre la interacció residual particle-forat a la capa *fp*.

D'altra banda, el nucli ^{56}Ni és l'isòtop produït més abundantment a la fase de combustió del silici a les estrelles de massa superior a 10 masses solars, i juntament amb el seu producte de desintegració, el ^{56}Co, juguen un important paper en la potència radiactiva irradiada a la majoria de supernoves.

El mecanisme de decaïment beta (β) està ben entès i ve dominat pels modes de desintegració Fermi (F) o Gamow-Teller (GT). Ambdós modes de desintegració converteixen un protó en un neutró o viceversa, per la qual cosa el nucli atòmic canvia i la tercera component d'isospí, definida com $T_z = (N - Z)/2$, varia en una unitat. La transició Fermi (operador τ) connecta l'estat inicial del nucli pare amb l'estat anàleg isobàric (en anglès, *Isobaric Analogue State*, IAS) en el nucli fill. Ambdós estats comparteixen la mateixa estructura i nombres quàntics moment angular (ò espí) total J^π i isospí T. L'operador τ és l'operador d'augment o disminució de la tercera component d'isospí, mentre que el moment angular orbital L i intrínsec S, i l'isospí es mantenen constants, és a dir, $\Delta L = 0$, $\Delta S = 0$ (i per tant, $\Delta J = 0$) i $\Delta T = 0$. D'altra banda, l'operador involucrat en la transició Gamow-Teller ($\sigma\tau$), a més del canvi al T_z del nucli, produeix una variació d'una unitat a l'espí i l'isospí. Així, $\Delta L = 0$ i $\Delta S = 1$ (i per tant, $\Delta J = 1$) i $\Delta T = 1$.

L'estudi del nucli ^{56}Co en el present treball fou inicialment motivat per l'observació de dos estats 0^+ en el seu nucli mirall ^{56}Cu en una experiment de decaïment β del ^{56}Zn realitzat a GANIL (Caen, França) [1]. Aquests dos estats són poblats mitjançant una desintegració de tipus Fermi i corresponen al desdoblament de l'IAS. Dos estats molt similars existeixen al nucli ^{56}Co i foren recentment investigats a l'experiment d'alta resolució d'intercanvi de càrrega (IC) ^{56}Fe(^{3}He,t)^{56}Co al *Research Centre for Nuclear Physics* (RCNP) a Osaka (Japó) [2].

Un dels objectius principals de l'experiment que presentam en aquest treball va ser estudiar detalladament la desexcitació gamma dels dos estats 0^+ als quals existeix mescla d'isospí (un és majoritàriament l'IAS i l'altre un estat molt pròxim en energia) al ^{56}Co i comparar els resultats amb l'observat al seu nucli mirall.

El mecanisme de desintegració β i les reaccions IC poden ser comparades sota certes condicions experimentals, concretament quan la reacció IC es duu a terme:

- a baixos angles pròxims a 0°,

- a energies incidents intermitges, generalment ($E \geq 100$ MeV/nucleó).

La motivació del present treball està definit a aquest context. La figura F.1 mostra la simetria mirall del multiplet d'isospí $T = 2$. El multiplet d'isospí està compost per $2T+1$ membres. La tercera component d'isospí $T_z = (N-Z)/2$ varia en una unitat entre membres veïns del multiplet. La desintegració β, $T_z = -2 \rightarrow -1$, connecta els nuclis ^{56}Zn i ^{56}Cu. D'altra banda, els estats excitats del ^{56}Co es poblen mitjançant la reacció IC de tipus (p,n), $T_z = +2 \rightarrow +1$, sobre ^{56}Fe. Els estats fonamentals dels nuclis pare $\mid T_z \mid = 2$, ^{56}Zn i ^{56}Fe, tenen els mateixos nombres quàntics $J^\pi = 0^+$ i $T = 2$. S'espera que es poblin dos tipus d'estats als corresponents nuclis fill en aquests processos: l'IAS, 0^+ amb $T = 2$ (mitjançant transició Fermi) i diversos estats 1^+ amb $T = 1$ (mitjançant transicions de tipus Gamow-Teller). El nucli doblement màgic ^{56}Ni es correspon amb el membre $T_z = 0$ del multiplet.

F.1.1 L'experiment de desintegració β del ^{56}Zn

La desintegració β del ^{56}Zn en ^{56}Cu es dugué a terme a GANIL [1]. L'experiment es realitzà a les instal.lacions LISE3 utilitzant un feix primari de ^{58}Ni^{26+}.

La intensitat (coneguda com "strength", en anglès) de la transició Fermi ve donada per l'expressió $\mid N-Z \mid = 4$. La *strength* Fermi a l'estat situat a 3508 keV d'energia d'excitació al ^{56}Cu (identificat prèviament com l'IAS de l'estat fonamental del ^{56}Fe) mesurada va ser $B(F) = 2.7(5)$. La intensitat perduda havia d'estar amagada al pic gruixat que fou observat a 3423 keV. Aquest fet fou la confirmació de que l'IAS al ^{56}Cu està fragmentat degut a la mescla d'isospí i així part de la desintegració al nivell situat a 3423 keV correspon a transició de tipus Fermi.

El desdoblament de la intensitat Fermi és degut a la mescla d'isospí entre nivells que tenen nominalment diferent valor d'isospí T. Aquesta mescla està causada per l'element de matriu fóra de la diagonal de la part del Hamiltonià de la interacció depenent de la càrrega, $\langle \mathcal{H}_c \rangle$. Així, siguin els estats mesclats $|\Psi_a\rangle$ i $|\Psi_b\rangle$, aquests

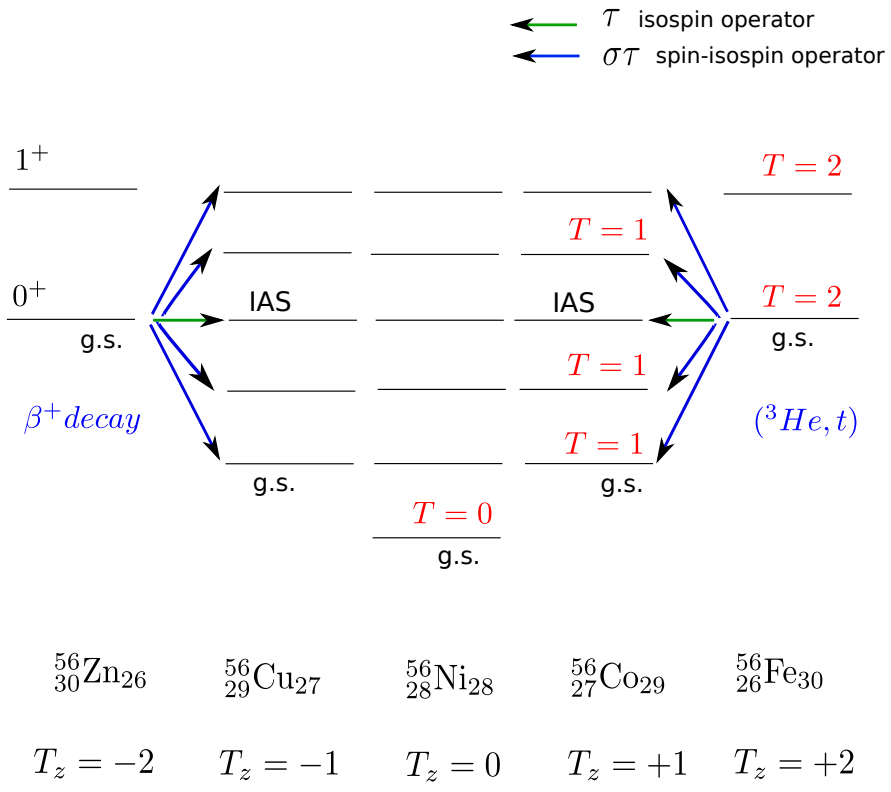

Figure F.1: Esquema gràfic del multiplet d'isospí $T = 2$ per nuclis amb nombre màssic $A = 56$. El decaïment β i les reaccions d'intercanvi de càrrega poden comparar-se sota certes condicions (veure text principal). La transició Fermi (operador τ) connecta l'estat inicial amb $T = 2$ del nucli pare amb l'IAS al nucli fill, tenint la mateixa estructura i els mateixos nombres quàntics J^π i isospí. La tercera component d'isospí $T_z = (N - Z)/2$ varia en una unitat entre membres veïns del multiplet. Les transicions a estats 1^+, amb $T = 1$, són de tipus Gamow-Teller (operador $\sigma\tau$).

poden descriure's en termes dels estats amb isospí com a bon nombre quàntic $|\Phi_a\rangle$ i $|\Phi_b\rangle$ segons l'expressió:

$$|\Psi_a\rangle = \beta|\Phi_a\rangle \pm \alpha|\Phi_b\rangle \tag{F.1a}$$
$$|\Psi_b\rangle = \mp\ \alpha|\Phi_a\rangle + \beta|\Phi_b\rangle. \tag{F.1b}$$

on el paràmetre α especifica la quantitat d'impuresa d'isospí, i α i β han de complir la condició $\alpha^2 + \beta^2 = 1$.

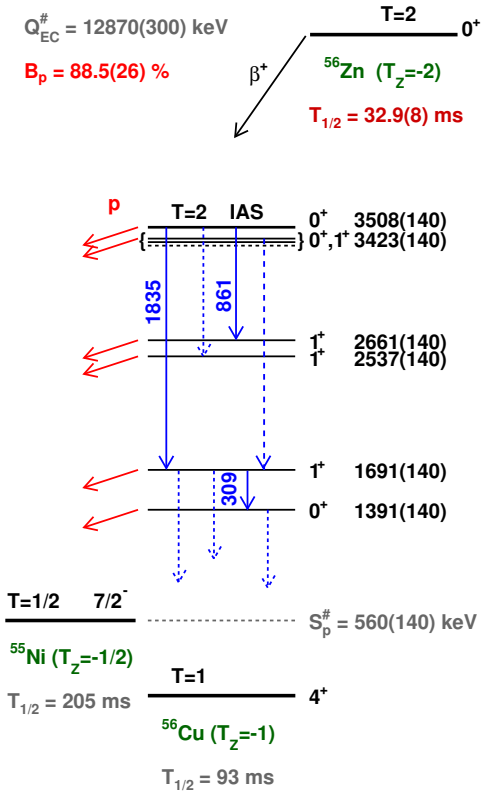

Figure F.2: ^{56}Zn decay scheme deduced from the ^{56}Zn β-decay experiment at GANIL. Observed proton or γ decays are indicated by solid lines. Transitions corresponding to those seen in the mirror ^{56}Co nucleus but not seen in ^{56}Cu are shown by dashed lines. The 140 keV-error comes from the uncertainty in S_p.

L'element $\langle \mathcal{H}_c \rangle$ i la impuresa d'isospí α^2 poden ser deduïts si les dades experimentals ho permeten. A l'experiment de desintegració β del ^{56}Zn va ser deduïda una impuresa d'isospí $\alpha^2 = 33(10)\%$.

Al seu torn aquest experiment fou motivat per la comparació amb la reacció mirall d'intercanvi de càrrega sobre ^{56}Fe, que pobla estats excitats del ^{56}Co, el nucli mirall de ^{56}Cu, i que explicam a la següent secció.

La figura F.2 mostra l'esquema de desintegració del ^{56}Zn deduït a partir de l'experiment de decaïment β. Els protons ò desintregracions γ observats a l'experiment estan indicats amb línies sòlides. D'altra banda, les transicions conegudes al seu nucli mirall, el ^{56}Co, però no observades a ^{56}Cu, estan indicades mitjançant línia discontínua. Podria ser que aquestes transicions no observades existissin però estigueren per davall el nivell de sensibilitat gamma de l'experiment. Cal esmentar que el nucli ^{56}Zn és exòtic i l'estadística que es va obtenir a l'experiment fou baixa. Dues transicions

γ foren observades i atribuïdes a la desexcitació de l'estat situat a 3508 keV. Tanmateix, cap desexcitació gamma va ser observada associada a l'estat a 3423 keV. Al moment de la realització d'aquest experiment, una transició gamma es coneixia desexcitant el seu nivell homòleg al ^{56}Co. Així, considerant que la mescla d'isospí és gran al ^{56}Cu, una pregunta interessant seria la següent: han de desexcitar-se de forma simil.lar els dos estats 0^+ als quals existeix mescla d'isospí? I, degut a la simetria d'isospí, no haurien el ^{56}Co i el ^{56}Cu de desexcitar de forma anàloga?

F.1.2 La reacció d'intercanvi de càrrega ^{56}Fe(^{3}He, t)^{56}Co

La reacció d'intercanvi de càrrega ^{56}Fe(^{3}He, t)^{56}Co va ser realitzada al *Research Centre for Nuclear Physics* (RCNP) a Osaka [2] amb alta resolució energètica. S'utilitzaren feixos de ^{3}He de 100 i 140 MeV/nucleó. La bona resolució aconseguida va fer possible estudiar l'estructura fina dels dos estats 0^+ molt pròxims en energia (que formen un doblet) al ^{56}Co i els estats excitats propers.

Les mesures foren realitzades a angles focalitzats entorn a la direcció del feix, incluint 0°, afavorint així una transferència de moment orbital $\Delta L = 0$. Llavors principalment estats 0^+ i 1^+ foren poblats a ^{56}Co.

Per tal de distingir entre la possible naturalesa 0^+ ò 1^+ dels estats, es pot aprofitar el fet què les *strengths* de les interaccions efectives de tipus τ o $\sigma\tau$ tenen diferent dependència amb l'energia incident del projectil. En les reaccions d'intercanvi de càrrega a energies intermitges i a prop de 0°, existeix una bona proporcionalitat entre les seccions eficaces de les interaccions GT i Fermi, σ_{GT} i σ_F, i el quadrat dels elements de matriu de transició. Perquè la *intensitat de transició reduïda*, B, és proporcional al quadrat de l'element de matriu de transició, podem escriure:

$$\sigma_{GT}(0^\circ) = \hat{\sigma}_{GT} B(GT) \tag{F.2a}$$

$$\sigma_F(0^\circ) = \hat{\sigma}_F B(F) \tag{F.2b}$$

on $\hat{\sigma}_{GT}$ i $\hat{\sigma}_F$ denoten les seccions eficaces unitàries GT i Fermi, respectivament. Un estudi sistemàtic en reaccions (p,n) per sota $E_p = 200$ MeV mostrà que el quocient de les seccions eficaces unitàries, $\hat{\sigma}_{GT}/\hat{\sigma}_F$, és pràcticament proporcional al quadrat de l'energia incident del feix de protons [3]. Això és causat pel fet què la intensitat del terme τ de la interacció lliure nucleó-nucleó es torna més gran a energies incidents baixes, mentre que la intensitat del terme $\sigma\tau$ roman pràcticament constant. Així doncs, s'espera que $\hat{\sigma}_F$ es torni major en comparació a $\hat{\sigma}_{GT}$ a energies incidents baixes. Així, els estats excitats mitjançant transició Fermi es veuran realçats en comparació amb els estats excitats mitjançant transició GT als espectres obtinguts.

Els espectres d'energia d'excitació de la reacció ^{56}Fe(^{3}He, t) a energies 100 i 140 MeV/nucleó es mostren a la Fig. F.3. Els espectres corresponen a les energies

mesurades del triti (t) i els pics estan etiquetats d'acord a les corresponents energies d'excitació al ^{56}Co. L'estat aïllat (intensament poblat mitjançant una transició GT) situat a 2.729 MeV fou utilitzat com a pic de normalització.

El quocient entre les seccions eficaces a 100 i 140 MeV/nucleó mostra quant la secció eficaç relativa augmenta a la mesura del primer respecte al segon. Com es pot veure clarament, l'estat a 3.599 MeV es troba realçat a l'espectre a 100 MeV/u. També ho està l'estat a 3.527 MeV. D'aquest resultat es va concloure que l'operador de tipus Fermi excita ambdós estats i que, llavors, existeix un desdoblament de la *strength* de la transició Fermi i, conseqüentment, de l'IAS. Així doncs els dos estats tenen $J^\pi = 0$ (el mateix que té l'estat fonamental del blanc, el nucli parell-parell ^{56}Fe).

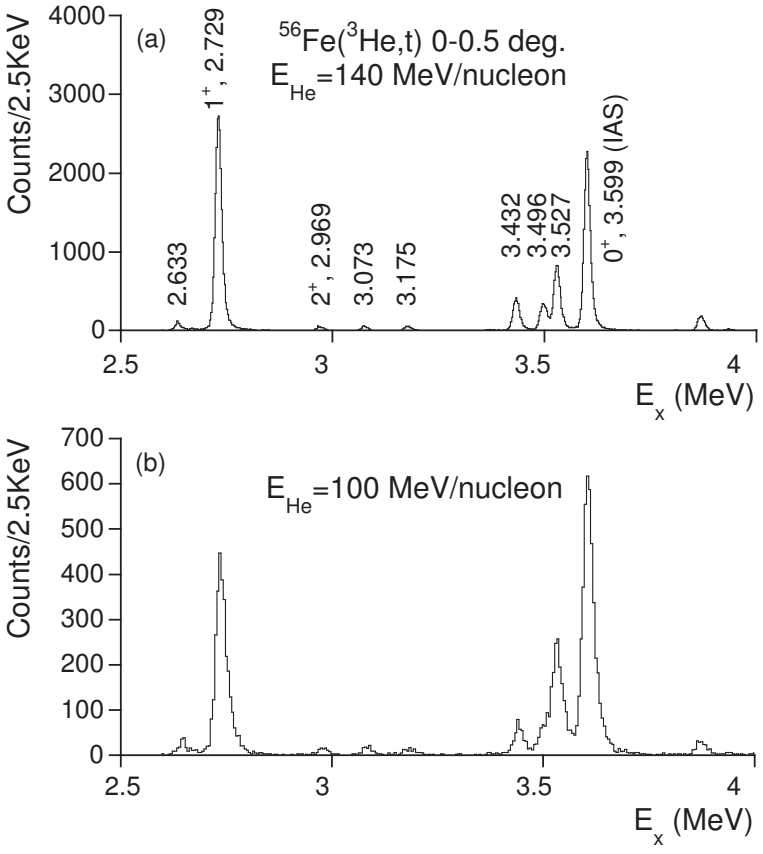

Figure F.3: Espectres d'energia d'excitació de la reacció ^{56}Fe(^{3}He, t)^{56}Co a 140 i 100 MeV/nucleó. L'estat aïllat intensament poblat mitjançant una transició GT situat a 2.729 MeV fou utilitzat com a pic de normalització.

Una impuresa d'isospí de $\alpha^2 = 28(1)\%$ va ser deduïda a aquest experiment. Aquest valor és compatible amb l'obtingut a l'experiment de desintegració β del ^{56}Zn, mostrant una bona simetria d'isospí.

Cal recordar que tant les transicions Fermi com les GT tenen una naturalesa $\Delta L = 0$. Així aquestes transicions poden ser identificades per la forma característica de distribució angular de les seccions eficaces de reacció, picades a 0°. Així el seu estudi permet realitzar una identificació de la J^π dels estats excitats. A aquest experiment, les distribucions angulars dels nivells a 2.633 i 3.073 MeV, associats prèviament a estats 1^+ a la literatura, diferien respecte a la forma esperada. Així, una possible millora a l'assignació J^π d'aquests dos estats fou una motivació més per estudiar en detall el nucli ^{56}Co.

F.2 L'experiment

F.2.1 El montatge experimental

Un estudi detallat de les propietats dels estats nuclears excitats requereix espectroscopia gamma d'alta resolució i múltiples detectors posicionats a diferents angles respecte al feix.

Totes les mesures analitzades i presentades al present treball foren fetes al Maier-Leibnitz-Laboratory (MLL) de la Universitat Tècnica de Munich (TUM, Munich, Alemanya). Els estats excitats al nucli ^{56}Co foren creats mitjançant la reacció de (principalment) fusió-evaporació ^{56}Fe(p,nγ)^{56}Co. La radiació gamma emesa a la desexcitació d'aquests estats fou mesurada *in-beam* (directament al voltant del blanc on es produeix la reacció) amb detectors MINIBALL d'alta resolució. El conjunt de detectors de MINIBALL és un espectròmetre de raigs γ optimitzat per assolir gran eficiència de fotopic i sensibilitat a la posició de la radiació mesurada. Els detectors MINIBALL consten de 3 cristalls de germani (Ge) cada un. Una gran granularitat és aconseguida per la segmentació dels electrodes de recolecció de càrrega dels cristalls de Ge. MINIBALL en la seva totalitat consta de vuit detectors triples. Per a l'experiment a Munich el montatge experimental constava de quatre d'ells, disposats a diferents angles respecte al blanc.

El MLL opera un accelerador Tandem-van-de-Graff el qual accelera ions a altes velocitats amb un voltatge de fins a 14 milions de volts. Pel nostre experiment, els protons foren accelerats fins a 10 MeV. Aquesta energia fou triada cercant optimitzar la creació del nucli ^{56}Co excitat a les energies d'excitació dels dos estats 0^+ que es troben mesclats en termes d'isospí i constitueixen una de les principals motivaciones del present treball (veure secció anterior).

Al nostre experiment, dos blancs de ^{56}Fe de diferent gruix foren utilitzats (1.1 i 2.1 mg/cm^2). Una vegada finalitzat el temps de feix, el primer d'ells fou utilitzat com a una de les fonts de calibració en energia del detectors. Cal esmentar que el blanc activat de ^{56}Fe, amb una certa quantitat de ^{56}Co, torna a desintegrar-se a ^{56}Fe mitjançant un decaïment β^+, amb una vida mitja de $t_{1/2} = 77.236 \pm 0.026$ dies.

L'electrònica utilitzada a l'experiment estigué basada principalment en mòduls estàndar de Mesytec [36]. Les dades foren enregistrades amb el sistema de múltiples branques (MBS, Multi Branch System, desenvolupat al GSI) basats en el sistema d'adquisició de dades MARaBOU [35] (principalment desenvolupat a la TUM) i guardades en archius binaris MED (MBS Event Data).

F.3 Procediment d'anàlisi

Les dades experimentals han de ser calibrades en energia i eficiència per tal de poder ser analitzades i extreure'n resultats. Per dur-ho a terme, s'utilitzaren fonts radioactives estàndar. Obtenir una curva d'eficiència en funció de l'energia és necessàri donada la forta dependència que presenta l'eficiència dels detectors de Ge amb l'energia de la radiació gamma mesurada.

Una vegada calibrades, les dades poden ser re-ordenades en histogrames d'una ò dues dimensions, anomenats espectres i matrius, respectivament.

L'espectre corresponent a la suma de tota l'estadística de l'experiment, cristall a cristall, s'anomena espectre de *Singles* ("individuals") de cada cristall, en referència a què no es requereix cap condició a les transicions per a la construcció de l'espectre (en contraposició al que vorem a la següent secció, al procés de construcció de les matrius bidimensionals). L'espectre de *Singles* una vegada se suma l'estadística del 10 cristalls MINIBALL (dos no foren utilitzats per presentar característiques indesitjades) s'anomena espectre de *Singles* total.

F.3.1 L'esquema de nivells del ^{56}Co

Per construir l'esquema de nivells d'un nucli és necessari col·locar les transicions γ observades a l'esquema de nivells i determinar la seva intensitat. Aquesta informació pot ser deduïda a partir de mesures de coincidències γ-γ, ja que la determinació de les relacions de coincidència entre transicions γ constitueix la base pel seu emplaçament a l'esquema de nivells. Llavors la contrucció de matrius bidimensionals de coincidència γ-γ és necessària. A l'hora de cercar coincidències, una condició de temps ha de ser establida per a decidir quan dos raigs γ són "coincidents", la qual s'anomena *finestra temporal*. La finestra temporal triada al present experiment fou de 312 ns.

Després de construir la matriu bidimensional de coincidència γ-γ, com a primer pas es generen les seves projeccions sobre els eixos x i y. Per ser matrius simètriques, les dues projeccions són idèntiques. Una vegada obtingudes les projeccions, i fent servir paquets d'anàlisi d'espectroscopia gamma apropiats, el procediment per construir l'esquema de nivells és el següent: es selecciona una regió principal de la projecció i tantes regions de fons com es desitgin. Aleshores, s'obté un espectre d'energies

gamma que correspon a totes les transicions gamma detectades en coincidència amb la prèvia regió seleccionada, una vegada sostret el fons. El fet d'observar un pic a aquest espectre indica que la transició corresponent a la regió seleccionada i la transició corresponent a aquest pic pertanyen a una mateixa cascada gamma. Per assegurar-se què aquesta coincidència és real, i no forma part de les coincidències aleatòries (transicions mesurades en coincidència que no pertanyen a una mateixa cascada de desexcitació), es comprova que s'obté la mateixa coincidència en la direcció inversa.

La complexitat de l'esquema de nivells obtingut a aquest treball va fer necessària la combinació de diferents mètodes per calcular les intensitats de les transiciones gamma. Les àrees dels pics han de ser corregides per la corresponent eficiència a l'energia del pic. Quan fou possible, les àrees eren mesurades als espectres de *Singles* total. Quan les transicions gamma eren dèbils ò pertanyien a un multiplet, les àrees s'obtingueren a partir de les matrius de coincidència γ-γ, seleccionant una transició en coincidència que permetera obtenir espectres més nets. Aquests valors havien de ser després normalitzats a l'espectre de *Singles* total. Totes les intensitats foren normalitzades de forma que $I_{158\,keV} = 100$. La transició gamma a 158 keV és la més intensa observada a la desexcitació del ^{56}Co i correspòn a la desexcitació des del seu primer estat excitat al nivell fonamental.

F.3.2 Distribucions angulars de transicions γ

Com s'ha explicat anteriorment, les mesures de coincidències γ-γ donen informació sobre l'energia dels nivells i la intensitat de les transicions que els connecten. Tanmateix, per realitzar assignacions d'espí J i paritat π un necessita investigar el caràcter (magnètic M ò elèctric E) i la multipolaritat de les transicions, on l'ordre multipolar és $L \geq 1$. En general, el/els ordre/s multipolar/s més baix/os, sempre i quan es compleixin les lleis de selecció, estan permesos per una determinada transició gamma, per exemple, una mescla de radiació M1 i E2. En aquests casos, el paràmetre de mescla δ està definit segons:

$$\delta = \frac{\langle J_f \| L_2 \| J_i \rangle}{\langle J_f \| L_1 \| J_i \rangle} \tag{F.3}$$

què representa el quocient entre les amplituds de les multipolaritats mesclades.

A una reacció nuclear el projectil transfereix moment angular als productes de la reacció. Així doncs, els estats excitats formats a reaccions nuclears estan en general orientats respecte a la direcció del feix, alineats a un pla perpendicular a aquest. Un pot utilitzar el fet què la intensitat de la radiació gamma emesa des d'un estat excitat orientat té una distribució espaial anisòtropa, la qual proveeix informació sobre l'ordre i la mescla multipolars de la radiació gamma.

La distribució angular direccional (o anisotropia) de la radiació gamma emesa per nuclis orientats pot escriure's com:

$$W(\theta_\gamma) = \sum_k A_k(\gamma) P_k(cos(\theta_\gamma)) \tag{F.4}$$

on $k = 2l$, i l és la multipolaritat de la transició. En general, aquesta expressió es trunca a segon ordre, i pot reescriure's segons:

$$W(\theta_\gamma) = 1 + A_2 P_2(cos(\theta_\gamma)) + A_4 P_4(cos(\theta_\gamma)) \tag{F.5}$$

Per obtenir les distribucions angulars d'una transició gamma es pot mesurar la seva intensitat a diferents angles respecte a la direcció del feix. En principi, la intensitat del raig gamma s'obtendria a partir de l'àrea del fotopic a l'espectre de *Singles* de cada cristall, i per tant angle a angle, corregida per l'eficiència del detector corresponent. Tanmateix, per tal de poder determinar la intensitat de transicions gamma dèbils ò que pertanyen a un multiplet, es construiren unes matrius de coincidència γ-γ especials. Aquestes matrius foren construides amb les coincidències entre un raig γ detectat a un detector en particular (a un angle en particular) i un raig γ detectat a qualsevol de la resta de detectors. Llavors es poden construir 12 matrius, que corresponen a 12 angles diferents.

Així doncs, es calcularen les intensitats d'una transició γ determinada angle a angle utilitzats cada una d'aquestes matrius, mesurant les àrees als espectres obtinguts en coincidència amb una altra transició γ de la mateixa cascada.

F.4 Els resultats experimentals

A aquesta secció presentam els resultats obtinguts a l'experiment de fusió-evaporació ^{56}Fe(p,nγ)^{56}Co amb una energia incident $E_p = 10$ MeV analitzat al present treball.

Malgrat la gran quantitat de treballs previs sobre l'estudi del nucli ^{56}Co [2, 5–9, 11–31], una enorme quantitat de nova informació ha estat obtinguda al present treball. A les següents línies resumim els principals resultats:

- Un total de 223 transicions gamma han estat observades i col·locades a l'esquema de nivells, de les quals 169 són transicions observades per primera vegada a aquest treball.

- S'ha assolit un nivell de sensibilitat molt major al referit a la literatura per a la desexcitació gamma de nivells del ^{56}Co, per nivells d'espí entre 0 i 6. Un total de 77 estats excitats han estat observats, 37 dels quals eren estats coneguts

pels quals no havia estat observada desexcitació gamma. A 42 dels casos, la precisió energètica dels nivells ha estat millorada. A part, 14 estats han estat observats per primera vegada a aquest treball.

- S'han realitzat 36 noves assignacions J^π, s'han suggerit 10 correccions a assignacions J^π prèvies i en 4 casos s'han resolt ambigüetats a assignacions realitzades amb anterioritat. A la resta de casos, les assignacions J^π referides a la literatura han estat confirmades.

Donada la complexitat de l'experiment, presentam un esquema de nivells del ^{56}Co simplificat, on només les transicions amb una intensitat $I_\gamma > 1.5$ són representades (veure Fig. F.4). Cal fer notar que els primers estats 6^+ i 7^+, així com els dos estats 0^+ d'interés, també estan representats a l'esquema, tot i que les seves transicions gamma no superaven l'umbral d'intensitat mencionat anteriorment. Ho feim així per tal de donar una idea del rang d'espins cobert al present experiment.

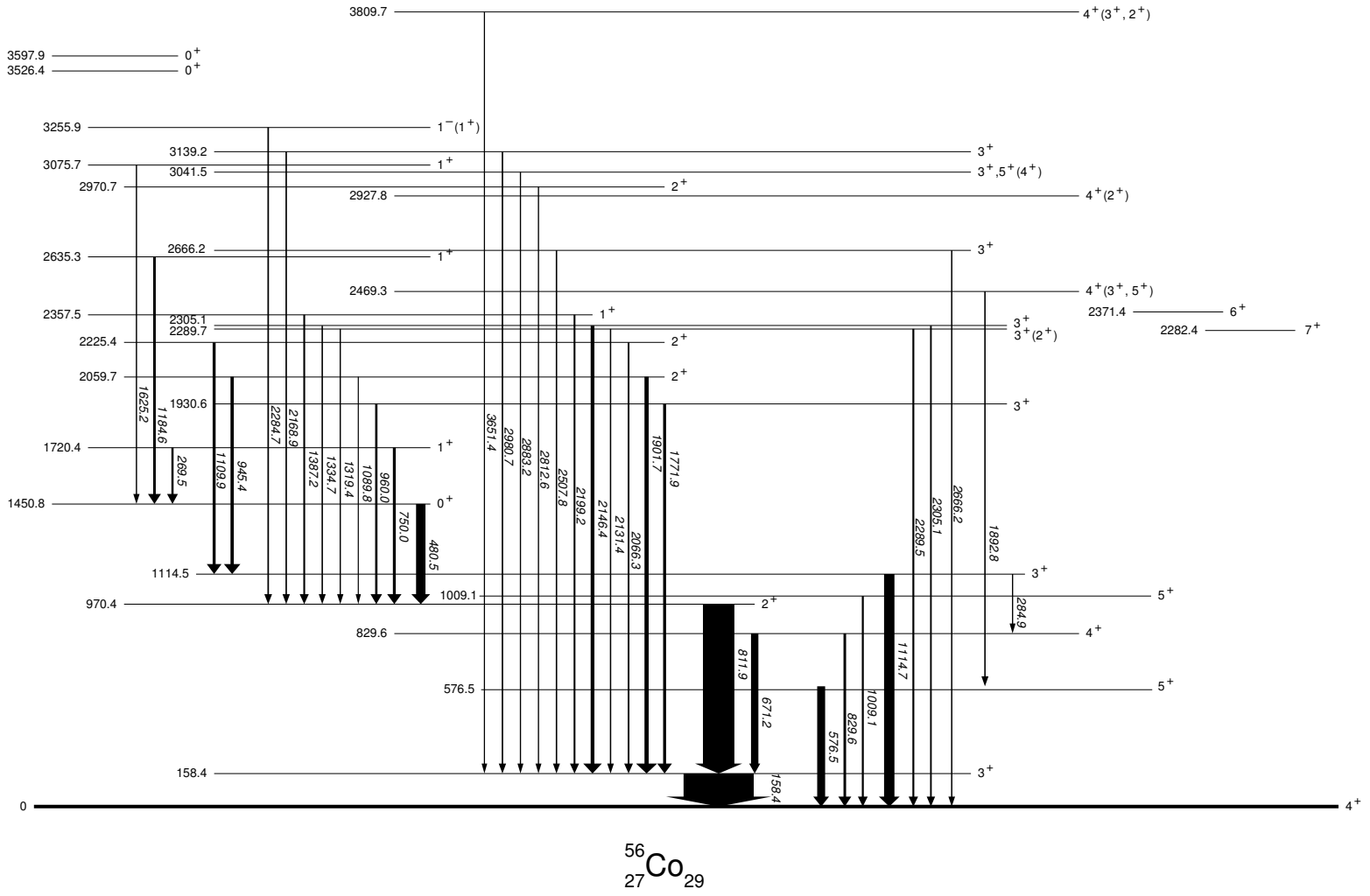

Figure F.4: L'esquema de nivells del ^{56}Co, on únicament les transicions gamma amb $I_\gamma > 1.5\%$ són mostrades. Les energies de les transicions gamma i dels nivells estan en keV. Cal fer notar que els primers estats 6^+ i 7^+, així com els dos estats 0^+ d'interés, també estan representats per completitut, tot i que les seves transicions gamma no superaven l'umbral d'intensitat mencionat anteriorment.

F.5 La interpretació teòrica

F.5.1 Model de capes i estats excitats del ^{56}Co

Les dades experimentals poden ser comparades amb prediccions teòriques per tal d'interpretar els resultats i/o comprobar la correcció de les descripcions teòriques. En el present treball utilitzàrem els Model de Capes com a aproximació teòrica. Els càlculs teòrics proveeixen espectres d'energia i transicions electromagnètiques dels estats individuals.

El nucli ^{56}Co pot ser vist com un cor de ^{56}Ni ($N = Z = 28$) amb un forat-protó a la capa $1f_{7/2}$ i un neutró fóra de l'esmentada capa. Llavors, dintre de la consideració més simple de model de capes, els estats excitats a més baixa energia d'excitació al ^{56}Co poden ser descrits en termes de configuracions de particle-forat (1p-1h, p≡ particle; h≡"hole", forat en anglès), és a dir, configuracions de la forma $(1f_{7/2})^{-1}_{\pi} \times (2p_{3/2}, 1f_{5/2}, 2p_{1/2})^{1}_{\nu}$ (veure Fig. F.5). Aquest espai de configuració dóna lloc als estats $T = 1$, $J^{\pi} = 1^+, ..., 6^+$. De la mateixa forma, configuracions de dues-particles-dos-forats (2p-2h) han de ser incloses per descriure els estats 0^+ al ^{56}Co. Amb aquest propòsit, interaccions efectives de dos cossos han de ser utilitzades.

Al present treball, càlculs de model de capes a un espai de valència de la capa *fp* truncat foren realitzats per Edward Simpson [64] utilitzant el codi NuShellX@MSU [61] i les interaccions efectives de dos cossos KB3G [59] i GXPF1a [60]. Als càlculs s'utilitzà un espai de valència de $q = 2$, on q és el nombre mínim de protons i neutrons que romanen a l'orbital $1f_{7/2}$.

En general, la identificació entre els nivells experimentals i les prediccions teòriques està basada inicialment en l'energia del nivell i el valor seu J^{π}. Per confirmar aquesta identificació es realitzà una comparació entre el patró de desintegració γ i les tases de desintegració, experimentals i predites. Hem observat que existeix un bon acord entre les energies d'excitació i les desexcitacions gamma dels estats excitats experimentals i teòrics fins a aproximadament 2.5 MeV per estats amb espins J = 3-7. Tanmateix, a aquestes energies per estats 1^+ i 2^+, i per sobre dels 2.5 MeV per la resta d'espins, la identificació comença a ser difícil degut a l'increment de densitat de nivells, la qual cosa fa que sigui qüestionable qualsevol altra identificació amb les prediccions teòriques.

F.5.2 Els estats 0^+ amb mescla d'isospí

Tal com s'ha explicat a la secció F.1 d'aquest resum, l'estudi dels dos estats 0^+ que es troben fortament mesclats en termes d'isospí al ^{56}Co fou una de les principals motivacions del present treball.

Experimentalment, els estats observats a 3526.4 i 3597.9 keV d'energia d'excitació

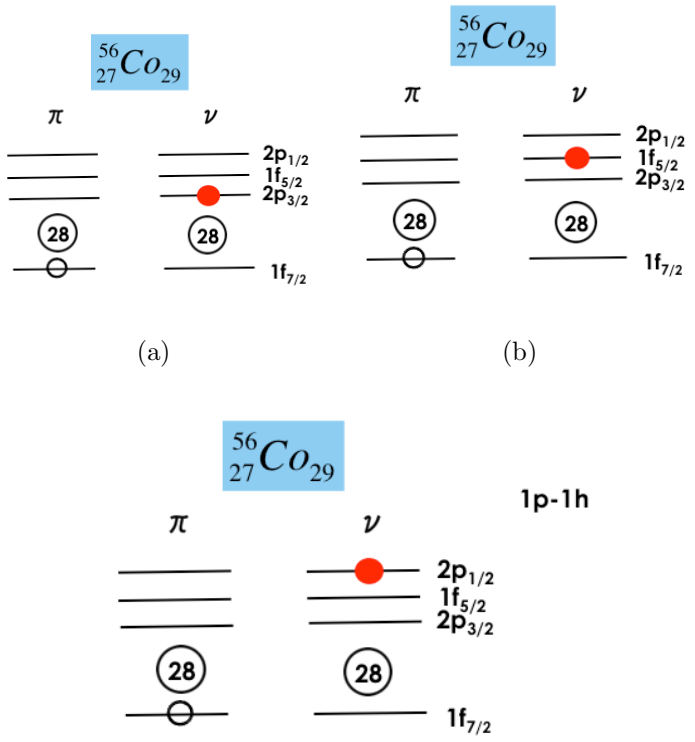

Figure F.5: Configuracions de particle-forat (1p-1h) a l'espai de valència de la capa *fp*, és a dir, $(1f_{7/2})^{-1}_{\pi} \times (2p_{3/2}, 1f_{5/2}, 2p_{1/2})^{1}_{\nu}$ ((a), (b) i (c), respectivament), que constitueixen la gran majoria d'estats de baixa energia d'excitació al ^{56}Co. Aquest espai de configuració dóna lloc als estats $T = 1$, $J^{\pi} = 1^{+}, ..., 6^{+}$.

corresponen a aquests dos estats 0^+, els quals tenen ambdós una component de l'IAS, com ha estat demostrat a diversos treballs [2, 7, 8]. L'estat a 3597.9 keV correspòn a la component del doblet amb (principalment) valor d'isospí $T = 2$. Així doncs, l'estat situat a 3526.4 keV és excitat mitjançant la part d'impuresa d'isospí ($T = 2$) de la funció d'ona i porta una part de la intensitat de la transició Fermi.

Un resum de la desexcitació gamma dels anteriors estats 0^+ es presenta a la Taula F.1. Es mateixos valors experimentals es troben representats en forma esquemàtica a la Fig. F.6. Apart de les transicions γ ja conegudes prèviament, al present treball s'han observat dues noves transicions desexcitant el nivell a més baixa energia. Així concloem que ambdós nivells desintegren als estats 1^+ situats a energies 1720.3, 2635.1 i 2729.1 keV. Es pot observar que els dos estats desexciten de forma molt diferent, en contra del nostre pensament inicial.

Table F.1: Resum de la desexcitació γ dels dos estats 0^+ fortament mesclats en termes d'isospí, situats a 3526.4 i 3597.9 keV. Les energies experimentals E_γ i les tases de desintegració (en anglès, *branching ratio*, BR) es mostren per cada nivell. Els valors de la vida mitja $t_{1/2}$ s'han pres de la referència [29]. Notar que totes les desintegracions són a estats 1^+.

E_{nivell}(keV)	$t_{1/2}$ (fs)	E_γ(keV)	$J_i^\pi \to J_f^\pi$	I_γ	BR	Comentaris
3526.4	6(5)	797.2(5)	$0^+ \to 1^+$	0.11(2)	10(2)	N
		891.5(4)	$0^+ \to 1^+$	c	1.8(5)	aN
		1806.1(3)	$0^+ \to 1^+$	1.13(12)	100(11)	
3597.9	18(5)	868.6(2)	$0^+ \to 1^+$	0.46(2)	62(3)	
		962.8(2)	$0^+ \to 1^+$	c	33(6)	b
		1877.9(3)	$0^+ \to 1^+$	0.74(5)	100(7)	

[N] Transició γ observada a aquest treball per primera vegada.

[a] Tasa de desintegració obtinguda utilitzant el valor de la tasa de desintegració de la transició γ de 962.8 keV i el quocient entre les intensitats relatives $I_{891.5}/I_{962.8}$ obtingut utilitzant una transició en coincidència a la matriu de coincidències γ-γ.

[b] Tasa de desintegració obtinguda de la referència [29].

[c] Intensitat relativa a una transició en coincidència a la matriu de coincidències γ-γ (és a dir, no normalitzada a l'espectre de *Singles* total).

Prediccions teòriques

Per la discussió de la desexcitació dels dos estats 0^+ que es troben mesclats en termes d'isospí, a més dels càlculs presentats a l'anterior secció (sec. F.5.1), càlculs de model de capes foren realitzats per Alfredo Poves [65] utilitzant una versió millorada de la interacció KB3G, la KB3GR [63], i fent servir el codi ANTOINE [62], amb una truncació $t = 7$, on t indica una configuració final on 7 nucleons poden estar fora de la capa $1f_{7/2}$.

Cap de les interaccions efectives utilitzades al present treball conté termes de no-conservació de l'isospí, com són la força de Coulomb entre d'altres. Llavors l'isospí és un bon nombre quàntic i els estats individuals calculats tenen valors purs d'isospí T. Així doncs, el càlcul de mescla d'isospí al present treball s'ha de fer una vegada calculats els estats de bon isospí.

La probabilitat de transició des d'un estat J_i a un estat J_f d'un raig γ d'energia E_γ i multipolaritat λ pot ser expressada segons l'equació extreta de [33]:

$$T(\sigma\lambda, J_i \to J_f) = \frac{8\pi(\lambda+1)}{\hbar\lambda(2\lambda+1)!!}\left(\frac{E_\gamma}{\hbar c}\right)^{2\lambda+1} B(\sigma\lambda : J_i \to J_f) \tag{F.6}$$

on σ denota transició elèctrica (E) o magnètica (M) i on,

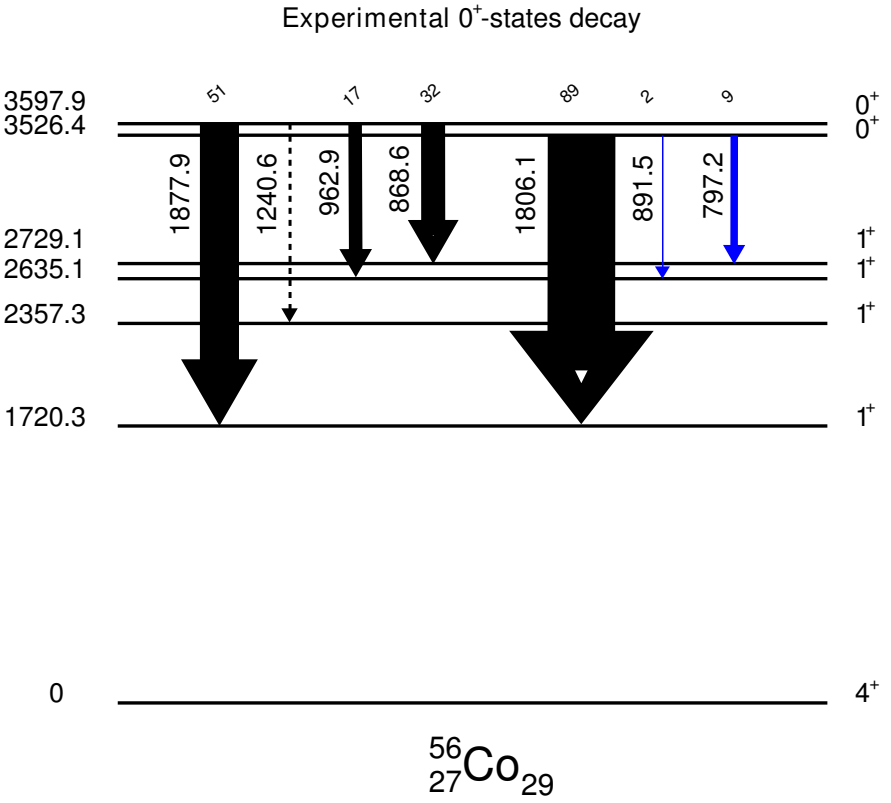

Figure F.6: Esquema dels resultats experimentals de la desexcitació γ dels dos estats 0^+ situats a 3526.4 i 3597.9 keV. El gruix de les fletxes és proporcional a la intensitat, i les tases de desintegració apareixen indicades a cada nivell. Les fletxes negres sòlides indiquen transicions γ coneixides prèviament a la literatura. Les fletxes blaves sòlides indiquen transicions γ observades per primera vegada a aquest treball. La fletxa en puntejat mostra una possible transició γ (predita als càlculs teòrics), l'existència de la qual no ha pogut confirmar-se ni descartar-se. Les energies de les transicions i els nivells es mostren en keV.

$$B(\sigma\lambda : J_i \to J_f) \equiv \sum_{\mu,m_f} |\langle f|\mathcal{M}(\sigma\lambda,\mu)|i\rangle|^2 = \sum_{\mu,m_f} \langle J_i m_i \lambda\mu | J_f m_f\rangle^2 |\langle f\|\mathcal{M}(\sigma\lambda)\|i\rangle|^2 \tag{F.7}$$

s'anomena *probabilitat de transició reduïda* [34]. El terme $|\langle f|\mathcal{M}(\sigma\lambda,\mu)|i\rangle|$ és l'element de matriu de transició, i $\langle f\|\mathcal{M}(\sigma\lambda)\|i\rangle$ s'anomena element reduït de matriu de transició. La probabilidad de transició reduïda no depèn de l'energia. Conseqüentment, en general és convenient convertir els valors $T(\sigma\lambda)$ a $B(\sigma\lambda)$.

Per la discussió de la desexcitació dels dos estats 0^+ esteim interessats només en transicions M1, donat que totes les desintegracions són del tipus $0^+ \rightarrow 1^+$.

Per aquest anàlisi utilitzàrem els valor teòrics de B(M1) obtinguts mitjançant càlculs de model de capes utilitzant la interacció efectiva KB3GR per les transicions d'interès. Tenint en compte les equacions de dos estats $|\Psi_a\rangle$ i $|\Psi_b\rangle$ amb mescla d'isospí presentades amb anterioritat (eqs. F.1a i F.1b) es poden calcular els valors de les probabilitats reduïdes B(M1) dels dos estats mesclats. Pel cas sota discussió, els estats $|\Psi_a\rangle$ i $|\Psi_b\rangle$ representen els dos estats 0^+ situats a 3597.9 i 3526.4 keV, respectivament, que anomenarem $|0^+_{sup}\rangle$ i $|0^+_{inf}\rangle$.

La figura F.7 mostra la comparació dels valors B(M1) experimentals amb les prediccions teòriques. Cal fer notar que degut a l'ortogonalitat dels dos estats què es troben mesclats, la opció de mescla constructiva a l'estat $|0^+_{sup}\rangle$ és compatible només amb la opció destructiva a l'estat $|0^+_{inf}\rangle$. Llavors, al gràfic presentam les solucions constructiva i destructiva al càlcul de la B(M1) de l'estat $|0^+_{sup}\rangle$, amb les opcions complementàries per la B(M1) de l'estat $|0^+_{inf}\rangle$.

S'ha de tenir en compte que les vides mitges dels dos estats 0^+ d'interès són grans [29], especialment la del nivell inferior ($t_{1/2} = 18 \pm 5$ fs pel nivell a 3597.9 keV, i 6 ± 5 fs pel nivell a 3526.4 keV). Llavors, les B(M1) experimentals tenen unes incerteses associades grans. Tanmateix, si un observa la desexcitació del nivell superior, que té associada una menor barra d'error, l'opció constructiva apareix clarament afavorida.

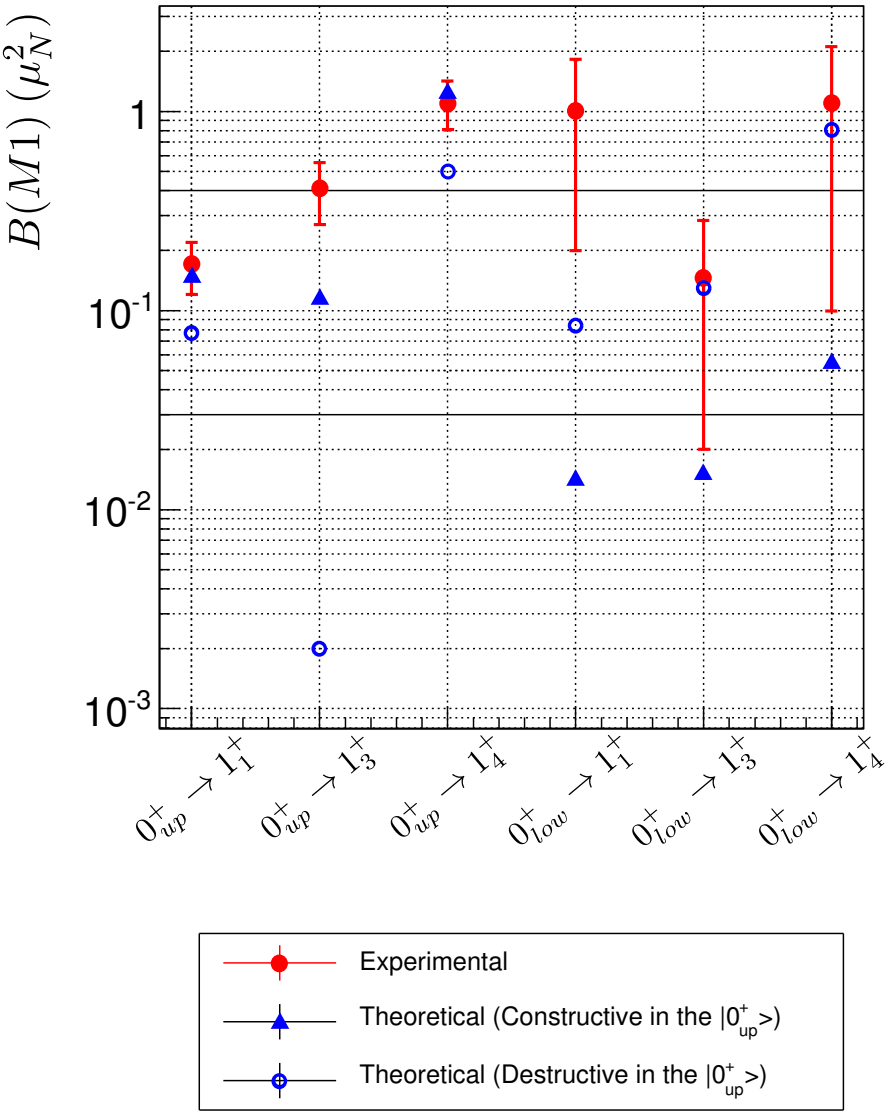

Figure F.7: Comparació dels valors B(M1) experimentals amb els càlculs de model de capes utilitzant un espai de València de la capa *fp* truncada, fent servir el codi ANTOINE amb la interacció efectiva KB3GR. El truncament utilitzat fou $t = 7$ (veure text principal). Les solucions constructiva i destructiva al càlcul de la B(M1) de l'estat $|0^+_{sup}\rangle$, amb les opcions complementàries per la B(M1) de l'estat $|0^+_{inf}\rangle$ es mostren al gràfic. Cal fer notar que els errors de les B(M1) experimentals provenen principalment de les vides mitges d'ambdós nivells.

F.6 Conclusions

Al present treball s'ha estudiat la reacció de fusió-evaporació ^{56}Fe(p,nγ)^{56}Co. La radiació gamma emesa a la desexcitació dels estats excitats del nucli imparell-imparell ^{56}Co fou mesurada *in-beam* (directament al voltant del blanc on es produeix la reacció) amb detectors MINIBALL d'alta resolució, al Maier-Leibnitz-Laboratory (MLL) de la Universitat Tècnica de Munich (TUM, Munich, Alemanya).

Malgrat l'extens treball previ realizat a l'estudi del ^{56}Co, al present treball s'ha obtingut una gran quantitat de nova d'informació, que implica una gran millora al coneixement de la seva estructura. En resum, els principals resultats obtinguts són:

- Un total de 223 transicions gamma han estat observades i col·locades a l'esquema de nivells, de les quals 169 són transicions observades per primera vegada a aquest treball.
- S'ha assolit un nivell de sensibilitat molt major al referit a la literatura per a la desexcitació gamma de nivells del ^{56}Co, per nivells d'espí entre 0 i 6. Un total de 77 estats excitats han estat observats, 37 dels quals eren estats coneguts pels quals no havia estat observada desexcitació gamma. A 42 dels casos, la precisió energètica dels nivells ha estat millorada. A part, 14 estats han estat observats per primera vegada a aquest treball.
- S'han realitzat 36 noves assignacions J^π, s'han suggerit 10 correccions a assignacions J^π prèvies i en 4 casos s'han resolt ambigüetats a assignacions realitzades amb anterioritat. A la resta de casos, les assignacions J^π referides a la literatura han estat confirmades.

D'altra banda, s'han realitzat càlculs teòrics de model de capes a un espai de valència de la capa *fp* truncat utilitzant el codi NuShellX@MSU [61] (amb les interaccions efectives de dos cossos KB3G [59] i GXPF1a [60]), i amb el codi ANTOINE i la interacció efectiva KB3GR. Hem pogut observar una bona descripció dels nivells de baixa excitació en termes de configuracions de particle-forat, que formen els diferents multiplets $(1f_{7/2})^{-1}_\pi \times (2p_{3/2}, 1f_{5/2}, 2p_{1/2})^1_\nu$. En general hem observat un bon acord entre energies i desexcitacions gamma dels nivells experimentals i les prediccions teòriques fins als 2.5 MeV, per espins J = 3-7. Tanmateix, pels estats 1^+ i 2^+ la identificació comença a ser difícil a aquestes energies degut a l'increment de densitat de nivells.

En quant a l'estudi dels dos estats 0^+ que es troben fortament mesclats en termes d'isospí, hem observat que aquests es desintegren de forma diferent, contràriament a la hipòtesi inicial. De l'estudi de les probabilitats de transició reduïda B(M1) hem conclòs que la mescla d'isospí és constructiva a l'estat de més alta energia d'excitació, mentre que l'estat 0^+ veí ha de tenir una mescla destructiva.

References

1. Orrigo, S. *et al. Phys. Rev. Lett.* **112,** 222501–1 (2014).
2. Fujita, H. *et al. Phys. Rev. C* **88,** 054329 (2013).
3. Taddeucci, T. *et al. Nucl. Phys. A* **469,** 125 (1987).
4. Lenske, H. *Nucl. Phys. A* **482,** 343c (1988).
5. Anderson, J. & Wong, C. *Phys. Rev. Lett.* **7,** 250 (1961).
6. Orihara, H. *et al. Phys. Lett. 106B,* 171 (1981).
7. Orihara, H. *et al. Nucl. Phys. A* **403,** 317 (1983).
8. Dzubay, T., Sherr, R., Becchetti, F. & Dehnhard, D. *Nucl. Phys. A* **142,** 488 (1970).
9. Zimmerman, W. R., J.J.Kraushaar, Schneider, M. & Rudolph, H. *Phys. Rev. C* **16,** 2432 (1977).
10. Osterfeld, F. *Rev. Mod. Phys.* **64,** 491 (1992).
11. Schneider, M. & Daehnick, W. *Phys. Rev. C* **4,** 1649 (1971).
12. Caldwell, T., Nathan, O., Hansen, O. & Bork, H. *Nucl. Phys. A* **202,** 225 (1973).
13. Okada, K., Kawa, J. & Yamagata, T. *Nucl. Phys. A* **349,** 125 (1980).
14. Rivet, E., Pehl, R., Cerny, J. & Harvey, G. *Phys. Rev.* **141,** 1021 (1965).
15. Nann, H., Chien, W., Saha, A. & Windenthal, B. *Phys. Lett. 60B,* 32 (1975).
16. Nann, H., Chien, W., Saha, A. & Windenthal, B. *Phys. Rev. C* **15,** 1959 (1977).
17. Haller, M & Kretschmer, W. *Nucl. Phys. A* **419,** 45 (1984).
18. Shang, R., Pilt, A., Vetterli, M., Trudel, A. & Kuehner, J. *Nucl. Phys. A* **425,** 411 (1984).
19. Frascaria, N., Didelez, J., Garron, J., Gerlic, E. & Roynette, J. *Phys. Rev. C* **10,** 1422 (1974).
20. Frascaria, N., Didelez, J., Chant, N. & Chang, C. *Phys. Rev. C* **16,** 603 (1977).
21. Glendenning, N. *Phys. Rev. B* **137,** 102 (1965).
22. Nann, H., Bacher, A., Jacobs, W., Jones, W. & Stephenson, E. *Phys. Rev. C* **24** (1981).

23. Bruge, G. & Leonard, R. *Phys. Rev. C* **2,** 2200 (1970).
24. Samuelson, L. *et al. Phys. Rev. C* **7,** 2379 (1973).
25. Hoffman, S. *Z. Phys.* **270,** 133 (1974).
26. Sur, B., Norman, E., Lesko, K., Browne, E. & Larimer, R. *Phys. Rev. C* **42,** 573 (1990).
27. DelVecchio, R., Gibson, R. & Daehnick, W. *Phys. Rev. C* **5,** 446 (1972).
28. Barker, J. & Sarantites, D. *Phys. Rev. C* **10,** 1407 (1974).
29. Kampp, W. D., Bodenmiller, K., Nagel, A. & Buhl, S. *Z. Phys. A* **288,** 167 (1978).
30. Sarantites, D., Urbon, J. & L.L. Rutlegde, J. *Phys. Rev. C* **14,** 1412 (1976).
31. Kampp, W. & Buhl, S. *Z. Phys. A* **284,** 117 (1978).
32. Koning, A. J. & Hilaire, S. in *Proceedings of the International Conference on Nuclear Data for Science and Technology (2007)* (2008), 211.
33. Morinaga, H. & Yamazaki, T. *In-beam Gamma-ray Spectroscopy* (North-Holland, 1976).
34. Harakeh, M. & van der Woude, A. *Giant Resonances* (Oxford Science Publications, 2001).
35. Lutter, R., Schaile, O., Schöffel, K., Steinberger, K. & Broude, C. *MARaBOU data adquisition system* 2003. `\url{http://www.bl.physik.uni-muenchen.de/marabou/html/}`.
36. Mesytec GmbH und Co. KG. 2014. `\url{http://www.mesytec.com/}`.
37. *Update of X Ray and Gamma Ray Decay Data Standards for Detector Calibration and Other Applications* IAEA (Vienna, 2007).
38. *Calibration Certificate Eu-152* Amersham Buchler, 1994.
39. *Calibration Certificate Ba-133* Calibration laboratory for measurements of radioactivity, Physikalisch-Technische Bundesanstalt, 2003.
40. *Calibration Certificate Co-60* Calibration laboratory for measurements of radioactivity, Physikalisch-Technische Bundesanstalt, 1987.
41. Jäckel, B., Westmeier, W. & Patzelt, P. *Nucl. Inst. Math. A* **261,** 543 (1987).
42. Ziegler, J., Ziegler, M. & Biersack, J. in *"SRIM - the stopping and range of ions in matter (2010)"* 1818–1823 (Nucl. Instrum. Methods Phys. Res. Sect. B, 2010).
43. Catford, W. *Catkin v2.02* University of Surrey. `\url{http://personal.ph.surrey.ac.uk/~phs1wc/kinematics/}`.
44. Fitzler, A. *Tv* Institute for Nuclear Physics, University of Cologne. `\url{http://www.ikp.uni-koeln.de/misc/doc/Tv_user-manual/Tv_user-manual.html}`.
45. Gulyás, J. *Eleven code* Institute for Nuclear Research (Debrecen, Hungary).

46. Kibédi, T., Burrows, T., Trzhaskovskaya, M., Davidson, P. & C. W. Nestor, J. 'Evaluation of theoretical conversion coefficients using BrIcc'. *Nucl. Instr. and Meth. A* **589,** 202–229 (2008).
47. Junde, H., Su, H. & Dong, Y. *Nuclear Data Sheets* **112,** 1513 (2011).
48. Mateosian, E. D. & Sunyar, A. W. *Tables of Attenuation Coefficients for Angular Distribution of Gamma Rays from Partially Aligned Nuclei.* 391 (1974).
49. Mateosian, E. D. & Sunyar, A. W. *Tables of Angular-Distribution Coefficients for Gamma Rays of Mixed Multipolarities emitted by Aligned Nuclei* 407 (1974).
50. Lenzi, S. & Bentley, M. *Lect. Notes Phys.* **764,** 57 (2009).
51. Smirnova, N. *et al. Phys. Rev. C* **93,** 044305 (2016).
52. Towner, I. & Hardy, J. *Phys. Rev. C* **82,** 065501 (2010).
53. Satula, W., Dobaczewski, J., Nazarewicz, W. & Rafalski, M. *Phys. Rev. Lett.* **106,** 132502 (2011).
54. Suzuki, T., Sagawa, H. & Colo, G. *Phys. Rev. C* **54,** 2954 (1996).
55. Vervier, J. *Nucl. Phys. A* **103,** 222 (1967).
56. Horie, H. & Ogawa, K. *Prog. Theor. Phys,* 439 (1971).
57. Hsieh, S. T., Wang, M. C., Chiang, H. C. & Lee, T. Y. *Phys. Rev. C,* 563 (1973).
58. Richter, W. FPD6. *Nucl. Phys. A* **523,** 325 (1991).
59. Poves, A., Sánchez-Solano, J., Caurier, E. & Nowacki, F. KB3G. *Nucl. Phys. A* **694,** 157 (2001).
60. Honma, M., Otsuka, T., Brown, B. & Mizusaki, T. GXPF1A. *Phys. Rev. C* **69,** 034335 (2004).
61. Brown, B. & Rae, W. NUSHELLX. *Nuclear Data Sheets* **120,** 115 (2014).
62. Caurier, E. & Nowacki, F. ANTOINE. *Acta Phys. Pol. B* **30,** 705 (1999).
63. Poves, A. KB3GR effective interaction, private communication.
64. Simpson, E. Shell-model calculations, private communication.
65. Poves, A. Shell-model calculations, private communication.
66. Pinto, P. & Woosley, S. *Nature* **333,** 534 (1988).
67. The LIGO Scientific Collaboration and the Virgo Collaboration. *GCN,* 21505, 21509, 21510, 21513, 21527 (2017).
68. Multi-messenger Observations of a Binary Neutron Star Merger. *The Astrophysical Journal Letters* **848,** L12 (2017).
69. Metzger, B. D. *et al. Mon. Not. R. Astron. Soc.* **406,** 2650 (2010).
70. Rosswog, S. *et al. A&A* **341,** 499 (1999).
71. Freiburghaus, C., Rosswog, S. & Thielemann, F. *ApJ* **525,** L121 (1999).
72. Lund, J., Martínez-Pinedo, G. & Langanke, K. *arXiv:nucl-th/9902005v1,* 1 (2017).

73. Rao, M.N. *Nuclear Data Sheets* **3,** 304 (1970).

74. Laget, J. & Gastebois, J. *Nucl. Phys. A* **122,** 431 (1968).

Acknowledgements/Agradecimientos

Quiero agradecer tanto y a tantísimas personas el haber hecho posible que estos años en Valencia hayan sido tan increíbles, que siento que me faltarán las palabras.

Ante todo, gracias al grupo de Espectroscopía Gamma y Neutrones del IFIC. A mi directora de tesis la Dra. Berta Rubio, por su paciencia y entusiasmo en entender cada pequeño detalle. Y por la confianza que siempre ha depositado en mí. De su actitud siempre positiva ante los pequeños contratiempos y momentos de agobio, y de su papel como mujer científica, he aprendido mucho. Gracias, Berta. Al Dr. Alejandro Algora, por su siempre amabilidad y cercanía para discutir cualquier cuestión. Al Dr. José Luis Taín, por su disponibilidad y ayuda siempre que lo he necesitado, y por su sabiduría.

Gracias a todo el grupo por la gran calidez humana que se respira. Por ser un grupo que destaca, no sólo por su excelencia científica, si no también por su calidad a nivel personal. A Jorge, por ser un amigo. Contigo he aprendido que la amistad traspasa barreras generacionales (yo suelo olvidar esa diferencia de edad, pero Kiko se encarga siempre de recordarme vuestro premio de 1987). Gracias por tu complicidad y apoyo, y por todos los buenos momentos. A Kike, por su inestimable ayuda. Por la increíble energía positiva que transmite y su generosidad. A Víctor, por ser mi compañero de tesis. Por su siempre ingeniosa respuesta y vivacidad. A Álvaro, que no ha podido ser mejor compañero. Por su predisposición siempre a ayudar, a dedicar una palabra de ánimo, y su bondad. A Anabel, porque se convirtió en una gran compañía diaria. Gracias por tu ayuda y cercanía, y por todas las conversaciones que hemos mantenido. A Pablo, por su compañerismo, amabilidad y disponibilidad. A Sonja, por sus siempre detalladas explicaciones a mis preguntas y su disponibilidad. A César, Loli, Luis, Ion... por vuestra siempre amable ayuda y compañía. A mi compi Ebhe, por ser única. Y por transmitir siempre esa alegría. A Roger, porque ha sido todos estos años un amigo en la distancia con el que he podido contar y al que agradezco muchas cosas. A Pancho, porque era ya un amigo antes de yo entrar en el grupo. To Ela. Thank you for your always kindness, sweetness and help. Y a Kiko, que visita nuestro despacho más que si fuera parte del grupo. Por su ayuda desinteresada y por nuestro saludo sincronizado.

To Prof. William Gelletly. Thank you for all, Bill. For all what I have learned from and with you, for your kind help and always kind words. For your patience and

humanity. To Prof. Yoshi Fujita. Thank you for your enthusiasm, encourage and always predisposition to teach and help.

I want to thank all the people I met in the E12 group at the TUM, and made me feel like home. To Dr. Dennis Mcher, for his energy and enthusiasm. To Steffi, for her generous help, kindness and sweetness. To Kathi, Michael and Dominik, for being such a good friends despite the short time we spent together.

Al Dr. Alfredo Poves, por sus amables explicaciones y su esfuerzo relativo a los cálculos Shell-Model realizados. I also want to thank Dr. Edward Simpson. I appreciated so much the fruitful discussions we had during his visit and his kindness and dedication during the next months. I also want to thank all the effort he did to performed such a huge amount of sets of calculations.

A mis amigos de "DoctoRandoms". Merece mención especial esta dedicatoria. Definitivamente habéis sido mi alegría diaria. Me siento muy afortunada de haber podido compartir mi día a día con vosotros. A mis queridos Rosa, Damián, Davide y Javi escalador, porque sin vosotros no hubiera sido lo mismo. Por conocerme tal y como soy, por hacerme reír y haberme visto llorar. Os quiero mucho. A Giulia, por todos los planes futuros que tenemos. A André, por valorar mi menospreciada nueva faceta musical con el huevo. A Dominik, Pablo León, Rebecca, Javi Barrios, Miguel Ángel, Alberto, Javi-nano, Daniele, Marta, Víctor (Babiano), Oleksii... A cada uno de vosotros, por haber hecho tan especial el haber pasado estos años en el IFIC.

A los que ya acabaron pero siguen en la secta de "DoctoRandoms", Elena y Sebas. Por tantas risas que hemos compartido y que así siga siendo por mucho tiempo. A Dani, que ha resultado ser la persona más fuerte y optimista que he conocido. Y que dentro de la adversidad de la situación, sabrá encontrar su sitio con brillo y energía únicos. Y a Pablo Ruíz y a Nacho.

A Vale y Paulina, gracias por vuestra complicidad y amistad. Porque es difícil tener tan buenas amigas, y me siento muy afortunada de teneros. Porque sois mucho más que "Encuentros de pasillo". Gracias por apoyarme en todo y cada día, os quiero mucho. Vale, que nuestra amistad siga cumpliendo años en Facebook, y aunque parezca difícil, se haga más bonita año tras año. Pau, honey, que mantengamos por muchos años nuestros gustos comunes, como sabes, en casi todo. Será muy triste separarme de vosotras.

A Núria, que ja no estàs tan a prop però la nostra amistat seguirà sent sempre igual de forta. Gràcies per tot el que hem passat juntes. Esper poder tornar a compartir els plans quotidians amb tu prest.

A mis queridas Irene y Ana, que han sido el escape del mundo de físicos, a pesar de haber entrado totalmente en él. Por todos los momentos únicos, el cariño y la complicidad compartidos. Por ser amigas en el sentido más profundo de la palabra.

A Carlos (bicho), por todos y cada uno de los días que hemos ido a patinar. Gracias a ellos estoy en forma. Y gracias por tu cariño y sentido del humor.

A amigas que se fueron pero con ellas sigue siendo todo como ayer. A Diana y a Mer. Que podamos reencontranos todas juntas pronto, y compartamos momentos tan bonitos como los que vivimos en Valencia. Y a los amigos que hice ya antes de empezar el doctorado. A Paco, Arnau, Carmen, Jose, Agustín... Porque hicieron de ese verano algo muy especial y la amistad con ellos ha continuado.

Por el resto de amigas que he encontrado a lo largo de estos años, y que han hecho que fueran aún mejores. A mi Mariana, que iluminaba cada momento que vivíamos juntas, a Beth, que con su locura y bondad aportaba la nota especial a nuestros días. Gracias por todo el cariño que me disteis y me seguís dando. A Tania, por las risas compartidas y su siempre disposición para escuchar y ayudar. A Ana (Gutiérrez), por todos los momentos en que me demostró lo que es ser una buena amiga. Porque aunque la distancia nos separe, mantengamos siempre esa amistad.

Y a mis padres y mi hermana, Merce, que son mi hogar y mi referente. Han sido y serán siempre mi apoyo. Con ellos he crecido día a día y gracias a ellos soy quién soy. Y porque me han enseñado que, ante todo, hay que ser feliz. Gracias por vuestra complicidad, por escucharme siempre, por vuestro amor incondicional.